

**Towards Self-sorting Materials using Hydrogen
Bonding Motifs**

Heather Marie Coubrough

Submitted in accordance with the requirements for the
degree of Doctor of Philosophy

The University of Leeds
School of Chemistry

November 2018

The candidate confirms that the work submitted is her own, except where work which has formed part of jointly-authored publications has been included. The contribution of the candidate and the other authors to this work has been explicitly indicated below. The candidate confirms that appropriate credit has been given within the thesis where reference has been made to the work of others.

Chapter 2 - Sequential self-sorting of hydrogen bonding motifs; the work reported in this chapter formed part of a research paper 'Supramolecular Self-Sorting Networks Using Hydrogen-Bonded Motifs', Chem. Eur. J., 2018, accepted article. The contributions of the authors are as follows: AJW and HMC (the candidate) designed the experimental research, HMC performed the experimental research and drafted the corresponding section of the manuscript. CFG and SCCL designed the computational research, SCCL performed the computational research and drafted the corresponding section of the manuscript. CP solved the x-ray crystal structures, MJH set up NOESY NMR experiments and AJW edited the manuscript into its present form.

This copy has been supplied on the understanding that it is copyright material and that no quotation from the thesis may be published without proper acknowledgement.

The right of Heather Marie Coubrough to be identified as author of this work has been asserted by her in accordance with the Copyright, Designs and Patents Act 1988. © 2018 The University of Leeds Heather Marie Coubrough

Acknowledgements

First and foremost, I would like to thank my PhD supervisor Prof Andrew Wilson for his support, guidance and encouragement throughout my PhD. His belief in the project and my abilities has been a huge motivation.

I would also like to thank several academic researchers that I have been lucky enough to collaborate with during my PhD; in particular, Prof Dr Célia Fonseca Guerra, Stephanie C. C. van der Lubbe and Dr Johan Mattsson. In addition, I would like to thank the many members of the academic and support staff at Leeds; in particular, Dr Mark J. Howard (NMR), Dr Christopher Pask (x-ray), Dr Daniel Baker and Matthew Reynolds (DSC) and Sam Parkinson and Dr Nicholas Warren (GPC). Thanks to Barbora Balonova and Barry Blight from University of New Brunswick, Canada for providing compound BB1.

A huge thank you goes to all the members of the Wilson groups, past and present. It's been a huge privilege to have been part of such a knowledgeable and talented research group. Their scientific guidance and emotional support over the past three years has been incredible, and many group members have become genuine friends over this time.

Many thanks must go to my family and friends who have lovingly supported me during my PhD. Special thanks to Emily and Sarah for proofreading this thesis. Thank you most of all to my mum and dad for always being there for me.

Abstract

Hydrogen bonding is one of the most useful of the non-covalent interactions. Highly directional and easily tuneable, the strength of hydrogen bonded arrays enable controlled assembly of macromolecular structures. The Wilson group has focused on utilising hydrogen bonded arrays in the development of orthogonal recognition pathways and in the controlled assembly of supramolecular polymers. The work presented in this thesis therefore combines these research areas and describes the efforts made to develop self-sorting supramolecular materials using hydrogen bonded arrays.

Chapter 1 introduces the area of hydrogen bonding motifs and the factors that control their interactions with each other through literature examples. Additionally, literature examples of the use of hydrogen bonding motifs in self-sorting supramolecular systems and supramolecular polymeric materials is explored. Chapter 2 outlines the examination of the hydrogen bonding interactions between six linear hydrogen bonding motifs, experimentally and computationally, leading to the development of a sequential self-sorting pathways and ultimately a self-sorting network. Chapter 3 focuses on the design of a responsive hydrogen bonding motif to allow reversible switching of self-sorted states in a network. Chapter 4 describes the efforts to synthesise and characterise supramolecular polymer blends capable of self-sorting with the potential to create self-sorting supramolecular materials.

Table of Contents

Acknowledgements	iii
Abstract	iv
Table of Contents	v
List of Tables	viii
List of Figures	ix
List of Schemes	xvii
List of Abbreviations	xix
1. Introduction	- 1 -
1.1 Hydrogen Bonding Motifs.....	- 1 -
1.1.1 Factors Influencing the Strength of Hydrogen Bonding.....	- 3 -
1.1.2 Number of Hydrogen Bonds.....	- 4 -
1.1.3 Secondary Electrostatic Effects.....	- 7 -
1.1.4 Pre-organisation.....	- 10 -
1.1.5 Intramolecular Hydrogen Bonding.....	- 12 -
1.1.6 Tautomerisation.....	- 15 -
1.2 Self-sorting Supramolecular Systems.....	- 17 -
1.3 Supramolecular Polymers.....	- 25 -
1.3.1 Linear Supramolecular Polymers.....	- 26 -
1.3.2 Cross-linked Supramolecular Polymers.....	- 37 -
1.4 Conclusion and project aims.....	- 45 -
2. Sequential self-sorting of hydrogen bonding motifs	- 47 -
2.1 Synthesis of Hydrogen Bonding Motifs.....	- 52 -
2.2 Analysing Pairwise Interactions.....	- 56 -
2.3 Self-sorting pathways.....	- 77 -
2.4 Self-sorting network.....	- 85 -
2.5 Conclusions.....	- 88 -
3. Responsive self-sorting of hydrogen bonding motifs	- 89 -
3.1 Analysis of a proton responsive hydrogen bonding motif.....	- 95 -
3.2 Switching the hydrogen bonding interactions of responsive hydrogen bonding motif with complementary motifs.....	- 100 -
3.3 Analysis of a non-coordinating responsive hydrogen bonding motif.....	- 106 -
3.4 Conclusions.....	- 110 -

4. Developing self-sorting supramolecular polymer blends.....	111
4.1 Monomer design and synthesis.....	121
4.1.1 DDA functionalised methacrylate monomers.....	121
4.1.2 AAD functionalised styrene monomers	129
4.1.3 ¹ H NMR Studies of Heterocomplementary Monomer Components.....	133
4.2 First generation co-polymerisation	137
4.2.1 RAFT co-polymerisation and characterisation.....	137
4.2.2 Blends formation	142
4.2.3 Differential scanning calorimetry analysis	145
4.2.4 Dynamic light scattering analysis	153
4.3 Second generation co-polymerisation	155
4.3.1 RAFT co-polymerisation second generation.....	157
4.3.2 Blend formation and characterisation	162
4.4 Conclusions.....	165
5. Summary and Future work	168
5.1 Thesis Summary	168
5.2 Future Directions	170
6. Experimental.....	172
6.1 General materials and methods for synthesis	172
6.2 Experimental Chapter 2.....	174
6.3 Experimental Chapter 3.....	182
6.4 Experimental Chapter 4.....	183
6.5 Crystal Structures.....	206
6.6 General procedures for ¹ H NMR Experiments.....	209
6.6.1 Pairwise analysis (chapter 2).....	209
6.6.2 Self-sorting pathways sequential addition (chapter 2)	209
6.6.3 Self-sorting pathways non-sequential addition (chapter 2).....	209
6.6.4 Switching interactions using system A (chapter 3)	210
6.6.5 Switching interactions using system B (chapter 3)	210
6.7 NOESY NMR experiments	211
6.8 Isothermal titration calorimetry (ITC)	211
6.9 Molecular structure calculations (Chapter 2):	211
6.10 Molecular modelling (Chapter 4):	212
6.11 Differential scanning calorimetry (DSC)	212

6.12 Optical microscopy	212
List of References	214
Appendix A	222
Appendix B	227
Appendix C	231
Appendix D	234
Appendix E	237
Appendix F.....	241
Appendix G	243

List of Tables

Table 1. Examples of interactions and their associated typical energies.	- 1 -
Table 2. The Gibbs free energies computed for all dimerisation interactions with implicit chloroform solvation at the BLYP-D3(BJ)/TZ2P level of theory (* denotes the interacting array of dimers seen experimentally).	- 60 -
Table 3. APC data for first generation test polymerisations created by solvent free polymerisation.....	139
Table 4. APC data for first generation co-polymers created by solvent free polymerisation.....	142
Table 5. Glass transition temperatures of polymers calculated from DSC experiments on polymer films.....	150
Table 6. APC and GPC data for first generation co-polymers created by solvent free polymerisation.....	155
Table 7. GPC data for the second generation polymer standards created by solvent free polymerisation.....	157
Table 8. GPC data for second generation co-polymers (*samples elute with solvent).	160

List of Figures

- Figure 1.** Schematic showing hydrogen bonding between (a) water molecules (oxygen in red, hydrogen in white and hydrogen bonds as red dashed lines) and (b) β sheets of peptides that can promote protein folding (hydrogen bonds as red dashed lines)..... - 2 -
- Figure 2.** Hydrogen bonding interaction between compounds 1.2 and 1.3 (hydrogen bonds shown as red dashed lines)..... - 3 -
- Figure 3.** Examples of hydrogen bonding motifs with (a) double, (b) triple, (c) quadruple and (d) sextuple hydrogen bonds (hydrogen bonds shown as red dashed lines)..... - 5 -
- Figure 4.** Hydrogen bonding interaction between compounds 11.12 (G-C), 13.14 (A-T), 15.16 and 15.17 (hydrogen bonds shown as red dashed lines)..... - 6 -
- Figure 5.** (a) Representation of the Jorgenson secondary electrostatic interaction model in triply hydrogen bonded motifs. *D* represents hydrogen donor groups and *A* represents hydrogen bond acceptors. Solid lines represent attractive interactions and dashed lines represent repulsive interactions. (b) Specific examples illustrating the change in binding constants, red atoms represent hydrogen bond donor groups and blue atoms represent hydrogen bond acceptors (hydrogen bonds shown as black dashed lines). - 8 -
- Figure 6.** Dimerisation interaction for compounds 18, 19 and 20 with hydrogen bonds shown as red dashed lines. - 9 -
- Figure 7.** Hydrogen bonding interaction of compound 21 (green) with freely rotating molecule 22 and macrocyclic ring 23 (hydrogen bonds shown as red dashed lines)..... - 10 -
- Figure 8.** (a) Hydrogen bonding interaction between compounds 24.25 with 2-alkoxyl group both *trans* and *cis* to *N* in compound 24 (green curves show steric repulsion interaction), (b) Hydrogen bonding interaction between compounds 26.25 (hydrogen bonds shown as red dashed lines)..... - 11 -
- Figure 9.** Dimerisation interaction for compounds 27 and 28 (hydrogen bonds shown as red dashed lines)..... - 12 -
- Figure 10.** (a) Conformational equilibria of compound 29 (*DDA* to *AD*), (b) conformational equilibria of compound 30 (*ADA* array) and (c) conformational equilibria of compound 31 (*DDA* array) (hydrogen bonds shown as red dashed lines)..... - 14 -
- Figure 11.** (a) Schematic showing possible tautomers and conformers of compound 32 and (b) Schematic showing possible tautomers and conformers of compound 33 (hydrogen bonds shown as red dashed lines)..... - 16 -
- Figure 12.** Schematic of self-sorting classifications (a) narcissistic nonintegrative, (b) social nonintegrative and (c) social integrative.. - 18 -

- Figure 13.** Hydrogen bonding aggregates shown to thermodynamically self-sort by Wu and Isaacs. - 20 -
- Figure 14.** Hexameric cyclic hydrogen bonding assembly of compound 42 through complementary *DDA·AAD* interactions. Hydrogen bonds represented at dashed lines. - 21 -
- Figure 15.** Hydrogen bonding interaction between compounds (a) 43·44 (*UG·DAN*) heterodimer, (b) 45-*I*·45-*I* (*UPy·UPy*) homodimer, (c) 45-*II*·44 (*UPy·DAN*) heterodimer and (d) 31·46 (*UIM·AIC*) heterodimer (hydrogen bonds shown as red dashed lines). - 23 -
- Figure 16.** (a) Schematic and chemical structure of the spontaneous self-sorting of DAN, UPy, UIM and AIC (hydrogen bonds shown as black dashed lines), (b) Schematic of the sequential self-sorting cascade for DAN, UPy, UIM and AIC and (c) Schematic of the photo activated sequential self-sorting cascade of DAN, UPy, UIM and masked AIC* and the chemical structure of the photo-cleavage reaction of masked AIC* 47 to AIC 46. - 24 -
- Figure 17.** Schematic showing (a) linear supramolecular polymers with end chain functionalisation and (b) cross-linked supramolecular polymers with side chain functionalisation. - 25 -
- Figure 18.** Supramolecular polymeric assembly of ditopic compounds 48 and 49 through linear hydrogen bonding (hydrogen bonds shown as red dashes lines). - 26 -
- Figure 19.** (a) Dimerisation interaction for compound 50, (b) Ditopic supramolecular monomer 51 with UPy end groups, (c) Supramolecular polymer of ditopic compounds 51 through linear hydrogen bonding and (d) Supramolecular polymer of ditopic compounds 51 with competition from UPy motif 50 (hydrogen bonds shown as red dashed lines). - 28 -
- Figure 20.** (a) Conformational equilibria of compound 52 and (b) Hydrogen bonding dimerisation interaction of compound 52-*I* (hydrogen bonds shown as red dashed lines). - 29 -
- Figure 21.** Supramolecular polymeric assembly of UCyt bis-functionalised polymers through linear hydrogen bonding. (a) Head-Head assembly and (b) tail-tail assembly. Hydrogen bonds shown as red dashed lines. - 30 -
- Figure 22.** AB diblock co-polymer through the dimerisation of duplexes 53 and 54 (hydrogen bonds shown as red dashed lines). - 31 -
- Figure 23.** (a) Chemical structure and schematic of ditopic supramolecular monomers 55 and 56 with UPy and DAN hydrogen bonding motifs respectively, (b) chemical structure and schematic of homopolymer of 55, (c) chemical structure and schematic of alternating block co-polymer of 55·56 and (d) schematic showing the change in polymer composition on addition of ditopic monomer 56 (hydrogen bonds shown as red dashed lines). - 33 -

- Figure 24.** Chemical structure and schematic of ditopic supramolecular monomer functionalised with (a) UG 57, (b) DAN 58 hydrogen bonding motifs and (c) schematic showing interaction of monomers 57 and 58 forming an alternating block polymer. - 34 -
- Figure 25.** (a) UIM functionalised polymeric chain extended monomer 59a, (b) Diamidoisocytosine (DAC) 60 and (c) supramolecular linear polymer created from 59a and 60 with soft and hard domains. - 36 -
- Figure 26.** General approach for synthesis of styrene based side chain functionalised co-polymers by (a) post polymerisation modification and (b) direct co-polymerisation. - 38 -
- Figure 27.** RAFT polymerisation mechanism. - 40 -
- Figure 28.** (a) UG functionalised PBMA co-polymer 61, (b) DAN functionalised PS co-polymer 62, (c) UPy functionalised PBMA co-polymer 63, (d) cross-linked polymer blend 61·62 with heterocomplementary interactions between UG·DAN and (e) mixture of cross-linked polymer blends 62·63 and 63·63 with heterocomplementary interactions between UPy·DAN and homocomplementary interactions between UPy·UPy. - 42 -
- Figure 29.** (a) ureidopyrimidine functionalised PMMA co-polymer 64, (b) diamidopyridine functionalised PS co-polymer 65, (c) triple hydrogen bonding interaction between ureidopyrimidine and diamidopyridine moieties of 64 and 65 co-polymers and (d) cross-linked polymer blend 64·65 with heterocomplementary interactions. - 44 -
- Figure 30.** (a) Heterodimers formed in an equimolar mixture of UIM, AIC, DAN and UPy hydrogen bonding motifs and (b) phototriggered reaction used to unmask AIC. - 48 -
- Figure 31.** The lowest energy dimerisation interactions between the six linear hydrogen bonding motifs with dashed lines showing intermolecular hydrogen bonds. - 51 -
- Figure 32.** (a-e) Different tautomeric configurations and conformations accessible by linear hydrogen-bonding array AUPy 66 and (f) X-ray crystal structure of AUPy 66 homodimer (carbon is shown in grey, nitrogen in blue, oxygen in red, hydrogens in white and hydrogen bonds as dashed lines, with D...A distances shown in Å). - 53 -
- Figure 33.** (a-c) Different tautomeric configurations and conformations accessible by linear hydrogen-bonding array NAPyO 67 and 72 and (d) X-ray crystal structure NAPyO 72 homodimer (carbon is shown in grey, nitrogen in blue, oxygen in red, hydrogens in white and hydrogen bonds as dashed lines, with D...A distances shown in Å). - 54 -
- Figure 34.** ¹H NMR (500 MHz, 10 mM, CDCl₃) for (a) AUPy 66·66, (b) 1:1 NAPyO·AUPy 66·67 and (c) NAPyO 67·67. - 57 -

- Figure 35.** Variable temperature ^1H NMR (500 MHz, 10 mM, CDCl_3) of 1:1 AUPy 66 and NAPyO 67 at (a) 244 K (b) 254 K (c) 264 K (d) 277 K. Resonances colour code; green = mixture of complexes, purple = AUPy homodimer 66-66, grey = NAPyO homodimer 67-67, pink = AUPy-NAPyO 66-67 heterodimer. - 58 -
- Figure 36.** Optimised dimer interactions and their Gibbs free energies between brackets [in kcal mol^{-1}] of (a) AUPy-NAPyO 66-67 heterodimer (*DADA*·*ADAD*) and (b) AUPy 66-66 homodimer (*DADA*·*ADAD*) with respect to their most stable tautomer *ADDA* (without alkyl chains). Computed at the BLYP-D3(BJ)/TZ2P level of theory (illustrations produced using CYLview)¹³¹. - 61 -
- Figure 37.** ^1H NMR (500 MHz, 10 mM, CDCl_3) for (a) AUPy 66-66, (b) 1:1 AUPy 66-66 and UPy 45-45 and (c) UPy 45-45. - 62 -
- Figure 38.** ^1H NMR (500 MHz, 10 mM, CDCl_3) for (a) NAPyO 67-67, (b) 1:1 NAPyO-UPy 67-45 and (c) UPy 45-45. - 63 -
- Figure 39.** Variable temperature ^1H NMR (500 MHz, 10 mM, CDCl_3) of 1:1 NAPyO 67 and UPy 45 at (a) 244 K (b) 254 K (c) 264 K (d) 277 K. - 64 -
- Figure 40.** UPy and AUPy tautomers and their Gibbs free energies between brackets [in kcal mol^{-1}] with respect to their most stable tautomer *ADDA* and the relevant Voronoi deformation density (VDD) charges [in me^-], computed at the BLYP-D3(BJ)/TZ2P level of theory (illustrations produced using CYLview)¹³¹. - 66 -
- Figure 41.** Optimised dimer interactions of AUPy, UPy and NAPyO, their Gibbs free energies between brackets [in kcal mol^{-1}] with respect to their most stable tautomer *ADDA*. Computed at the BLYP-D3(BJ)/TZ2P level of theory (illustrations produced using CYLview)¹³¹. - 67 -
- Figure 42.** ^1H NMR (500 MHz, 10 mM, CDCl_3) for (a) AUPy 66-66, (b) 1:1 AUPy-DAN 66-44 and (c) DAN 44. - 68 -
- Figure 43.** ^1H NMR (500 MHz, 10 mM, CDCl_3) for (a) DAN 44, (b) 1:1 DAN-UPy 44-45 and (c) UPy 45-45. - 69 -
- Figure 44.** 2D ^1H - ^1H NOESY NMR (600 MHz, 50 mM, CDCl_3 , 278 K) for 1:1 AUPy-DAN 66-44. Green cross-peaks show NOE interactions and red cross-peaks show EXSY interactions. Grey circles highlight the NOE cross peaks between NH resonances of AUPy and DAN (H^3 - H^{11} and H^2 - H^{11}). - 70 -
- Figure 45.** (a) ITC thermograms and (b) binding isotherm for the addition of a solution of DAN 44 (1 mM) into AUPy 66 (0.1 mM) in CHCl_3 . .. - 71 -
- Figure 46.** Single crystal structure of AUPy-DAN 66-81 heterodimer (carbon is shown in grey, nitrogen in blue, oxygen in red, hydrogens in white and hydrogen bonds as dashed lines, with D...A distances shown in Å). - 72 -
- Figure 47.** ^1H NMR (500 MHz, 10 mM, CDCl_3) for (a) AUPy 66-66, (b) 1:1 AUPy-UIM 66-31 and (c) UIM 31. - 73 -

- Figure 48.** ^1H NMR (500 MHz, 10 mM, CDCl_3) for (a) UIM 31, (b) 1:1 UPy-UIM 45-31 and (c) UPy 45-45. - 74 -
- Figure 49.** Analysis of pairwise interactions and preferences for AUPy 66, DAN 44 and UPy 45 by ^1H NMR (10 mM, CDCl_3) (a) 1:1 AUPy 66: DAN 44, (b) 2:1:1 DAN 44: AUPy 66: UPy 45, (c) 1:1:1 DAN 44: AUPy 66: UPy 45, (d) 1:1 DAN 44: AUPy 66 (e) UPy 45. - 76 -
- Figure 50.** ^1H NMR (500 MHz, 10 mM, CDCl_3) for (a) NAPyO 67-67, (b)1:1 AUPy-DAN 66-44, (c)1:1:1 AUPy 66, NAPyO 67 and DAN 44, (d) 1:1 AUPy-NAPyO 66-67 and (e) AUPy 66-66..... - 78 -
- Figure 51.** Five component signalling pathway studied by ^1H NMR (10 mM, CDCl_3) (a) AUPy 66, NAPyO 67, DAN 44, UIM 31 and AIC 46, (b) AUPy 66, NAPyO 67, UIM 31 and AIC 46, (c) AUPy 66, UIM 31 and AIC 46, (d) AUPy 66, UIM 31 and (e) AUPy 66..... - 80 -
- Figure 52.** Pathway E ^1H NMR (500 MHz, 10 mM, CDCl_3) (a) AUPy 66, NAPyO 67, DAN 44, UPy 45, UIM 31, and AIC 46, (b) AUPy 66, NAPyO 67, UPy 45, UIM 31, and AIC 46, (c) AUPy 66, UPY 45, UIM 31, and AIC 46, (d) AUPy 66, UPy 45, and UIM 31, (e) AUPy 66 and UPy 45 and (f) UPy 45. - 82 -
- Figure 53.** Pathway G ^1H NMR (500 MHz, 10 mM, CDCl_3) (a) AUPy 66, NAPyO 67, DAN 44, UPy 45, UIM 31, and AIC 46, (b) AUPy 66, NAPyO 67, UPy 45, UIM 31, and AIC 46, (c) AUPy 66, NAPyO 67, UPy 45 and UIM 31, (d) AUPy 66, NAPyO 67 and UPy 45 and (e) AUPy 66 and UPy 45. - 84 -
- Figure 54.** Schematic showing the self-sorting behaviour of pathways A to G in forming hydrogen bonding dimers. - 87 -
- Figure 55.** X-ray crystal structures of 2-amino *tert*butyl imidazole hydrochloride salt (intermediate 78) (a) showing chloride bridge hydrogen bonding interaction $\text{NH}\dots\text{Cl}\dots\text{HN}$ between two molecules, (b) side view showing the chain like packing structure with molecules liked up antiparallel and (c) top view showing extended crystal packing (carbon is shown in grey, nitrogen in blue, oxygen in red, hydrogens in white, chloride in yellow and hydrogen bonds as red dashed lines, $\text{D}\dots\text{A}$ bond distances given in Å). - 91 -
- Figure 56.** Structure highlighting the interacting hydrogen bonding array of (a) hydrochloride salt of intermediate 78 (*DD*) and (b) protonated UIM 31* (*DDD*). - 92 -
- Figure 57.** Examples of cationic hydrogen bonding pairs reported in the literature (hydrogen bonds shown as red dashed lines). - 93 -
- Figure 58.** System A proton switch studied by ^1H NMR (500 MHz, 10 mM, CDCl_3) (a) UIM-HCl 31* (protonated with 4M HCl in 1,4-dioxane cycle 2), (b) UIM 31 (deprotonated with NaHCO_3 cycle 1), (c) UIM-HCl 31* (protonated with 4M HCl in 1,4-dioxane cycle 1) and (d) UIM 31. - 96 -

- Figure 59.** Titration of HCl into UIM studied by ^1H NMR (500 MHz, 5 mM, CDCl_3) (a) UIM 31 with 3 eq. HCl, (b) UIM 31 with 1 eq. HCl, (c) UIM 31 with 0.75 eq. HCl, (d) UIM 31 with 0.5 eq. HCl, (e) UIM 31 with 0.25 eq. HCl and (f) UIM 31. - 97 -
- Figure 60.** System B proton switch studied by ^1H NMR (500 MHz, 5 mM, CDCl_3) (a) UIM 31 (deprotonated with 3 eq DABCO), (b) UIM 31 (deprotonated with 1 eq DABCO), (c) UIM-TFA 31* (protonated with TFA), (d) UIM 31. - 99 -
- Figure 61.** Self-sorting behaviour of proton responsive UIM 31 (system A) with AIC 46 studied by ^1H NMR (500 MHz, 5 mM, CDCl_3) (a) UIM.AIC 31.46 dimer formed after washing UIM-HCl 31* and AIC 46 mixture with NaHCO_3 , (b) UIM-HCl 31* (protonated with 4M HCl in 1,4-dioxane) and AIC 46, (c) UIM-HCl 31* (protonated with 4M HCl in 1,4-dioxane), (protonated with 4M HCl in 1,4-dioxane), (d) UIM 31 and (e) UIM.AIC 31.46 dimer. - 101 -
- Figure 62.** Self-sorting behaviour of proton responsive UIM 31 (system B) with AIC 46 studied by ^1H NMR (500 MHz, 5 mM, CDCl_3) (a) UIM.AIC 31.46 (dimer formed after washing UIM-TFA 31* and AIC 46 mixture with 3 eq. DABCO), (b) mixture of UIM-TFA 31* and AIC 46 (formed after protonated with TFA) and (c) UIM.AIC 31.46 dimer. - 102 -
- Figure 63.** Self-sorting behaviour of proton responsive UIM 31 (system A) with AIC 46 and BB1 85 studied by ^1H NMR (500 MHz, 5 mM, CDCl_3) (a) UIM.AIC 31.46 dimer and BB1 85 formed after washing UIM-HCl.BB1 31*.85 dimer and AIC 46 mixture with NaHCO_3 (b) UIM-HCl.BB1 31*.85 dimer (protonated with 4M HCl in 1,4-dioxane) and AIC 46, (c) UIM-HCl 31* (protonated with 4M HCl in 1,4-dioxane) and AIC 46, (d) UIM.AIC 31.46 dimer, (e) UIM.AIC 31.46 dimer and BB1 85 and (f) BB1 85. - 104 -
- Figure 64.** Self-sorting behaviour of proton responsive UIM 31 (system B) with AIC 46 and BB1 85 studied by ^1H NMR (500 MHz, 5 mM, CDCl_3) (a) UIM.AIC 31.46 dimer and BB1 85 formed after washing UIM-HCl.BB1 31*.85 dimer and AIC 46 mixture with 3 eq. DABCO, (b) UIM-TFA.BB1 31*.85 dimer (protonated with TFA) and AIC 46 and (c) UIM.AIC 31.46 dimer and BB1 85. - 105 -
- Figure 65.** Showing potential chloride coordination in UIM-HCl and dimerisation. - 106 -
- Figure 66.** Formation of non-interacting motif UIM-HPF₆ and subsequent deprotonation to form UIM 31 studied by ^1H NMR (500 MHz, 5 mM, CDCl_3) (a) UIM 31 (deprotonated UIM-HPF₆ with NaHCO_3), (b) UIM-HPF₆ (formed on the addition of AgPF_6 to UIM-HCl 31*), (c) UIM-HCl 31* (protonated with 4M HCl in 1,4-dioxane) and (d) UIM 31. - 107 -
- Figure 67** Self-sorting behaviour of proton responsive UIM-HPF₆ with AIC 46 and BB1 85 studied separately by ^1H NMR (500 MHz, 5 mM, CDCl_3) (a) AIC 46, (b) UIM-HPF₆ and AIC 46, (c) UIM-HPF₆, (d) UIM-HPF₆.BB1 dimer and (e) BB1 85. - 108 -

- Figure 68.** Self-sorting behaviour of proton responsive of UIM-HPF₆ with AIC 46 and BB1 85 combined studied by ¹H NMR (500 MHz, 5 mM, CDCl₃) (a) AIC 46 (b) UIM-HPF₆:BB1 dimer and AIC 46, (c) UIM-HPF₆ and (d) BB1 85. - **109** -
- Figure 69.** Schematic showing the use of sequential self-sorting of hydrogen bonding motifs to create self-sorting supramolecular polymers. **112**
- Figure 70.** The Flory-Huggins Lattice Model comparing the possible configurations of (a) monomers, (b) small polymers and (c) long polymers in a lattice. Circles represent monomers which make up polymer chains, blue and red show different types of monomers/polymers..... **114**
- Figure 71.** Phase diagram showing the single, metastable and two-phase regions possible for polymer-polymer system in terms of composition and temperature. LCST (black dot), binodal curve (blue), spinodal curve (red) and metastable phase (green)..... **115**
- Figure 72.** A schematic showing potential self-sorting in polymer blends due to side chain functionalisation with self-sorting hydrogen bonding motifs..... **117**
- Figure 73.** A schematic outlining the strategy for the formation of a supramolecular blend between UIM-PMMA and AIC-PS copolymers. **119**
- Figure 74.** The product from the reaction of tert-butyl imidazole amine 78 with isocyanate 89 (a) structure and (b) crystal structure..... **123**
- Figure 75.** ¹H NMR (400 MHz, DMSO, 5 mM) (a) MMA-UIM monomer 90, (b) MMA-UIM monomer 90 and AIC-Styrene co-monomer 117 and (c) AIC-Styrene monomer 117. **133**
- Figure 76.** ¹H NMR (400 MHz, CDCl₃, 5 mM) (a) UIM-butyl analogue 119, (b) 1:1 UIM-butyl analogue 119 and AIC-Styrene monomer 117 and (c) AIC- Styrene monomer 117. **135**
- Figure 77.** Molecular model diagram of the lowest energy conformation found when merge MMA-UIM monomer 90 and Styrene-AIC monomer 117 showing the desired intermolecular and intramolecular hydrogen bonding interaction. MMA-UIM monomer 90 in green, styrene-AIC monomer 117 in blue, hydrogen bonds in yellow. **136**
- Figure 78.** Films of (a) 122 (PS), (b) 126 (PMMA) and (c) 1:1 mixture of 122 and 126 (PS:PMMA). **143**
- Figure 79.** Films of 1:1 mixtures of co-polymers (a) 122 (PMMA) and 126 (PS), (b) 129 (3% UIM-PMMA) and 126 (PS), (c) 122 (PMMA) and 135 (3% AIC-PS), (d) 129 (3% UIM-PMMA) and 135 (3% AIC-PS), (e) 131 (3% UIM-PMMA) and 135 (3% AIC-PS) and (f) 132 (6% UIM-PMMA) and 136 (6% AIC-PS)..... **144**

- Figure 80.** Schematic of a DSC thermogram showing typical phase transitions; glass transition (T_g), crystallisation (T_c) and melting (T_m)..... **146**
- Figure 81.** DSC thermogram on heating of polymer 122 (PMMA) blue, polymer 126 (PS) red and 1:1 mixture of 122 and 126 (PMMA:PS) green (dashed line highlighting the calculated T_g)..... **148**
- Figure 82.** DSC thermogram on heating of co-polymer 129 (PMMA with 3% UIM co-monomer 90) blue, polymer 126 (PS) red and 1:1 mixture of 129 and 126 (3%UIM-PMMA:PS) green (dashed line highlighting the calculated T_g).. **149**
- Figure 83.** DSC thermogram on heating of co-polymer 129 (PMMA with 3% UIM hydrogen bonding motifs 90) blue, co-polymer 135 (PS with 3% AIC hydrogen bonding motifs 117) red and 1:1 mixture of 129 and 135 (3% UIM-PMMA:3% AIC-PS) green (dashed line highlighting the calculated T_g).. **152**
- Figure 84.** Films of 1:1 mixtures of co-polymers (a) 138 (PMMA) and 142 (PS), (b) 146 (2% UIM-PMMA) and 142 (PS), (c) 138 (PMMA) and 148 (2.5% AIC-PS), (d) 146 (2% UIM-PMMA) and 148 (2.5% AIC-PS), and (e) 146 (2% UIM-PMMA) and 149 (4.5% AIC-PS). **162**
- Figure 85.** DSC thermogram on heating of co-polymer 146 (2% UIM hydrogen bonding motifs) blue, co-polymer 149 (4.5% AIC hydrogen bonding motifs) red and 1:1 mixture of 146 and 149 (2% UIM-PMMA:4.5% AIC-PS) green (dashed line highlighting the calculated T_g).. **163**
- Figure 86.** DSC thermogram on heating of co-polymer 146 (2% UIM hydrogen bonding motifs) blue, co-polymer 148 (2.5% AIC hydrogen bonding motifs) red and 1:1 mixture of 146 and 148 (2% UIM-PMMA:2.5% AIC-PS) green (dashed line highlighting the calculated T_g).. **164**

List of Schemes

Scheme 1. Synthesis of UIM functionalised monomers 59a (chain extended) and 59b (chain capped).....	- 35 -
Scheme 2. The synthetic route for the preparation of AUPy 66.....	- 52 -
Scheme 3. The synthetic route for the preparation of NAPyO 67 and NAPyO 72.....	- 54 -
Scheme 4. The synthetic route for the preparation of AIC 46.....	- 55 -
Scheme 5. The synthetic route for the preparation of UIM 31.....	- 55 -
Scheme 6. The synthetic route for the preparation of DAN (isobutyryl analogue) 81.....	- 72 -
Scheme 7. Synthetic conditions for the isolation of tert-butyl imidazole amine hydrochloride salt 78.....	- 91 -
Scheme 8. Suggested switching of conformers of UIM when neutral 31 and protonated 31* together with suitably complementary hydrogen bonding motifs AIC 46 and BB1 85 respectively.....	- 94 -
Scheme 9. Systems tested for the protonation and deprotonation of UIM 31 (a) system A:HCl and NaHCO ₃ and (b) system B:TFA and DABCO.....	- 96 -
Scheme 10. Formation of non-interacting motif UIM-HPF ₆ from UIM-HCl and subsequent deprotonation to form UIM.....	- 107 -
Scheme 11. The synthetic route for preparation of methacrylate monomers (a) 90 and (b) 92 adapted from synthesis previously reported by the Wilson group. ¹⁰⁶	121
Scheme 12. The synthetic route for preparation of methacrylate monomer 93 adapted from the syntheses previously reported by the Wilson group. ^{40,106}	122
Scheme 13. Potential products of the reaction between tert-butyl imidazole amine 78 and isocyanate 89.....	123
Scheme 14. Potential rearrangement reaction for the formation of 95.....	123
Scheme 15. The synthetic route for the formation of 31, 97 and 95.....	125
Scheme 16. The proposed synthesis of methacrylate monomer 93 using Fmoc protection.....	126
Scheme 17. The proposed synthesis of methacrylate monomer 93 forming the urea prior to the tert-butyl imidazole.....	127
Scheme 18. Potential synthetic route for preparation of an aromatic containing methyl methacrylate monomer 106.....	128
Scheme 19. The synthetic route for preparation of styrene monomer 112 adapted from a synthesis previously reported by the Wilson group. ¹⁰⁶	130

Scheme 20. The synthetic route A for the preparation of styrene monomer 117.	131
Scheme 21. The alternative synthetic route B for the preparation of styrene monomer 117.	132
Scheme 22. Synthesis of n-butyl imidazole UIM analogue 119.	134
Scheme 23. First generation RAFT co-polymerisation of (a) MMA and MMA-UIM co-monomer (b) styrene and PS-AIC co-monomer.	140
Scheme 24. Second generation RAFT co-polymerisation of (a) MMA and MMA-UIM co-monomer (b) styrene and PS-AIC co-monomer. ...	158

List of Abbreviations

A	Hydrogen bonding acceptor site
Å	Angstrom
ADF	Amsterdam density functional
AFM	Atomic force microscopy
AIBN	Azobisisobutyronitrile
AIC	Amido <i>s</i> ocytosine
AIC*	Masked amido <i>s</i> ocytosine
APC	Advance polymer chromatography
aq.	Aqueous
Ar	Aryl
AUPy	Aminoureidopyrimidine
BB1	Benzo[f]isoquinolino[3,4-b][1,8]naphthyridine
Boc	Di- <i>tert</i> -butyl dicarbonate
br (NMR, IR)	Broad (NMR, IR)
Bu	Butyl
C	Cytosine
CDCl ₃	Deuterated chloroform
COSMO	Conductor-like screening model
COSY	¹ H- ¹ H correlation NMR spectroscopy
CTA	Chain transfer agent
<i>D</i>	Hydrogen bonding donor site
d (NMR)	Doublet (NMR)
DABCO	1,4-diazabicyclo[2.2.2]octane
DAC	Diamido <i>s</i> ocytosine
DAN	2,7-Diamido-1,8-naphthyridine
DBU	1,8-Diazabicyclo[5.4.0]undec-7-ene
DCM	Dichloromethane
DeAP	Deazapterin
DFT	Density functional theory
DLS	Dynamic light scattering
DMF	N,N-dimethylformamide
DMSO	Dimethylsulfoxide

DMSO- <i>d</i> ₆	Deuterated dimethylsulfoxide
DNA	Deoxyribonucleic acid
DP	Degree of polymerisation
DSC	Differential scanning calorimetry
eq.	Equivalent
ESI	Electrospray ionisation
EXSY	Exchange spectroscopy
Fmoc	Fluorenylmethyloxycarbonyl chloride
FTIR	Fourier transform infra-red spectroscopy
g	Gram(s)
G	Guanosine
GPC	Gel-permeation chromatography
HCl	Hydrogen Chloride
HI	Hydrogen Iodide
HBM	Hydrogen bonding motif
HPF ₆	Hexafluorophosphoric acid
HPLC	High performance liquid chromatography
hr	Hour(s)
HRMS	High resolution mass spectrometry
Hz	Hertz
I	Initiator
IR	Infra-red
ITC	Isothermal titration calorimetry
J	Coupling constant in Hz
<i>K</i> _a	Association constant
<i>K</i> _{dim}	Dimerisation constant
kJ	Kilojoule(s)
LC-MS	Liquid chromatography-mass spectrometry
M	Molar concentration/monomer
m (NMR)	Multiplet (NMR)
m/z	Mass-to-charge ratio
MCMM	Monte Carlo Molecular Mechanics
MDI	4,4'-methylenediphenyl diisocyanate
mg	Milligram(s)

min	Minute(s)
mL	Millilitre(s)
MMA	Methylmethacrylate
MMFF	Merck Molecular Force Field
mmol	Millimole(s)
M_n	Number average molar mass
Mol	Moles
MS	Mass spectrometry
M_w	Mass average molar mass
n	Reaction stoichiometry
NaHCO_3	Sodium hydrogen carbonate
NaOH	Sodium hydroxide
NAPyO	Naphthyridinone
nm	Nanometer(s)
NMR	Nuclear magnetic resonance
NOE	Nuclear Overhauser effect
NOESY	Nuclear Overhauser effect spectroscopy
PBMA	Poly(butyl methacrylate)
PDI	Polydispersity
PEG	Poly(ethylene glycol)
PF_6	Hexafluorophosphate
PMMA	Polymethylmethacrylate
PPG	Poly(propylene glycol)
ppm	Parts per million
PS	Polystyrene
PTM	Post-translational modification
PUPY	Phenylureidopyrimidine
Py	Pyridine
R	Alkyl group
RAFT	Reversible addition-fragmentation chain transfer
ROESY	Rotating-frame Overhauser Effect Spectroscopy
ROMP	Ring-opening metathesis polymerisation
RT	Room temperature
s	Singlet (NMR)

SMP	Supramolecular polymer
T	Thymine/Temperature
t	Time/ triplet (NMR)
<i>tert</i>	Tertiary
TFA	Trifluoroacetic acid
TFAB	Ortho-tatrefluorinated azobenzene
T _g	Glass transition temperature
THF	Tetrahydrofuran
TLC	Thin-layer chromatography
T _m	Melting temperature
TOF	Time of flight
UCyt	Ureidocytosine
UG	Ureidoguanosine
UIM	Ureidoimidazole
UPy	Ureidopyrimidine
UV	Ultraviolet
VDD	Voronoi deformation density
vis	Visible light
VT	Variable temperature
δ	Chemical shift
ΔG	Gibbs free energy
ΔH	Enthalpy
ΔS	Entropy

1. Introduction

1.1 Hydrogen Bonding Motifs

Hydrogen bonding is an important non-covalent interaction as it is highly directional, reversible and can also be selective.^{1,2} Hydrogen bonds are much weaker than covalent bonds, yet are considered to be strong when compared to other non-covalent interactions (Table 1). The strength of hydrogen bonds are found to be more profound when used multivalently.

<i>Non-covalent interaction</i>	<i>Typical Energy Range (kJ mol⁻¹)</i>
Ion-Ion	50-400
Ion-Dipole	50-200
Dipole-Dipole	4-40
Cation- π	5-80
π - π	4-20
Solvation	4-40
Hydrogen Bonding	4-120
Covalent Carbon-Carbon bond	300-600

Table 1. Examples of interactions and their associated typical energies.

Hydrogen bonding occurs between an acceptor atom, an electronegative heteroatom (e.g. O or N), and a donor atom, a hydrogen attached to an electronegative atom (e.g. OH or NH).³ The electronegative acceptor atom is attracted to the electropositive hydrogen atom. This specific acceptor-donor interaction results in selectivity and directionality as the electronegative atoms repel each other to position themselves as far apart as possible. Hydrogen bonding between oxygen and hydrogen atoms in water molecules is

considered a classic example (Figure 1 (a)). Hydrogen bonding is fundamental for biological assembly processes such as protein folding and DNA pairing. Figure 1(b) illustrates hydrogen bonding between β sheet peptides can stabilise the secondary structure of proteins.⁴

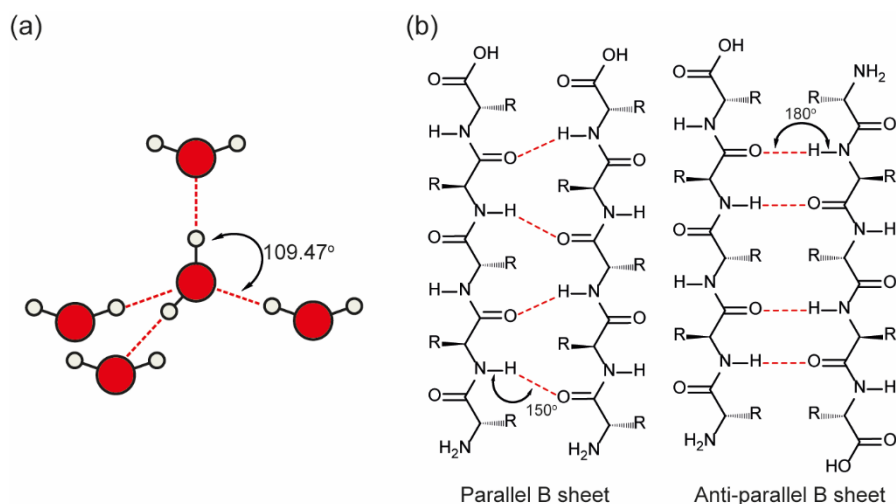


Figure 1. Schematic showing hydrogen bonding between (a) water molecules (oxygen in red, hydrogen in white and hydrogen bonds as red dashed lines) and (b) β sheets of peptides that can promote protein folding (hydrogen bonds as red dashed lines).

The attractive properties of hydrogen bonds have led to their exploitation in the construction of many synthetic self-assemblies.^{2,3} Etter confirmed hydrogen bonds as key in the design of solid state organic compounds.⁵ Work carried out by Wuest and co-workers revealed the use of hydrogen bonds in long range superstructures, such as organic diamondoid networks.^{6,7} Hamilton's research on molecular recognition relied on hydrogen bonding to develop artificial receptors capable of strong and selective binding.⁸⁻¹⁰ In addition, the Hamilton group revealed the use of hydrogen bonding to control the assembly of molecular sheets through complementarity of carboxylic acids with 2-aminopyridine derivatives resulting in formation of a rod-like structure.^{11,12}

1.1.1 Factors Influencing the Strength of Hydrogen Bonding

To fully utilise hydrogen bonding in molecular design/engineering, the factors governing association and the strength of interactions between molecules must be understood. The relative strength of individual hydrogen bonds can be understood in terms of the acidity of the donor (positive charge) and basicity of the acceptor (negative charge).¹³ Meijer and co-workers showed that binding affinity can increase by using more acidic donors and more basic acceptors.¹⁴ The group acetylated 2,6-diaminopyridine **2** to form 2,3-diacetamidopyridine **3** with more acidic amide protons and compared the binding association constants with compound **1**. The association constant increased significantly from $K_a = 84 \text{ M}^{-1}$ for complex **1·2** to $K_a = 920 \text{ M}^{-1}$ for complex **1·3** (Figure 2).¹⁴

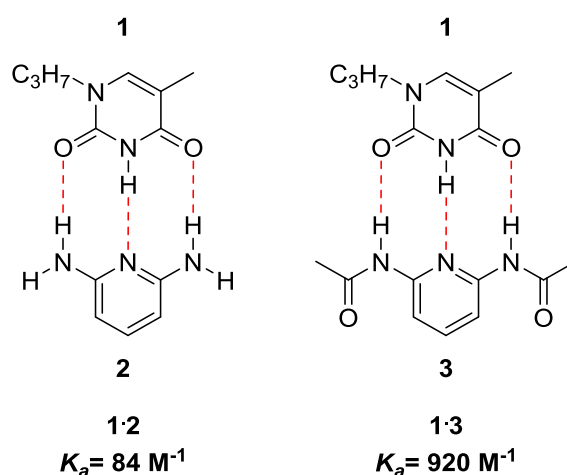


Figure 2. Hydrogen bonding interaction between compounds **1·2 and **1·3** (hydrogen bonds shown as red dashed lines).**

Hence, relative acidity and basicity of individual functional groups can be used to estimate stability of complexes.¹⁵ However, in hydrogen bond arrays, molecules in which hydrogen bond donor and acceptors are contiguous; the effects of specific hydrogen bonds cannot readily be distinguished. Often, the

hydrogen bond donors and acceptors in the array are connected to each other through conjugation and intramolecular interactions, and so there are many influences on the strength of hydrogen bonding.¹ Important principles to consider include: number of intermolecular hydrogen bonds; pre-organisation; intramolecular hydrogen bonding; secondary interactions; tautomerisation and electronic substituent effects.¹

1.1.2 Number of Hydrogen Bonds

As previously discussed, a single hydrogen bond is relatively weak, so multiple hydrogen bonds are often used collectively when creating hydrogen-bonding arrays. Arrays consisting of two, three, four and six hydrogen bonds have been reported with a range of binding affinities (Figure 3).¹⁶⁻²²

Several studies have shown that the addition of an extra hydrogen bond can increase the binding association by two or three orders of magnitude. For example, the DNA base pair guanosine-cytosine (G-C **11·12**) containing three hydrogen bonds is more than two orders of magnitude more stable than the adenine-thymine (A-T **13·14**) pair containing two hydrogen bonds (Figure 4).²³ Alternatively, the association constant is three times larger for complex **15·16** than **15·17** with an increase of one hydrogen bond group (Figure 4).^{24,25} Hydrogen bond arrays containing three or four intermolecular bonds are the most useful in terms of reversible assembly properties. Fewer hydrogen bonds do not give strong enough interactions to yield stable assemblies, whereas the interaction between more than four hydrogen bonds are often too strong to easily reverse the dimerisation.

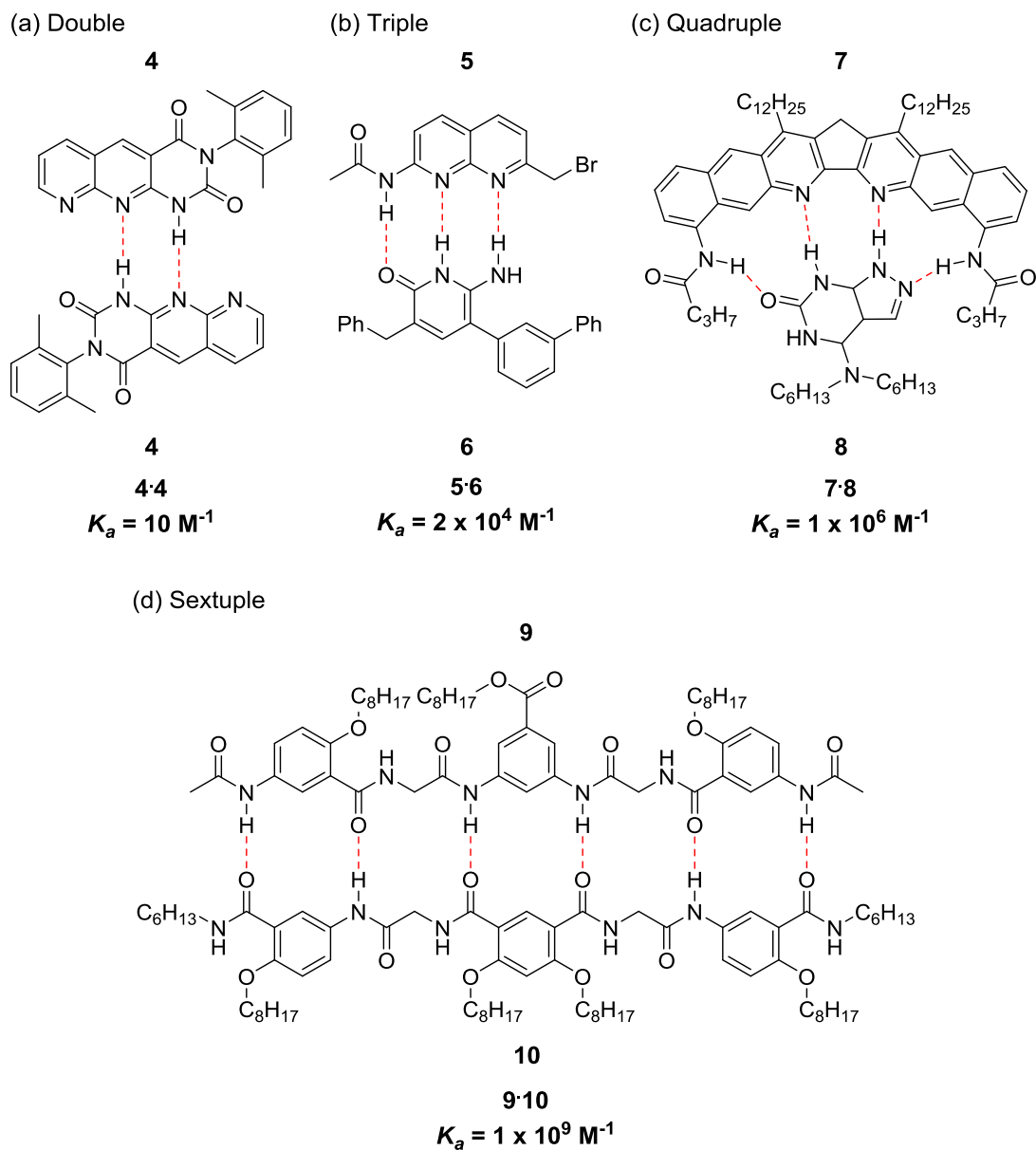


Figure 3. Examples of hydrogen bonding motifs with (a) double, (b) triple, (c) quadruple and (d) sextuple hydrogen bonds (hydrogen bonds shown as red dashed lines).

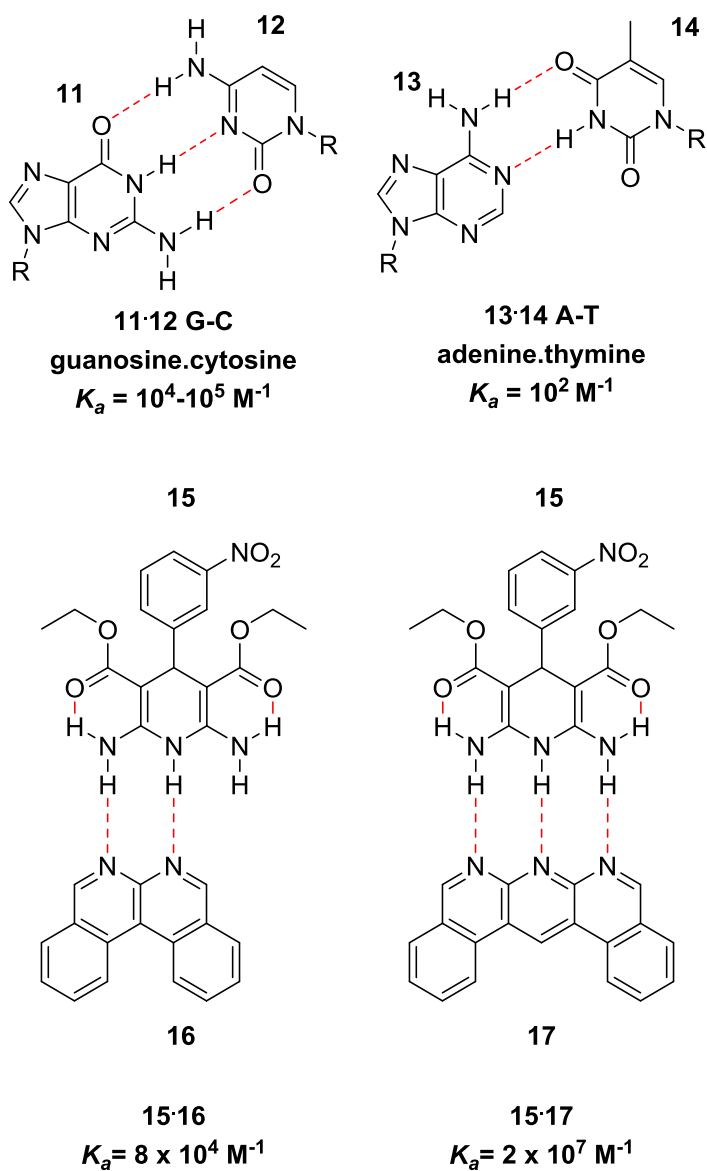


Figure 4. Hydrogen bonding interaction between compounds 11·12 (G-C), 13·14 (A-T), 15·16 and 15·17 (hydrogen bonds shown as red dashed lines).

1.1.3 Secondary Electrostatic Effects

As well as the number of donor and acceptor groups in an array, the order of adjacent interacting groups has a significant effect on the binding affinity of the complex. Secondary electrostatic interactions occur between adjacent hydrogen bond donors (*D*) and acceptors (*A*). The Jorgensen model illustrates the potential attractive and repulsive interactions present in triple hydrogen bond motifs (Figure 5 (a)).^{26,27} Unsurprisingly, *DDD-AAA* arrays (**15-17**) exhibit the strongest binding affinities ($K_a = 2 \times 10^7 \text{ M}^{-1}$) because they contain four attractive secondary electrostatic interactions. *DDA-AAD* arrays (**4-5**) contain two attractive and two repulsive secondary electrostatic interactions ($K_a = 10^4 \text{ M}^{-1}$)^{20,26,28,29} and *DAD-ADA* arrays (**1-3**) have the lowest binding affinity due to having four repulsive secondary electrostatic interactions ($K_a = 10^2 \text{ M}^{-1}$).^{15,29,30} Computational studies were able to predict the association constants of dimers without having to synthesise and test each molecule.³¹ It was calculated that primary hydrogen bonds increased the binding affinity by 7.9 kJ mol⁻¹ and secondary electrostatic interactions added ± 2.9 kJ mol⁻¹ depending on whether they were attractive or repulsive in nature.³² It is possible to remove these secondary interaction effects by separating the interacting groups in space.¹ Wuest and co-workers introduced an alkyne spacer between two lactam groups allowing dimerisation of a *ADAD* motif **18** with strong affinity ($K_{dim} = 6 \times 10^4 \text{ M}^{-1}$) (Figure 6).³³ Gong and co-workers were also able to eliminate these interactions in the formation of hydrogen bonded duplexes **19** (*DADA*) ($K_{dim} = 4.4 \times 10^4 \text{ M}^{-1}$) and **20** (*DDAA*) ($K_{dim} = 6.5 \times 10^4 \text{ M}^{-1}$) (Figure 6).³⁴ The binding associations of the arrays were of the same magnitude indicating that secondary electrostatic interactions had no influence.

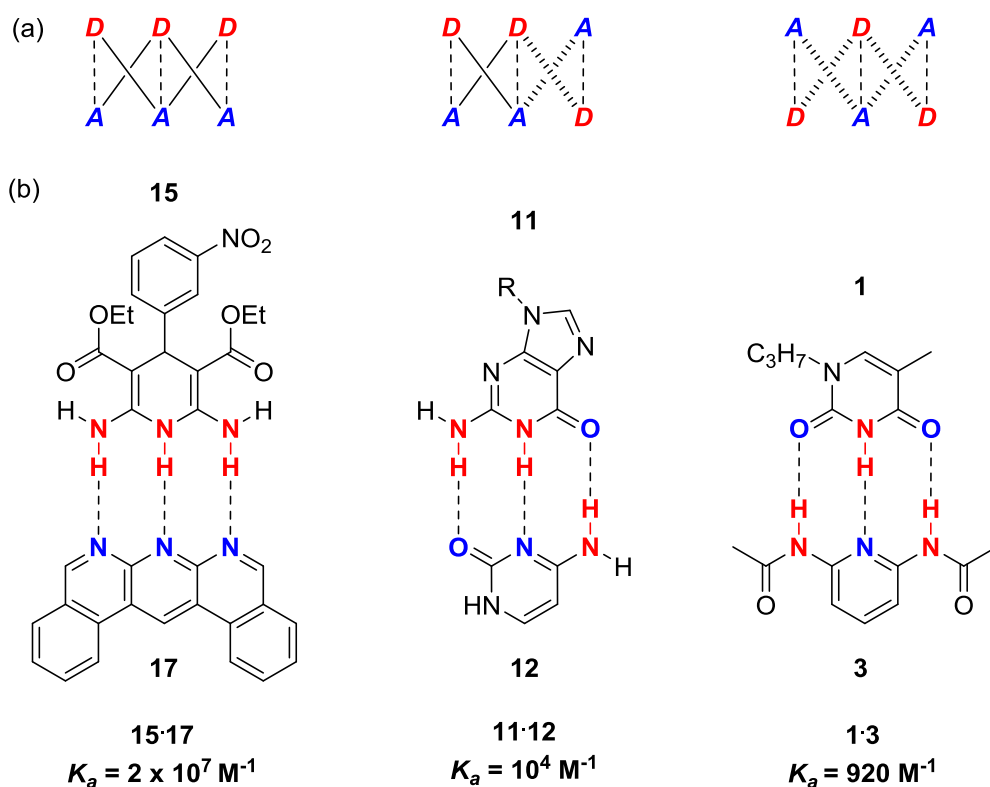
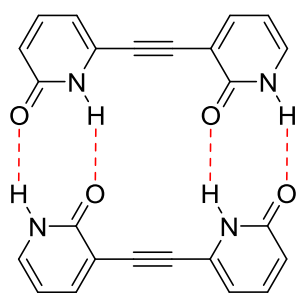
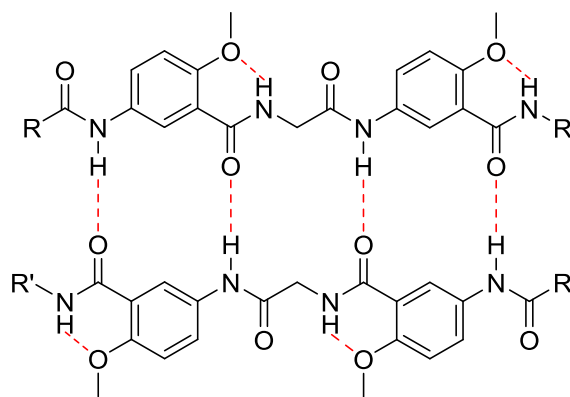


Figure 5. (a) Representation of the Jorgenson secondary electrostatic interaction model in triply hydrogen bonded motifs. *D* represents hydrogen donor groups and *A* represents hydrogen bond acceptors. Solid lines represent attractive interactions and dashed lines represent repulsive interactions. (b) Specific examples illustrating the change in binding constants, red atoms represent hydrogen bond donor groups and blue atoms represent hydrogen bond acceptors (hydrogen bonds shown as black dashed lines).

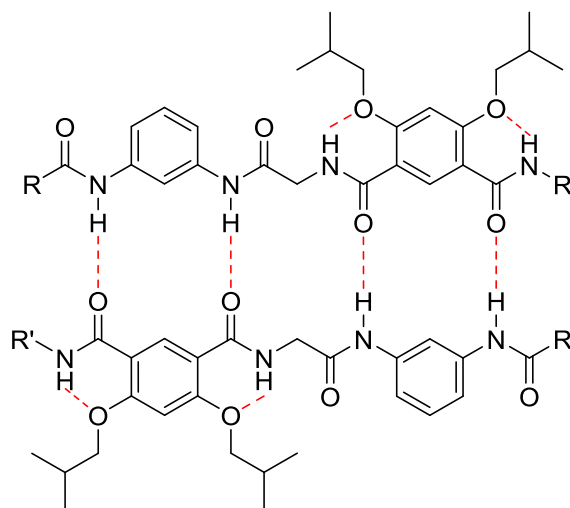


18·18
 $K_{dim} = 6 \times 10^4 \text{ M}^{-1}$



$R = (\text{CH}_2)_8\text{CH}_3$ $R' = \text{CH}_2\text{CH}(\text{CH}_3)_2$

19·19
 $K_{dim} = 4.4 \times 10^4 \text{ M}^{-1}$



$R = \text{C}_5\text{H}_{11}$ $R' = \text{C}_6\text{H}_{13}$

20·20
 $K_{dim} = 6.5 \times 10^4 \text{ M}^{-1}$

Figure 6. Dimerisation interaction for compounds 18, 19 and 20 with hydrogen bonds shown as red dashed lines.

1.1.4 Pre-organisation

Pre-organisation is a key tool in the design of hydrogen bonding motifs to maximise stability and binding affinity.³⁵ Often, pre-organisation involves the use of a rigid aromatic framework to position the atoms of interacting groups in a specific conformation to present all the interacting sites simultaneously. Consequently, there is a reduced entropic penalty to fix freely rotating bonds in position; so the entropic cost is limited as it is paid on binding of the first hydrogen bond.¹ The influence of pre-organisation on binding affinity was described by Chang and co-workers when comparing the binding association of compound **21** with an acyclic molecule **22** and a macrocyclic ring **23**. In the macrocyclic ring, all the hydrogen bonding groups were held in the desired position and K_a in chloroform was increased by 100-fold, from 10^4 M^{-1} (**21**·**22**) to 10^6 M^{-1} (**21**·**23**) (Figure 7).¹⁰

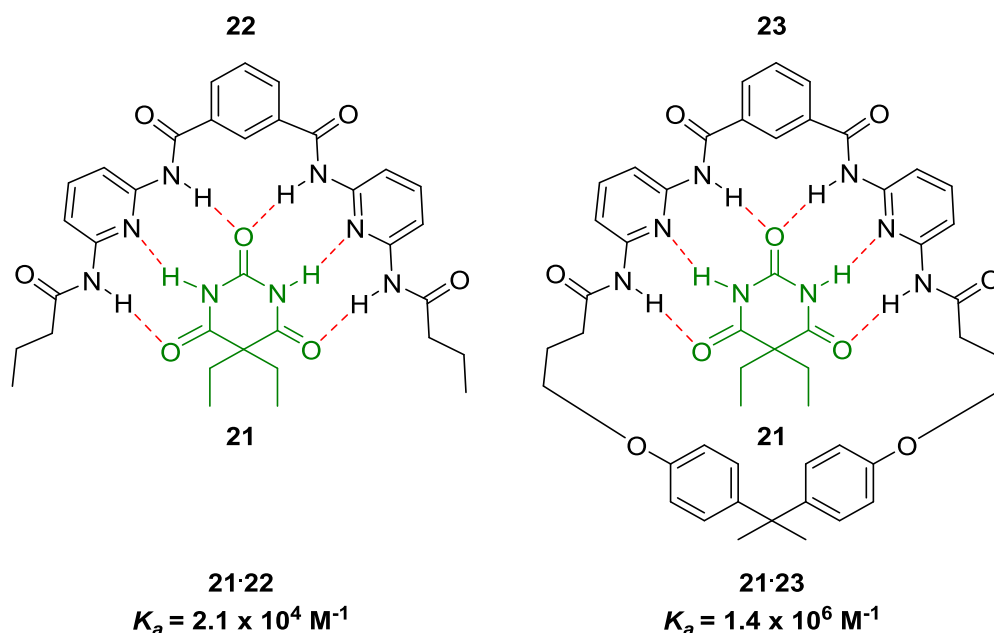


Figure 7. Hydrogen bonding interaction of compound **21** (green) with freely rotating molecule **22** and macrocyclic ring **23** (hydrogen bonds shown as red dashed lines).

In addition to fixing non-interacting functional groups, pre-organisation can eliminate steric repulsion between hydrogen bonding arrays. Murray implied that steric interactions can lead to a lower than expected association constant for example complex **24·25** ($K_a = 208 \text{ M}^{-1}$).³⁶ It was hypothesised that the 2-alkoxyl group in compound **24** can orientate to create steric repulsion with **25** (Figure 8 (a)). Whereas, for a fixed conformation analogue (**26**), the binding association of **26·25** was significantly increased ($K_a = 10^4 \text{ M}^{-1}$) (Figure 8 (b)).

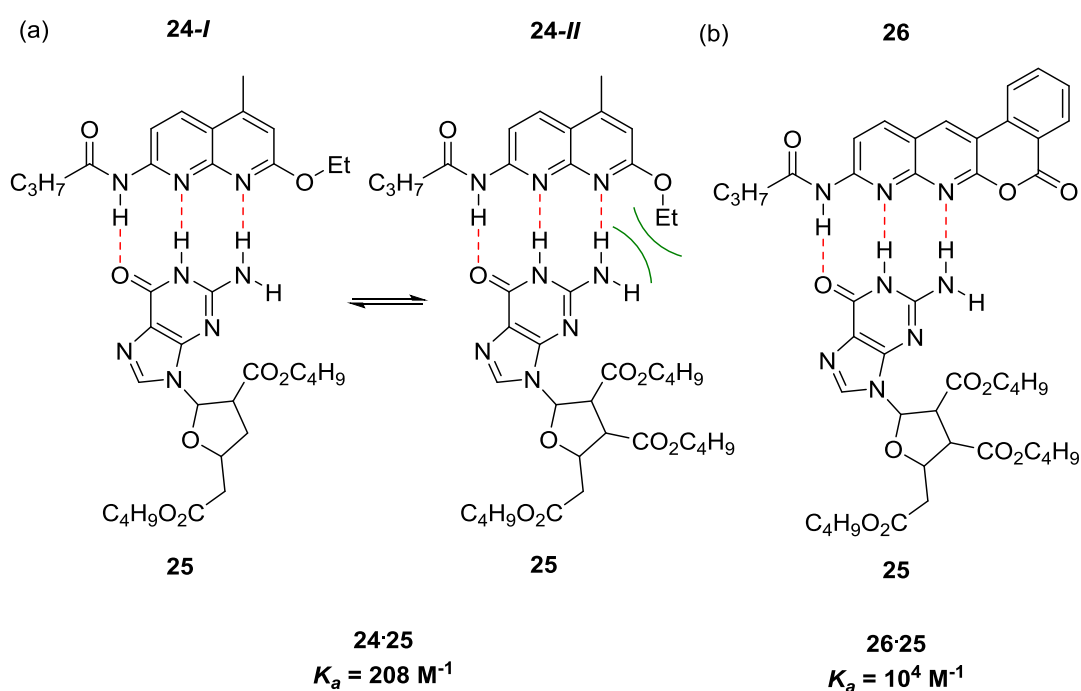


Figure 8. (a) Hydrogen bonding interaction between compounds **24·25 with 2-alkoxyl group both *trans* and *cis* to *N* in compound **24** (green curves show steric repulsion interaction), (b) Hydrogen bonding interaction between compounds **26·25** (hydrogen bonds shown as red dashed lines).**

hydrogen bond then must be broken for the desired triple hydrogen bonding interaction to take place.⁴⁰ Intramolecular interactions can be controlled somewhat through substituent effects; for example, the addition of electron withdrawing groups to the phenyl substituted 2-pyridyl urea increases the binding association with a cytosine derivative.⁴¹ By understanding intramolecular interaction preferences, hydrogen-bonding motifs have been designed which utilise intramolecular hydrogen bonds to favour a desired interacting conformer. The Wilson group have synthesised phenylureidopyrimidine (PUPY) **30** and phenylureidoimidazole (UIM) **31** with desired *ADA* and *DDA* arrays, respectively (Figure 10 (b) & (c)).^{40,42} The pyrimidine ring used in PUPY **30** contains two nitrogen atoms which are both able to form intramolecular hydrogen bonds to present the desired *ADA* array irrespective of the conformer **30-I** or **30-II** (Figure 10 (b)).⁴² An imidazole moiety was employed to give the conformer independent *DDA* array **31**. The NH group of the imidazole acts as donor to the carbonyl group of the urea (**31-I**); alternatively, the nitrogen in the imidazole ring can act as an acceptor to the NH of the urea (**31-II**) (Figure 10 (c)). The association constant of conformer independent **31** with a complementary *AAD* array is greatly increased ($K_a = 8400 \text{ M}^{-1}$) when compared to that of **29** ($K_a = 30 \text{ M}^{-1}$).^{39,40}

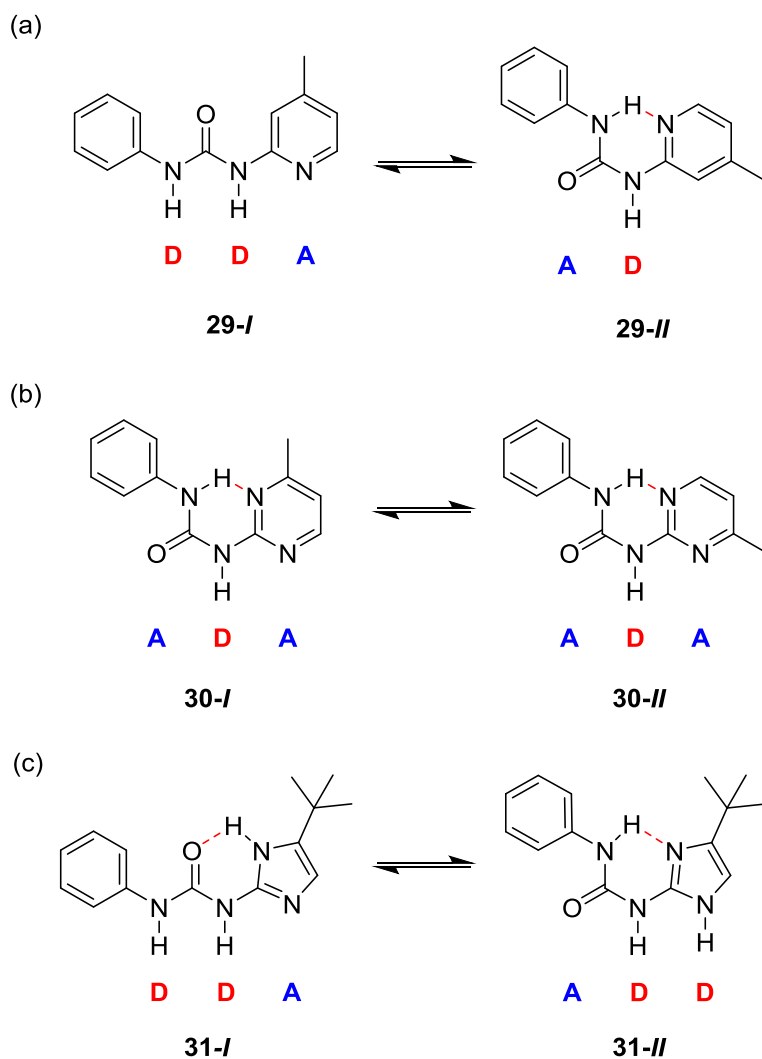


Figure 10. (a) Conformational equilibria of compound 29 (DDA to AD), (b) conformational equilibria of compound 30 (ADA array) and (c) conformational equilibria of compound 31 (DDA array) (hydrogen bonds shown as red dashed lines).

1.1.6 Tautomerisation

Tautomerisation can be problematic in the design of heteroaromatic hydrogen bonding arrays. Different tautomeric states can result in the presentation of non-complementary arrays and so prevent the desired intermolecular interaction. This was illustrated by Meijer in the design of ureidopyrimidine (UPy) **32**, an AADD array which was hypothesised to self-associate.⁴³ However, it was found to adopt three different tautomeric states (Figure 11 (a)). Generally, the AADD array was more dominant than the ADAD array as it contained less repulsive secondary electrostatic interactions as a hydrogen bonded homodimer. In addition, Meijer and co-workers were able to control the preferred array through changing the nature of the substituents by changing the electron density of the interacting atoms. Electron withdrawing substituents on the urea favour the AADD array, whereas electron donating substituents favour the ADAD array.⁴³ Zimmerman and co-workers tried to increase the strength of homodimerisation with the design of deazapterin (DeAP) **33** to ensure that all tautomers display an AADD array.^{44,45} DeAP had a slightly higher dimerisation constant than UPy, with the lower limit of **33** estimated as $K_{dim} > 5 \times 10^8 \text{ M}^{-1}$ by fluorescence spectroscopy; however, unwanted arrays (DAAD and AADA) were still presented (Figure 11 (b)). Generally, with triply hydrogen bonding motifs there are fewer potential tautomers and conformers.

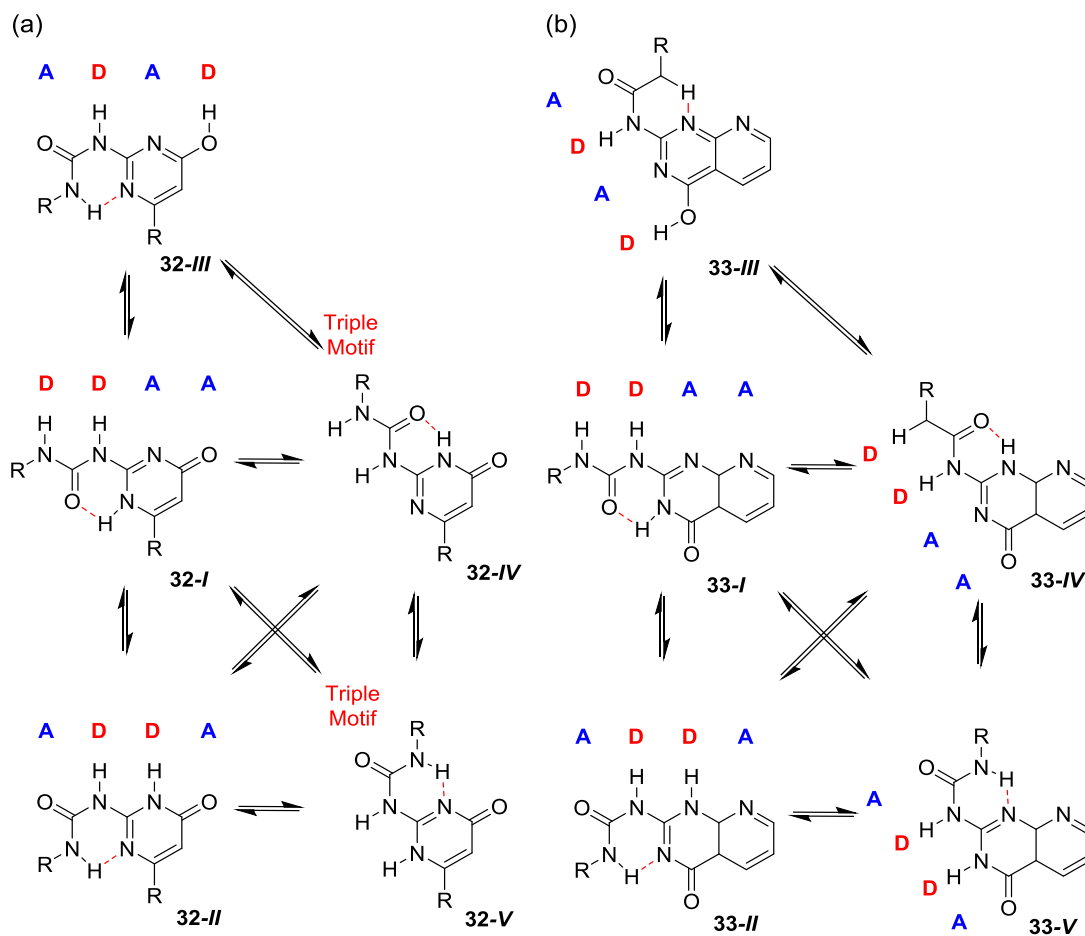


Figure 11. (a) Schematic showing possible tautomers and conformers of compound 32 and (b) Schematic showing possible tautomers and conformers of compound 33 (hydrogen bonds shown as red dashed lines).

1.2 Self-sorting Supramolecular Systems

Nature has the ability to assemble multiple functional assemblies simultaneously, in defined locations, and, with temporal precision.⁴⁶ For example, in a cell, multiple levels of compartmentalisation arising from the self-sorting of their molecular components allow the coexistence of different functional architectures acting independently. However, many of the artificial self-assemblies reported are only considered as isolated systems. Systems chemistry has begun to examine the interactions of different components in complex mixtures; which are not always possible in isolated systems.⁴⁷⁻⁴⁹ An objective of systems chemistry is to understand self-sorting behaviour in complex mixtures, i.e. how artificial molecules bind or ignore a specific partner in a complex multicomponent environment.⁵⁰ Self-sorting can be generally defined as high fidelity recognition between molecules and ions within complex mixtures.⁵¹ It can be categorised based on the affinity of the components, as social (self-loathing), narcissistic (self-loving)^{52,53} or, in terms of the final product, as integrative (one final complex), non-integrative (more than one complex) (Figure 12).^{54,55} Additionally, self-sorting systems can be considered as at thermodynamic equilibrium (majority of cases) or a trapped species under kinetic control.^{51,55,56}

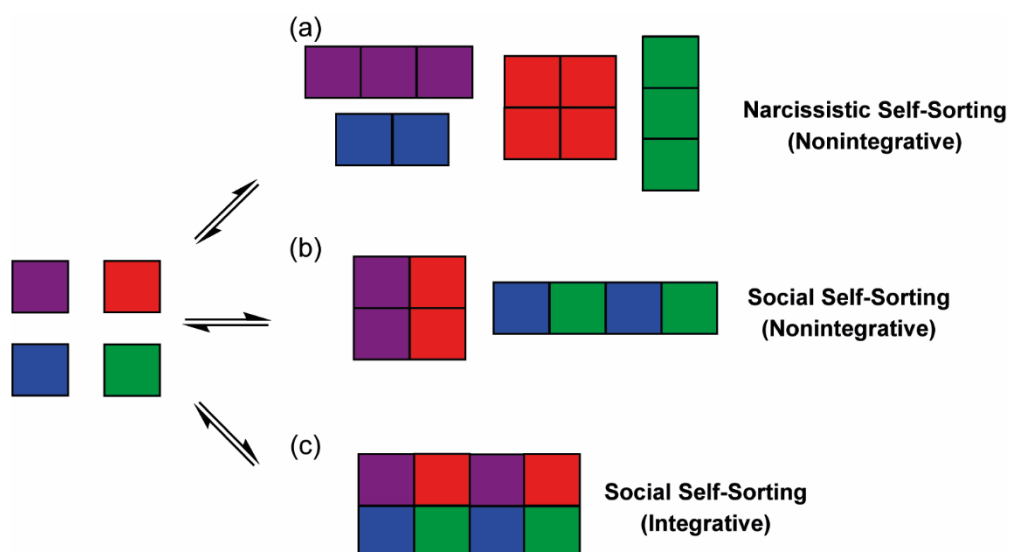


Figure 12. Schematic of self-sorting classifications (a) narcissistic nonintegrative, (b) social nonintegrative and (c) social integrative.

Many artificial molecules have been shown to exhibit high levels of selectivity within complex mixtures. Several factors known as “molecular codes” have been shown to control these molecular recognition events. Geometrical parameters, size and shape play the most prominent role and can be considered a prerequisite before other molecular codes (complementarity, non-covalent interactions, sterics, coordination sphere of metal ions and charge-transfer) can come into play and eventually direct self-sorting processes. It is noteworthy that, as well as molecular recognition, self-sorting processes depend to a great extent on the external variables (solvent, temperature, concentration, pH, etc.) that can differently influence the equilibrium and/or the stability of independent recognition processes involving different noncovalent interactions.^{57,58} Many different supramolecular architectures reported to undergo self-assembly historically have been implicated in self-sorting processes. Schmittel and co-workers have shown

self-sorting of metal-ligand complexes and Nitschke and co-workers have described this behaviour in metal cages.^{59,60} Cucurit[n]uril, cryptand and cyclodextrin building blocks have also been exploited to create self-sorting systems, with a particular emphasis on the ability to self-sort in aqueous media.^{61–65} Self-sorting of supramolecular building blocks has been the driving force in the formation of several pseudo rotaxanes.^{54,66–68} Isaacs and co-workers have reported the use of such building blocks to create molecular clips capable of self-sorting.^{64,69} Adams and co-workers have described a series of low molecular weight gelators, based on diketopyrrolopyrrole, oligophenylvinylene, perylene bisimide and stilbene structures, that can produce self-sorted fibres on gelation.^{70–73} A study by Wu and Isaacs combined eight well-defined supramolecular structures including self-assembled ionophores, molecular clips and calixarenes (Figure 13 (a-h)).⁵¹ The ¹H NMR of the mixture of all eight components revealed thermodynamic narcissistic self-sorting of the system.

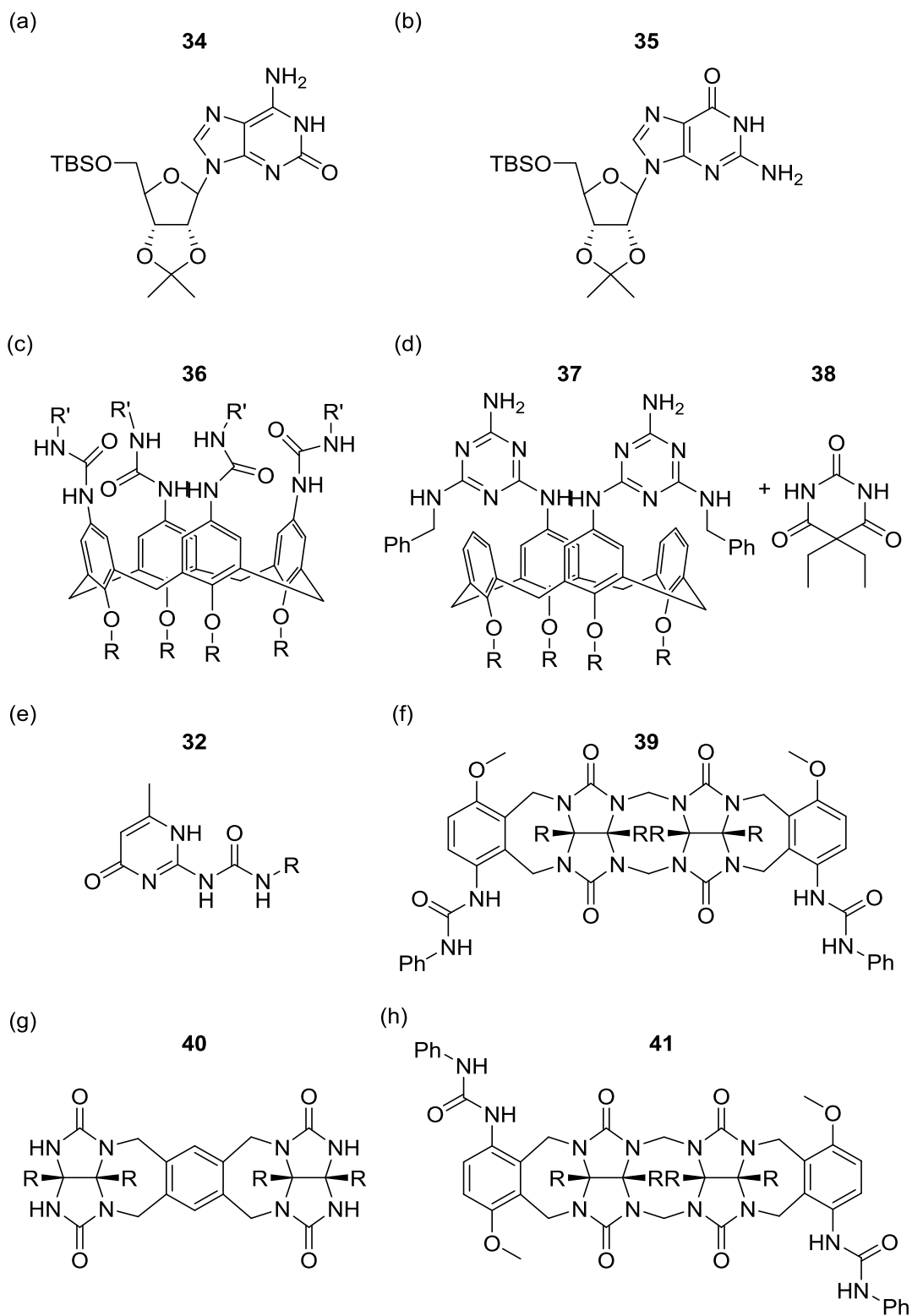


Figure 13. Hydrogen bonding aggregates shown to thermodynamically self-sort by Wu and Isaacs.

Self-sorting systems utilising the complementarity of hydrogen bond motifs have also been described. Zimmerman and co-workers highlighted self-sorting in mixtures of hydrogen-bonded cyclic assemblies based on a fixed complementary *DDA·AAD* interacting array **42** (Figure 14). The self-sorting events of the hexamer **42₆** were influenced by the attachment of different sized R groups (dendrons).⁷⁴

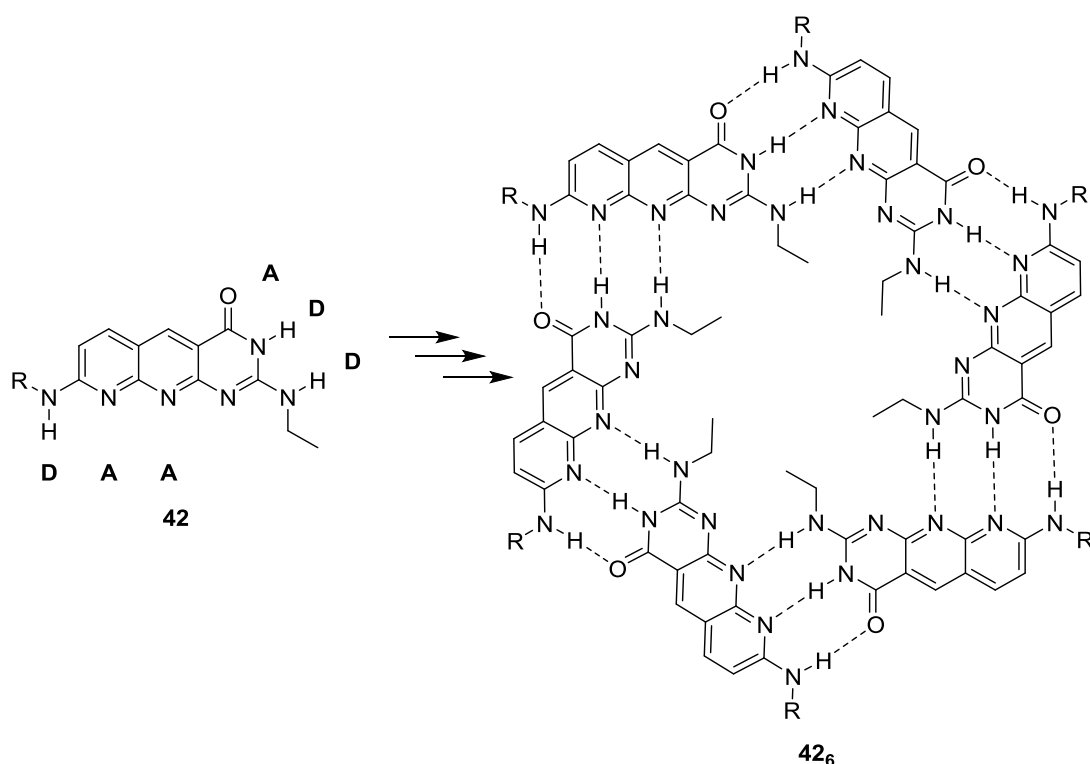


Figure 14. Hexameric cyclic hydrogen bonding assembly of compound 42 through complementary *DDA·AAD* interactions. Hydrogen bonds represented at dashed lines.

Other systems developed by Zimmerman and co-workers have focussed on linear arrays exhibiting high fidelity molecular recognition.^{75,76} The ureidoguanosine-diamidonaphthyridine complex (UG·DAN **43·44**) forms with high fidelity with nominal interference from competing arrays (Figure 15 (a)).⁷⁵ However, UPy analogue **45** has a low fidelity as it is able to form both homodimers (**45-I**) and heterodimer (**45-II**) with DAN motif **44** through tautomerisation (Figure 15 (b) & (c)).^{77,78} Wilson and co-workers reported complementary triply hydrogen bonding complexes ureidoimidazole (UIM) **31** and amido/isocytosine (AIC) **46** formed a strong heterodimer UIM·AIC **31·46** (Figure 15 (d)).^{40,79,80} Additionally, the Wilson group then showed that strong heterodimers **45·44** (UPy·DAN) and **31·46** (UIM·AIC) were able to assemble in the presence of each other in solution.⁸¹ These four hydrogen bonding motifs could spontaneously self-sort to give two heterodimers (Figure 16 (a)). Using these findings, it was possible to develop an artificial signalling cascade (Figure 16 (b)) which utilises the differing fidelity of arrays of UPy, DAN, UIM and AIC to associate and dissociate in a sequential manner. The addition of a photo-cleavable motif to the AIC motif (AIC* **47**) led to an extension of the cascade to five phases (Figure 16 (c)). This self-sorting system described by Wilson and co-workers provides the foundation for the development of the self-sorting network outlined in Chapter 2.

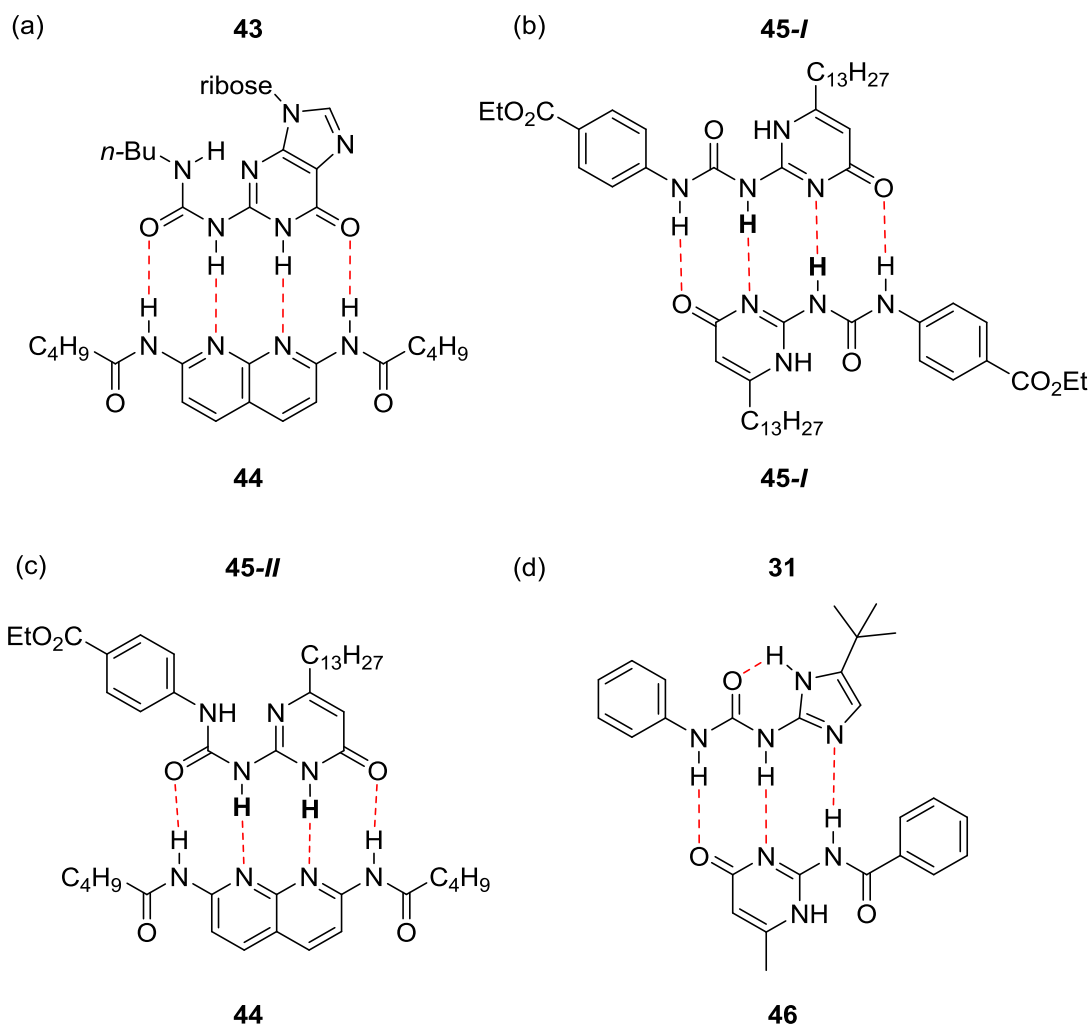


Figure 15. Hydrogen bonding interaction between compounds (a) 43·44 (UG·DAN) heterodimer, (b) 45-I·45-I (UPy·UPy) homodimer, (c) 45-II·44 (UPy·DAN) heterodimer and (d) 31·46 (UIM·AIC) heterodimer (hydrogen bonds shown as red dashed lines).

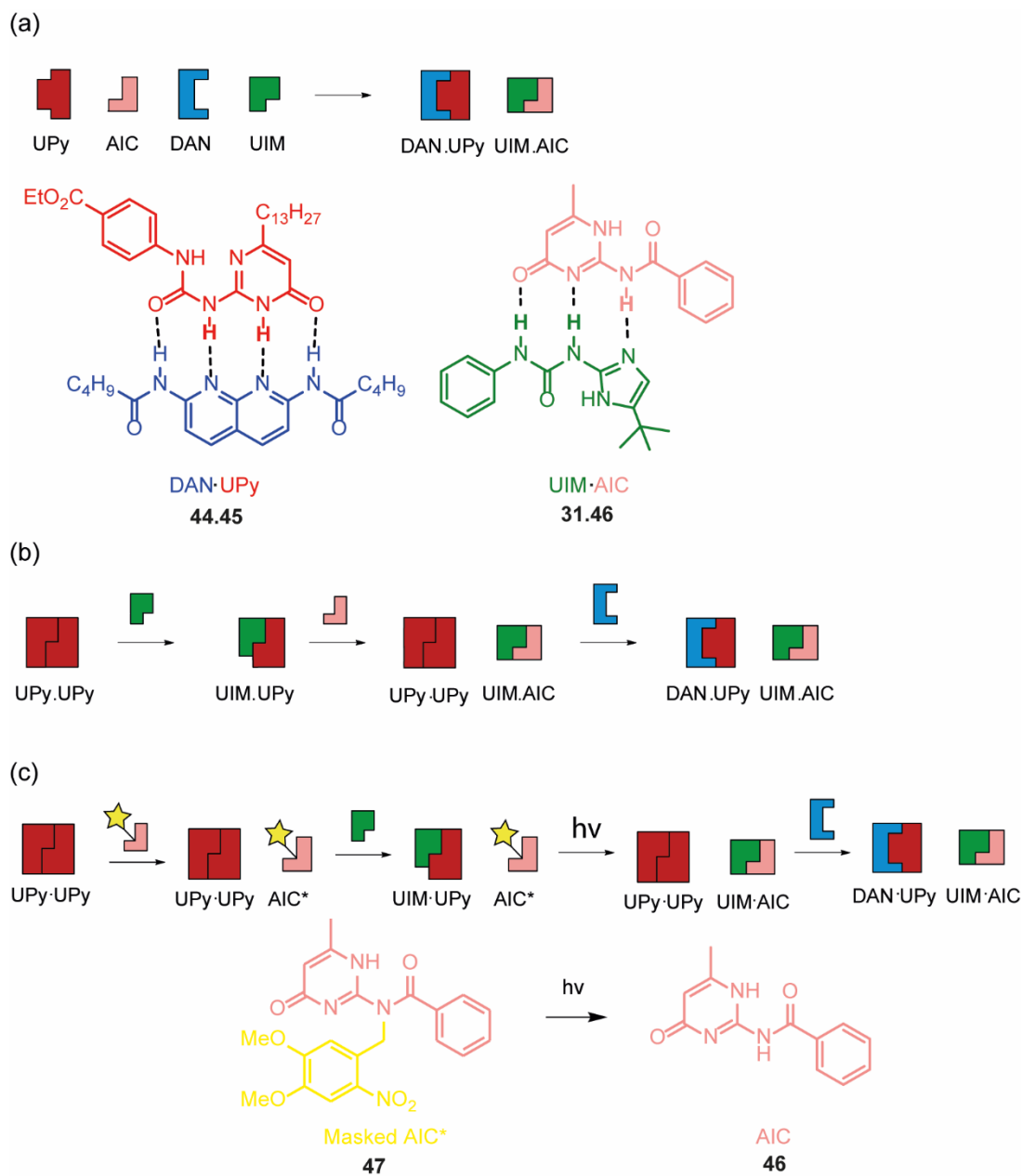


Figure 16. (a) Schematic and chemical structure of the spontaneous self-sorting of DAN, UPy, UIM and AIC (hydrogen bonds shown as black dashed lines), (b) Schematic of the sequential self-sorting cascade for DAN, UPy, UIM and AIC and (c) Schematic of the photo activated sequential self-sorting cascade of DAN, UPy, UIM and masked AIC* and the chemical structure of the photo-cleavage reaction of masked AIC* 47 to AIC 46.

1.3 Supramolecular Polymers

There has been considerable interest in the use of non-covalent interactions to create supramolecular polymers (SMP). In the bulk state, these supramolecular polymers should display mechanical properties of covalent polymers as well as the reversibility and stimuli-responsive properties of non-covalent molecular arrays.⁸² The degree of polymerisation and material properties can be controlled by the nature of the non-covalent interactions.¹ As a result of the directionality, selectivity and strength of hydrogen bonds discussed above, hydrogen bonding arrays are a commonly used interaction for the formation of linear supramolecular polymers and cross-linked networks (Figure 17). Many of the hydrogen bonding motifs discussed previously in this chapter have been utilised in the creation of supramolecular polymers.

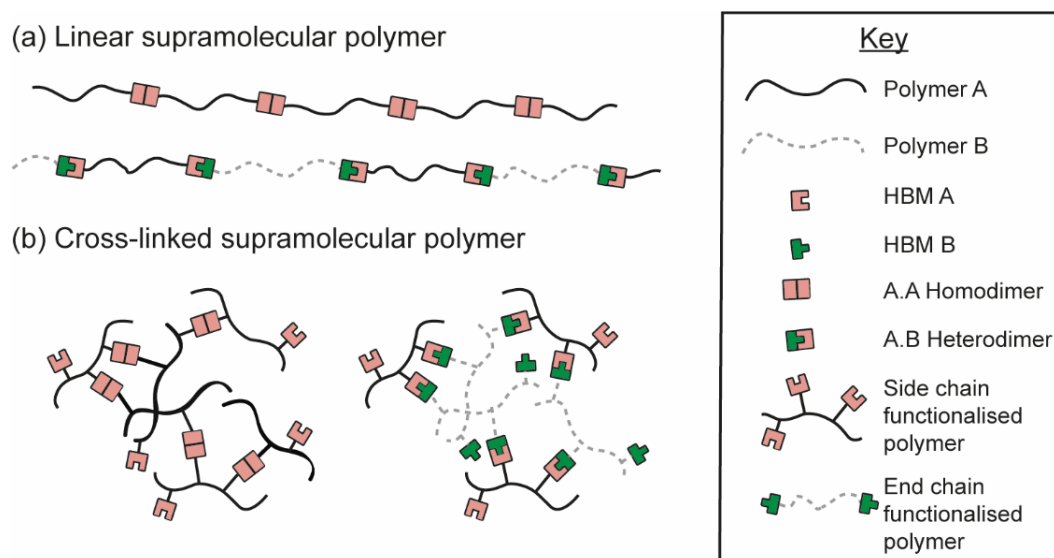


Figure 17. Schematic showing (a) linear supramolecular polymers with end chain functionalisation and (b) cross-linked supramolecular polymers with side chain functionalisation.

1.3.1 Linear Supramolecular Polymers

Lehn and co-workers described one of the first SMP assemblies using 2,6-diamidopyridine **48** and thymine-functionalised **49** building blocks to form liquid crystals through ditopic linear hydrogen bonding (Figure 18).^{83–85} The stabilities of these assemblies were not sufficient to be classed as true SMPs but revealed that self-recognition can transform molecules into macromolecules.

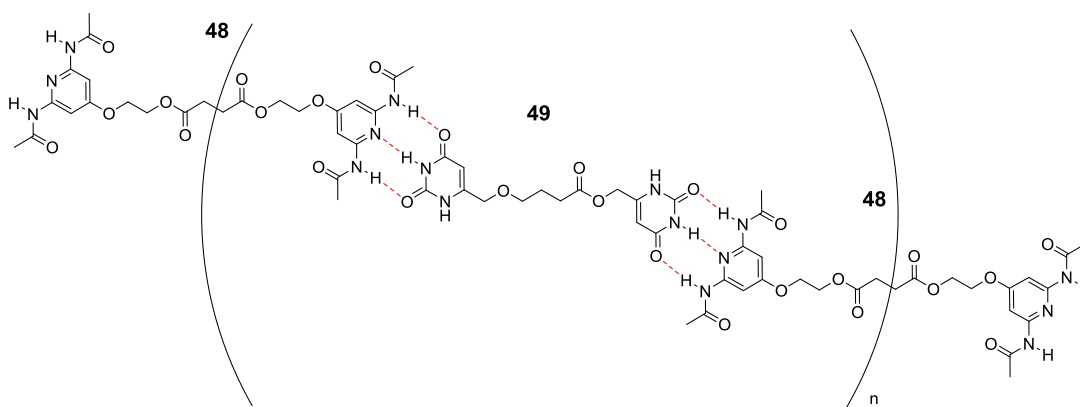


Figure 18. Supramolecular polymeric assembly of ditopic compounds 48 and 49 through linear hydrogen bonding (hydrogen bonds shown as red dashes lines).

Development of SMPs was accelerated when Meijer and co-workers introduced the self-complementary 2-ureido-4-pyrimidine (UPy) motifs. Analogue **50** was shown to self-associate in chloroform with a dimerisation constant greater than $4.5 \times 10^5 \text{ M}^{-1}$ (Figure 19 (a)).⁴³ Ditopic supramolecular monomers **51** were synthesised from alkyl chains functionalised with UPy groups at each end (Figure 19 (b)).⁸⁶ These ditopic monomers were shown to assemble into polymeric linear chains in dilute solution (Figure 19 (c)). The

polymers obey the criteria of conventional condensation polymers defined by Carothers, as polymers and small molecules are formed rather than addition where only polymer is created.^{87,88} In addition, they have the properties associated with reversibility due to self-complementary hydrogen-bonding. For example, Meijer *et al.* showed that the bifunctional UPy motif **51** exhibited viscosity changes that were dependent on both concentration and temperature.⁸⁶ Addition of monofunctional UPy unit **50** reduced the viscosity of the solution, implying a decrease in degree of polymerisation due to competition with the bifunctional motif resulting in the disruption of polymer chains (Figure 19 (d)). The monofunctional UPy monomers **50** end cap the polymer chains, hence decreasing the degree of polymerisation of the homopolymer. The UPy motif has been employed in several supramolecular polymers⁸⁹ and has been used commercially.⁹⁰

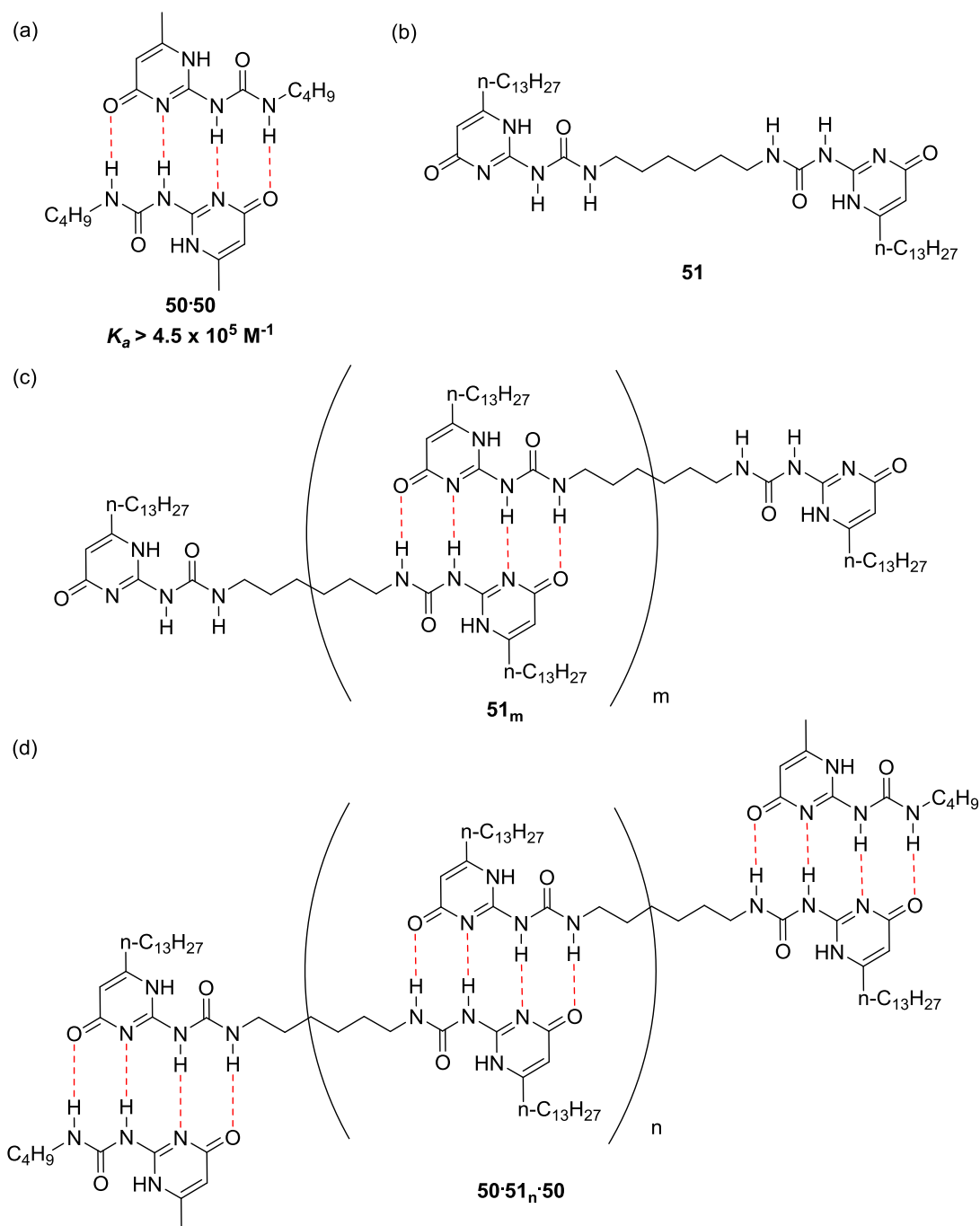


Figure 19. (a) Dimerisation interaction for compound 50, (b) Ditopic supramolecular monomer 51 with UPy end groups, (c) Supramolecular polymer of ditopic compounds 51 through linear hydrogen bonding and (d) Supramolecular polymer of ditopic compounds 51 with competition from UPy motif 50 (hydrogen bonds shown as red dashed lines).

Hailes and co-workers also reported a linear polymer built with hydrogen bonding motifs. Ureido functionalised cytosine (UCyt) **52** were used as an alternative self-complementary hydrogen bonding array to UPy **50**.⁹¹ The UCyt motif **52** exists in both folded **52-II** and unfolded **52-I** states (Figure 20 (a)).^{92,93} In apolar solvents, UCyt **52** exclusively adopts an unfolded **52-I** state with an AADD hydrogen bonding motif and exhibited a dimerisation constant of more than $2.5 \times 10^5 \text{ M}^{-1}$ in CDCl_3 (Figure 20 (b)).^{91,93} In very polar solvents, such as dimethylsulfoxide, the folded conformer **52-II** is preferred. UCyt DDAA-based bis-functionalised polymeric assemblies could be constructed via the attachment of polymeric chains at both N-1 (giving tail-tail) and N-9 positions (giving head-head) (Figure 21).⁹² The group investigated the effect of N-substituents and showed that longer alkyl chains give rise to more of the unfolded conformer **52-I**.⁹³ The chain length at the N-9 position had a smaller effect on the rotamer ratio, than at the N-1 position, and was dependent on the substituent at the N-1 position.⁹³

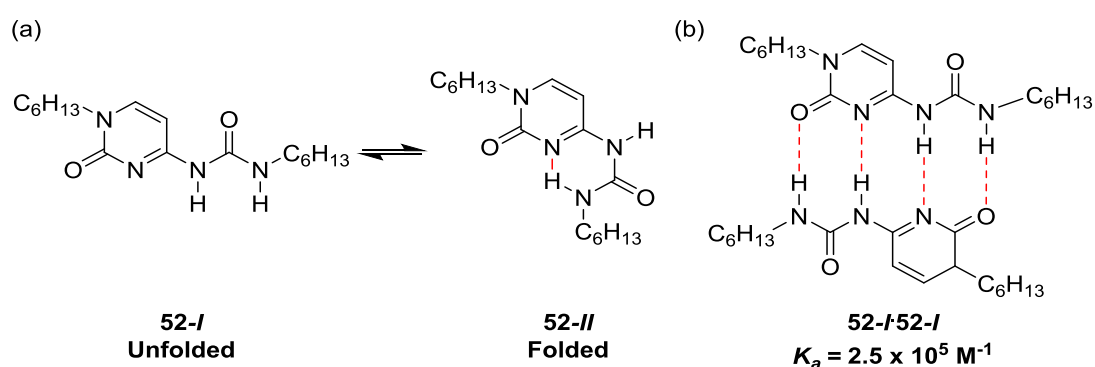
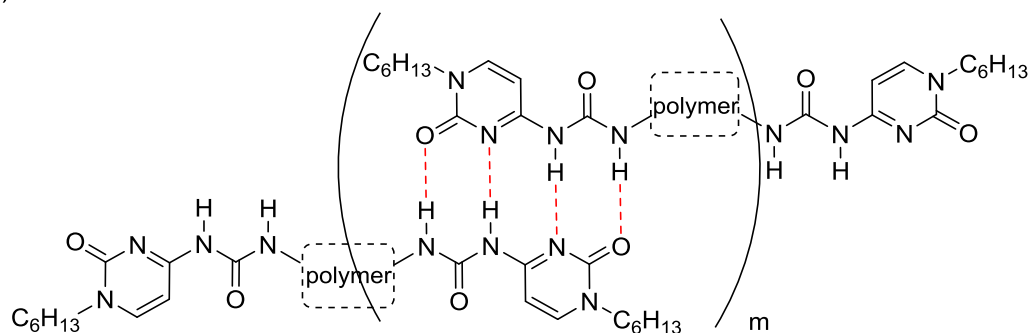


Figure 20. (a) Conformational equilibria of compound 52 and (b) Hydrogen bonding dimerisation interaction of compound 52-I (hydrogen bonds shown as red dashed lines).

(a) Head-Head



(b) Tail-Tail

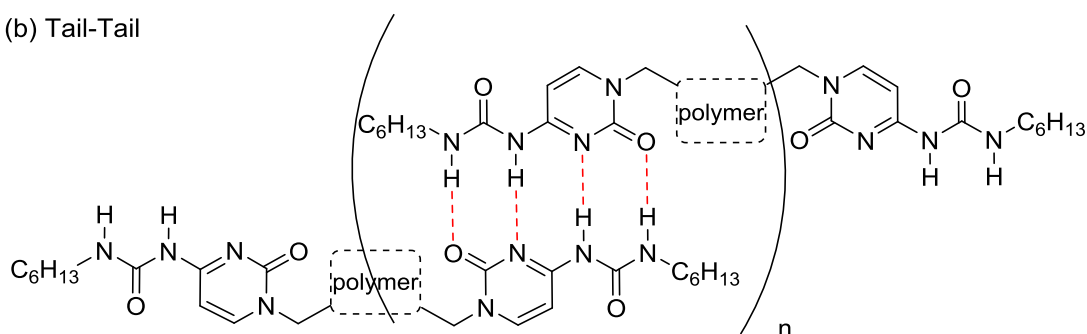
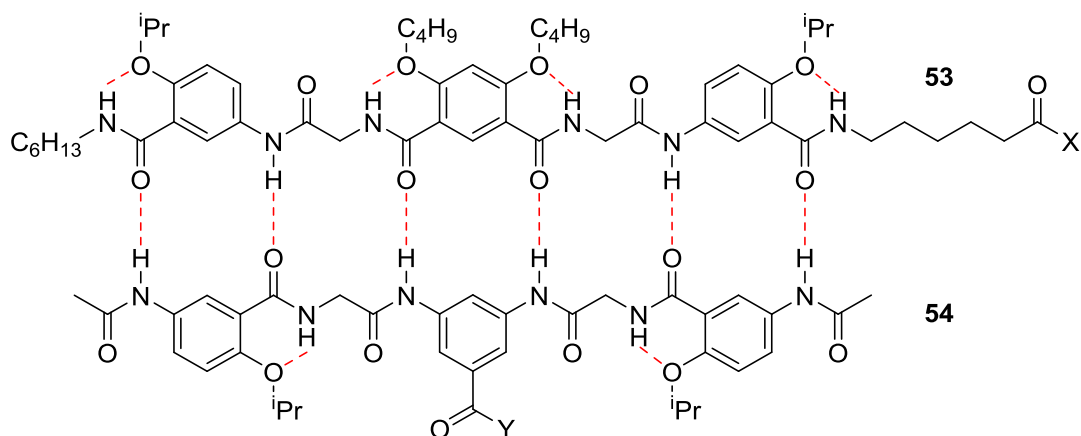


Figure 21. Supramolecular polymeric assembly of UCyt bis-functionalised polymers through linear hydrogen bonding. (a) Head-Head assembly and (b) tail-tail assembly. Hydrogen bonds shown as red dashed lines.

Heterocomplementary assemblies are desirable as they are able to form more complex structures such as supramolecular block co-polymers.¹ This type of supramolecular assembly requires high affinity between different monomers and low affinity for homodimerisation, as well as high selectivity. Gong and co-workers described the assembly of an AB diblock co-polymer through the dimerisation of hydrogen bonding duplexes **53** and **54** (Figure 22).⁹⁴ **53** and **54** were synthesised by the termination of polystyrene (PS) and poly(ethylene glycol) (PEG) with two complementary aromatic oligoamide strands respectively. Shorter polymer chains resulted in disordered block co-polymers whereas the longer chains underwent microphase separation.



53a: X = OMe

54a: Y = OMe

53b: X = OPS ($M_w = 1.7 \times 10^3 \text{ g mol}^{-1}$)

54b: Y = OPEG ($M_w = 350 \times 10^3 \text{ g mol}^{-1}$)

53c: X = OPS ($M_w = 3.2 \times 10^3 \text{ g mol}^{-1}$)

54c: Y = OPEG ($M_w = 2.0 \times 10^3 \text{ g mol}^{-1}$)

53d: X = OPS ($M_w = 20 \times 10^3 \text{ g mol}^{-1}$)

54d: Y = OPEG ($M_w = 5.0 \times 10^3 \text{ g mol}^{-1}$)

Figure 22. AB diblock co-polymer through the dimerisation of duplexes 53 and 54 (hydrogen bonds shown as red dashed lines).

As discussed above, UPy has poor fidelity recognition behaviour as it can form strong homodimers and strong heterodimers with DAN **44**; suggesting that the formation of a heteromeric supramolecular block copolymer would be difficult. However, Meijer and co-workers have reported the formation of a supramolecular AA–BB-type block co-polymer using macromonomers **55** and **56** functionalised with UPy and DAN hydrogen bonding motifs (Figure 23 (a)).⁹⁵ The homopolymer is first assembled from a telechelic polytetrahydrofuran macromonomer functionalised with a UPy end group **55** (Figure 23 (b)).⁹⁵ The macromonomers are held together by hydrogen bonding between the complementary motifs. Stoichiometric control can be used to tune the composition of the polymer from a pure supramolecular homopolymer to a strictly alternating heteropolymer as a result of the low fidelity of UPy. The

supramolecular structure is retained upon the addition of a dimeric DAN monomer **56** until 1 equivalent of DAN had been added after which the viscosity significantly decreases indicating depolymerisation (Figure 23 (c)). This indicates that the DAN monomer **56** is inserting into the polymer backbone when up to one equivalent is added, creating an alternating block co-polymer. When the ratio of DAN monomer **56** added is greater than UPy monomer **55**, DAN monomer **56** caps the polymer chain ends, hence reducing the length of the polymer chains (Figure 23 (d)). Another example was reported by Zimmerman and co-workers who described the formation of a multi-block co-polymer with a strict alternating structure. This was achieved by co-polymerisation of macromonomers **57** and **58** terminated with high fidelity UG or DAN motifs respectively (Figure 24).⁹⁶

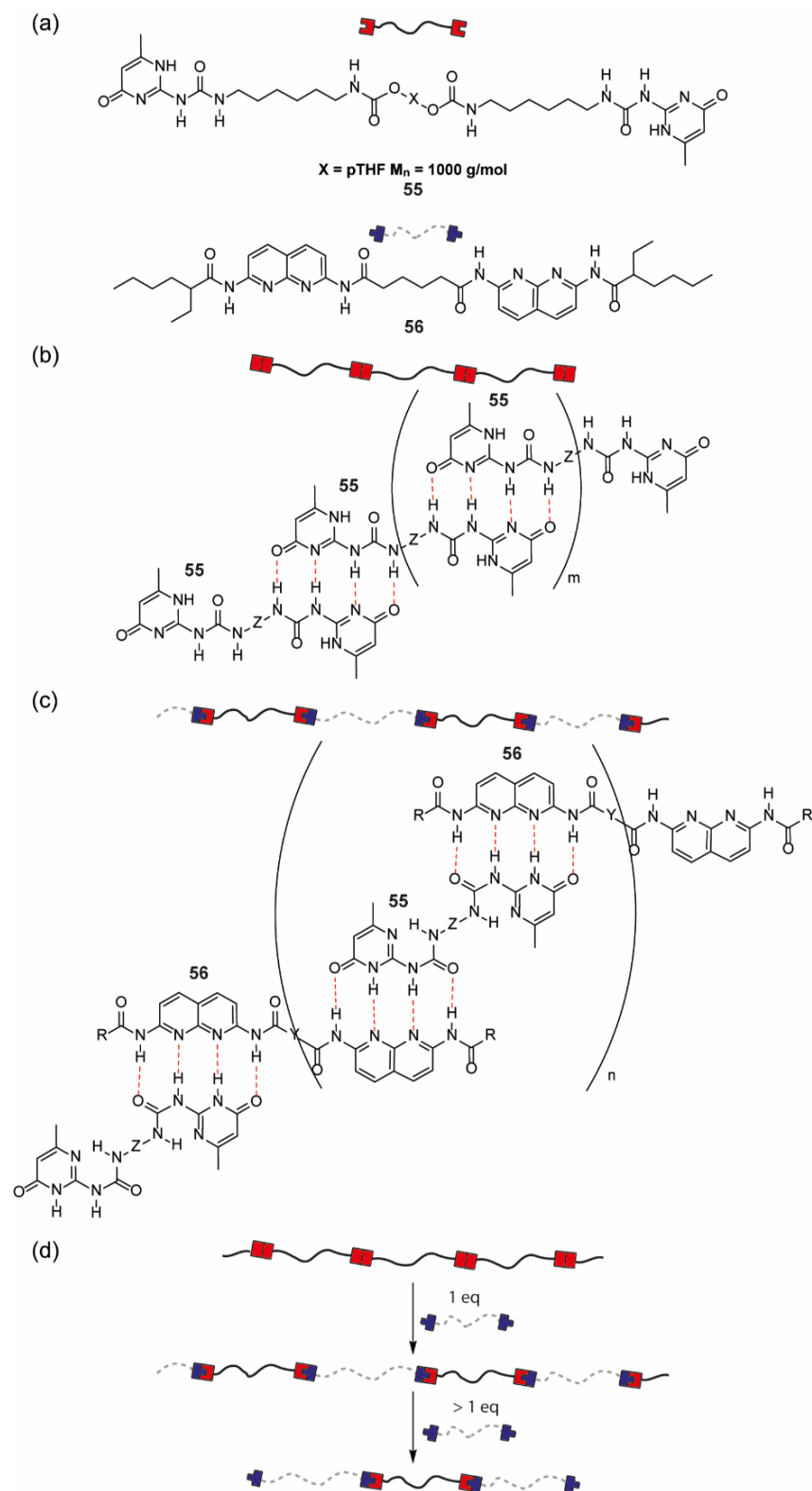


Figure 23. (a) Chemical structure and schematic of ditopic supramolecular monomers 55 and 56 with UPy and DAN hydrogen bonding motifs respectively, (b) chemical structure and schematic of homopolymer of 55, (c) chemical structure and schematic of alternating block co-polymer of 55·56 and (d) schematic showing the change in polymer composition on addition of ditopic monomer 56 (hydrogen bonds shown as red dashed lines).

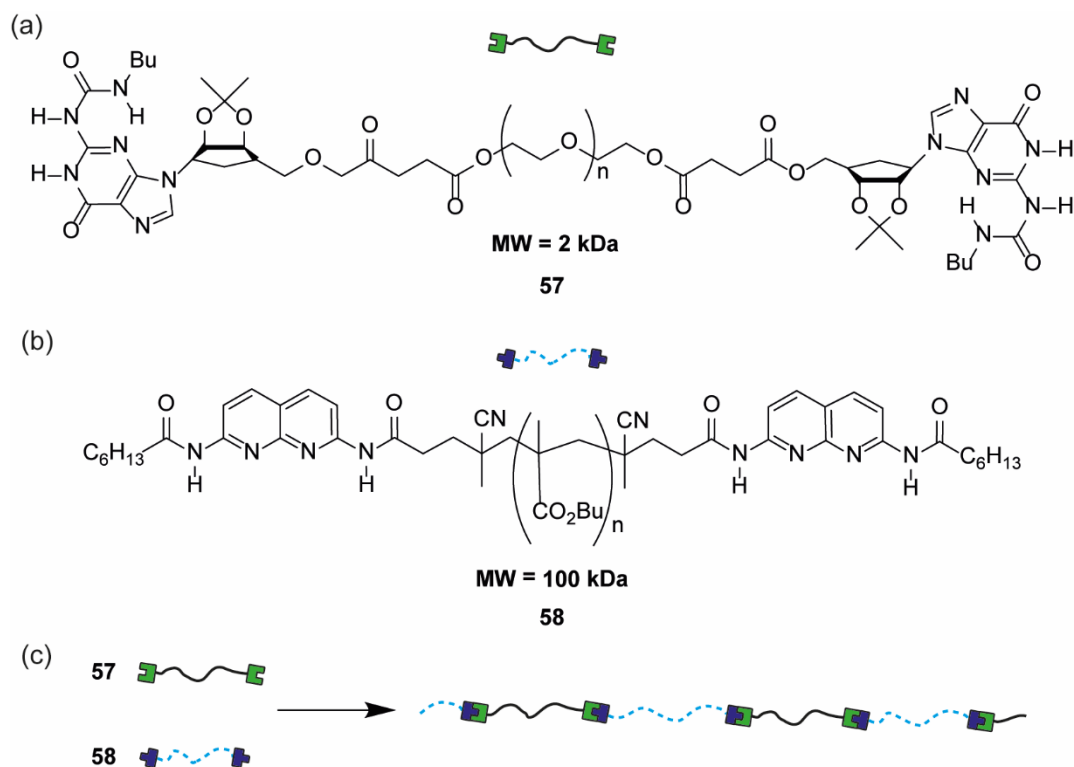
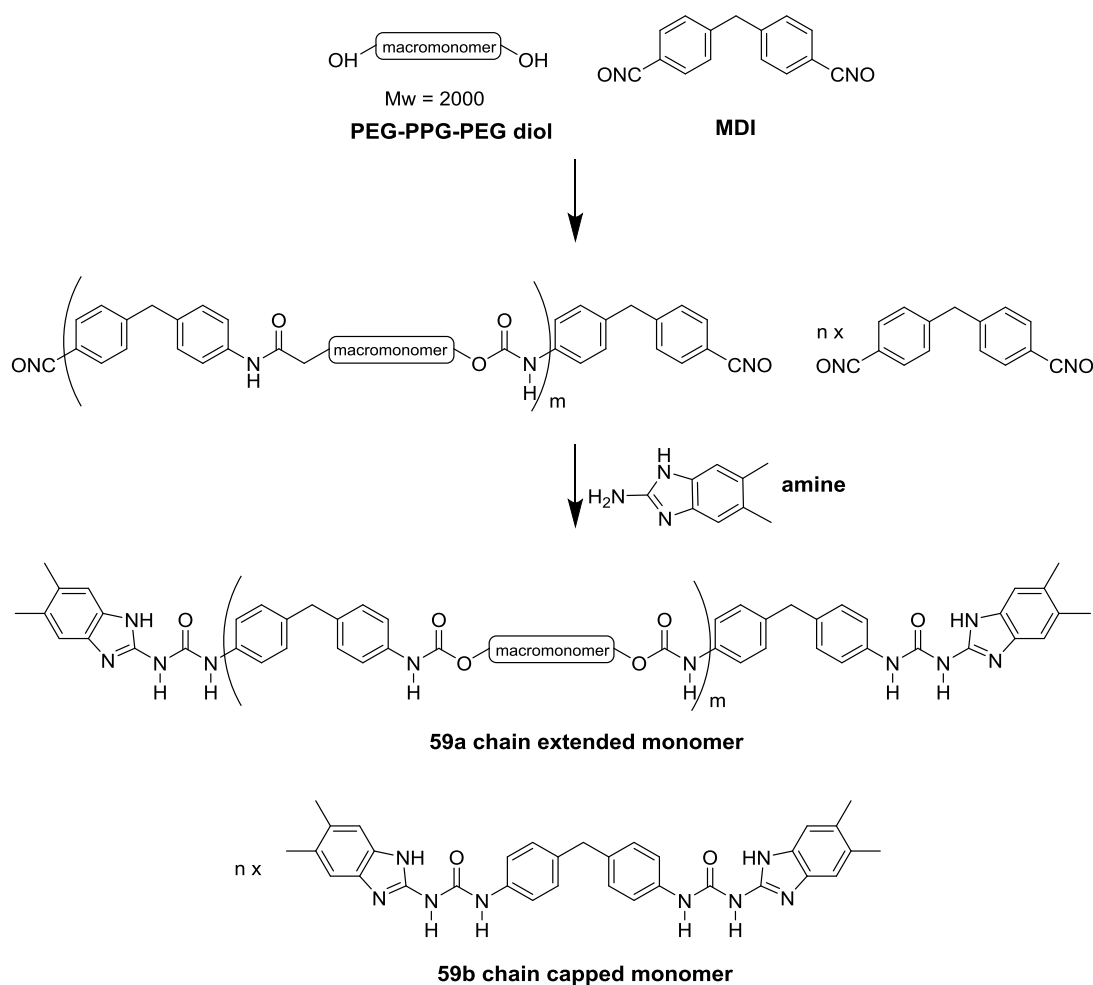


Figure 24. Chemical structure and schematic of ditopic supramolecular monomer functionalised with (a) UG 57, (b) DAN 58 hydrogen bonding motifs and (c) schematic showing interaction of monomers 57 and 58 forming an alternating block polymer.

The Wilson group developed a self-assembled elastomer using UIM·AIC **31·46** type intermolecular interaction to hold the polyurethane monomers together.^{40,79,97} The UIM functionalised monomer **59** was synthesised by reacting poly(ethylene glycol)-poly(propylene glycol)-poly(ethylene glycol) diol (PEG-PPG-PEG) macromolecule with bifunctional isocyanate (MDI) followed by the addition of 2-amino-5,6-dimethylbenzimidazole to create chain extended monomer **59a** and chain capped monomer **59b** (Scheme 1).⁹⁸ The supramolecular polymer is subsequently formed on the addition of heterocomplementary diamido/socytosine (DAC) **60** to chain extending monomer **59a** (Figure 25). The blend consists of soft domains derived from the PEG diol in **59** and hard domains comprised of the aromatic functional

groups and the heterocomplementary intermolecular interaction between **59** and **60**. This supramolecular polymer displayed two unique features: first, assembly only occurs when both **59** and **60** are present, and secondly, the mechanical properties of the polymer can be controlled by the ratio of **59** and **60** used during synthesis.⁹⁸



Scheme 1. Synthesis of UIM functionalised monomers 59a (chain extended) and 59b (chain capped).

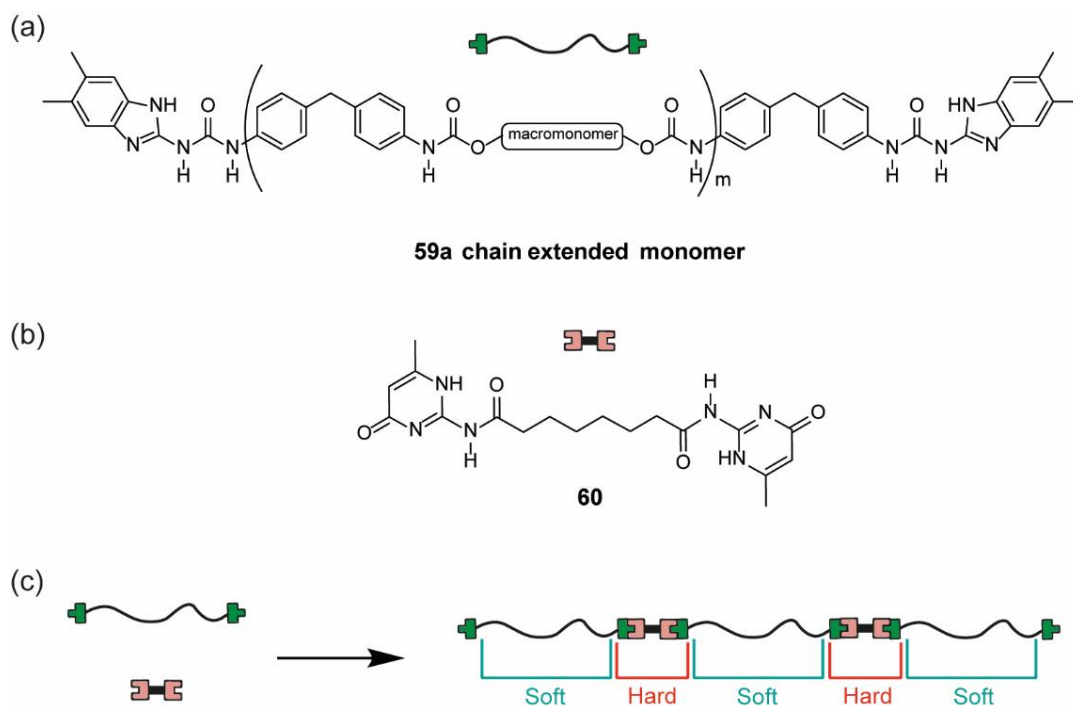


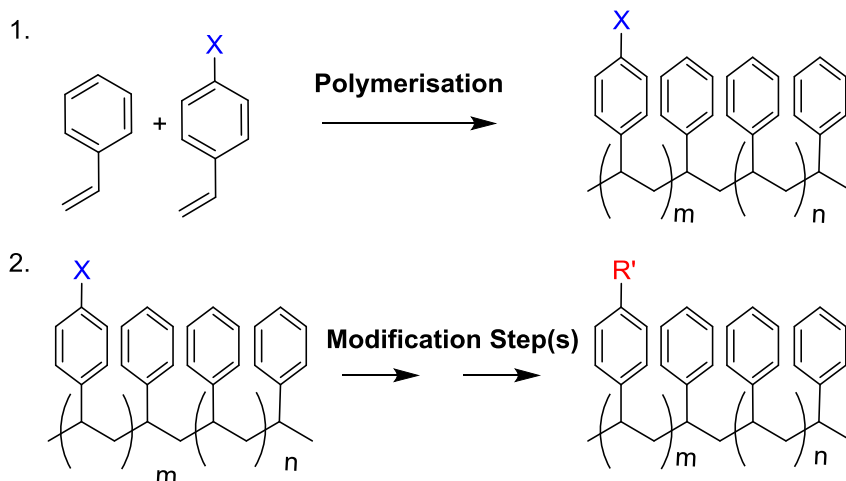
Figure 25. (a) UIM functionalised polymeric chain extended monomer 59a, (b) Diamidoisocytosine (DAC) 60 and (c) supramolecular linear polymer created from 59a and 60 with soft and hard domains.

1.3.2 Cross-linked Supramolecular Polymers

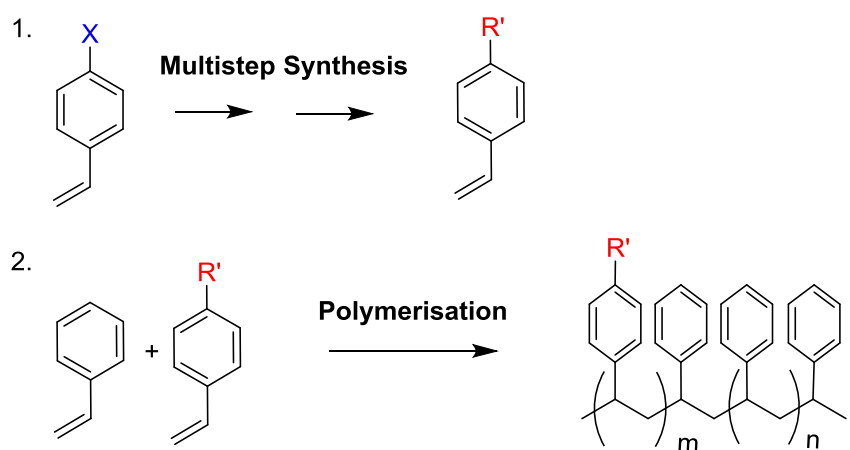
As well as in the formation of linear SMPs, hydrogen bonding motifs have been exploited to create cross-linked polymer networks.⁹⁹ In linear SMPs, hydrogen bonds between complementary motifs link macromolecules together to generate the polymer backbone (Figure 17a). However, in the formation of cross-linked supramolecular polymers, covalent polymer chains make up the backbone and the hydrogen bonds between complementary motifs create the cross-links between different polymer chains (Figure 17b). In both systems, the interaction between complementary hydrogen bonding motifs govern the formation of the SMP. Consequently, the selection of appropriate hydrogen bonding motifs is key to control the properties of the supramolecular polymer.

The hydrogen bonding motifs selected for both linear and cross-linked polymer systems are often similar but the synthetic route for polymerisation is significantly different. For a cross-linked polymer, a covalent polymer is functionalised with a hydrogen bonding moiety to create a co-polymer. This functionalisation can occur by post polymerisation modification reactions or by direct co-polymerisation of a monomer and functionalised co-monomer (Figure 26). For post polymerisation modification, a monomer such as styrene is co-polymerised with a similar monomer with a reactive handle, such as X (e.g. 4-vinylbenzylchloride), the hydrogen bonding motif (R') is then introduced to the polymer through the reactive handle (Figure 26 (a)). For direct polymerisation, a co-monomer containing both a hydrogen bonding moiety and polymerisable group is synthesised and then co-polymerised with the relevant monomer (Figure 26(b)).

(a) Post polymerisation modification



(b) Direct co-polymerisation



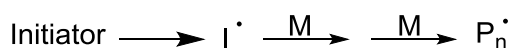
X = reactive handle **R' = hydrogen bonding motif**

Figure 26. General approach for synthesis of styrene based side chain functionalised co-polymers by (a) post polymerisation modification and (b) direct co-polymerisation.

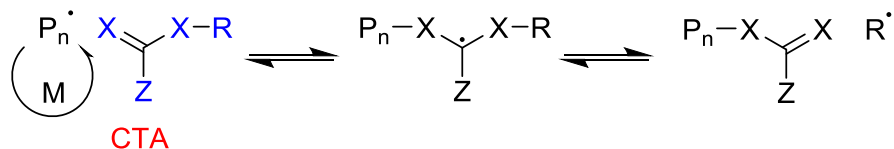
Several polymerisation techniques have been reported in the literature for such systems; however, living polymerisation is considered to offer the best control. Reversible addition fragmentation chain transfer polymerisation (RAFT) was used previously in the Wilson group and chosen for this project. The benefits of this technique include low polydispersity, application to many different polymerisable monomers, tolerance to unprotected functionality in monomers and solvent, and ease of implementation.¹⁰⁰ The mechanism for

RAFT polymerisation progresses through several steps outlined in Figure 27.¹⁰⁰⁻¹⁰² The first stage is initiation which can be triggered by thermal, photochemical or redox methods. Reversible chain transfer or pre-equilibrium RAFT propagation occurs next, in which the chain transfer reagent (CTA) is introduced. The CTA must have several key features; a reactive S=C double bond, a weak S-C single bond between X-R, a free radical leaving group R which is capable of reinitiation and a suitable Z activating group to control the S=C activity and the rate of addition fragmentation. For more activated groups (such as MMA and styrene), Z is ideally a thiol with low volatility to minimise retardation, where retarder molecules react mildly with the initiating radical and slow down polymerisation, while maintaining a high fraction of living chains. The next stage is reinitiation of the free radical leaving group followed by chain equilibration or main equilibrium RAFT propagation. The final stage is termination of polymer radicals to give “dead” polymer chain ends which inhibits any further chain propagation.

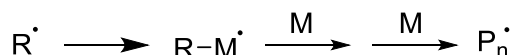
(a) Initiation



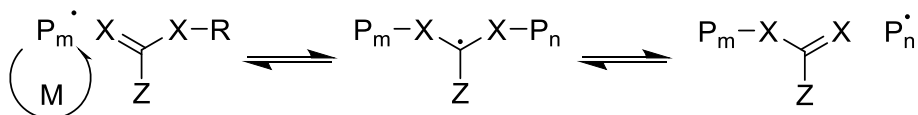
(b) Reversible chain transfer



(c) Reinitiation



(d) Main chain equilibrium



(e) Termination



Figure 27. RAFT polymerisation mechanism.

There have been reports of cross-linked supramolecular polymers employing both homocomplementary and heterocomplementary hydrogen bonding motifs.¹⁰³ In the cases where heterocomplementary hydrogen bonding motifs are used to functionalise immiscible polymers, the hydrogen bonding interactions of the side chains can drive blend formation.

Cross-linked polymer blends have been reported by Zimmerman and co-workers based on the complementary quadruple hydrogen bonding motifs UG:DAN **43-44**, with functionalised (poly)butyl methacrylate (PBMA) and (poly)styrene (PS) groups to form **61** and **62** respectively (Figure 28 (a) & (b)).^{76,104} The PS/PBMA pair is usually immiscible; however, it was thought

than when the polymers are functionalised with hydrogen bonding motifs UG **43** and DAN **44**, hydrogen bonding would create a miscible cross-linked polymer **61·62** (Figure 28 (d)). It was shown these polymers form colourless transparent films. The films did not show microphase separation and differential scanning calorimetry (DSC) studies indicated a homogenous blend as it contained a single glass transition. It is suggested that this blend is formed due to the high stability and fidelity of the **43·44** complex.^{76,104} In addition, the group also investigated the possible formation of a polymer blend between a PBMA monomer functionalised with a UPy motif **61** and PS-DAN monomer **62** (Figure 28 (c)).¹⁰⁵ It was revealed that the **62·63** mixture (with DAN·UPy HBMs) was less viscous than **61·62** (with UG·DAN HBMs) suggesting that the ability of the UPy motif to self-dimerise inhibits the formation of a polymer blend because a similar viscosity was observed on blending, irrespective of the percentage of **63**.¹⁰⁵ When there is an excess of UPy PBMA monomer it was cross link with its self (Figure 28 (e)).

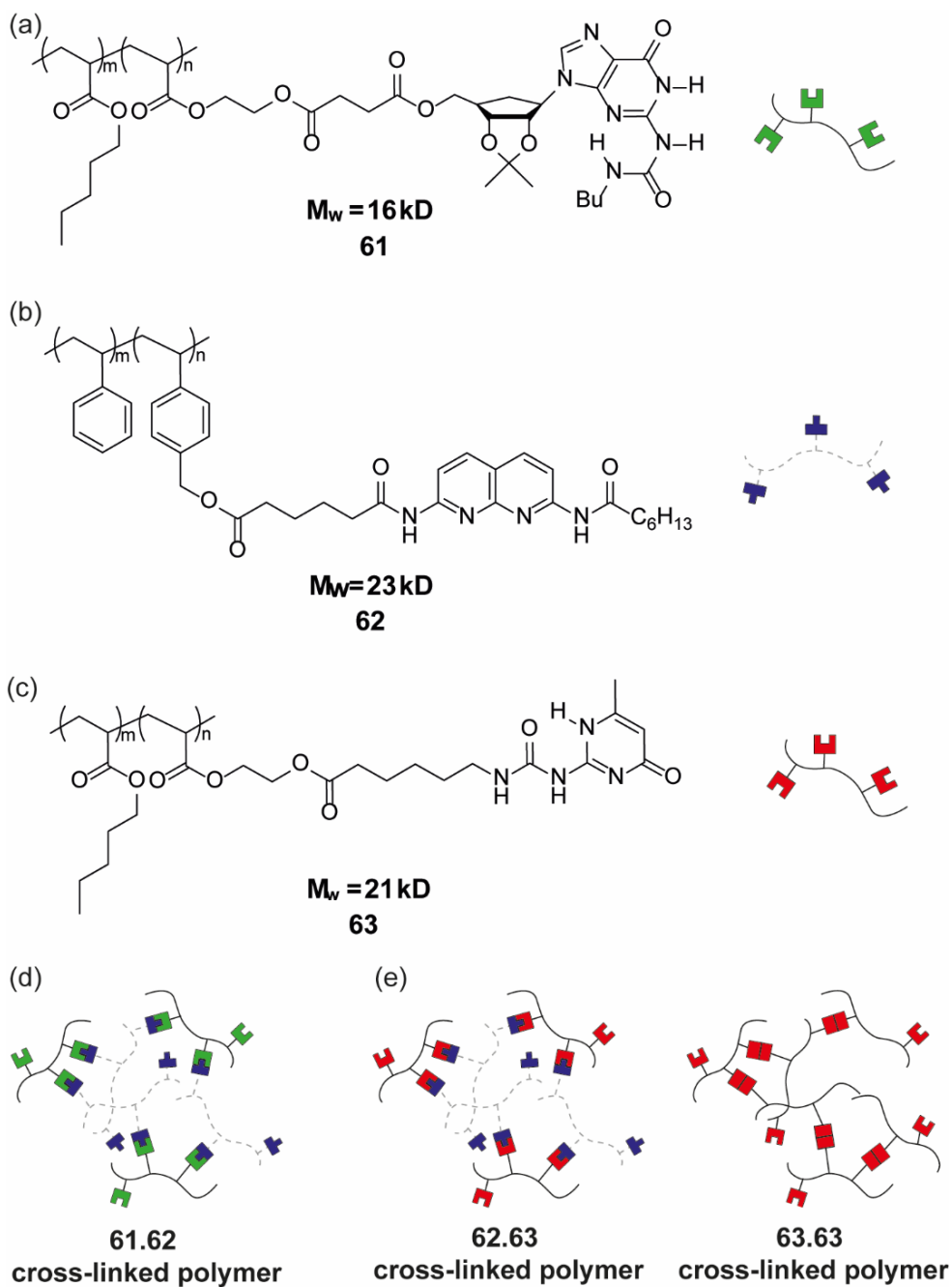


Figure 28. (a) UG functionalised PBMA co-polymer 61, (b) DAN functionalised PS co-polymer 62, (c) UPy functionalised PBMA co-polymer 63, (d) cross-linked polymer blend 61·62 with heterocomplementary interactions between UG·DAN and (e) mixture of cross-linked polymer blends 62·63 and 63·63 with heterocomplementary interactions between UPy·DAN and homocomplementary interactions between UPy·UPy.

The Wilson group formed an alternative polymer blend incorporating complementary triple hydrogen bonding arrays, ureidopyrimidine and diamidopyridine. The group synthesised methacrylate-functionalised ureidopyrimidine and styrene-functionalised diamidopyridine macromonomers **64** and **65** using RAFT living polymerisation (Figure 29 (a) & (b)).¹⁰⁶ Mixtures of the macromonomers **64** and **65** with a high proportion of hydrogen bonding motifs (6-14%) lead to the assembly of the cross-linked polymer blend (Figure 29 (d)) which was shown to form a transparent film. DSC studies of the film confirmed the formation of a miscible polymer blend. The role of intermolecular hydrogen bonding in promoting miscibility was further highlighted by infra-red (IR) and Atomic Force Microscopy (AFM) analyses as a higher fraction of hydrogen bonding motifs decreased the surface roughness of the polymer.¹⁰⁶

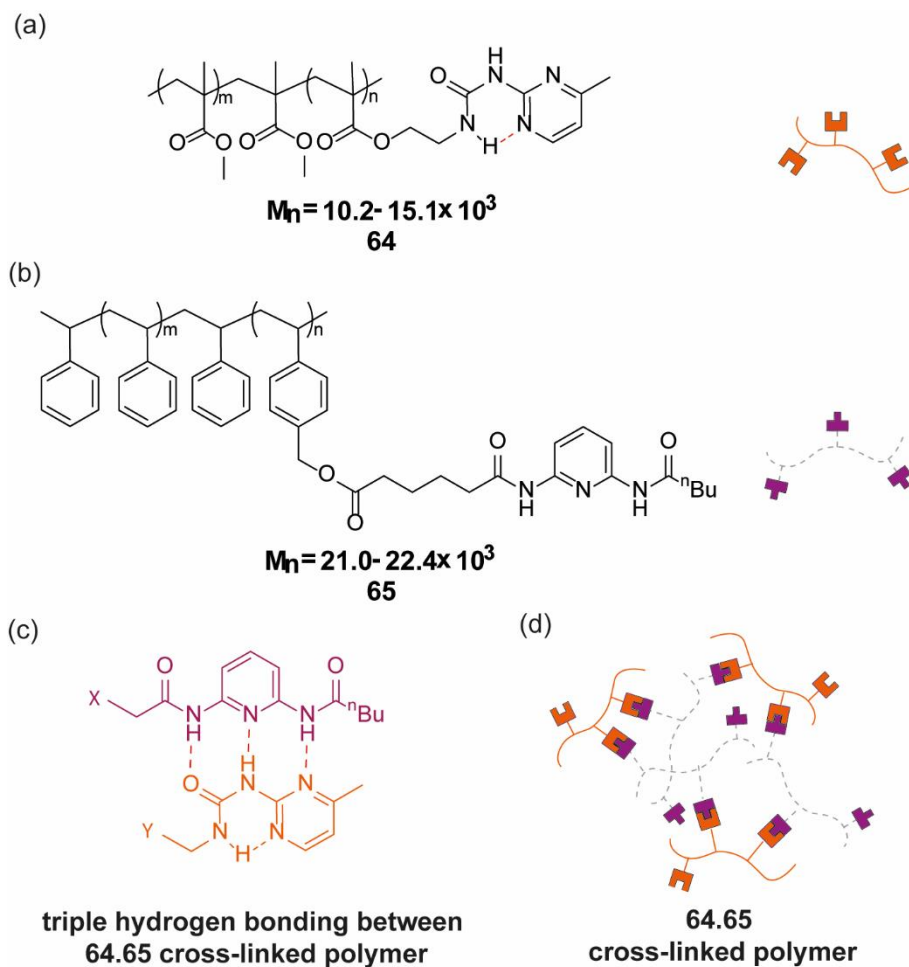


Figure 29. (a) ureidopyrimidine functionalised PMMA co-polymer 64, (b) diamidopyridine functionalised PS co-polymer 65, (c) triple hydrogen bonding interaction between ureidopyrimidine and diamidopyridine moieties of 64 and 65 co-polymers and (d) cross-linked polymer blend 64.65 with heterocomplementary interactions.

1.4 Conclusion and project aims

This thesis aims to utilise hydrogen bonding motifs and combine the areas of self-sorting and supramolecular polymers to create self-sorting supramolecular materials. Chapter 1 has introduced the topic of hydrogen bonding motifs and the factors that control their interactions with each other through literature examples. Additionally, the use of hydrogen bonding motifs in self-sorting supramolecular systems and supramolecular polymeric materials has been described with appropriate literature examples. The aim of Chapter 2 was to understand the pairwise interactions of six different hydrogen bonding motifs experimentally, using NMR spectroscopy, calorimetry and crystallography, and computationally, using density functional theory (DFT). And hence use this knowledge to development of series of sequential self-sorting pathways and networks. Chapter 3 focused on introducing reversibility to the sequential self-sorting pathways developed in Chapter 2. Here a responsive hydrogen bonding motif is created and it's ability to induce switching of self-sorted states in a network of complementary hydrogen bonding motifs was explored. Chapter 4 describes the efforts to syntheses and characterise supramolecular polymer blends capable of self-sorting with the potential to create self-sorting supramolecular materials. The objective was to first create a supramolecular polymer blend between two immiscible polymers (PMMA and polystyrene) via hydrogen bonding between side chains functionalised with two complementary triple hydrogen bonding motifs (UIM and AIC) respectively. Subsequently, the aim was to analysis the properties of this system in comparison to previously developed supramolecular polymer blends to confirm the strategy of hydrogen bonding

mediated blending is reliable. The long term aim to use the knowledge of the properties of these supramolecular blends to design self-sorting systems between orthogonally functionalised co-polymers, and hence self-sorting materials.

2. Sequential self-sorting of hydrogen bonding motifs

Nature has the ability to assemble multiple functional assemblies simultaneously, in defined locations, and, with temporal precision.⁴⁶ For example, in a cellular signaling cascade, individual proteins interact selectively with certain proteins during one stage of a cascade and then with different proteins at another stage, driven by protein expression levels and enzymatically manipulated post-translational modifications (PTMs).^{46,107} Regulatory control in a cellular context thus requires molecular recognition motifs capable of selective but adaptive recognition behaviour.^{46,108} In terms of biomimetic systems, that can reproduce these features, supramolecular assemblies employing multiple consecutive narcissistic and/or social integrative self-sorting^{109,110} events have been used to transition between well-defined – and, in some instances functional^{111,112} – complexes.^{59,60,113–116} The parallel assembly of different complexes and transitions to express different architectural complexity has also been demonstrated.¹¹¹ However, these multicomponent systems have typically relied on shape and geometrical complementary together with dative coordination bonds. In contrast, non-integrative systems capable of transitioning between different self-sorted configurations are less established, as is the exploitation of weaker interactions e.g. hydrogen-bonding set within the context of a recognition pattern of donors (*D*) and acceptors (*A*).¹ Achieving this objective is a fundamental challenge and more accurately mimics many of the bimolecular associations that control cellular processes including those that occur within the context of multicomponent protein assemblies (e.g. the binding of co-activators to transcription factor complexes).¹¹⁷

Previously, the Wilson group described a supramolecular system termed a self-sorting cascade;⁸¹ it exploited both orthogonal and promiscuous recognition behavior of linear arrays of hydrogen bonds to achieve sequential self-sorting depending on which components were present (Chapter 1, Figure 14). Comprising four different hydrogen bonding motifs: UIM, AIC, DAN, UPy, four rounds of self-sorting could be achieved with different complexes forming depending on the sequence in which the components were added to give DAN·UPy and AIC·UIM heterodimers (Figure 30 (a)). Furthermore, the transitions could be triggered, albeit irreversibly, using a light mediated reaction to unmask one of the hydrogen bonding motifs (AIC) (Figure 30 (b)), thus mimicking the process of post-translational regulation.

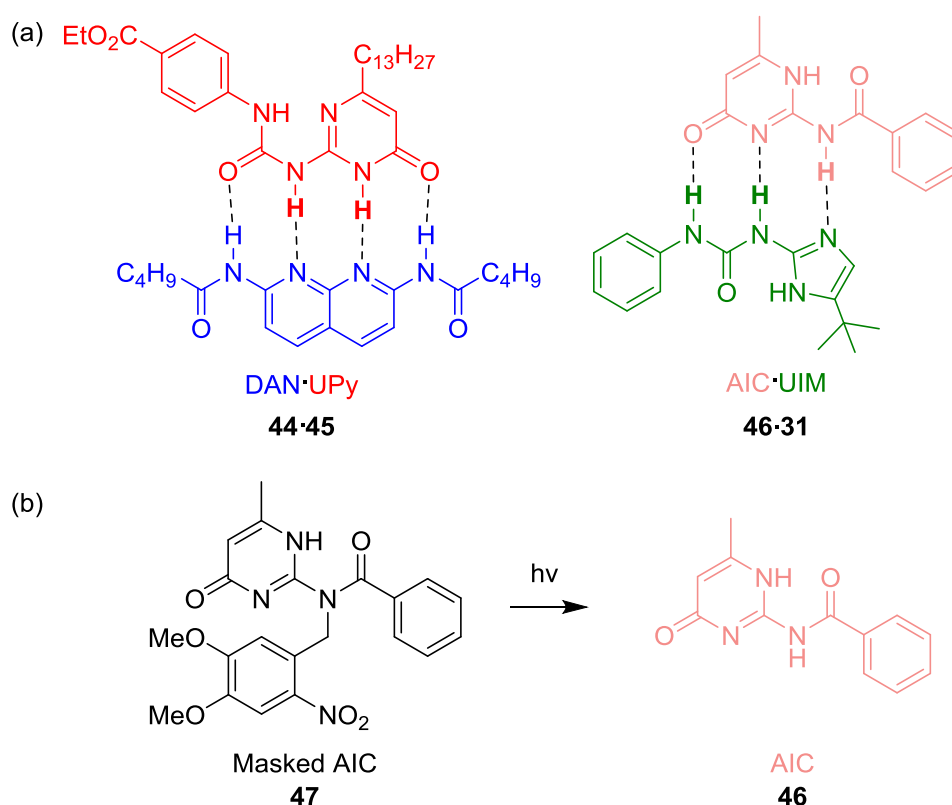


Figure 30. (a) Heterodimers formed in an equimolar mixture of UIM, AIC, DAN and UPy hydrogen bonding motifs and (b) phototriggered reaction used to unmask AIC.

This work focuses on understanding in greater detail the ability of linear arrays of hydrogen-bonds to self-sort using a combination of experimental (x-ray single crystal and ^1H NMR) and computational (DFT) methods. The aim was to extend the scope of the sequential self-sorting cascade to six components and construct pathways that operate in the presence of each other but with cross-talk, recapitulating a novel aspect of biological signaling, leading to the development of a self-sorting network.

To extend the scope of the self-sorting cascade previously reported involving UIM, AIC, DAN, UPy, initially the literature was examined and AUPy and NAPyO were identified as suitable hydrogen bonding motifs to be added.⁸¹ Prior work by Sijbesma and co-workers established dialkylaminoureidopyrimidinone (AUPy) motifs e.g. **66** and amidonaphthyridone (NAPyO) motifs e.g. **67** could be used to form alternating supramolecular copolymers through heterocomplexation, with tunable polymer composition.¹¹⁸ These building blocks were also shown to be self-complementary and thus displayed the low fidelity recognition behavior in the same way as ureidopyrimidinone (UPy) **45** as described previously. This variable recognition behavior, shown to arise through tautomeric and conformational change, is an essential requirement for the assembly of a sequential self-sorting pathway.⁴³ Equally the use of motifs such as diamidonaphthyridine (DAN) **44**, ureidoimidazole (UIM) **31** and amidoisocytosine (AIC) **46** with more restricted molecular recognition properties, enforced by a solitary arrangement of donors and acceptors in each case, is also considered necessary for effective assembly of a self-

sorting pathway. This combination of hydrogen bonding motifs with both high and low molecular recognition fidelity is essential for extending the scope of the sequential self-sorting pathway.

Figure 31 outlines the potential homodimers and heterodimers formed through three and four intermolecular bonds (dashed lines) between the six hydrogen bonding motifs studied. In the prior study, motifs **31**, **44**, **45** and **46** were shown to form a pair of tightly bound heterodimers **44·45** and **31·46** in chloroform, resulting in effective self-sorting. Therefore, this study commenced with a deeper analysis of the recognition properties of these compounds with an emphasis on their recognition with AUPy **66** and NAPyO **67**.

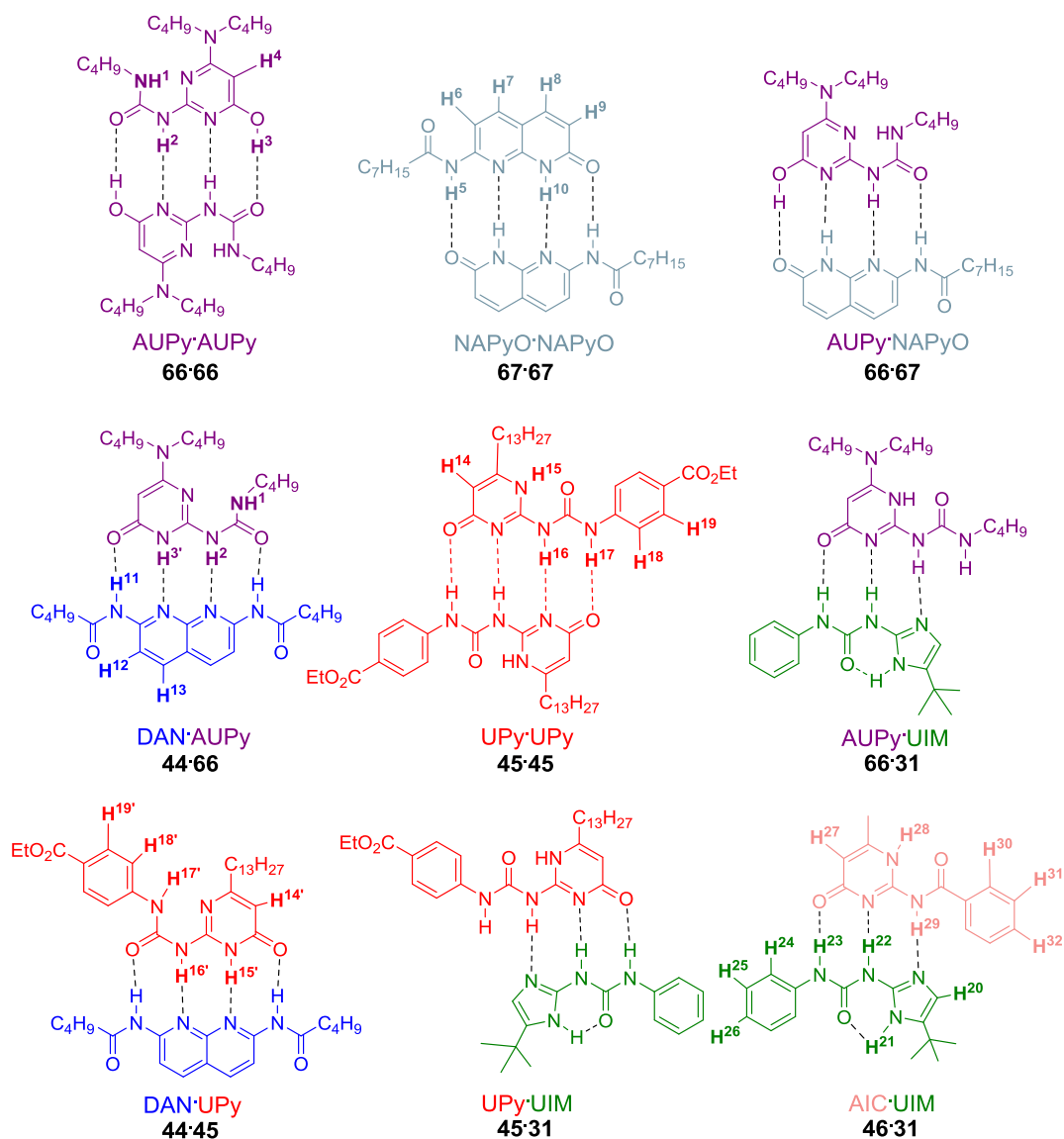
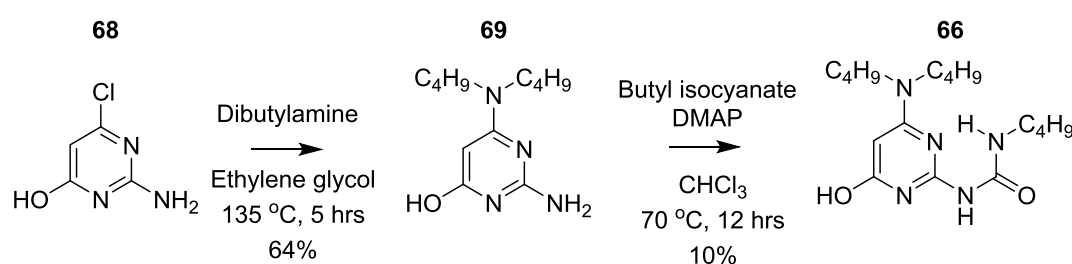


Figure 31. The lowest energy dimerisation interactions between the six linear hydrogen bonding motifs with dashed lines showing intermolecular hydrogen bonds.

2.1 Synthesis of Hydrogen Bonding Motifs

The synthesis of AUPy **66** was adapted from a previously described method by de Greef and co-workers (Scheme 2).¹¹⁹ For ease of synthesis and characterisation, as well as solubility in chloroform, **66** was synthesised with butyl chains, rather than the previously reported motif with a dodecyl carbon chain adjacent to the urea.



Scheme 2. The synthetic route for the preparation of AUPy 66.

Like UPy **45**, AUPy **66** has the potential to adopt at least five different tautomers/conformers (Figure 32 (a-e)), three of which present a quadruple hydrogen-bond array. A single crystal analysis confirmed that AUPy **66** forms a quadruple hydrogen-bonded homodimer **66-66** in the solid state; in this case, with the monomer adopting the *DADA* presenting tautomeric conformer (Figure 32 (f)). 1D and 2D NMR analysis of AUPy **66** in CDCl₃ suggests the *DADA* homodimer is also present in solution. Firstly in the ¹H NMR spectrum three resonances are shifted above 9 ppm suggesting hydrogen bonding protons. Additionally assignment of the resonances using 2D NMR experiments (see Appendix B for spectra) and in combination with previously reported structures indicated the *DADA* tautomer.

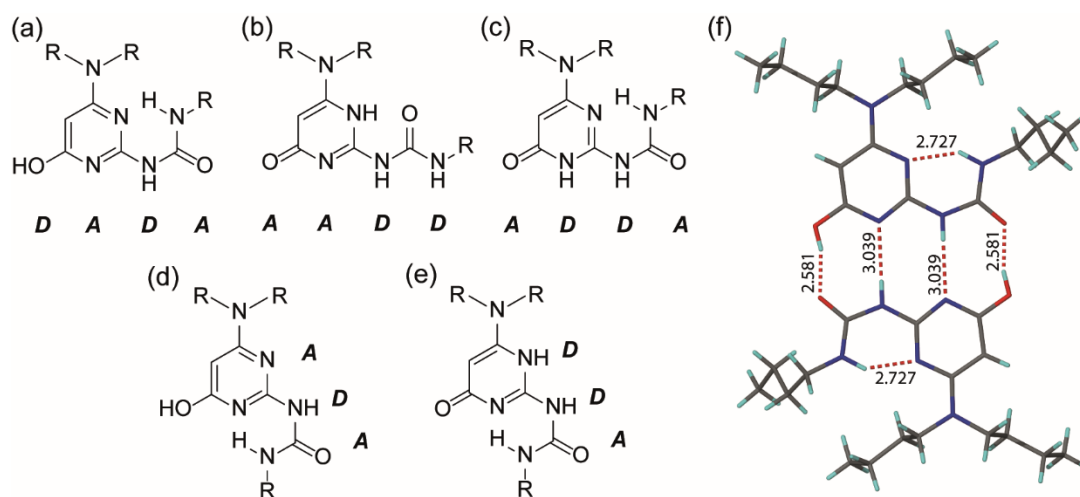
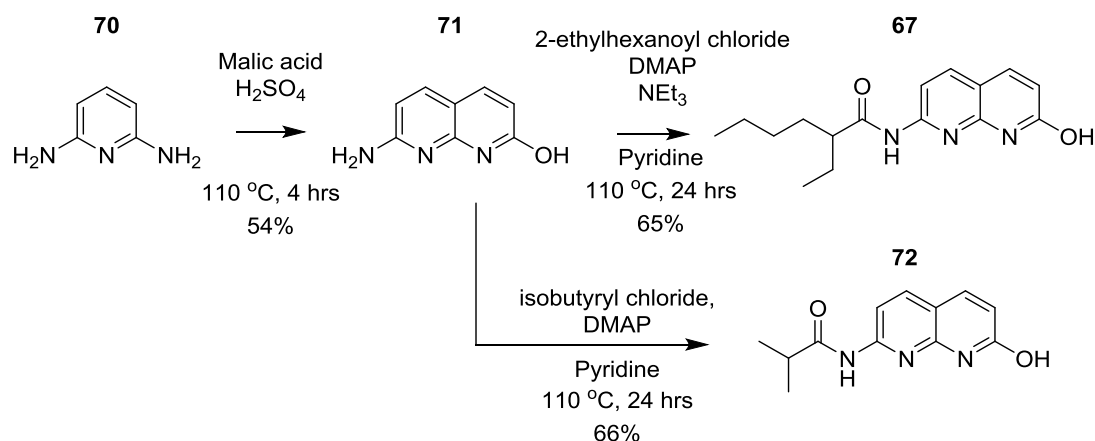


Figure 32. (a-e) Different tautomeric configurations and conformations accessible by linear hydrogen-bonding array AUPy 66 and (f) X-ray crystal structure of AUPy 66 homodimer (carbon is shown in grey, nitrogen in blue, oxygen in red, hydrogens in light blue and hydrogen bonds as dashed lines, with D...A distances shown in Å).

The synthesis of NAPyO **67** was achieved by the adaptation of previously described methods, ethyl hexanoyl was chosen as a suitable R group to ensure solubility in chloroform for NMR experiments (Scheme 3).^{118,120} Similarly to AUPy **66**, NAPyO **67** may feasibly access more than one tautomeric configurations (Figure 33(a-c)). Efforts were made to obtain an x-ray crystal structure of NAPyO **67** to confirm the preferred tautomer in the solid state. However, this was not possible with the ethyl hexanoyl analogue NAPyO **67** in the solvent systems tested, likely due to the chiral nature of the R group. Consequently, a less soluble isobutyryl analogue of NAPyO **72**, which was considered more susceptible to crystallisation, was synthesised (Scheme 3). It was possible to obtain a single x-ray crystal of this isobutyryl analogue of NAPyO **72**, which revealed a quadruple hydrogen-bonded homodimer **72·72** in which the monomer was present as the pyrimidinone tautomer resulting in a *DADA* array in the solid state (Figure 33d). As with AUPy **66**, NMR analysis and assignment of NAPyO **67** in CDCl₃ indicated the

DADA array is also present in solution (see Appendix B for representative 2D NMR spectrum).



Scheme 3. The synthetic route for the preparation of NAPyO 67 and NAPyO 72.

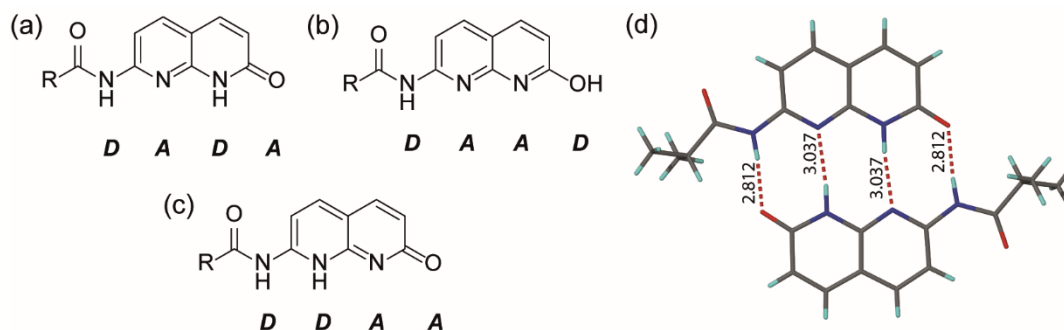
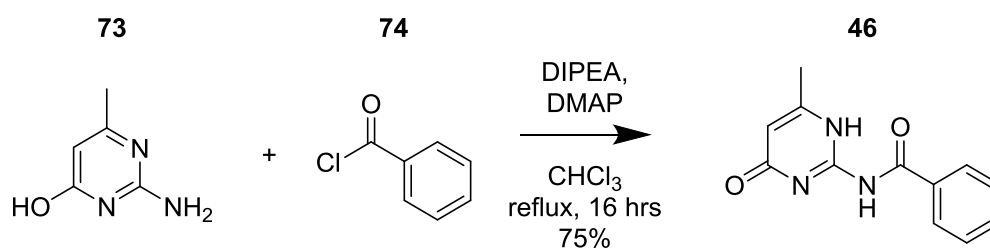
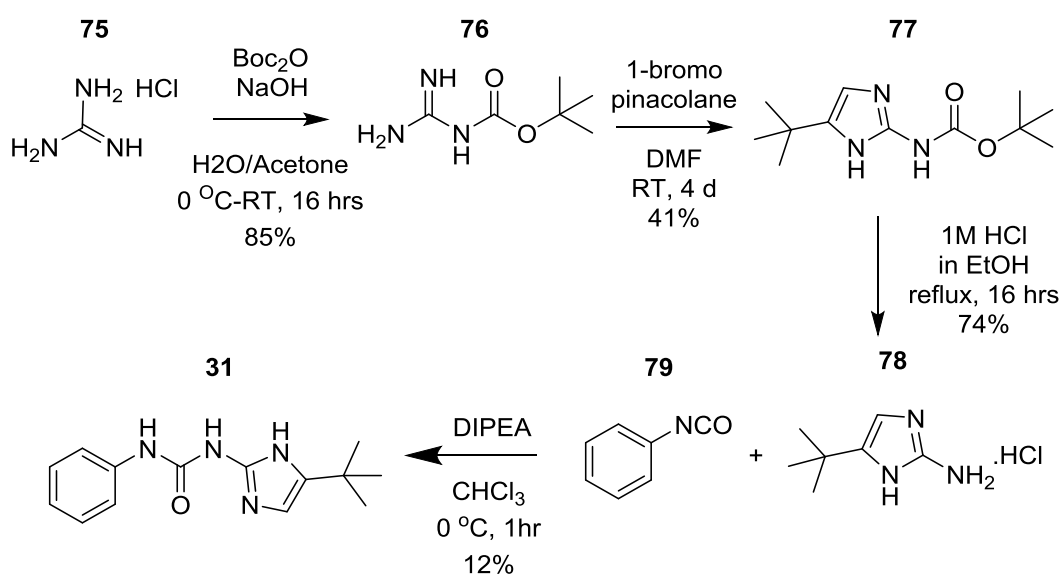


Figure 33. (a-c) Different tautomeric configurations and conformations accessible by linear hydrogen-bonding array NAPyO 67 and 72 and (d) X-ray crystal structure NAPyO 72 homodimer (carbon is shown in grey, nitrogen in blue, oxygen in red, hydrogens in light blue and hydrogen bonds as dashed lines, with D...A distances shown in Å).

Of the remaining hydrogen bonding motifs used in this study, DAN **44**¹²¹ and UPy **45** were provided by Dr Maria Pellizzaro, a former member of the group. AIC **46** was synthesised following the literature procedure outlined in Scheme 4.¹²² The synthesis of UIM **31** outlined in Scheme 5 was adapted slightly from the literature procedure as intermediate **78**, which was originally believed to be unstable, was isolated as a hydrochloride salt (refer to Chapter 3 on proton responsive behaviour for more details).¹²³



Scheme 4. The synthetic route for the preparation of AIC 46.



Scheme 5. The synthetic route for the preparation of UIM 31.

2.2 Analysing Pairwise Interactions

Prior to the creation of an extended sequential self-sorting pathway, the pairwise interactions of all the hydrogen bonding motifs needed to be well understood and characterised. ^1H NMR was selected as an appropriate technique to identify the dimerisation interactions between two hydrogen bonding motifs. CDCl_3 was chosen as the solvent for these studies, as an aprotic solvent CDCl_3 should not strongly influence hydrogen bonding between the species in solution. Hydrogen bonding induced chemical shifts were used to distinguish between the presence of homodimers and heterodimers in solution. ^1H NMR spectra of separate species were compared to the ^1H NMR spectrum of a 1:1 mixture of each species. Changes in the chemical shift of specific resonances in the mixture relative to the separate samples indicate a change in environment which can be inferred as a change in hydrogen bonding for these species. In this study the change in chemical shift was not quantified but it is clear from the range of 0.1-2.5 ppm, that the greater the change in environment the larger the change in the chemical shift. Additionally sharpening and broadening of specific resonances in a mixture relative to separate species can indicate if species are hydrogen bonding or in chemical exchange.

Initially, the interaction between the two additional components AUPy **66** and NAPyO **67** was investigated using ^1H NMR in CDCl_3 . The ^1H NMR resonances of separate samples of AUPy **66-66** and NAPyO **67-67** homodimers were compared to a 1:1 mixture of AUPy **66** and NAPyO **67** (Figure 34). The broadening of resonances along with small, yet notable, changes in the chemical shift of the NH resonances (H^1 and H^5) and aromatic CH resonance

H⁹ relative to the homodimers were indicative of complex formation and consistent with reported interactions.¹¹⁸ Attempted 2D ¹H-¹H NOESY analyses were confounded by the presence of exchange peaks for NH/OH resonances, preventing a more in depth structural interpretation, although such exchange peaks are entirely consistent with an interaction between AUPy **66** and NAPyO **67**.

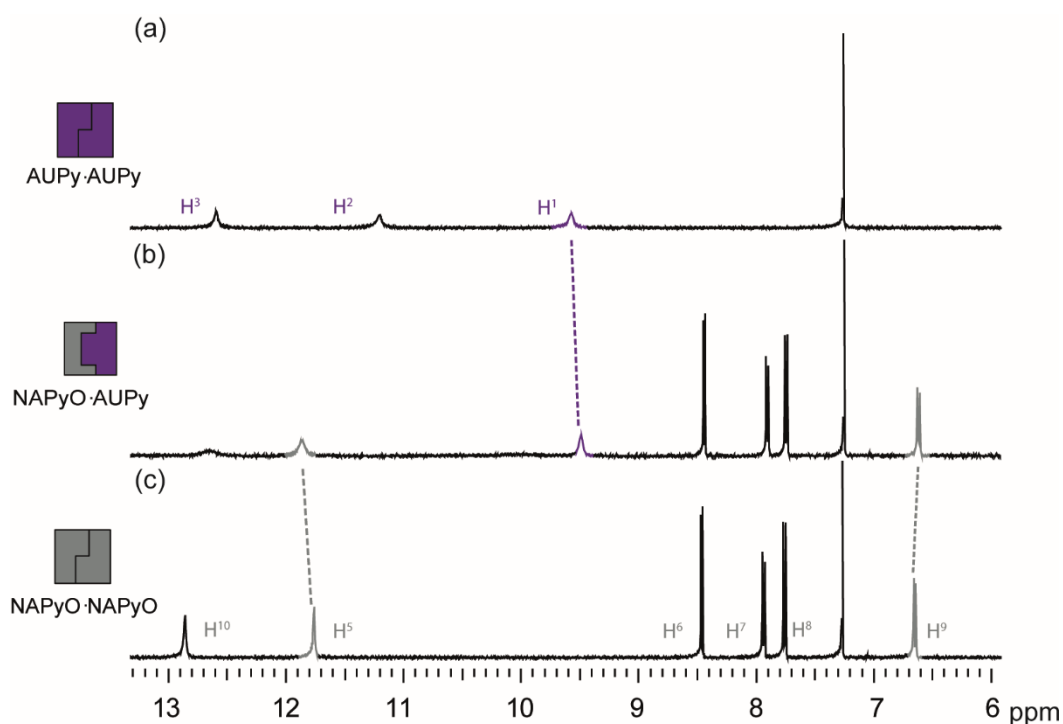


Figure 34. ¹H NMR (500 MHz, 10 mM, CDCl₃) for (a) AUPy **66-66**, (b) 1:1 NAPyO-AUPy **66-67** and (c) NAPyO **67-67**. Refer to Figure 31 for the resonance assignment and chemical structure.

To further confirm the presence of a heterodimer, variable temperature (VT) NMR analyses were performed (Figure 35). As the temperature was reduced from 277K to 244K, the broad NH/OH resonances in the region 9-15 ppm sharpened and split to reveal additional resonances consistent with the presence of homodimers of AUPy **66-66** and NAPyO **67-67** as well as AUPy·NAPyO **66-67** heterodimer as the dominant species; at 253 K the ratio

of homodimer:heterodimer was observed to be 1:2. This indicates fast exchange between homodimers **66-66/67-67** and heterodimer **66-67** at room temperature. This is a property that is useful in the context of the sequential self-sorting pathways and network discussed later, in that recognition simply needs to translate into a response e.g. a signal change and not necessarily diagnostic resonances associated with particular complexes.

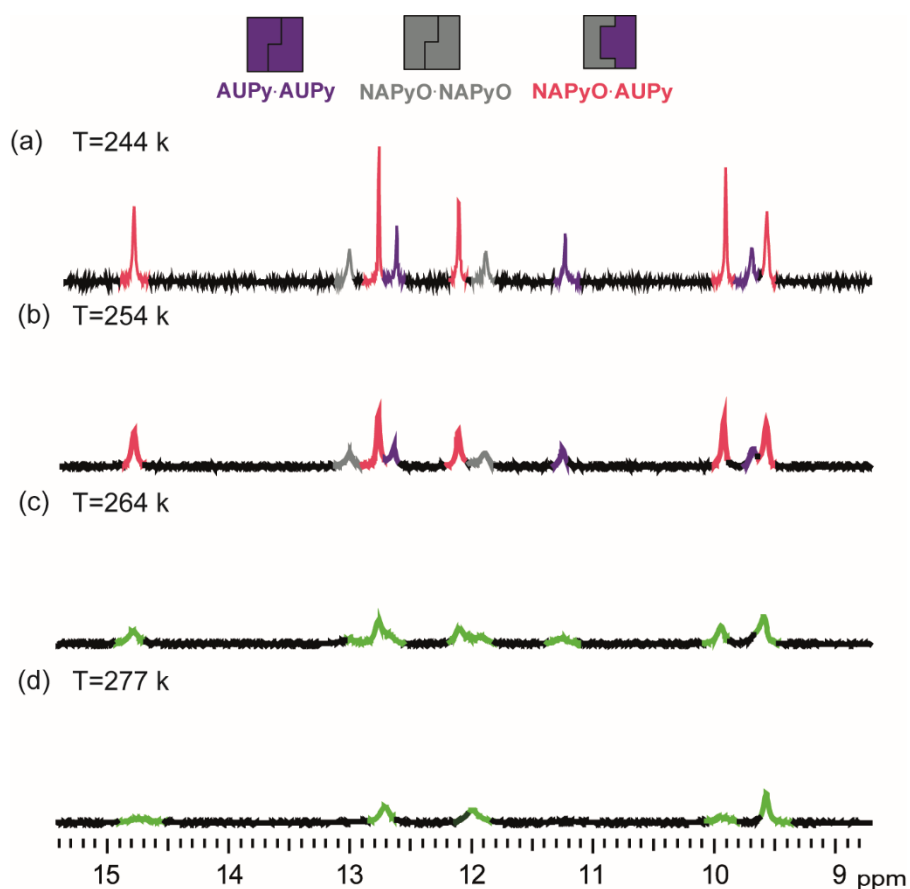


Figure 35. Variable temperature ^1H NMR (500 MHz, 10 mM, CDCl_3) of 1:1 AUPy 66 and NAPyO 67 at (a) 244 K (b) 254 K (c) 264 K (d) 277 K. Resonances colour code; green = mixture of complexes, purple = AUPy homodimer 66-66, grey = NAPyO homodimer 67-67, pink = AUPy-NAPyO 66-67 heterodimer.

To further understand the observations gleaned from ^1H NMR analyses, computational analyses were carried out in collaboration with Stephanie van der Lubbe and Prof. Dr. Célia Fonseca Guerra from Vrije Universiteit

Amsterdam. Stephanie computed the Gibbs free energies of dimerisation (ΔG) at the BLYP-D3(BJ)/TZ2P¹²⁴⁻¹²⁷ level of theory by applying Amsterdam Density Functional (ADF) 2017.108¹²⁸ with implicit chloroform solvation at 298K. To make the calculations viable, the R groups of all the monomers were replaced by hydrogens. By comparison of the calculated monomers and dimers to reported crystal structures, as well as literature precedent, it was concluded the appropriate level of theory was used for the system to accurately represent the strength and length of hydrogen bonds.¹²⁹ Solvent effects were accounted for by using the implicit conductor-like screening model (COSMO), in which the solute molecule is surrounded by a dielectric medium.¹³⁰ The Gibbs free energies for the AUPy **66-66** and NAPyO **67-67** homodimers were -2.2 and -3.5 kcal mol⁻¹ respectively (Table 2). The lowest energy AUPy-NAPyO **66-67** heterodimer was seen for the *ADAD-DADA* interacting array with a Gibbs free energy of -2.3 kcal mol⁻¹ (Figure 36). Hence the dimerisation energy of the AUPy **66-66** homodimer is close to that of the AUPy-NAPyO **66-67** heterodimer, which is consistent with experimental observations of a mixture of homodimers and heterodimer at room temperature.

Hydrogen Bonding Motif	Interacting Array	ΔG (kcal mol ⁻¹)
<i>Homodimers</i>		
AUPy	<i>ADAD*</i>	-2.2
AUPy	<i>AADD</i>	0.6
UPy	<i>ADAD</i>	-2.6
UPy	<i>AADD*</i>	-6.9
NAPyO	<i>ADAD*</i>	-3.5
NAPyO	<i>AADD</i>	7.4
<i>Heterodimers</i>		
AUPy·DAN	<i>ADDA·DAAD*</i>	-5.0
UPy·DAN	<i>ADDA·DAAD*</i>	-4.8
AUPy·NAPyO	<i>ADAD·DADA*</i>	-2.3
AUPy·NAPyO	<i>AADD·DDAA</i>	4.1
AUPy·NAPyO	<i>ADDA·DAAD</i>	0.0
UPy·NAPyO	<i>ADAD·DADA</i>	-2.6
UPy·NAPyO	<i>AADD·DDAA</i>	0.8
UPy·NAPyO	<i>ADDA·DAAD</i>	0.5
AUPy·UPy	<i>ADAD·DADA</i>	-2.4
AUPy·UPy	<i>AADD·DDAA</i>	-3.1

Table 2. The Gibbs free energies computed for all dimerisation interactions with implicit chloroform solvation at the BLYP-D3(BJ)/TZ2P level of theory (* denotes the interacting array of dimers seen experimentally).

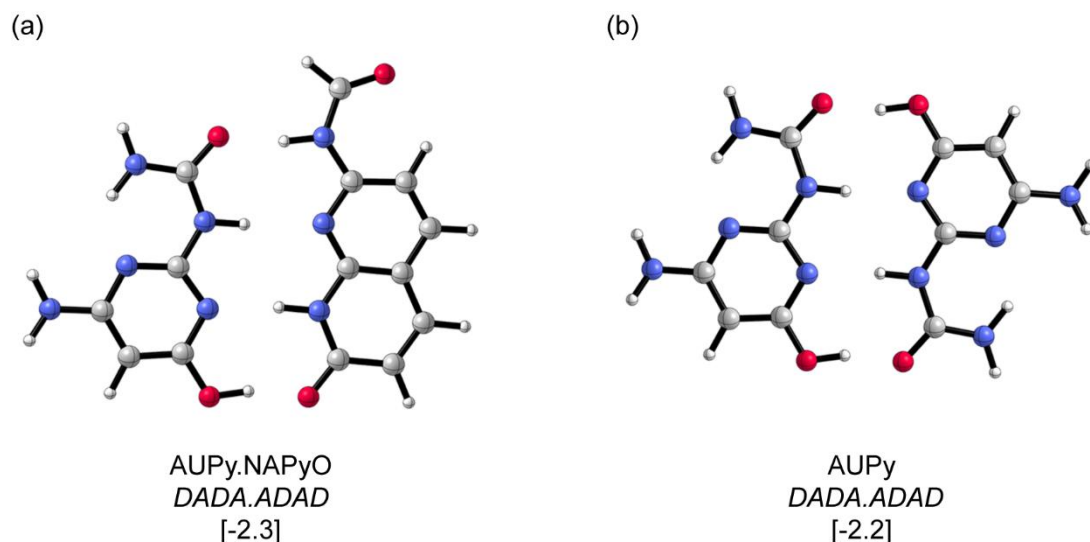


Figure 36. Optimised dimer interactions and their Gibbs free energies between brackets [in kcal mol⁻¹] of (a) AUPy-NAPyO 66-67 heterodimer (*DADA·ADAD*) and (b) AUPy 66-66 homodimer (*DADA·ADAD*) with respect to their most stable tautomer *ADDA* (without alkyl chains). Computed at the BLYP-D3(BJ)/TZ2P level of theory (illustrations produced using CYLview)¹³¹.

Next, the interactions of AUPy **66** and NAPyO **67** with UPy **45** were examined. Previous studies have highlighted the promiscuous nature of UPy **45** to interact through several hydrogen bonding arrays.^{81,119} Surprisingly, ¹H NMR suggested there was no significant interaction of UPy **45** with AUPy **66** in a 1:1 mixture, illustrated by no change in chemical shift of diagnostic resonances of the 1:1 mixture compared to individual samples (Figure 37). The transient formation of AUPy-UPy (**66-45**), as described previously in toluene-*d*₈, was not observed on the timescale the NMR experiment was carried out.¹¹⁹ The formation of AUPy-UPy (**66-45**) was previously reported after 18 seconds, however it was not possible to acquire data on this timescale with the spectrometer used, consequently each sample was allowed to equilibrate for a minimum of ten minutes.

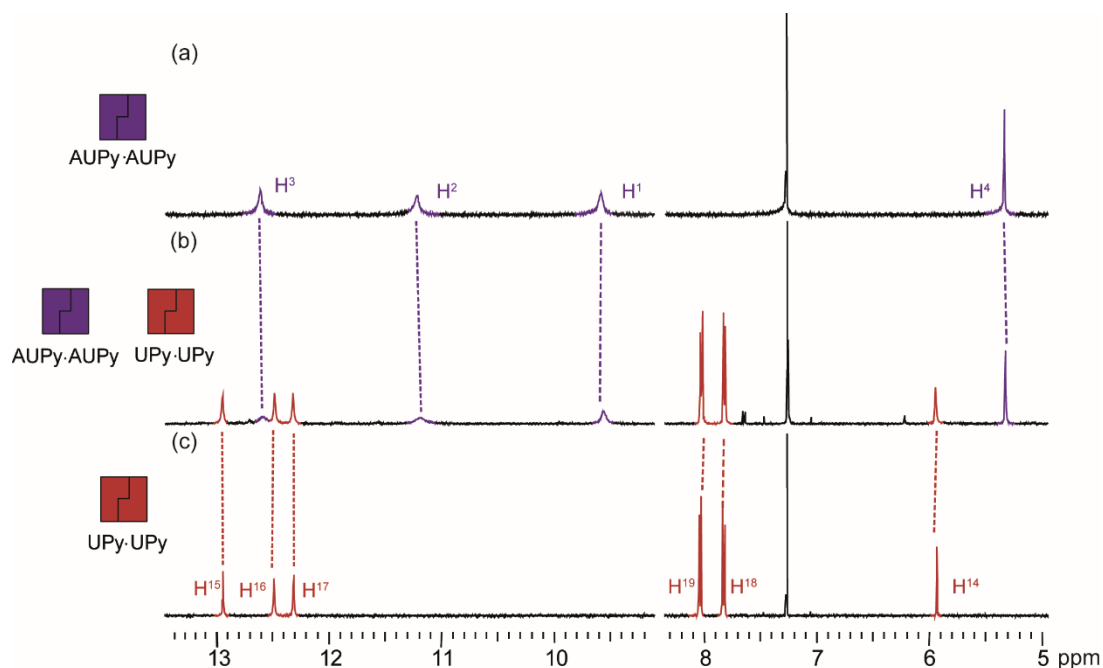


Figure 37. ¹H NMR (500 MHz, 10 mM, CDCl₃) for (a) AUPy 66-66, (b) 1:1 AUPy 66-66 and UPy 45-45 and (c) UPy 45-45. Refer to Figure 31 for the resonance assignment and chemical structure.

For the ¹H NMR of a 1:1 mixture of UPy **45** with NAPyO **67**, there were no significant changes in chemical shifts observed for the resonances associated with UPy **45**, but there were subtle changes in the NH resonances (H⁵ and H¹⁰) of NAPyO **67** (Figure 38). Hence, a variable temperature ¹H NMR analysis of a 1:1 mixture of NAPyO **67** and UPy **45** was carried out. Upon cooling the sample, no changes in the resonances were observed further confirming narcissistic self-sorting (Figure 39). Thus, UPy **45** remained as homodimer **45-45** and did not show heterodimer interactions with AUPy (66-45) or NAPyO (67-45).

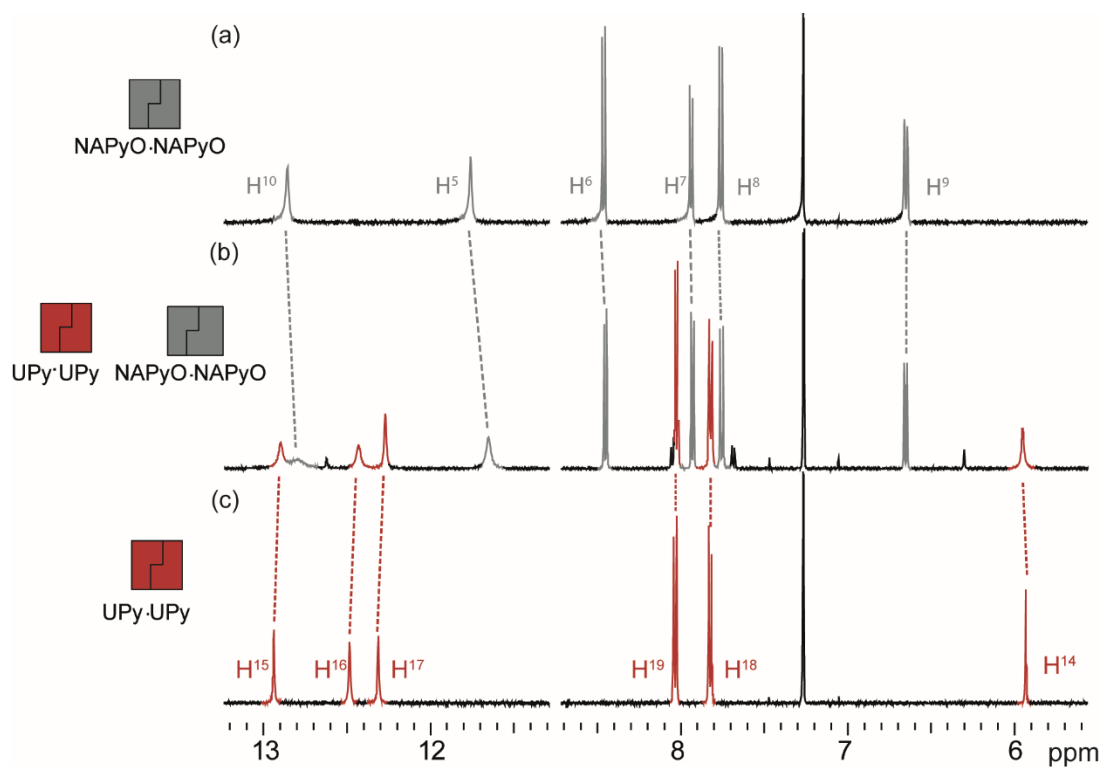


Figure 38. ¹H NMR (500 MHz, 10 mM, CDCl₃) for (a) NAPyO 67-67, (b) 1:1 NAPyO-UPy 67-45 and (c) UPy 45-45. Refer to Figure 31 for the resonance assignment and chemical structure.

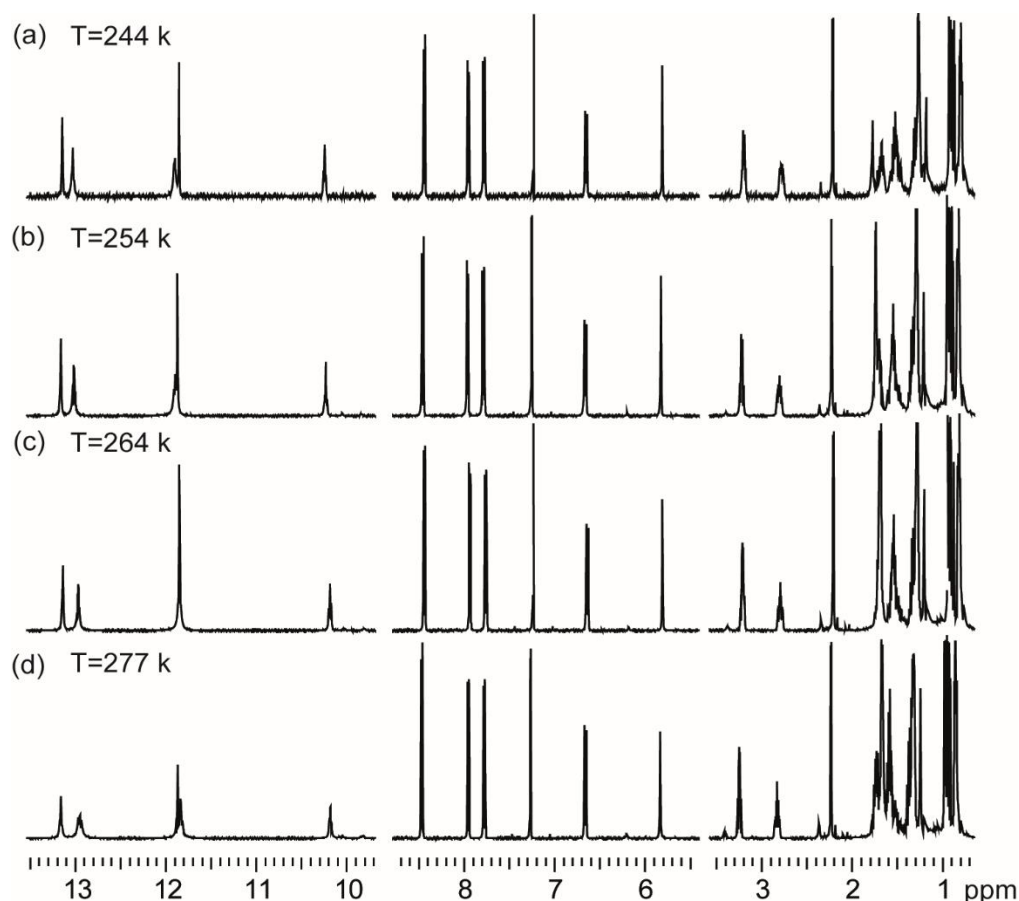


Figure 39. Variable temperature ^1H NMR (500 MHz, 10 mM, CDCl_3) of 1:1 NAPyO **67 and UPy **45** at (a) 244 K (b) 254 K (c) 264 K (d) 277 K.**

Taken together, these observations raised the following interesting points: (i) AUPy **66** has a preference to adopt a *DADA* pyrimidinol tautomer in the homodimer in contrast to the extensively observed *DDAA* pyrimidinone tautomer seen for UPy **45** and (ii) AUPy **66** has the ability to form a heterodimer with NAPyO **67** whereas UPy **45** does not. To investigate these observations further, DFT calculations were carried out (in collaboration as discussed above). The preference of the homodimers of AUPy **66** to adopt a *DADA* pyrimidinol tautomer and UPy **45** to adopt a *DDAA* pyrimidinone tautomer can be explained simply in terms of the lowest calculated ΔG . The lowest energy homodimer of AUPy **66** has a ΔG value of $-2.2 \text{ kcal mol}^{-1}$ for the *DADA* tautomer whereas the *DDAA* tautomer is $0.6 \text{ kcal mol}^{-1}$. Conversely,

the *DADA* tautomer of UPy **45** has a ΔG value of $-2.6 \text{ kcal mol}^{-1}$ compared the lowest energy *DDAA* tautomer with ΔG value of $-6.9 \text{ kcal mol}^{-1}$. To understand why this preference occurred, the molecular basis for the tautomeric difference between AUPy and UPy was assessed. Naturally, the secondary electrostatic model proposed by Jorgensen²⁶ and verified by Zimmerman¹³² dictates that the *DDAA* array should be a higher affinity interaction than the *DADA* array, but nevertheless the *DADA* tautomer is preferred by AUPy **66-66**. The DFT calculations revealed that this is caused by the differences in tautomerisation energy ΔG_{taut} . For this, Voronoi deformation density (VDD) was applied to the different tautomers of AUPy **66** and UPy **45** (Figure 40).¹³³ By the comparison of AUPy **66** and UPy **45**, in terms of the substitution at position 4 of the pyrimidinone/pyrimidinol ring, it can be seen that the NR_2 group of AUPy **66** is more electron donating than the R group of UPy **45**. This is reflected by the VDD charges (red squares), which are more positive for AUPy than for UPy. This flow of electron density is favourable for the *ADDA* and *DADA* tautomers, because the hydrogen bond acceptor atoms N (blue squares) become more negatively charged. On the other hand, the same flow of electron density has a destabilising effect in the *DDAA* conformation, because the NH hydrogen bond donating groups become less positively charged. Since these stabilising (*ADDA* and *DADA*) and destabilising (*DDAA*) effects are more pronounced when $\text{R}=\text{NH}_2$ (AUPy **66**) compared to when $\text{R}=\text{H}$ (UPy **45**), the energetic differences between the AUPy tautomers are larger than the energetic differences of the UPy tautomers. Consequently, the tautomerisation energy (energetic penalty) is larger for AUPy to adopt *DDAA*, which explains why AUPy forms *DADA* homodimers while UPy forms *DDAA* homodimers.

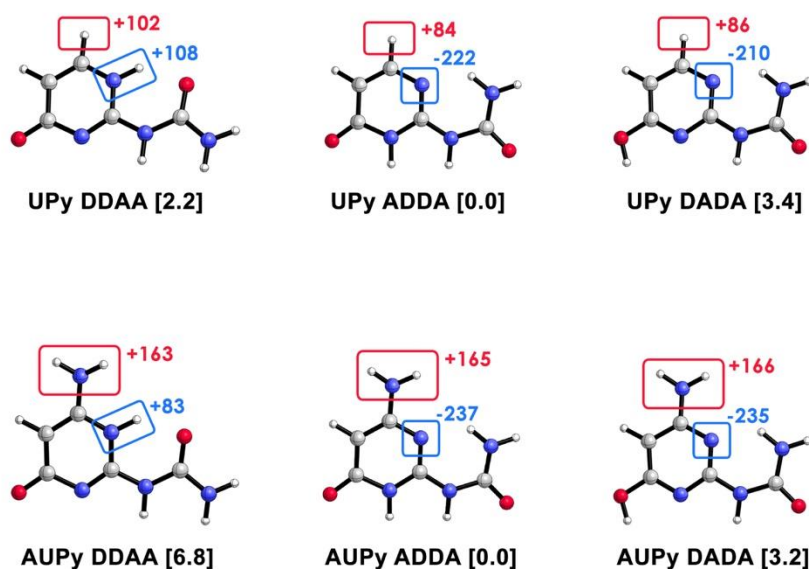


Figure 40. UPy and AUPy tautomers and their Gibbs free energies between brackets [in kcal mol⁻¹] with respect to their most stable tautomer *ADDA* and the relevant Voronoi deformation density (VDD) charges [in me⁻], computed at the BLYP-D3(BJ)/TZ2P level of theory (illustrations produced using CYLview)¹³¹.

When considering the second point as to why AUPy forms heterodimers but UPy does not, the ΔG values of all the possible dimers were compared (Table 2). These showed the most stable UPy **45-45** and AUPy **66-66** homodimers to have a ΔG of -6.9 and -2.2 kcal mol⁻¹, while the most stable UPy-AUPy **45-66**, UPy-NAPyO **45-67** and AUPy-NAPyO **66-67** heterodimers have ΔG values of -3.1, -2.6 and -2.3 kcal mol⁻¹, respectively (Figure 41). Hence, the dimerisation energy of UPy (i.e. to form **45-45**) is considerably stronger than the potential heterodimers (**66-45** and **67-45**) so UPy prefers to remain as a homodimer. Whereas, the difference in ΔG between the AUPy (**66-66**) homodimer and AUPy-NAPyO (**66-67**) heterodimer is very small (possibly within experimental error considering the simplification of molecules) explaining why AUPy can form heterodimers.

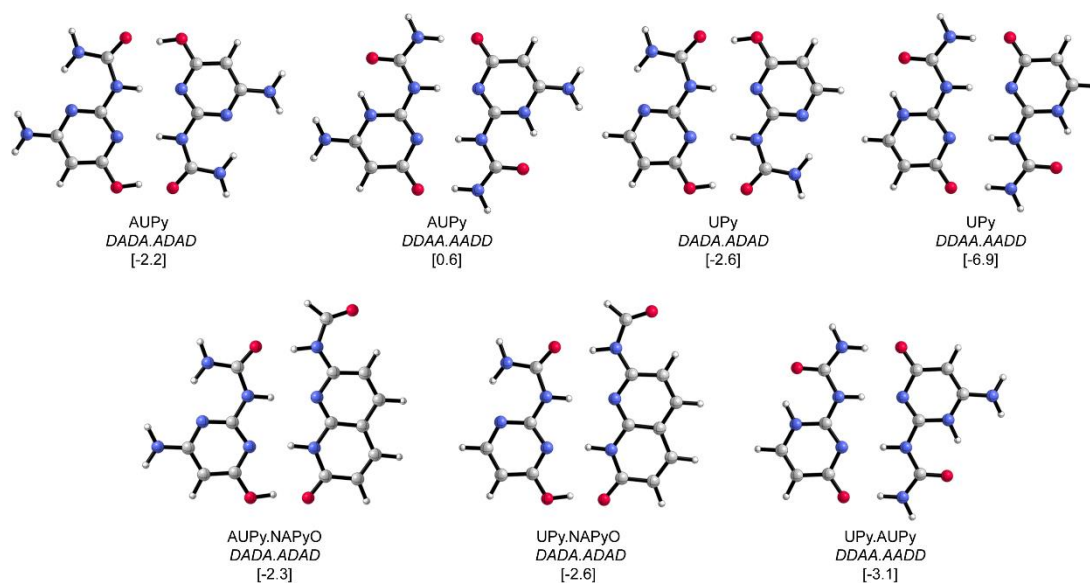


Figure 41. Optimised dimer interactions of AUPy, UPy and NAPyO, their Gibbs free energies between brackets [in kcal mol⁻¹] with respect to their most stable tautomer *ADDA*. Computed at the BLYP-D3(BJ)/TZ2P level of theory (illustrations produced using CYLview)¹³¹.

The interactions of the additional components, AUPy **66** and NAPyO **67**, with DAN **44**, presenting only a *DAAD* arrangement of hydrogen bonding functionalities, were then characterised. ¹H NMR analyses on 1:1 mixtures of NAPyO **67** and DAN **44** demonstrated no interaction as expected, given the incompatible linear arrays. In contrast, ¹H NMR analyses on a 1:1 mixture of AUPy **66** and DAN **44** indicated heterodimer **66-44** formation (Figure 42). The NH resonance of DAN **44** (H¹¹) shifts downfield significantly and broaden in comparison to the isolated sample of DAN **44**. Additionally, a change in chemical shifts of the CH on the imidazole ring (H⁴) and NH resonances (H¹, H² and H³) of AUPy **66** was also observed. A similar observation is made for ¹H NMR analysis of the formation of heterodimer **44-45** (Figure 43).⁸¹ Again,

the NH resonance of DAN **44** (H^{11}) shifts downfield significantly and there is a change in chemical shift for resonances H^{14-19} of UPy **45**.

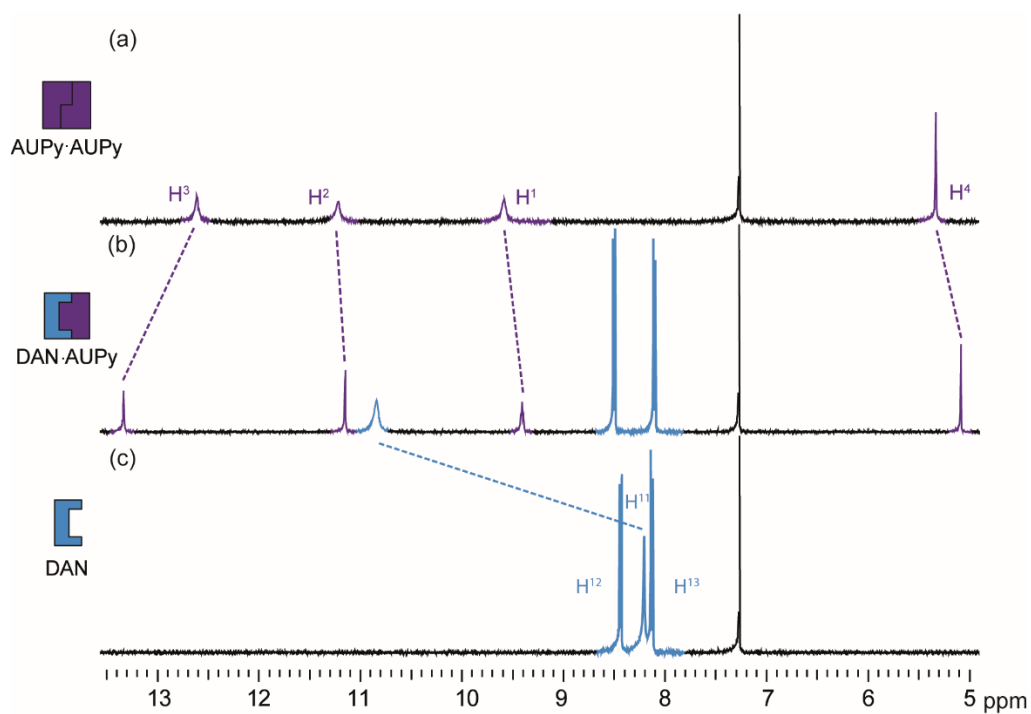


Figure 42. ^1H NMR (500 MHz, 10 mM, CDCl_3) for (a) AUPy 66-66, (b) 1:1 AUPy-DAN 66-44 and (c) DAN 44. Refer to Figure 31 for the resonance assignment and chemical structure.

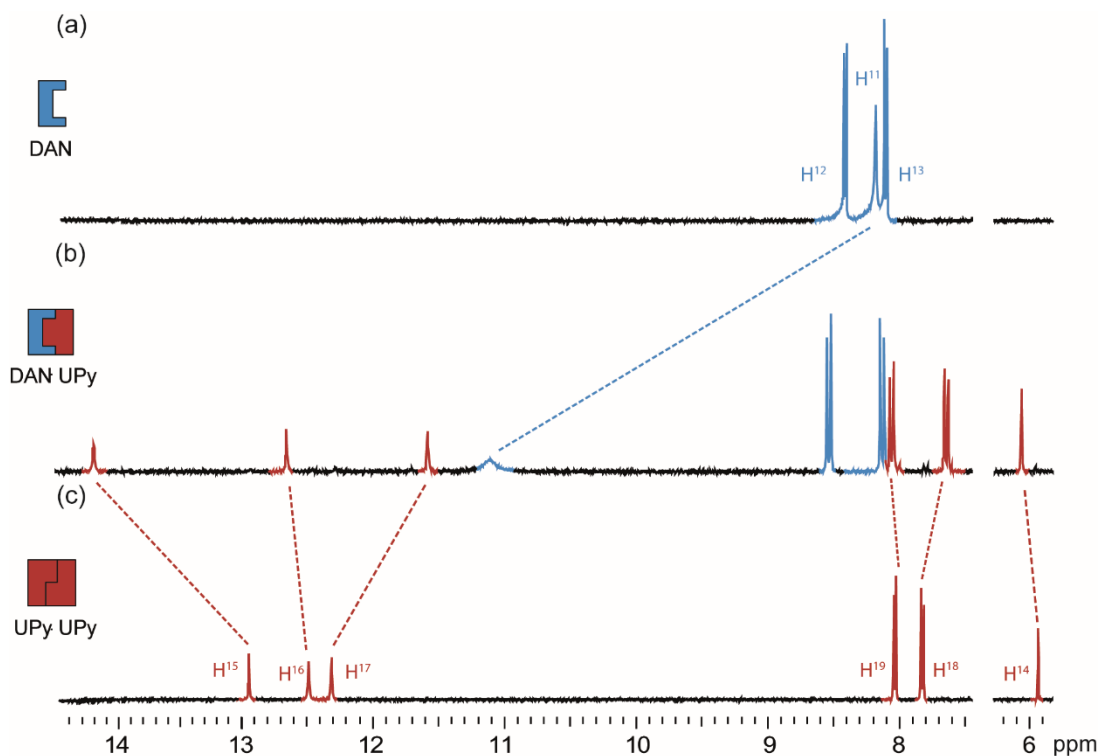


Figure 43. ^1H NMR (500 MHz, 10 mM, CDCl_3) for (a) DAN 44, (b) 1:1 DAN-UPy 44-45 and (c) UPy 45-45. Refer to Figure 31 for the resonance assignment and chemical structure.

2D ^1H - ^1H NOESY analyses also supported the formation of a heterodimer with NOE cross peaks between NH resonances of both AUPy 66 and DAN 44 (Figure 44). The grey circles in Figure 44 highlight the NOE interactions seen between H³-H¹¹ and H²-H¹¹ which are as expected for the AUPy·DAN 66·44 heterodimer.

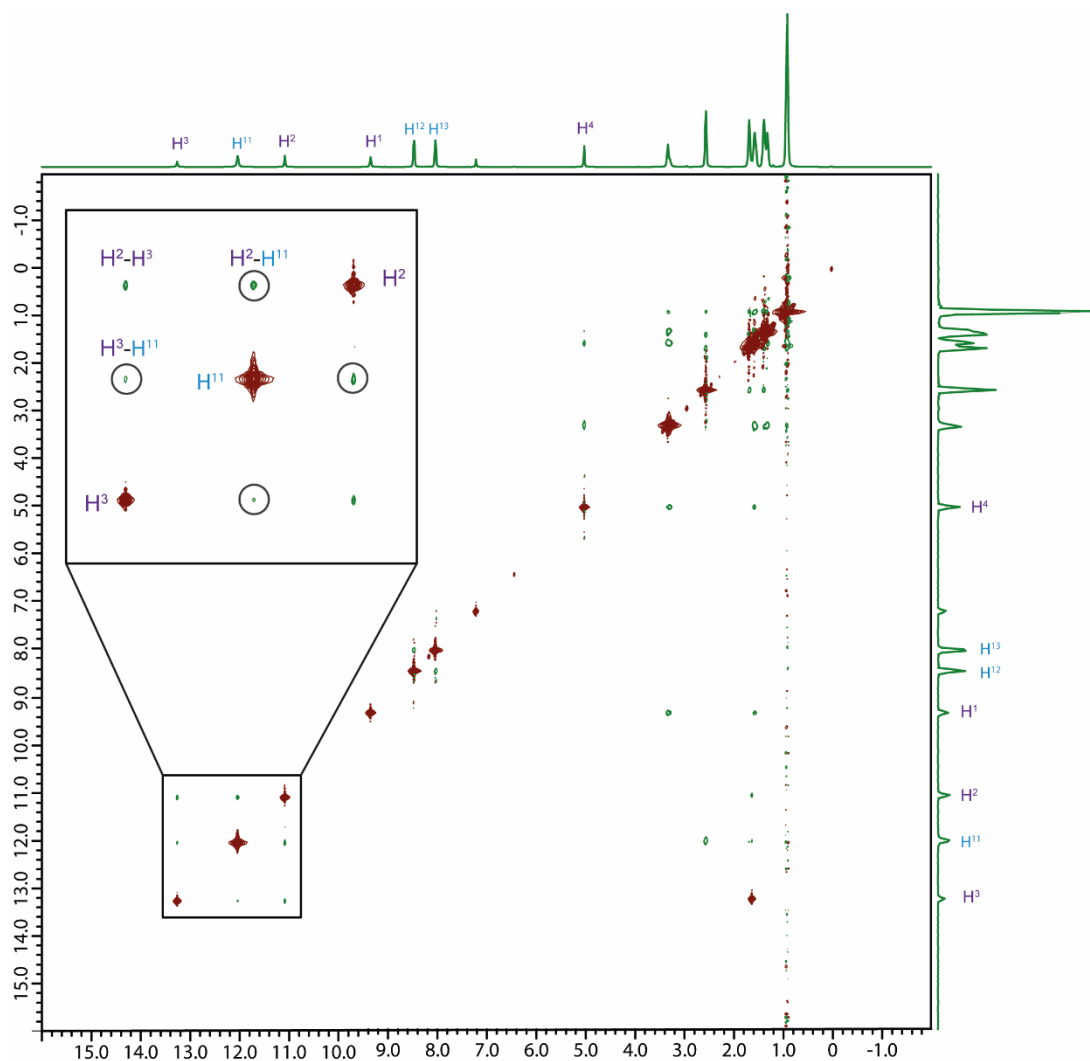


Figure 44. 2D ^1H - ^1H NOESY NMR (600 MHz, 50 mM, CDCl_3 , 278 k) for 1:1 AUPy-DAN 66-44. Green cross-peaks show NOE interactions and red cross-peaks show EXSY interactions. Grey circles highlight the NOE cross peaks between NH resonances of AUPy and DAN (H^3 - H^{11} and H^2 - H^{11}). Refer to Figure 31 for the resonance assignment and chemical structure.

Isothermal titration calorimetry is a technique typically used to measure the interactions of biomolecules. It directly measures the heat that is either released or absorbed during a biomolecular binding event. Measuring this heat transfer enables accurate determination of binding constants (K_a), reaction stoichiometry (n), enthalpy (ΔH) and entropy (ΔS).¹³⁴ In this study, isothermal titration calorimetry (ITC) was used to confirm a strong interaction

between AUPy **66** and DAN **44** with an association constant of $K_a=10^6 \text{ M}^{-1}$ in chloroform (Figure 45). The change in heat was measured during the gradual addition of DAN **44** (1 mM) into AUPy **66** (0.1 mM) resulting in a series of peaks until saturation was reached (Figure 45 (a)). Origin fitting software was then used to integrate the area of each peak and plot it against the molar ratio of the two components revealing a 1:1 binding and the K_a (Figure 45 (b)).

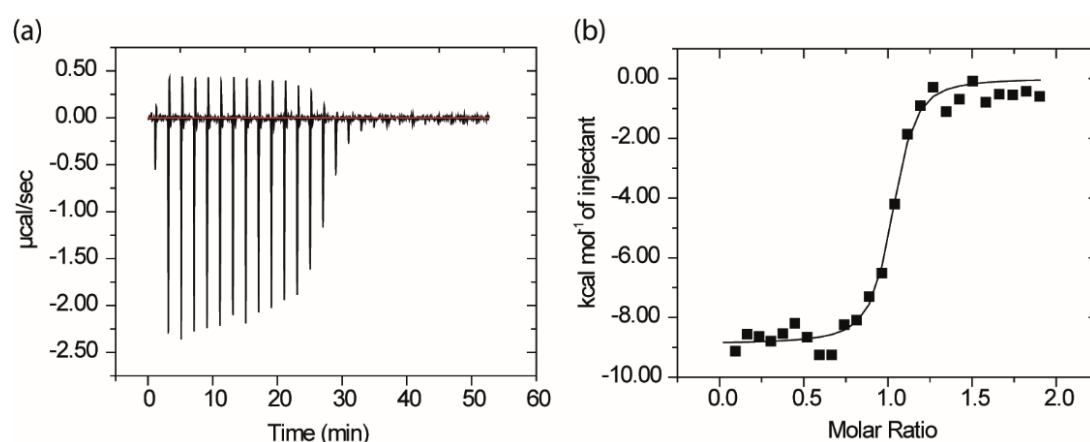
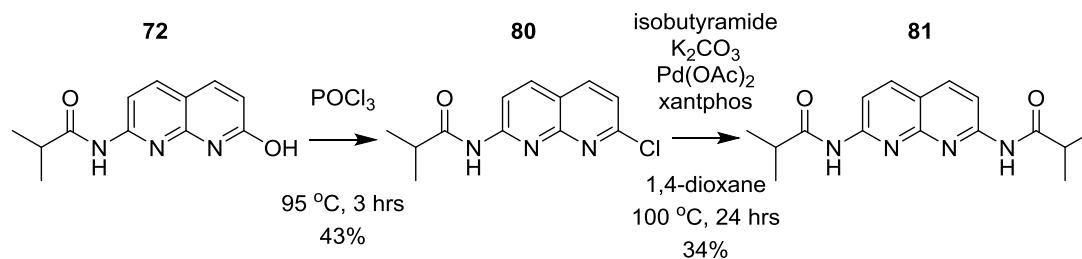


Figure 45. (a) ITC thermograms and (b) binding isotherm for the addition of a solution of DAN **44 (1 mM) into AUPy **66** (0.1 mM) in CHCl_3 .**

Attempts to crystallise the AUPy-DAN **66-44** heterodimer were unsuccessful in the tested solvent systems; nevertheless, it was possible to isolate a single crystal of AUPy **66** interacting with an isobutyryl analogue of DAN **81**. The synthesis of isobutyryl analogue of DAN **81** is outlined in Scheme 6. Chlorination of NAPyO **72** using phosphorus oxychloride gave **80**. The subsequent reaction with isobutyramide in the presence of palladium acetate, potassium carbonate and xantphos to give **81** via a Buchwald-Hartwig amidation reaction. X-ray diffraction of the co-crystal revealed the anticipated *ADDA*·*DAAD* **66-81** heterodimer interaction (Figure 46).



Scheme 6. The synthetic route for the preparation of DAN (isobutyryl analogue) 81.

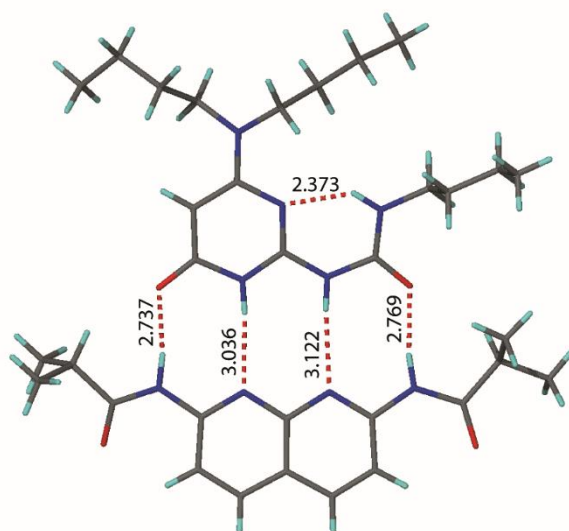


Figure 46. Single crystal structure of AUPy-DAN 66-81 heterodimer (carbon is shown in grey, nitrogen in blue, oxygen in red, hydrogens in light blue and hydrogen bonds as dashed lines, with D...A distances shown in Å).

The final novel pairwise interaction identified was between AUPy **66** and UIM **31**. In the 1:1 mixture small downfield shifts of the aromatic resonances (H²⁴⁻²⁶) of UIM **31** were observed as well as the broadening of NH resonances (H¹⁻³) of AUPy **66** (Figure 47). This is consistent with the changes in chemical shifts observed on the formation of the UPy·UIM **45·31** heterodimer previously reported (Figure 48).⁸¹ On the formation of UPy·UIM **45·31** heterodimer aromatic resonances (H²⁴⁻²⁶) of UIM **31** also shift downfield and NH

resonances (H^{15-17}) of UPy **45** broaden. Additionally, a diagnostic shift and broadening is observed for the aromatic H^{18} resonance of UPy **45**. No heterodimer interactions were observed by 1H NMR between NAPyO and UIM or AIC as well as between AUPy and AIC. This was not a surprising observation, considering of the mismatch configuration donor and acceptors in the hydrogen bonding arrays and the small association energies of related dimers, previously reported in the literature.⁸¹

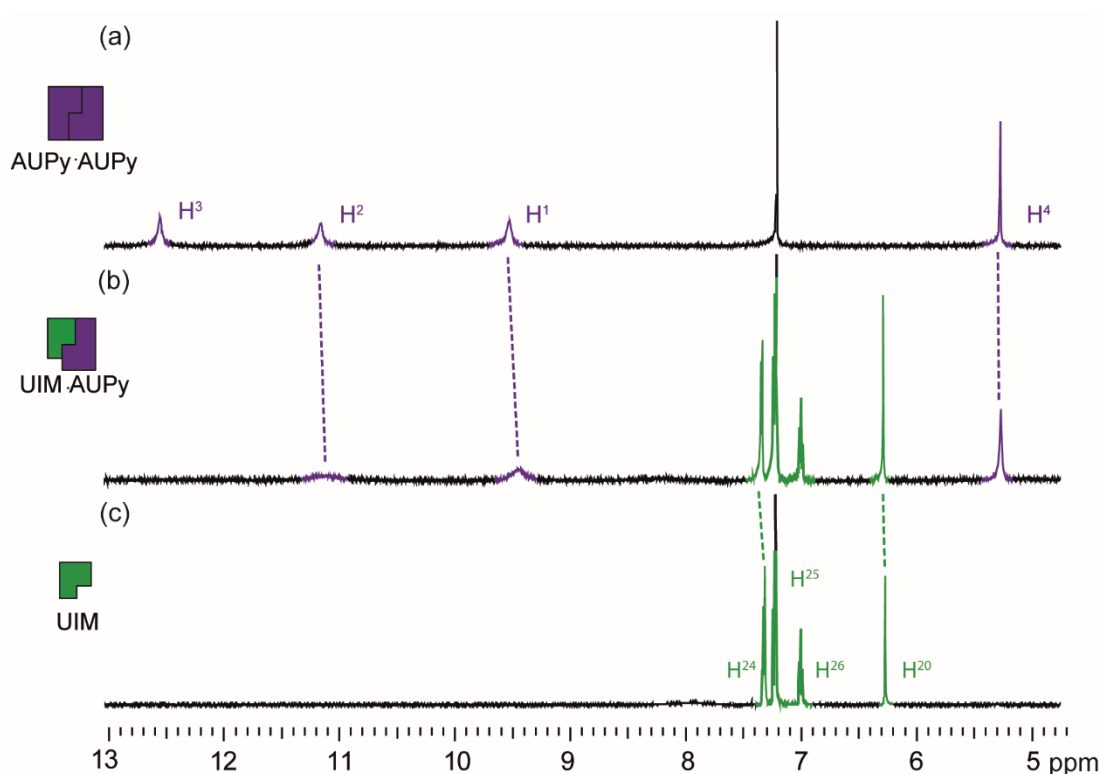


Figure 47. 1H NMR (500 MHz, 10 mM, $CDCl_3$) for (a) AUPy 66-66, (b) 1:1 AUPy-UIM 66-31 and (c) UIM 31. Refer to Figure 31 for the resonance assignment and chemical structure.

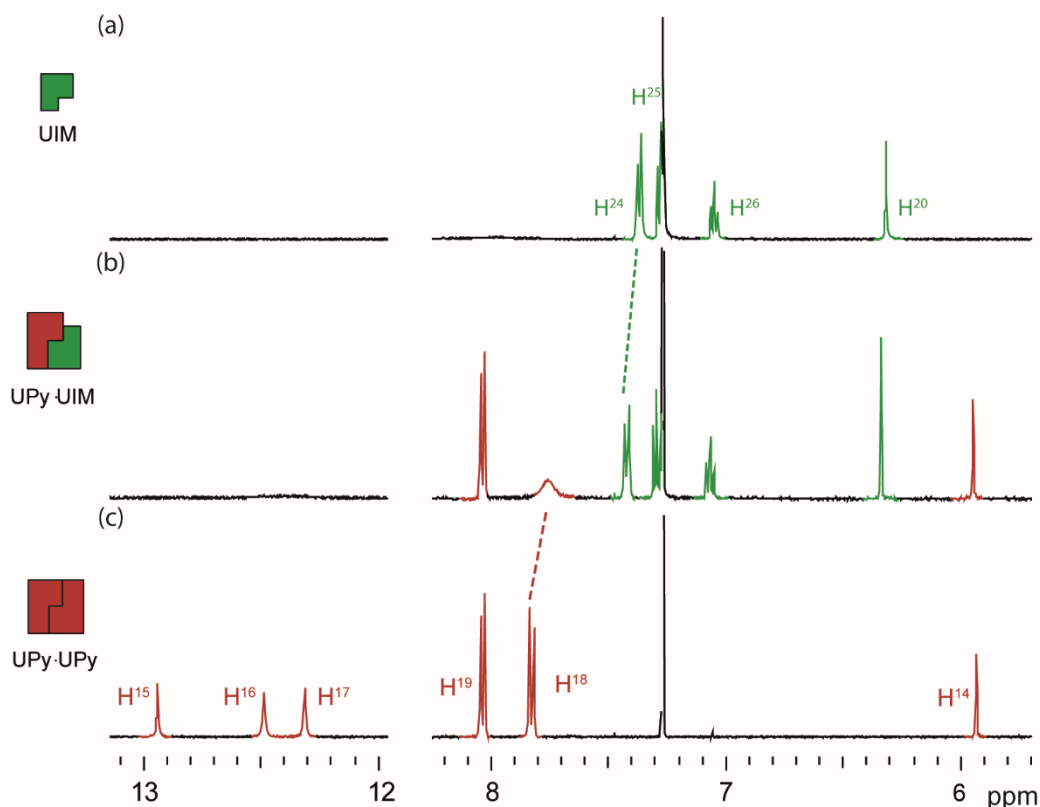


Figure 48. ^1H NMR (500 MHz, 10 mM, CDCl_3) for (a) UIM 31, (b) 1:1 UPy-UIM 45-31 and (c) UPy 45-45. Refer to Figure 31 for the resonance assignment and chemical structure.

Content with understanding which hydrogen bonding motifs can potentially interact and which dimers can form in bimolecular mixture, the next goal was to test which dimers would “win out” in a three-component mixture with the potential for several outcomes. For this purpose, hydrogen bonding motifs AUPy **66**, DAN **44** and UPy **45** were combined in a 1:1:1 ratio. The ^1H NMR data was indicative of a mixture of UPy **45-45** homodimer and AUPy-DAN **66-44** heterodimer (Figure 49 (c)), consistent with prior observations.¹¹⁸ The DFT analyses indicated no significant Gibbs free energy difference ΔG between UPy-DAN **44-45** ($-4.8 \text{ kcal mol}^{-1}$) and AUPy-DAN **66-44** ($-5.0 \text{ kcal mol}^{-1}$) (Table 2). Thus, the energetic difference between the two heterodimers fails to explain the preferential AUPy-DAN (**66-44**) heterodimer formation.

Instead, the behaviour is explained by considering the free energy change in this system and the additive effects of each dimer formed. Again, the high stability of the UPy **45-45** homodimer drives the behaviour of the system; because the ΔG for the UPy **45-45** homodimer is lower (i.e. more negative) than both heterodimers by 1.9 (AUPy-DAN **66-44**) and 2.1 (UPy-DAN **45-44**) kcal mol⁻¹, UPy **45** dimerises with itself instead of with DAN **44**, and the AUPy **66-66** homodimer consumes two equivalents on DAN **44** to form the AUPy-DAN **66-44** heterodimer. Even though calculations reveal AUPy-DAN **66-44** is 2.8 kcal mol⁻¹ (Table 2) more stable than the AUPy **66-66** homodimer, the requirement to maximise hydrogen-bonding interactions dictates this behaviour. To provide further evidence that the overall number of hydrogen bonds in the system must first be maximised before considering the strength of the dimerisation interaction and lowest energy conformers, a further ¹H NMR experiment was performed with DAN **44**, AUPy **66** and UPy **45** in 2:1:1 ratio (Figure 49b). This predictably resulted in an equal amount of AUPy-DAN **66-44** and UPy-DAN **45-44** heterodimers with no homodimers present. Here, the excess of DAN **44** drives the formation of the UPy-DAN **45-44** heterodimer over the UPy **45-45** homodimer, despite an energetic bias towards the later.

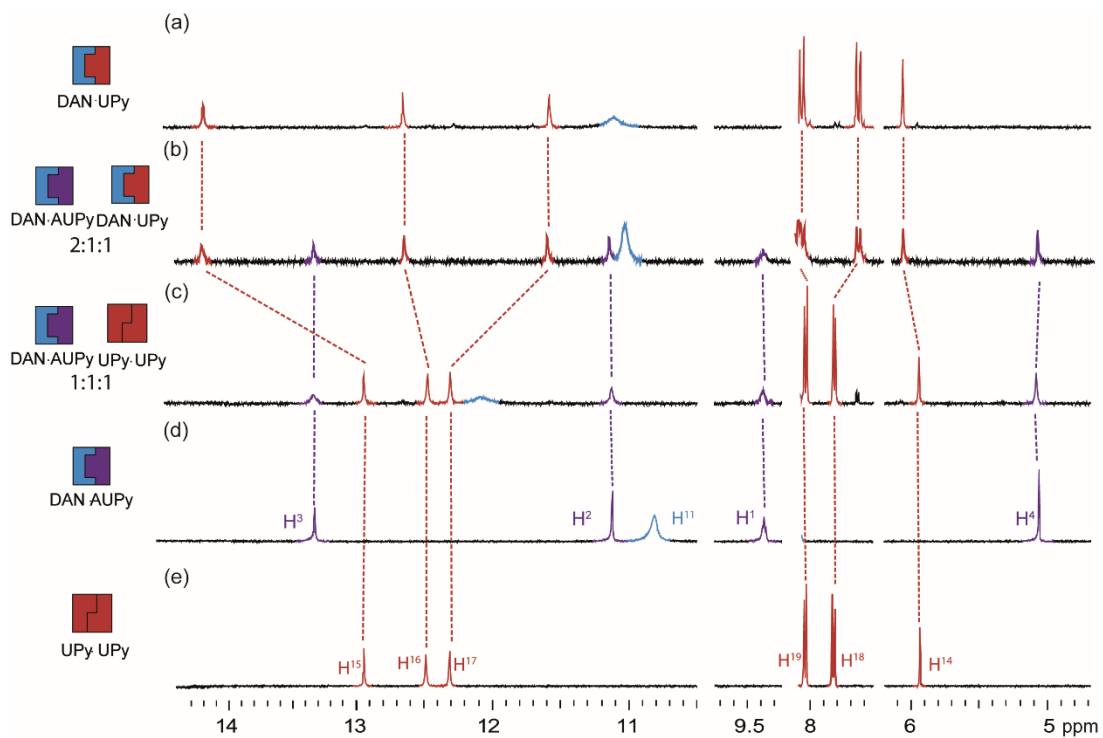


Figure 49. Analysis of pairwise interactions and preferences for AUPy 66, DAN 44 and UPy 45 by ^1H NMR (10 mM, CDCl_3) (a) 1:1 AUPy 66: DAN 44, (b) 2:1:1 DAN 44: AUPy 66: UPy 45, (c) 1:1:1 DAN 44: AUPy 66: UPy 45, (d) 1:1 DAN 44: AUPy 66 (e) UPy 45. Refer to Figure 31 for the resonance assignment and chemical structure.

2.3 Self-sorting pathways

Having characterised the pairwise dimerisation behaviour of the individual components, this allowed the construction of a number of self-sorting pathways. The simplest of which was conceived through the addition of NAPyO **67** to AUPy **66** (Figure 50 (e) & (d)) followed by the addition of DAN **44** (Figure 50 (c)). Starting with AUPy **66** homodimer (Figure 50 (e)), on the addition of NAPyO **67** (Figure 50 (d)) AUPy-NAPyO **66-67** heterodimer is formed. On the addition of DAN **44** to the weak AUPy-NAPyO **66-67** heterodimer (Figure 50 (c)), NAPyO **67** is displaced resulting in the formation of the AUPy-DAN **66-44** heterodimer (see Figure 50 (b) for comparison spectra) and the NAPyO **67-67** homodimer (see Figure 50 (a) for comparison spectra). The NMR experiments on this simple self-sorting pathway were carried out in a non-sequential manner (see experimental for more details). This can be readily explained in terms of both maximising the number of hydrogen bonds in a system and association strength. Unsurprisingly, DFT computations mirror these experimental observations; AUPy-NAPyO **66-67** and AUPy-DAN **66-44** heterodimers have a ΔG of -2.3 and -5.0 kcal mol⁻¹ (Table 2).

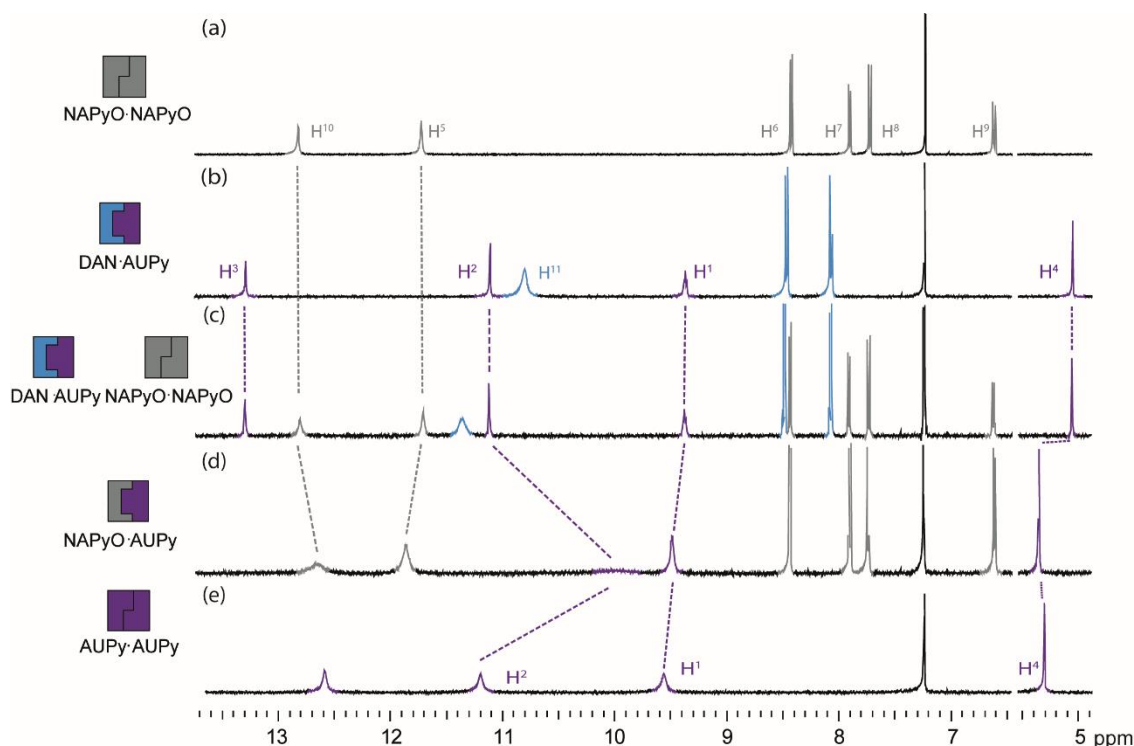


Figure 50. ^1H NMR (500 MHz, 10 mM, CDCl_3) for (a) NAPyO 67-67, (b) 1:1 AUPy-DAN 66-44, (c) 1:1:1 AUPy 66, NAPyO 67 and DAN 44, (d) 1:1 AUPy-NAPyO 66-67 and (e) AUPy 66-66. Refer to Figure 31 for the resonance assignment and chemical structure.

More complex self-sorting pathways exploiting five hydrogen bonding motifs were also investigated (Figure 51). This series of NMR experiments were carried out in a sequential manner (see experimental for more details). Beginning with the AUPy-AUPy **66-66** homodimer (Figure 51 (e)), the addition of UIM **31** (Figure 51 (d)) resulted in a small shift in the H^4 resonance of AUPy **66** and broadening of the NH resonances, consistent with the weak AUPy-UIM **66-31** heterodimer formation (Figure 47). The AIC **46** motif was then added to the mixture (Figure 51(c)) resulting in the formation of the UIM-AIC.**31-46** heterodimer indicated by the downfield shift in the H^{24} resonance and broadening of the H^{20} resonance of UIM **31**. Concomitant recovery of the AUPy homodimer **66-66** was observed on the basis of the restoration of its NH resonances towards the expected frequency. Upon the addition of NAPyO

67 (Figure 51 (b)) the interaction between AIC.UIM **46.31** was unchanged, but small changes in chemical shifts of the NH resonances of AUPy **66** were observed, consistent with formation of AUPy·NAPyO **66-67** as the dominant species comprising either component (as previously discussed). The pathway was completed by the addition of DAN **44** (Figure 51 (a)); the AIC.UIM **46-31** heterodimer remained with no resonances in the ¹H NMR affected. However a significant upfield shift for proton H⁴ and sharpening of NH resonances for AUPy **66** indicated formation of AUPy·DAN **66-44** and the displacement of NAPyO **67** from complexation with AUPy **66** (Figure 42 & Figure 50). Based on this reasoning the final mixture was comprised of AUPy·DAN **66-44** and AIC.UIM **46-31** heterodimers as well as NAPyO·NAPyO **67-67** homodimer (as predicted) and a clear pathway of sequential self-sorting established for five components.

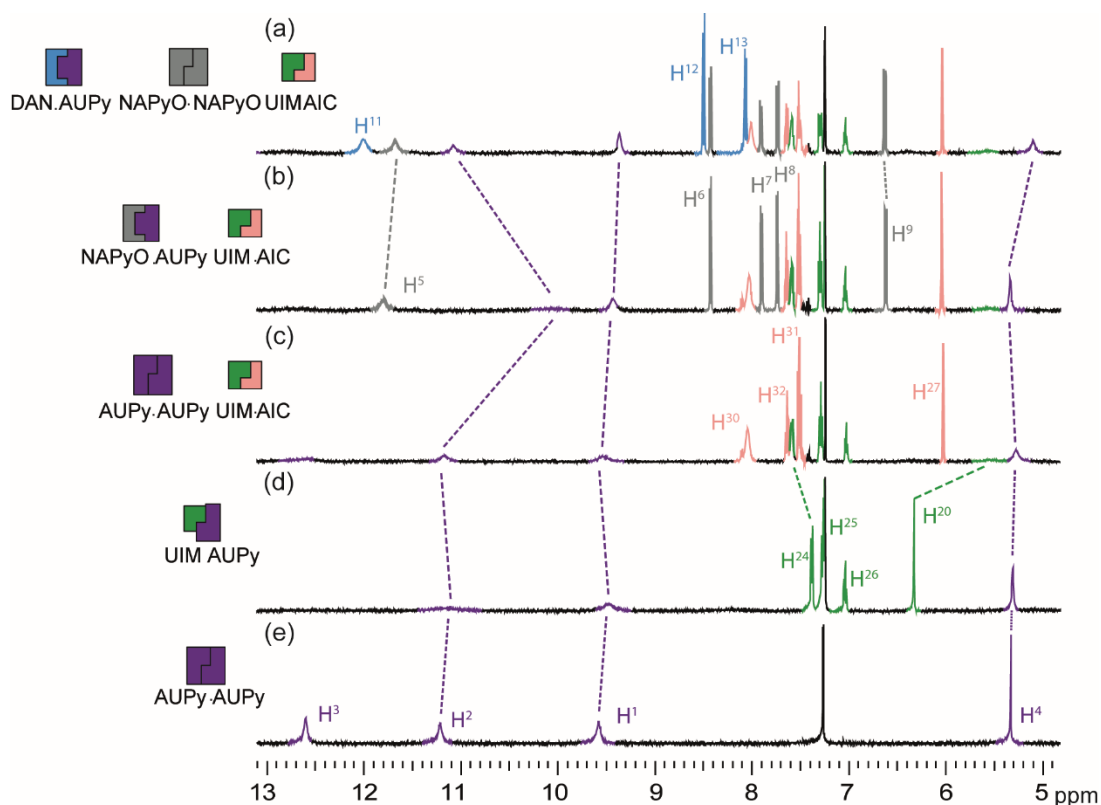


Figure 51. Five component self-sorting pathway studied by ^1H NMR (10 mM, CDCl_3) (a) AUPy 66, NAPyO 67, DAN 44, UIM 31 and AIC 46, (b) AUPy 66, NAPyO 67, UIM 31 and AIC 46, (c) AUPy 66, UIM 31 and AIC 46, (d) AUPy 66, UIM 31 and (e) AUPy 66. Refer to Figure 31 for the resonance assignment and chemical structure.

A series of ^1H NMR experiments were then performed to exemplify a six component pathway (Figure 52). The first six component pathway (referred to as Pathway E in the final section of this chapter on self-sorting network) was initiated with the UPy **45-45** homodimer; the addition of AUPy **66** lead to no change in chemical shifts consistent with narcissistic self-sorting of UPy **45-45** and AUPy **66-66** homodimers (Figure 52 (e)). Upon the addition of UIM **31**; UPy.UIM **45-31** and AUPy.UIM **66-31** heterodimers were formed as major products (Figure 52 (d)). This was indicated by the upfield shift and broadening of H^{18} of UPy **45** as well as the upfield shift of H^4 and broadening

of NH resonances of AUPy **66**, in line with heterodimerisation observed in the two component mixture (Figure 47 & Figure 48). Noteworthy here, is the fact that a distinct spectral change is sufficient to distinguish this phase of the pathway from the preceding and subsequent phases, demonstrating the absence of clear speciation may be tolerated in pathway (see earlier discussion on AUPy·NAPyO **66-67**). AIC **46** was then added (Figure 52 (c)) resulting in strong heterodimer formation with UIM **31** (illustrated by the downfield shift of H²), and simultaneous reformation of the UPy **45-45** and AUPy **66-66** homodimers. Formation of the AUPy·NAPyO **66-67** heterodimer occurred on addition of NAPyO **67** to the pathway in the presence of UPy **45-45** homodimer and UIM-AIC **31-46** heterodimers (Figure 52 (b)). The addition of DAN **44**, as expected, disrupted AUPy·NAPyO **66-67** complexation resulting in AUPy·DAN **66-44** heterodimer and NAPyO **67-67** homodimers (Figure 52 (a)). Thus, a final product distribution with four major components AUPy·DAN **66.44**, UIM-AIC **31-46** heterodimers and NAPyO **67-67**, UPy **45-45** homodimers was observed. This series of NMR experiments were tested in a sequential manner, the final product distribution was also identified as the sample when the NMR experiments were carried out in a non-sequential manner (see experimental for more details).

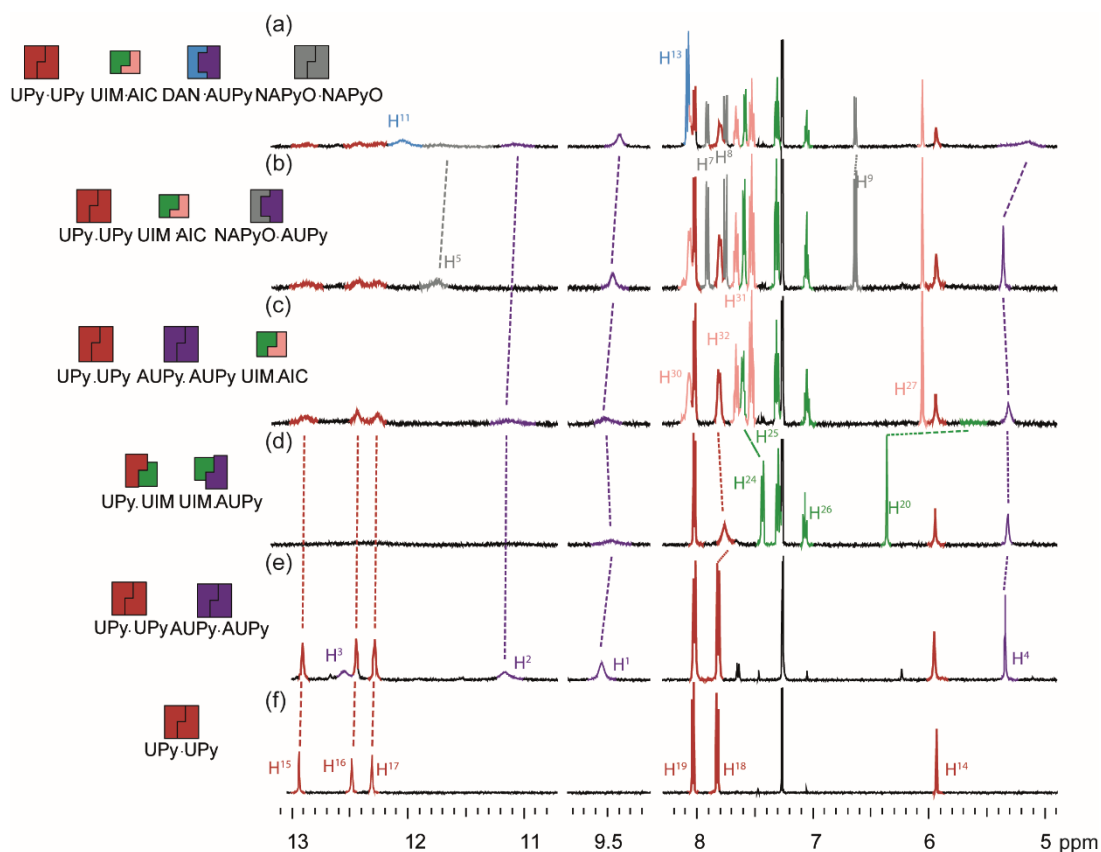


Figure 52. Pathway E ^1H NMR (500 MHz, 10 mM, CDCl_3) six component self-sorting pathway (a) AUPy 66, NAPyO 67, DAN 44, UPy 45, UIM 31, and AIC 46, (b) AUPy 66, NAPyO 67, UPy 45, UIM 31, and AIC 46, (c) AUPy 66, UPY 45, UIM 31, and AIC 46, (d) AUPy 66, UPy 45, and UIM 31, (e) AUPy 66 and UPy 45 and (f) UPy 45. Refer to Figure 31 for the resonance assignment and chemical structure.

In an attempt to closer mimic the property of multiple cellular signalling cascades, which occurring in parallel (but comprising components capable of cross-talk), an approach to perform two orthogonal self-sorting pathways was developed (Pathway G, Figure 53). The aim was to create two parallel pathways which can operate in sequence in spite of the ability of complexes from both pathways to interact with one another in different scenarios. Starting with a mixture of UPy **45-45** and AUPy **66-66** homodimers (Figure 53 (e)), the pathway could be split in two with the UPy **45-45** homodimer at the

head of one channel and the AUPy **66-66** homodimer at the head of the other. On the addition of NAPyO **67** (Figure 53 (d)); the “UPy channel” is unchanged, whereas, in the “AUPy channel”, AUPy **66** interacts with NAPyO **67** to form the AUPy-NAPyO **66-67** heterodimer. Upon addition of UIM **31** to this three component mixture (Figure 53 (c)); the “AUPy channel” is unchanged and UPy-UIM **45-31** heterodimer formed in the “UPy channel”. With the addition of AIC **46** (Figure 53 (b)); the “AUPy channel” is unchanged through a further stage but in the “UPy channel” the UPy-UIM **45-31** heterodimer is disrupted to form the UPy **45-45** homodimer and the UIM-AIC **31-46** heterodimer. The pathway is completed with the addition of DAN **44**; here the “UPy channel” is unchanged but DAN **44** interacts with AUPy **66** in the “AUPy channel” to form the AUPy-DAN **66-44** heterodimer liberating the NAPyO **67-67** homodimer (Figure 53 (a)). Overall, four social self-sorting transitions occur, two in one channel and two in the other; however, the transitions do not cross over, thus exemplifying an orthogonal pathway. Simply changing the point at which one motif is added could alter this pathway resulting in cross-talk. For example, if UIM **31** was added before NAPyO **67** it would interact with both AUPy **66** and UPy **45** and the “channels” would no longer be orthogonal.

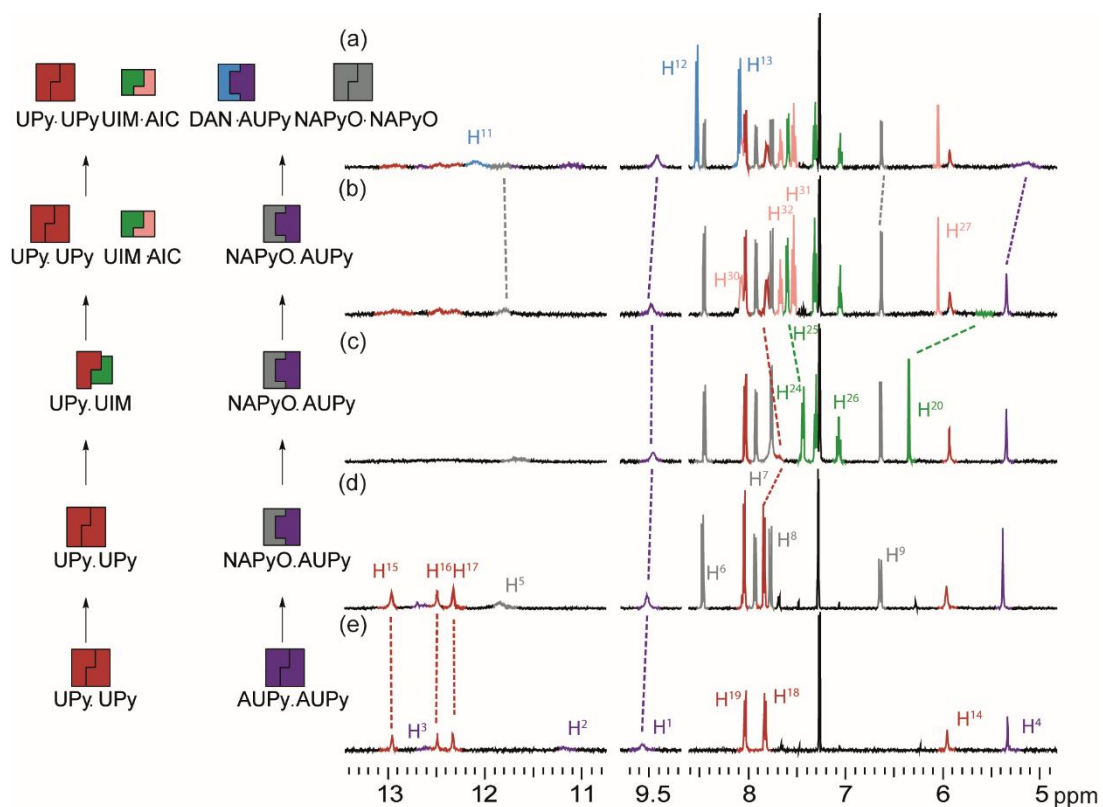


Figure 53. Pathway G ^1H NMR (500 MHz, 10 mM, CDCl_3) (a) AUPy 66, NAPyO 67, DAN 44, UPy 45, UIM 31, and AIC 46, (b) AUPy 66, NAPyO 67, UPy 45, UIM 31, and AIC 46, (c) AUPy 66, NAPyO 67, UPy 45 and UIM 31, (d) AUPy 66, NAPyO 67 and UPy 45 and (e) AUPy 66 and UPy 45. Refer to Figure 31 for the resonance assignment and chemical structure.

2.4 Self-sorting network

To elaborate a self-sorting network, several different additional pathways were exemplified; understanding potential hydrogen bonding interactions between the six motifs used was key in creating this self-sorting network bearing intersecting points (Figure 54). By comparing the ^1H NMR spectra of each mixture with the distinct chemical shifts of heterodimers and homodimers the major components at point of each pathway were identified. This allowed for several different self-sorting pathways to be plotted together to create a network map based on their product distribution. The resulting self-sorting network consists of diverging and converging paths with the same end point (Figure 54). For example, pathway B (red Figure 54) initiates with the UPy **45-45** homodimer and the addition of DAN **44** led to production of the DAN-UPy **44-45** heterodimer (Figure 43). Pathway B continues with the addition of AUPy **66** resulting in disassembly of the DAN-UPy **44-45** heterodimer at the expense of forming the DAN-AUPy **44-66** heterodimer, together with regeneration of the UPy **45-45** homodimer (Appendix A Figure 2 (d) for ^1H NMR data). The hydrogen bonding interactions are unchanged on the addition of NAPyO **67** which is present as **67-67** homodimer (Appendix A Figure 2 (c) for ^1H NMR data). UIM **31** is able to interfere with the UPy **45-45** homodimer interactions to form the UPy.UIM **45.31** heterodimer (Appendix A Figure 2 (b) for ^1H NMR data) which is in turn disassembled to form the UIM.AIC **31.46** heterodimer with concomitant UPy **45-45** homodimer formation on the addition of AIC **31**. Pathway C (yellow Figure 54) takes a different route from pathway B in that UIM **31** and AIC **46** are successively added to the DAN-UPy **44-45** heterodimer (considered here as an

interchange) to create UPy-UIM **45-31** and UIM-AIC **31-46** heterodimers successively (Appendix A Figure 3 for ^1H NMR data). The ability of UIM **31** to disrupt the DAN-UPy **44-45** heterodimer is moderate, and a series of low-fidelity complexes are formed –nonetheless, the resultant ^1H NMR spectrum is diagnostic of a distinct state within the network, and, the addition of AIC **46** restores a well-resolved spectrum indicative of a well-defined self-sorted configuration. Finally, in pathway C the addition of AUPy **66** switches the configuration from DAN-UPy **44-45** and UIM-AIC **31-46** to AUPy-DAN **66-44**, UPy **45-45** and UIM-AIC **31-46** with subsequent addition of NAPyO **67-67** promoting no change in the distribution of the other components (Appendix A Figure 3 for ^1H NMR data). Pathways A, D and F further exemplify the different network configurations that can be obtained depending on which components are present and therefore expressed in the system (Appendix A Figure 1, Appendix A Figure 4 and Appendix A Figure 5 for ^1H NMR data).

2.5 Conclusions

Detailed analyses of molecular recognition behavior of hydrogen-bonding motifs by experiment and computation has allowed a complex self-sorting network made up of several sequential self-sorting pathways to be created. The sequential addition of six linear hydrogen motifs has led to self-sorting pathways capable of both narcissistic and social self-sorting phases, as well as a mixture of both. Through the examination of interactions between individual components of each pathway, the product distribution of the overall system can be understood in terms of orthogonal recognition. This study illustrated that thermodynamically less preferential complexes can be formed during self-sorting, driven by the stability of the whole system, and that this can be influenced by the configuration and conformation of the hydrogen-bonding motif. The varying degrees of fidelity and promiscuity of the hydrogen bonding interactions of these motifs, and critically, an understanding of their behavior was essential in developing the sequential self-sorting pathways comprising the self-sorting network. These pathways include, for the first-time, parallel cascades that operate in the presence of each other, but which contain building blocks capable of cross-talk. Future studies will centre on exploiting these motifs as components of self-sorting and reconfigurable materials, on developing reversible transitions between the different phases of the pathway. Beyond this, developing approaches to temporarily perturb the system may provide access to out-of-equilibrium networks with emergent behaviour, and hence close mimic signaling cascades in biological processes that often occur away from thermodynamic equilibrium.

3. Responsive self-sorting of hydrogen bonding motifs

There has been a significant amount of research in creating responsive self-assemblies due to potential applications of the materials. For example, stimuli responsive supramolecular polymers, dendrimers and nanoparticles have all been exploited for drug delivery and nanomedicine.^{135–138} However, switchable systems, in which self-assemblies can change from two discrete states reversibly due to a stimuli, are less well explored. The most progress in this area has involved host guest chemistry and the use of cucurbit[*n*]uril type molecules as hosts.^{61,67} Several photo-switchable systems have been reported which exploit the cis-trans switch of azobenzene moieties to induce a change of state.^{67,139,140} Other stimuli such as redox, pH, metal driven selection and competitive binding have also been employed to create switchable systems.^{141–145} Isaacs and co-workers have additionally generated switchable systems capable of self-sorting.^{62,69} Schalley and co-workers described an orthogonally switchable self-sorting network consisting of dynamic libraries of cucurbit[8]uril complexes.¹⁴⁶ The use of external stimuli (pH and redox) can switch a 1 : 1 : 1 heteroternary complex to a 2 : 1 homoternary complex.

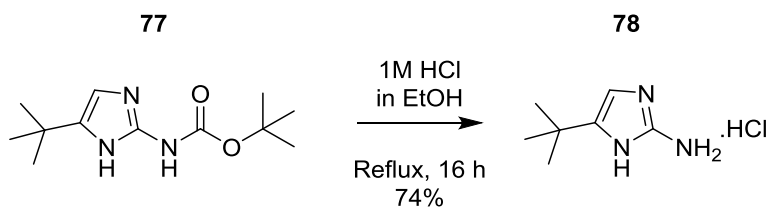
Far fewer switchable systems have focused on the switching of hydrogen bonding mediated assemblies. Hecht and co-workers reported a photoswitchable hydrogen bonding motif, in which light switched the motif to a ring closed state and in turn increased the binding affinity to a complementary motif.¹⁴⁷ Another system reported by Zhang and co-workers linked two hydrogen bonding motifs (UPy) with a photochromic ortho-tetrafluorinated azobenzene (TFAB) to create a supramolecular polymer.¹³⁹

The supramolecular polymer could be reversibly switched from a gel to sol by the photo-isomerisation of the TFAB moiety. To our knowledge, there are no reports of self-sorting behaviour of switchable hydrogen bonding motifs.

A limitation of the sequential self-sorting pathways and network described in Chapter 2 is that the self-sorting transitions can only proceed in a forward direction; therefore the final product distribution is always the same for a given mixture of hydrogen bonding motifs. The objective of this work was to use an external stimulus to reversibly switch the self-sorting preferences of the system. Ideally this would allow for the sequential self-sorting pathways described in Chapter 2 to be reversed. Moreover, for a mixture of hydrogen bonding motifs, the final product distribution of the system could be tuned by an external stimuli. This required identification and/or design of stimuli responsive hydrogen bonding motifs which switch their interacting array in situ.

UIM **31** was identified as a potential responsive hydrogen bonding motif as during the synthesis of UIM **31** the intermediate **78**, previously believed to be unstable, was isolated as a hydrochloride salt (Scheme 7). The single crystal X-ray structure (Figure 55) revealed protonation of the five-membered imidazole ring and a chloride ion bridging two imidazole rings via a $N^+H...Cl^-...HN^+$ hydrogen bonding interaction. The crystal packing structure shows a chloride bridged chain-link structure, with four hydrogen bonds to each chloride ion and an equal number of monomers to chloride ions (Figure 55 (b) & (c)). The hydrochloride salt of the intermediate **78** with both nitrogen atoms on the imidazole ring suggests a *DD* interacting array (Figure 56 (a)). It was

theorised that if UIM **31** was protonated in the same way, a cationic hydrogen bonding motif with an *DDD* array would be formed (Figure 56 (b)).



Scheme 7. Synthetic conditions for the isolation of tert-butyl imidazole amine hydrochloride salt **78.**

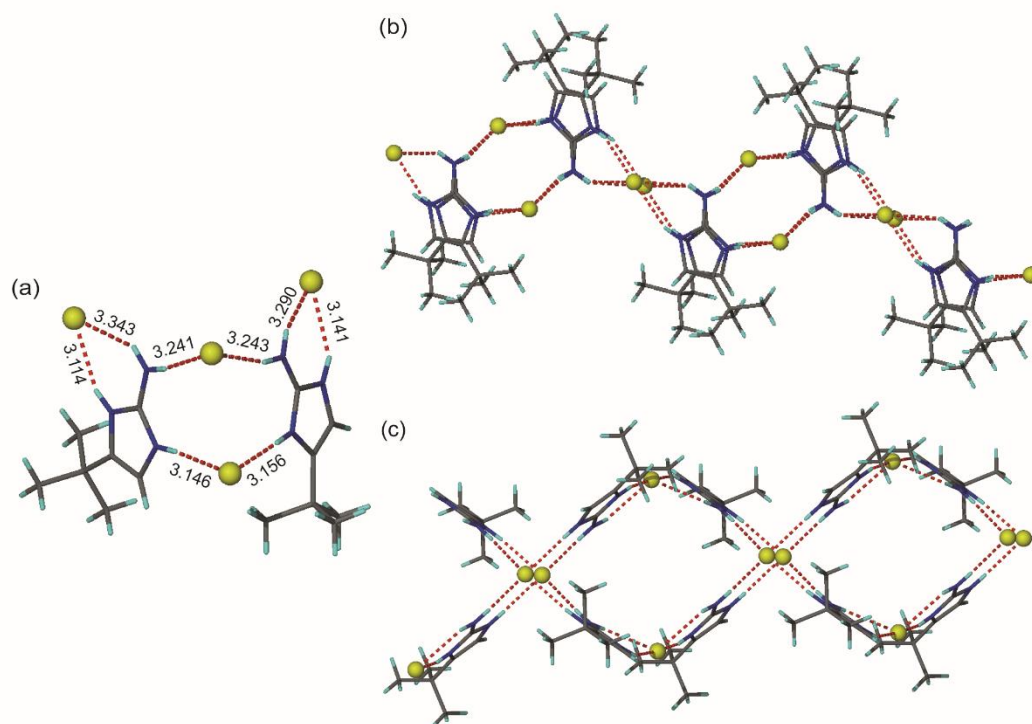


Figure 55. X-ray crystal structures of 2-amino tert-butyl imidazole hydrochloride salt (intermediate **78) (a) showing chloride bridge hydrogen bonding interaction NH...Cl...HN between two molecules, (b) side view showing the chain like packing structure with molecules linked up antiparallel and (c) top view showing extended crystal packing (carbon is shown in grey, nitrogen in blue, oxygen in red, hydrogens in white, chloride in yellow and hydrogen bonds as red dashed lines, D...A bond distances given in Å).**

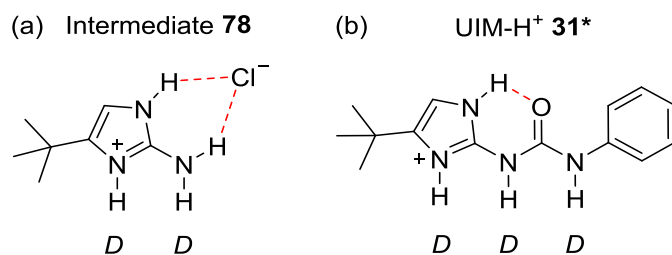


Figure 56. Structure highlighting the interacting hydrogen bonding array of (a) hydrochloride salt of intermediate 78 (*DD*) and (b) protonated UIM 31* (*DDD*).

Cationic mediated hydrogen bonding systems, similar to that hypothesised in this work, have been previously reported in the literature. Bell and Anslyn were the first to describe a cationic *AAA-DDD* interaction with a $K_a > 5 \times 10^5 \text{ M}^{-1}$ in CH_2Cl_2 as determined by UV-vis spectroscopy (Figure 57 (a)).¹⁴⁸ Leigh and co-workers reported the strongest bound triple hydrogen bonded system *AAA-DDD* by using a more stable cationic hydrogen bonding motif to give a $K_a = 3 \times 10^{10} \text{ M}^{-1}$ (Figure 57 (b)).²⁴ This system was subsequently elaborated further to create a quadruple *AAAA-DDDD* interaction where the cation mediated interaction could be switched 'off' and 'on' by deprotonation with DBU and reprotonation with HI (Figure 57 (c)).^{149,150}

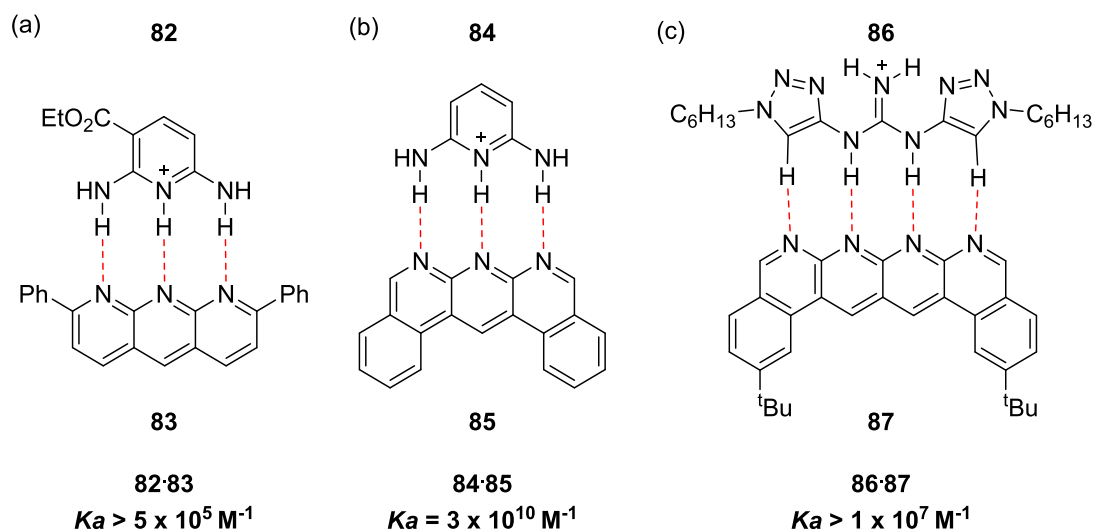
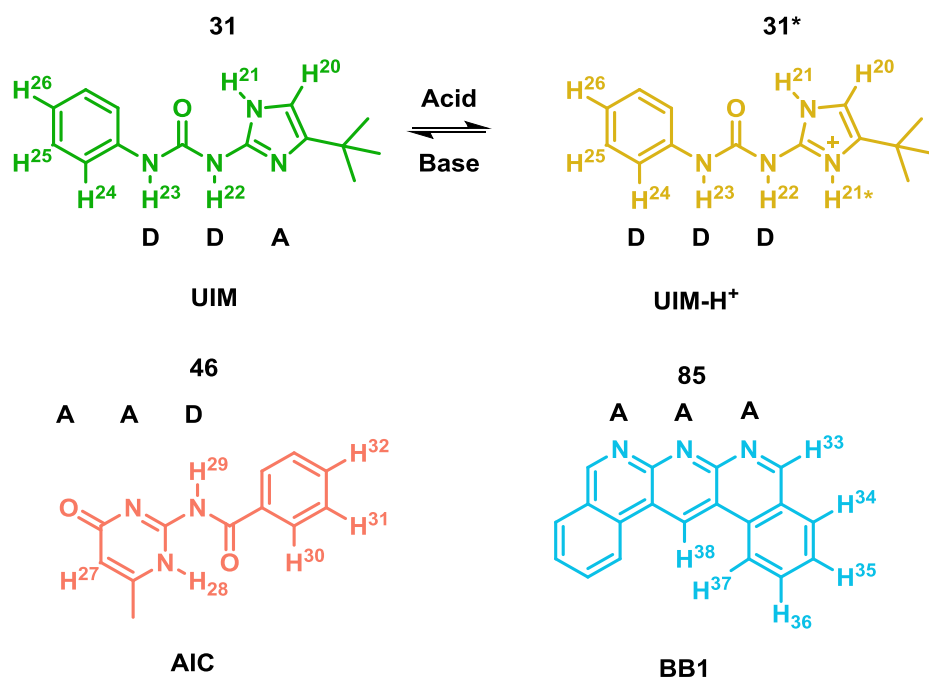


Figure 57. Examples of cationic hydrogen bonding pairs reported in the literature (hydrogen bonds shown as red dashed lines).^{24,148–150}

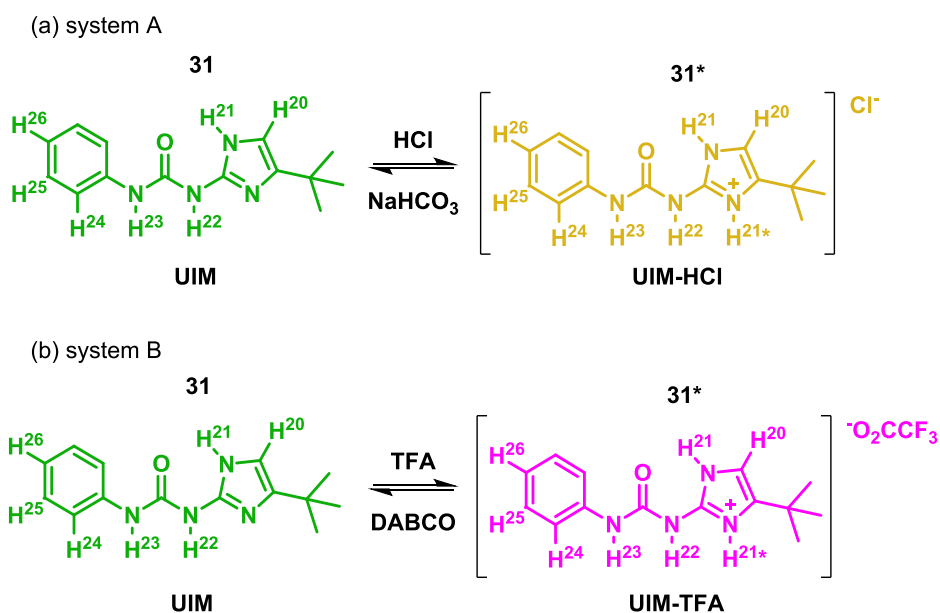
Encouraged by both the crystal structure of intermediate **78** and the reported switching ‘on’ and ‘off’ for cationic mediated interactions, the aim of this work was to switch the interacting array of UIM **31** by protonation and hence change its self-sorting preferences in a pathway or network. Scheme 8 illustrates the potential switching between the *DDA* array of neutral UIM **31** and the *DDD* array of protonated UIM- H^+ **31***. The variety of possible approaches to achieve protonation and deprotonation in situ, such as acids and bases, offers additional benefits for developing this UIM responsive hydrogen bonding motif. In turn it would be expected that this responsive hydrogen bonding motif would interact preferentially with different complementary hydrogen bonding motifs depending on the conditions. For example, neutral UIM **31** would interact with AIC **46**, whereas protonated UIM- H^+ **31*** should interact with a complementary *AAA* array such as BB1 **85** (Scheme 8).



Scheme 8. Suggested switching of conformers of UIM when neutral 31 and protonated 31* together with suitably complementary hydrogen bonding motifs AIC 46 and BB1 85 respectively.

3.1 Analysis of a proton responsive hydrogen bonding motif

Inspired by the crystal structure of **78** protonation of UIM **31** using hydrochloric acid (HCl) was attempted, (system A, Scheme 9 (a)). ^1H NMR analysis in chloroform showed the potential to switch from a neutral UIM **31** to a protonated UIM with chloride ion, UIM-HCl **31*** (Figure 58). On the addition of excess (4 equivalents) 4M HCl in 1,4-dioxane to UIM **31** (10 mM) a distinct downfield change in chemical shifts was observed the proton resonances H^{20} , H^{24} , H^{25} and H^{26} (Figure 58 (c)). Additionally, NH resonances H^{21} , H^{22} and H^{23} , which are too broad in UIM **31**, were observed as well as an additional NH signal H^{21*} , illustrating the protonation to create UIM-HCl **31***. This protonation event could be switched back to the neutral UIM **31** by washing with excess basic sodium hydrogen carbonate (NaHCO_3) solution and extraction (see experimental for details). The ^1H NMR spectrum showed the broadening of NH resonances and chemical shift of aromatic protons consistent with the presence of UIM **31** (Figure 58 (b)). This switching event could be repeated for several cycles by addition of acid and base respectively.



Scheme 9. Systems tested for the protonation and deprotonation of UIM 31 (a) system A:HCl and NaHCO₃ and (b) system B:TFA and DABCO.

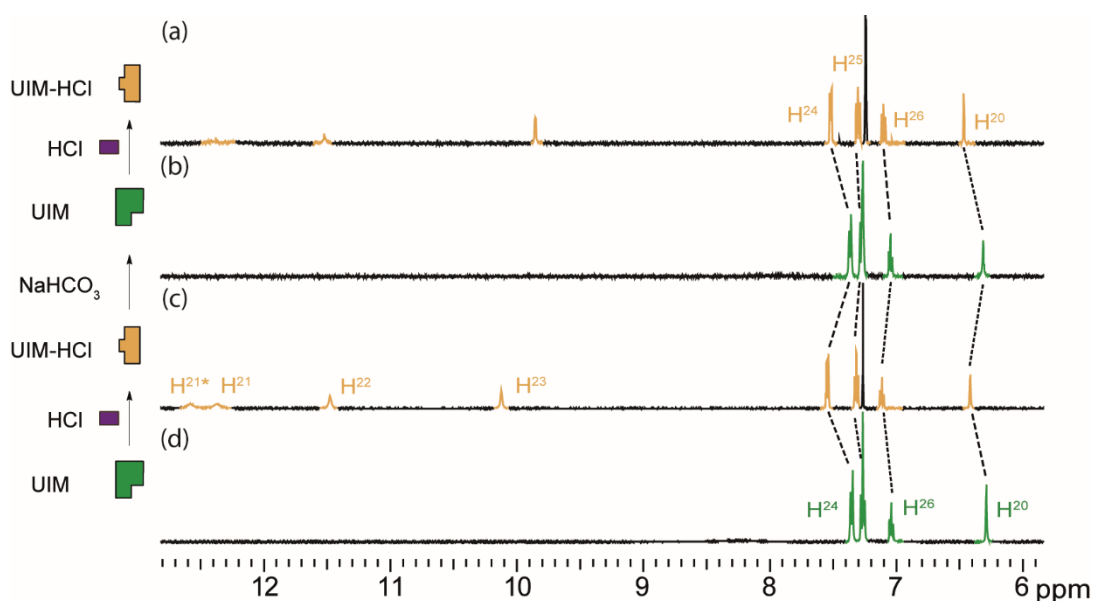


Figure 58. System A proton switch studied by ¹H NMR (500 MHz, 10 mM, CDCl₃) (a) UIM-HCl 31* (protonated with 4M HCl in 1,4-dioxane cycle 2), (b) UIM 31 (deprotonated with NaHCO₃ cycle 1), (c) UIM-HCl 31* (protonated with 4M HCl in 1,4-dioxane cycle 1) and (d) UIM 31. Refer to Scheme 8 for the resonance assignment and chemical structure.

An additional ^1H NMR titration experiment was carried out to calculate the equivalence of acid required to protonate the UIM motif **31**. At 5 mM of UIM in chloroform 0.25, 0.5, 0.75, 1 and 3 equivalents of 4M HCl in 1,4-dioxane were added (Figure 59). This series of NMR experiments were carried on separate samples. This demonstrated that the characteristic chemical shift of the aromatic protons occurred even at 0.5 equivalents of hydrochloric acid. With 1 equivalent of hydrochloric acid the broad NH resonances of UIM **31** fully sharpened ensuring clean preparation of UIM-HCl **31*** for the remaining experiments.

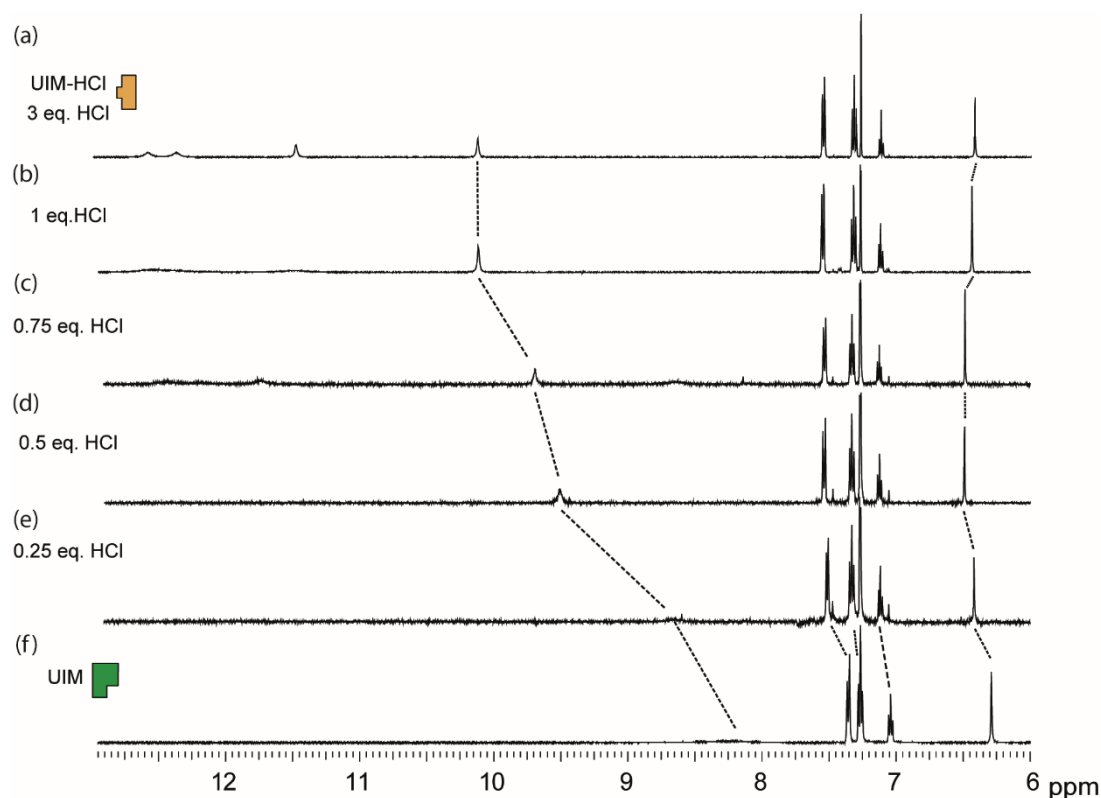


Figure 59. Titration of HCl into UIM studied by ^1H NMR (500 MHz, 5 mM, CDCl_3) (a) UIM **31** with 3 eq. HCl, (b) UIM **31** with 1 eq. HCl, (c) UIM **31** with 0.75 eq. HCl, (d) UIM **31** with 0.5 eq. HCl, (e) UIM **31** with 0.25 eq. HCl and (f) UIM **31**.

After multiple protonation and deprotonation cycles, the ^1H NMR spectrum was less well resolved. This was likely due to sample being lost during the method of deprotonation, in which the sample in chloroform was washed with basic NaHCO_3 solution, aqueous is separated and organic dried. Therefore, an alternative set of acid and base reagents were tested which could be added in situ (System B, Scheme 9 (b)). ^1H NMR study revealed a change in the diagnostic chemical shifts (H^{20} , H^{24} , H^{25} and H^{26}) on the addition of 1 equivalence of trifluoroacetic acid (TFA) in a 5 mM chloroform solution suggesting protonation of UIM (Figure 60 (c)). To reverse the protonation one equivalent of 1,4-diazabicyclo[2.2.2]octane (DABCO) was added to the 5 mM solution of UIM-TFA **31*** (Figure 60 (b)). This resulted in small changes in the chemical shifts of the diagnostic protons H^{20} , H^{24} , H^{25} and H^{26} but the resonances did not fully align with those observed for neutral UIM **31** (or UIM-DABCO mixture) suggesting a mixture of neutral and protonated UIM. However, with the addition of excess DABCO (3 eq.) the diagnostic protons H^{20} , H^{24} , H^{25} and H^{26} shifted further upfield, consistent with the formation of UIM **31** as the dominant species (Figure 60 (a)).

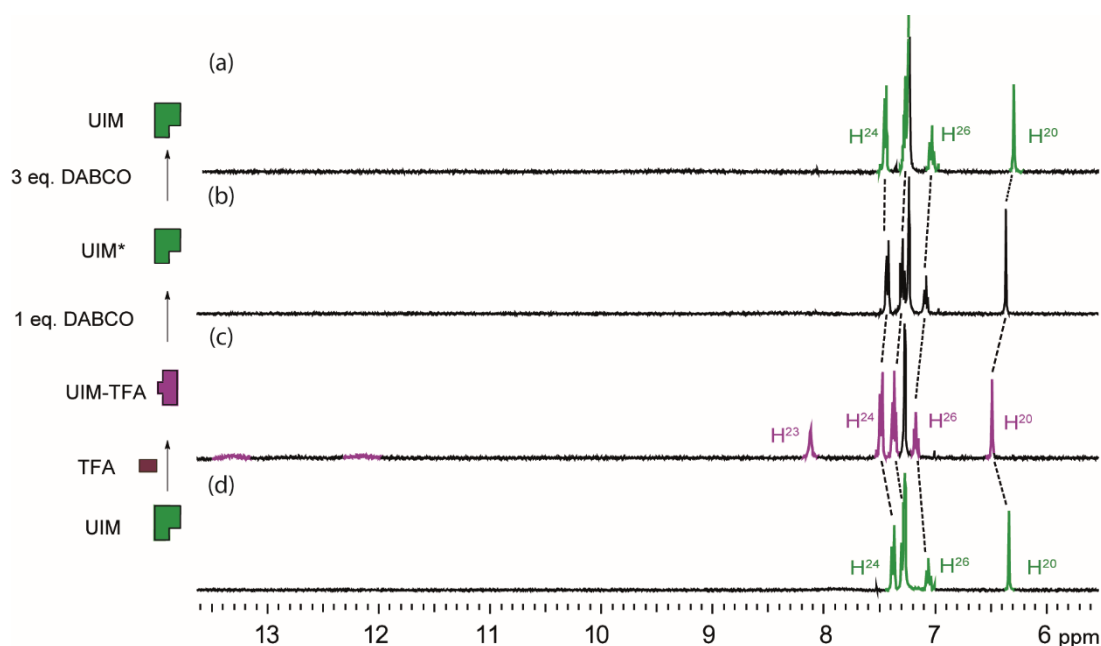


Figure 60. System B proton switch studied by ^1H NMR (500 MHz, 5 mM, CDCl_3) (a) UIM 31 (deprotonated with 3 eq DABCO), (b) UIM 31 (deprotonated with 1 eq DABCO), (c) UIM-TFA 31* (protonated with TFA), (d) UIM 31. Refer to Scheme 8 for the resonance assignment and chemical structure.

Comparison of the two systems highlighted that system A (HCl and NaHCO_3) resulted in sharper and more reproducible spectra in which there was a clear distinction between the neutral UIM (*ADD*) and protonated UIM (*DDD*) motifs. System B (TFA and DABCO) was practically simpler but the deprotonation step was more difficult to control. It was decided, despite the limitations, to take both systems forward to investigate their ability to self-sort in a comparative manner.

3.2 Switching the hydrogen bonding interactions of responsive hydrogen bonding motif with complementary motifs

The ability of neutral UIM **31** and cationic UIM **31*** to interact with complementary HBMs was tested by the addition of AIC **46**. The dimerisation interaction of UIM **31** and AIC **46** through hydrogen bonds has been well studied¹²³ and can be identified by the diagnostic downfield shift of H²⁴, H²⁵ and H²⁶ resonances and the upfield shift and broadening of resonance H²⁰ in ¹H NMR relative to UIM **31** (Figure 61 (e)). The aim was to switch 'off' and 'on' this interaction by protonation and deprotonation of UIM **31**.

System A illustrated this process efficiently, starting from **31** (Figure 61 (d)) the addition of hydrochloric acid gave UIM-HCl **31*** (Figure 61 (c)). Upon the addition of AIC **46** to UIM-HCl **31*** no significant binding was observed between UIM-HCl **31*** and AIC **46** indicated by the presence of sharp H²⁰ and H²⁷ resonances (Figure 61 (b)). The complementary *ADD-DAA* interaction was thus switched 'off' giving a non-interacting *DDD-DAA* pair. This interaction could be restored by washing the mixture of UIM-HCl **31*** and AIC **46** with sodium hydrogen carbonate to give the UIM·AIC **31.46** dimer (Figure 61 (a)). Here, the H²⁰ resonance was broadened and shifted as expected and the overall spectrum aligned well with that observed for the UIM·AIC **31.46** dimer (Figure 61 (e)). It is clear that although, the ¹H NMR spectrum in Figure 61 (a) and (e) line up indicating the presence of the UIM·AIC **31.46** dimer, there are differences in the resonances. This likely due to loss of compound during the deprotonation with NaCO₃ which results in a slight change in concentration. This revealed a proton dependent three component self-sorting sequence in

which AIC **46** can dimerise with UIM **31** but not with the protonated species UIM-HCl **31***.

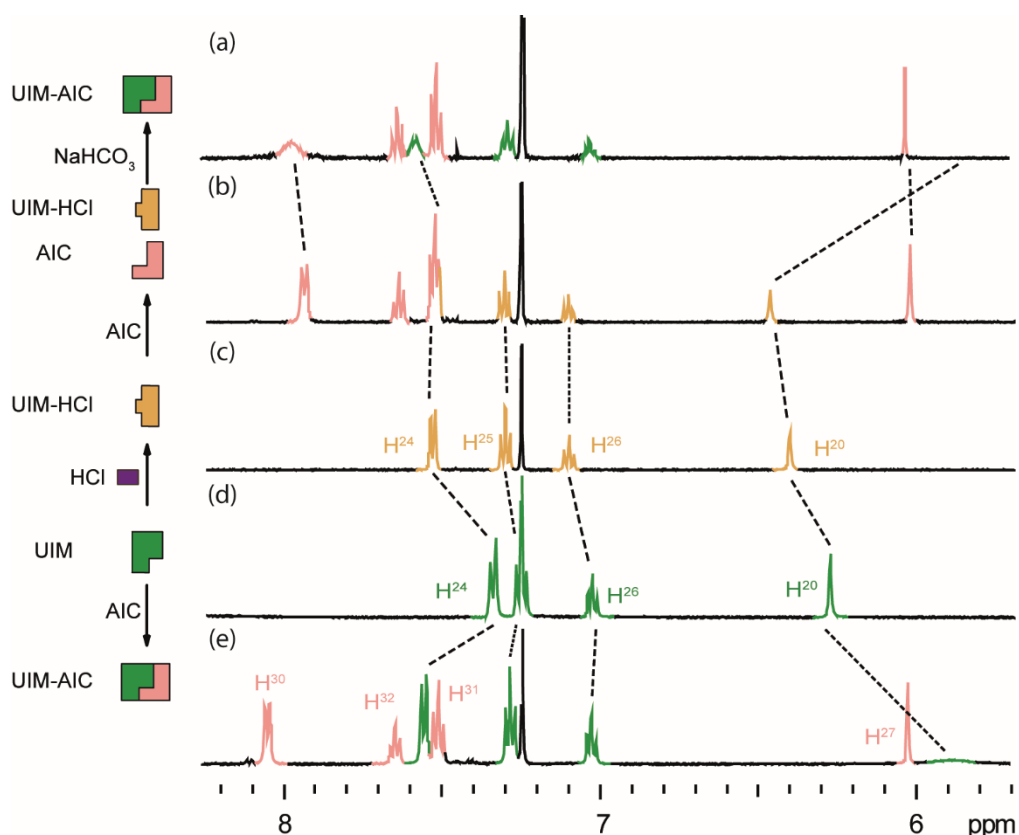


Figure 61. Self-sorting behaviour of proton responsive UIM **31** (system A) with AIC **46** studied by ^1H NMR (500 MHz, 5 mM, CDCl_3) (a) UIM.AIC **31.46** dimer formed after washing UIM-HCl **31*** and AIC **46** mixture with NaHCO_3 , (b) UIM-HCl **31*** (protonated with 4M HCl in 1,4-dioxane) and AIC **46**, (c) UIM-HCl **31*** (protonated with 4M HCl in 1,4-dioxane), (protonated with 4M HCl in 1,4-dioxane), (d) UIM **31** and (e) UIM.AIC **31.46** dimer. Refer to Scheme 8 for the resonance assignment and chemical structure.

With system B the addition of TFA clearly disrupted the *ADD-DAA* **31·46** dimer seen by the downfield chemical shift and well resolved H^{20} resonance (Figure 62 (b)). The addition of DABCO to this mixture indicated that the *ADD-DAA* dimer was reformed by the upfield shift and broadening of the H^{20} resonance. However, some of the resonances, H^{24} and H^{26} , did not align as anticipated. This could be due to the presence of TFA and DABCO salts in the mixture,

leading to competing interactions (fast in the NMR timescale) and/or intermolecular complex formation.

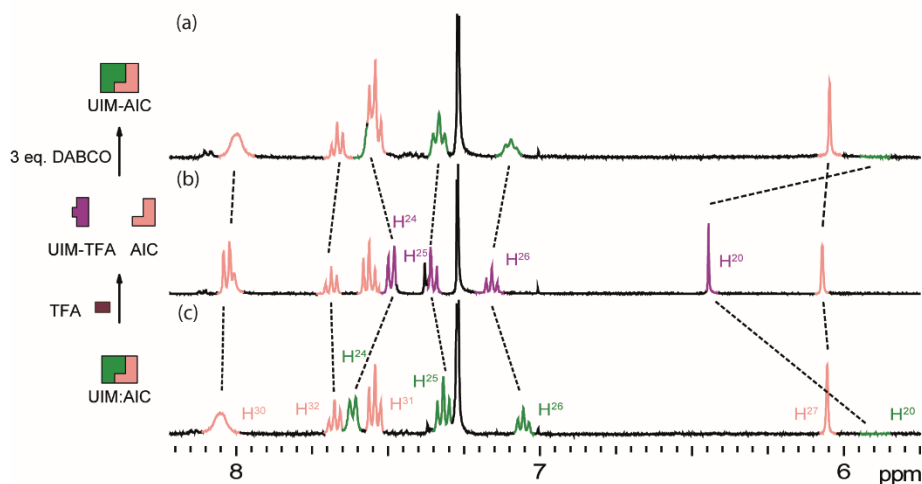


Figure 62. Self-sorting behaviour of proton responsive UIM 31 (system B) with AIC 46 studied by ^1H NMR (500 MHz, 5 mM, CDCl_3) (a) UIM:AIC 31·46 (dimer formed after washing UIM-TFA 31* and AIC 46 mixture with 3 eq. DABCO), (b) mixture of UIM-TFA 31* and AIC 46 (formed after protonated with TFA) and (c) UIM:AIC 31·46 dimer. Refer to Scheme 8 for the resonance assignment and chemical structure.

To further explore the self-sorting ability of the switchable HBM **31***, a complementary HBM **85** (BB1 with AAA moiety) was added to create a four component self-sorting system. Compound **85** BB1 was provided by Barbora Balonova and Barry Blight from University of New Brunswick, Canada. On the addition of the AAA motif BB1 **85** to the **31·46** dimer (UIM:AIC), the dimer remained bound and the resonances of the BB1 **85** motif were unchanged when compared to the separate ^1H NMR spectra (Figure 63 (d-f)). As expected the HBM UIM **31** favoured the matched triple hydrogen bonding interaction with AIC **46** over the mismatched array of BB1 **85**. However, when BB1 **85** was added to a mixture of AIC **46** and UIM- H^+ **31*** (created using system A) interaction was observed between BB1 **85** and UIM- H^+ **31***. ^1H

NMR (Figure 63 (b-c)) showed changes in the chemical shifts of H²⁰, H²³, H²⁴, H²⁵ and H²⁶ resonances correlating to BB1·UIM-H⁺ **31***·**85** interaction, whereas the chemical shifts of **46** were unaffected in comparison to an isolated sample. This highlighted the preference for UIM-H⁺ **31*** to hydrogen bond with BB1 **85** rather than AIC **46**. The self-sorting behaviour of UIM-H⁺·BB1 **31***·**85** in the presence of AIC **46** could be reverted to favour the UIM·AIC **31**·**46** dimer in the presence of BB1 **85** by washing with basic sodium hydrogen carbonate solution (Figure 63 (a)).

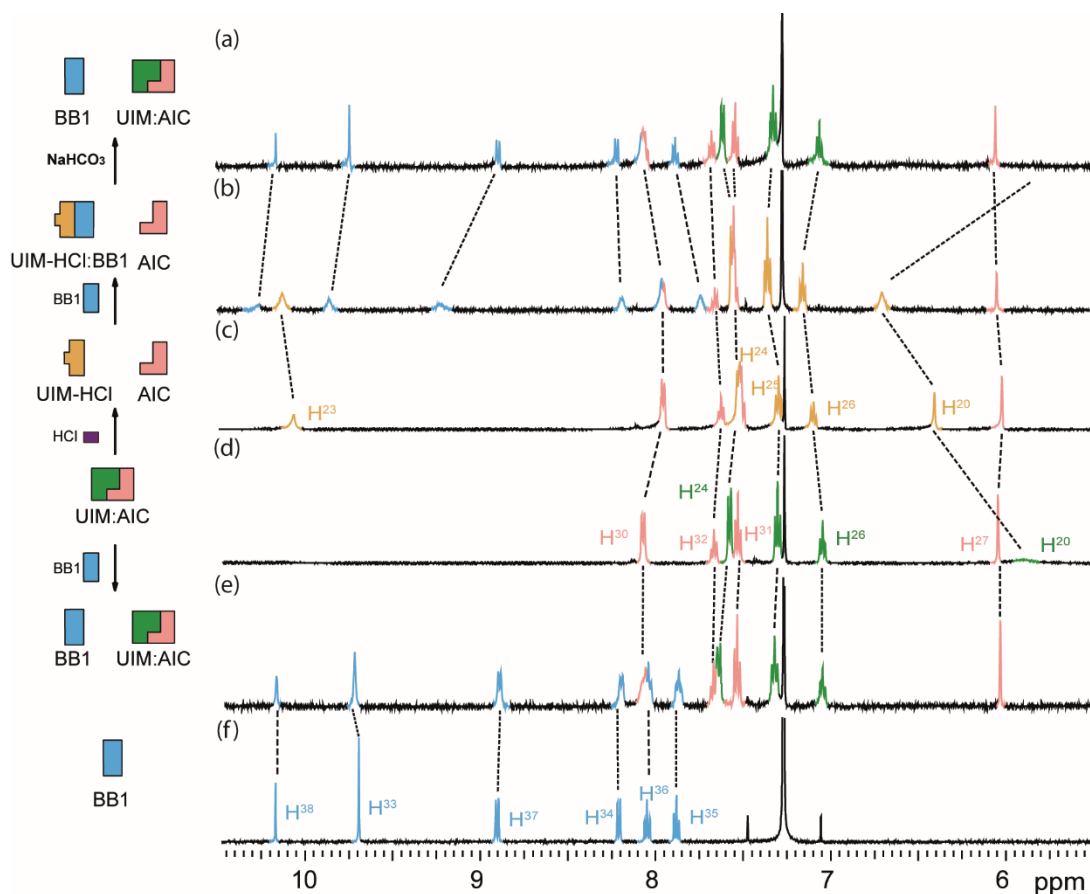


Figure 63. Self-sorting behaviour of proton responsive UIM 31 (system A) with AIC 46 and BB1 85 studied by ^1H NMR (500 MHz, 5 mM, CDCl_3) (a) UIM·AIC 31·46 dimer and BB1 85 formed after washing UIM-HCl·BB1 31*·85 dimer and AIC 46 mixture with NaHCO_3 (b) UIM-HCl·BB1 31*·85 dimer (protonated with 4M HCl in 1,4-dioxane) and AIC 46, (c) UIM-HCl 31* (protonated with 4M HCl in 1,4-dioxane) and AIC 46, (d) UIM·AIC 31·46 dimer, (e) UIM·AIC 31·46 dimer and BB1 85 and (f) BB1 85. Refer to Scheme 8 for the resonance assignment and chemical structure.

A similar series of ^1H NMR experiments carried out using system B mirrored this behaviour (Figure 64). The addition of TFA to a mixture of the UIM·AIC 31·46 dimer and HBM BB1 85 disrupted the UIM·AIC 31·46 dimer generating a mixture of the UIM-TFA·BB1 31*·85 dimer in presence of AIC 46 (Figure 64 (b)). The addition of 3 equivalents of DABCO to this mixture switched back 'on' the UIM·AIC 31·46 dimerisation and liberated BB1 85 (Figure 64 (a)). Overall, both systems demonstrated the ability of UIM 31 to undergo proton responsive switching in a mixture and hence switch the self-sorting behaviour

of the system. The addition of acid or base can promote switching between the UIM·AIC **31·46** and the UIM-H⁺·BB1 **31*·85** dimers.

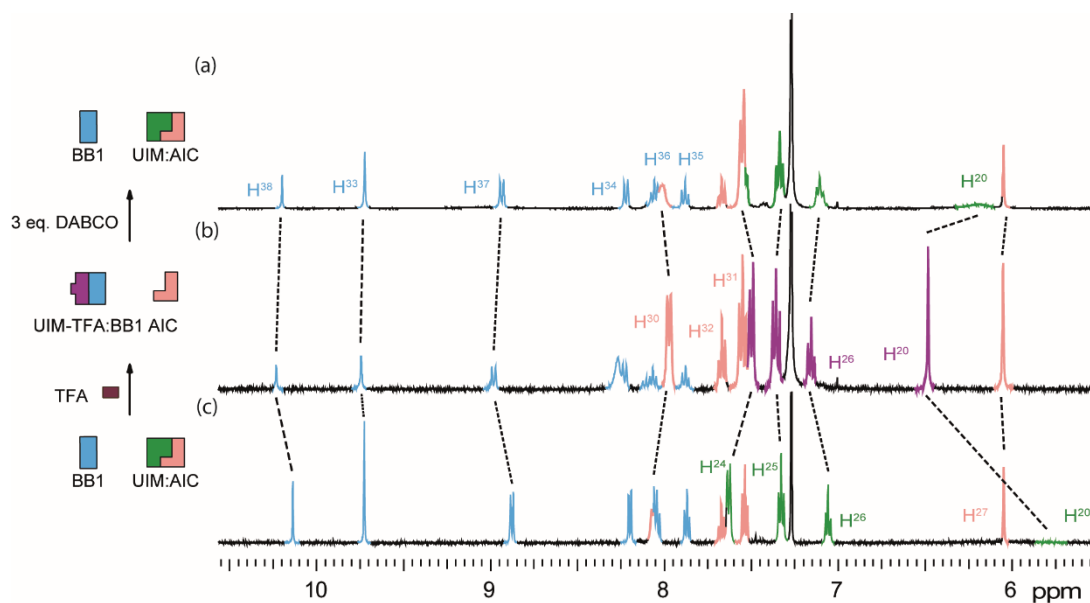


Figure 64. Self-sorting behaviour of proton responsive UIM 31 (system B) with AIC 46 and BB1 85 studied by ¹H NMR (500 MHz, 5 mM, CDCl₃) (a) UIM·AIC 31·46 dimer and BB1 85 formed after washing UIM-HCl·BB1 31*·85 dimer and AIC 46 mixture with 3 eq. DABCO, (b) UIM-TFA·BB1 31*·85 dimer (protonated with TFA) and AIC 46 and (c) UIM·AIC 31·46 dimer and BB1 85. Refer to Scheme 8 for the resonance assignment and chemical structure.

3.3 Analysis of a non-coordinating responsive hydrogen bonding motif

Reflecting on the original crystal structure of the intermediate **78** (Figure 55) where the chloride ion bridges four NH groups, the effect of the chloride ion on dimerisation was considered. In the studies described above, the chloride ion was treated as non-interfering in solution; however, this is likely to be an oversimplification as the chloride ion may coordinate with NH moieties effecting the hydrogen bonding (Figure 65). The coordination of a chloride ion could change the arrangement of the hydrogen bond donors and accepters and thus change the preferred dimer interactions.

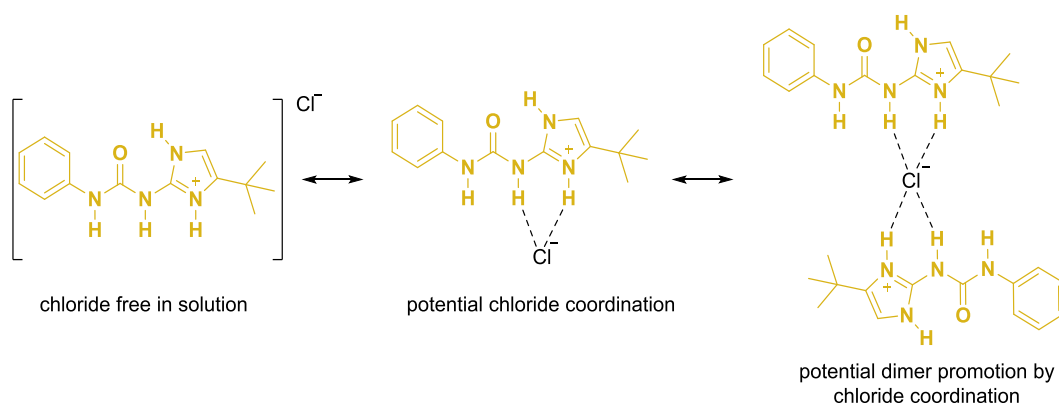
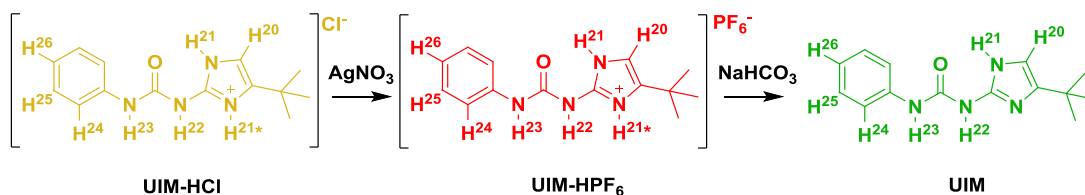


Figure 65. Showing potential chloride coordination in UIM-HCl and dimerisation.

To probe this, the chloride ion was exchanged for a non-interacting anion, hexafluorophosphate (PF₆) using silver hexafluorophosphate to create UIM-HPF₆ (Scheme 10).



Scheme 10. Formation of non-interacting motif UIM-HPF₆ from UIM-HCl and subsequent deprotonation to form UIM.

¹H NMR suggested that the UIM was still protonated as the chemical shift of the imidazole CH (H²⁰) was similar to that observed for UIM-HCl and the NH resonances were sharp (Figure 66 (b)). However, the NH resonances had shifted significantly implying a different environment. Next the proton dependent switching of UIM-HPF₆ was explored, revealing it was possible to deprotonate motif UIM-HPF₆ by washing with NaHCO₃ in the same way UIM-HCl was deprotonated in system A (Figure 66 (a)).

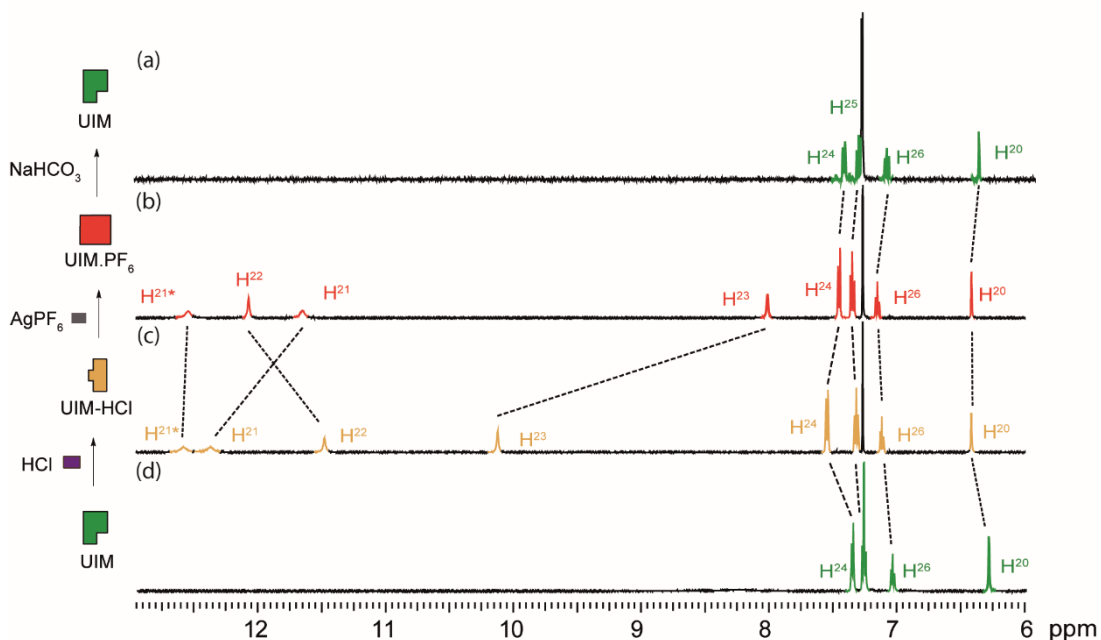


Figure 66. Formation of non-interacting motif UIM-HPF₆ and subsequent deprotonation to form UIM 31 studied by ¹H NMR (500 MHz, 5 mM, CDCl₃) (a) UIM 31 (deprotonated UIM-HPF₆ with NaHCO₃), (b) UIM-HPF₆ (formed on the addition of AgPF₆ to UIM-HCl 31*), (c) UIM-HCl 31* (protonated with 4M HCl in 1,4-dioxane) and (d) UIM 31. Refer to Scheme 10 for the resonance assignment and chemical structure.

The self-sorting preference of UIM-HPF₆ compared to UIM-HCl **31*** was investigated by ¹H NMR upon the addition of AIC **46** and BB1 **85** (Figure 67). As expected UIM-HPF₆ was able to form an interaction with complementary BB1 **85** (Figure 67d) and no interaction was seen on the addition of AIC **46** (Figure 67b). This agreed with the behaviour observed for UIM-HCl **31***.

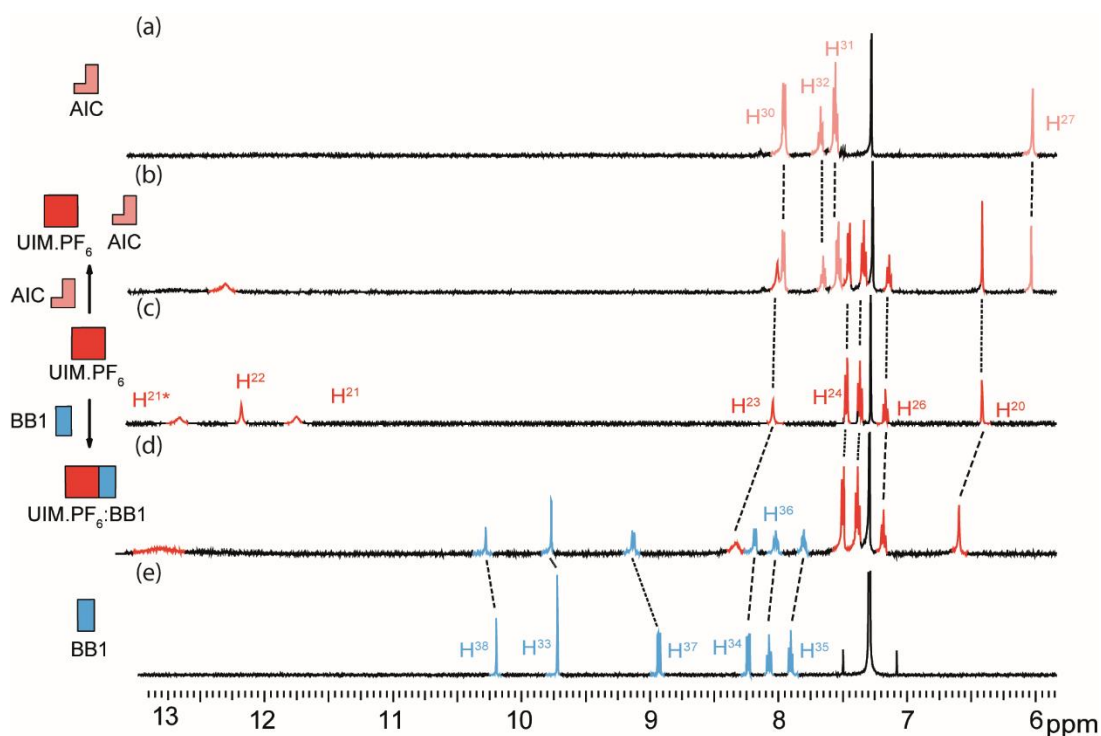


Figure 67 Self-sorting behaviour of proton responsive UIM-HPF₆ with AIC **46 and BB1 **85** studied separately by ¹H NMR (500 MHz, 5 mM, CDCl₃) (a) AIC **46**, (b) UIM-HPF₆ and AIC **46**, (c) UIM-HPF₆, (d) UIM-HPF₆.BB1 dimer and (e) BB1 **85**. Refer to Scheme 8 & 10 for the resonance assignment and chemical structure.**

When AIC **46** and BB1 **85** were combined with UIM-HPF₆, the ¹H NMR spectrum was indicative of an interaction between BB1 **85** and UIM-HPF₆ while the chemical shifts of AIC **46** were unchanged in comparison to the isolated samples (Figure 68). Efforts were made to switch this self-sorting behaviour 'off' by the addition of base to reform the UIM·AIC **31**·**46** dimer in

the presence of BB1 **85**. However due to the low solubility of BB1 **85** and the process of washing with NaHCO_3 , sample was being lost thus it was not possible to obtain a well resolved ^1H NMR spectra with equal ratios of hydrogen bonding motifs. The low solubility of the HBM BB1 **85** in CDCl_3 was problematic throughout these series of experiments, but it was more profound the system using PF_6 salts than the acid containing systems. It is logical that the acidic UIM samples are more soluble than the UIM- HPF_6 species, which could led to an enhanced solubility of the HBM BB1 **85** in the acid containing systems.

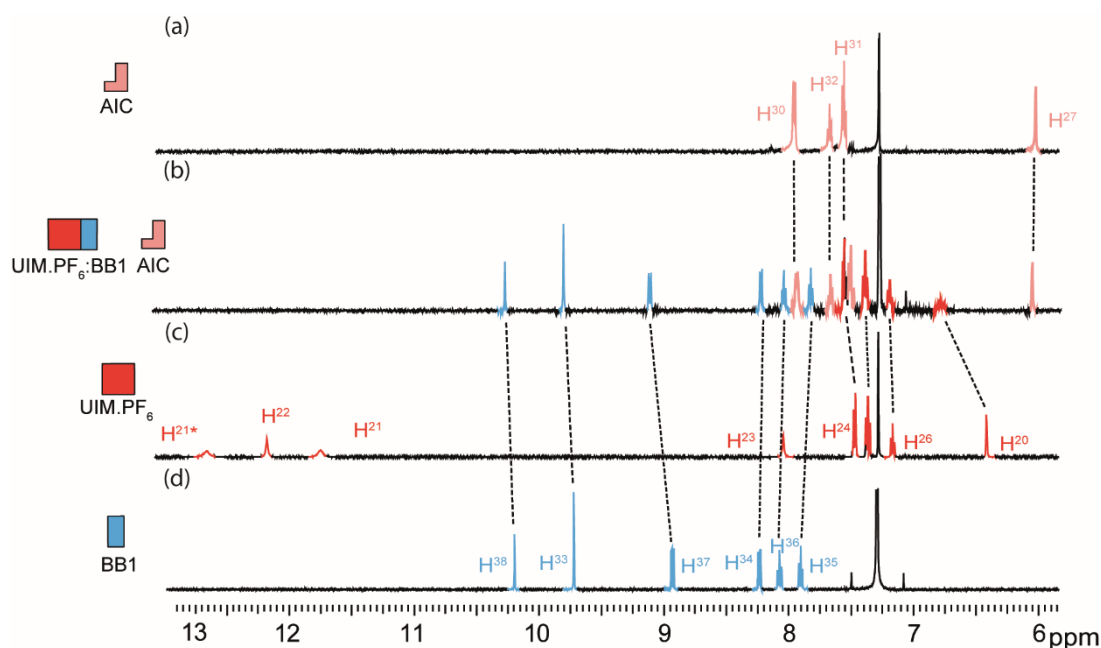


Figure 68. Self-sorting behaviour of proton responsive of UIM- HPF_6 with AIC 46 and BB1 **85 combined studied by ^1H NMR (500 MHz, 5 mM, CDCl_3) (a) AIC 46 (b) UIM- HPF_6 :BB1 dimer and AIC 46, (c) UIM- HPF_6 and (d) BB1 **85**. Refer to Scheme 8 & 10 for the resonance assignment and chemical structure.**

Overall, the self-sorting behaviour exhibited by UIM- HPF_6 closely mimics the preferences exhibited by HBM UIM- HCl ; and so, it difficult to conclude if the chloride ion is coordinating to the hydrogen bonding motifs and influencing the

dimerisation interactions. Efforts to obtain crystal structures of the different salts and dimers were futile.

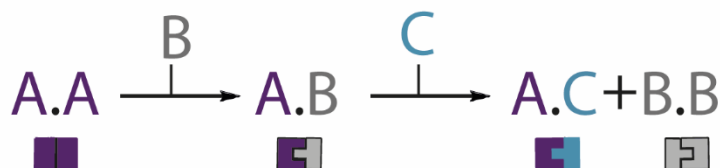
3.4 Conclusions

A responsive cationic hydrogen bonding motif **31*** was created via protonation of the triple hydrogen bonding motif UIM **31**. Protonation of UIM **31** changed the hydrogen bonding array from *DDA* to *DDD*. Reversible switching between the neutral and protonated species was achieved through the addition of a variety of acids and bases. This switching behaviour was identified and monitored by ¹H NMR experiments. The formation of cationic hydrogen bonding motifs with both interacting and non-interacting anions was explored. The neutral and protonated species of UIM were shown to preferentially interact, self-sort, with their complementary partners, AIC **46** and BB1 **85** respectively. In a system containing the responsive hydrogen bonding motif (**31**) and the two complementary partners (**46** and **85**) the molecular recognition could be reversibly switched between two self-sorted states. This illustrates that *in situ* switching of molecular recognition between hydrogen bonding motifs is possible in a simple self-sorting network. Future efforts would explore the incorporation of this and other responsive hydrogen motifs in more complicated self-sorting pathways and networks. Development of pathways with multiple orthogonal responsive motifs could offer reversible control over several phases of self-sorting and drive the final product distribution away from equilibrium.

4. Developing self-sorting supramolecular polymer blends

Building on the understanding of self-sorting behaviour of hydrogen bonding motifs discussed in Chapter 2, this chapter focuses on efforts to develop supramolecular polymers capable of self-sorting. It was thought that the sequential self-sorting behaviour of basic molecular hydrogen bonding motifs (A, B and C for simplicity) could be translated into macromolecular systems that assemble into supramolecular polymers (Figure 69). The strategy would be to combine the known self-sorting hydrogen bonding motifs (discussed in Chapter 2) with polymers through side chains functionalisation, that could then assemble into cross-linked supramolecular polymers. It was hypothesised that self-sorting could occur between hydrogen bonding motifs on side chains groups (A, B and C) without dramatically influencing the materials behaviour of the polymer backbone (Figure 69 (b)). This could lead to subtle changes in the material properties on self-assembly and self-sorting.

(a) Sequential self-sorting of A, B and C hydrogen bonding motifs.



(b) Sequential self-sorting of polymers functionalised with A, B and C hydrogen bonding motifs.

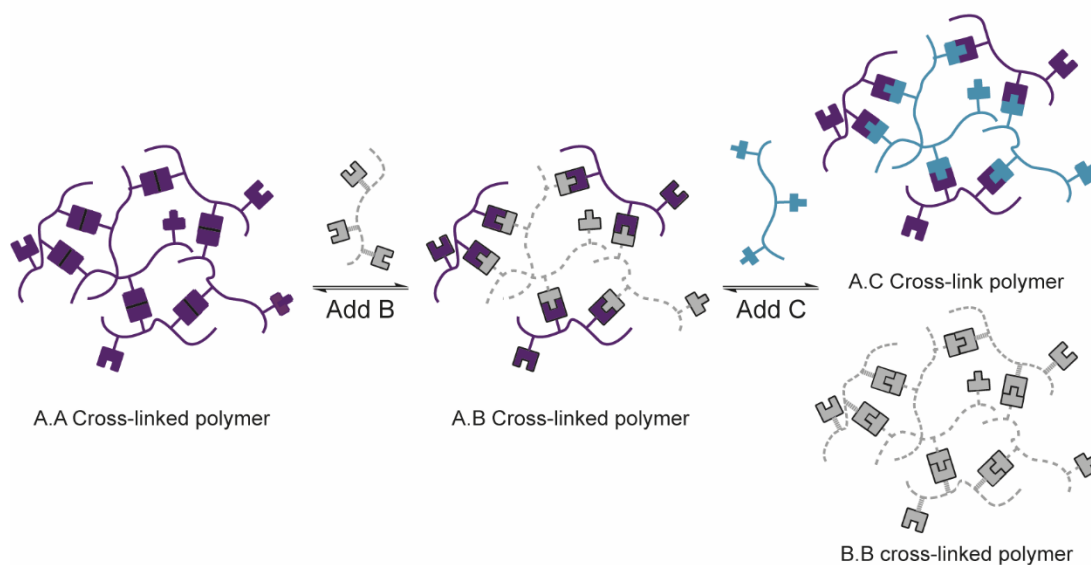


Figure 69. Schematic showing the use of sequential self-sorting of hydrogen bonding motifs to create self-sorting supramolecular polymers.

Polymeric blends were selected to test this hypothesis. Polymer blends are physical mixtures of two or more polymers, these could be homopolymers or copolymers.¹⁵¹ The major incentive to develop blends is to enhance the properties of the individual homopolymers and co-polymers, which can lead to various industrial applications based on their properties (e.g. the aircraft industry).¹⁵² For this to be viable, the polymers must be compatible, which means that they must form stable mixtures at the molecular level. If the polymers are not compatible, phase-separation occurs and the system will exhibit undesirable or ill-defined mechanical properties.¹⁵³ The behaviour of

polymer blends depends, in general, on the degree of mixing of the components and their mutual interaction, as well as the individual properties of the components. This difference in the properties means that most pairs of polymers are not miscible on a molecular level (e.g (poly)styrene (PS) and (poly)methylmethacrylate (PMMA)), and, in the majority of cases, the mixing of two polymers results in phase separation.^{154,155}

The compatibility of polymers can be understood in terms of thermodynamics specifically from the relationship between the Gibbs free energy (ΔG_m), enthalpy (ΔH_m) and entropy (ΔS_m) on mixing.^{156,157} For complete miscibility of two polymers on mixing, Equation 1 must be fulfilled. Hence the Gibbs free energy on mixing must be less than zero for a miscible blend. Taking this assumption $\Delta G_m < 0$, Equation 2 highlights that for a single phase on mixing, the entropic contribution must be larger than the enthalpic contribution.

Equation 1 $\Delta G_m = \Delta H_m - T\Delta S_m < 0$

Equation 2 $\Delta H_m < T\Delta S_m$

According to the Flory-Huggins theory, entropy on mixing is always positive due to the increased number of possible configurations that a given molecule can exhibit when the two components are mixed, hence miscibility is always promoted.¹⁵⁸⁻¹⁶⁰ However for large molecular weight polymers this entropic contribution is negligible. This can be considered in terms of the lattice model (Figure 70). For small molecules/monomers there are many possible positions

the monomer can move in the lattice and so the entropy is large (Figure 70 (a)). When small polymers are placed in a lattice each monomer occupies a lattice site but consecutive monomers in the chain must be in adjacent sites (Figure 70 (b)) so there are less possible configurations of each monomer and the entropy is reduced. However, when high molecular weight polymer chains are placed in a lattice (Figure 70 (c)), the number of possible configurations is greatly reduced, due to the increased number of monomers and constraints of the polymer chain, the entropy becomes insignificant. Consequently, the enthalpic contribution often controls the miscibility of a polymer blend system. Favourable enthalpic interactions such as hydrogen bonding interactions can improve the enthalpy on mixing and hence decrease the Gibbs free energy to stimulate single phase formation over phase separation.¹⁶¹

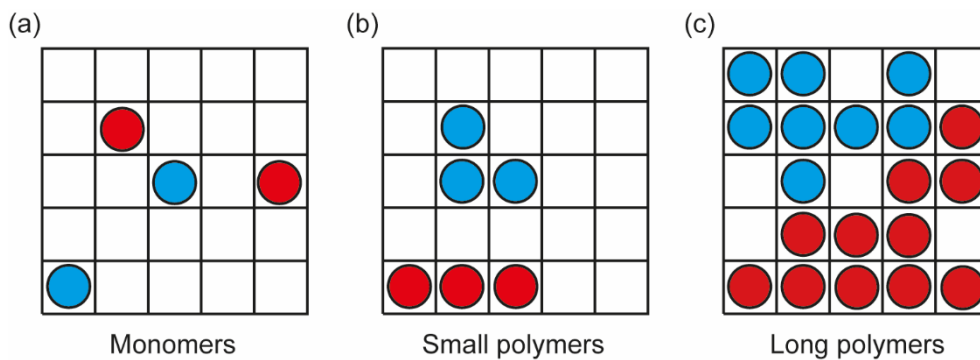


Figure 70. The Flory-Huggins Lattice Model comparing the possible configurations of (a) monomers, (b) small polymers and (c) long polymers in a lattice. Circles represent monomers which make up polymer chains, blue and red show different types of monomers/polymers.

Phase separation of a two component mixture can be understood through a generic phase diagram in terms of temperature (Figure 71).^{156,162} Polymer-polymer mixtures largely exhibit lower critical solution temperature (LCST). This is the minimum of the boundary curves (binodal and spinodal) at which both the single and two-phase regions are identical. The binodal curve (blue curve) separates the single phase and metastable region (green area), the spinodal curve (red curve) separates the metastable and two-phase region. Phase separation can occur by two methods; nucleation and growth mechanism (through a metastable region) or spinodal decomposition mechanism (directly jump to a two-phase region) and can be triggered by a change of composition, temperature or pressure.¹⁶³ It is thought that the favourable interactions between complementary hydrogen bonding motifs can stabilise the polymer blends in the single phase region.

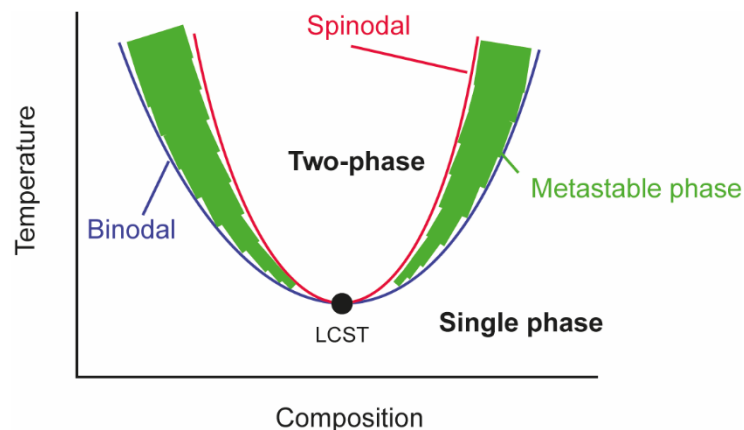


Figure 71. Phase diagram showing the single, metastable and two-phase regions possible for polymer-polymer system in terms of composition and temperature. LCST (black dot), binodal curve (blue), spinodal curve (red) and metastable phase (green).

The long-term goal would be to combine several different co-polymers functionalised with complementary hydrogen bonding motifs. The self-sorting behaviour of the hydrogen bonding motifs of each polymer would control the cross-linked state of the polymer. The presence or absence of complementary hydrogen bonding motifs could drive transitions between cross-linked polymers and differing degrees of phase separation.

Figure 72 illustrates how the self-sorting behaviour of known hydrogen bonding motifs (described in Chapter 2) may be applied to polymer blends. AUPy and NAPyO are known to form a heterodimer through hydrogen bonds, if these motifs are used to functionalise immiscible polymers the hydrogen bonding interactions should result in a compatible blend between the (poly)styrene and (poly)methyl methacrylate backbones. On the addition of a (poly)methyl methacrylate co-polymer functionalised with DAN, the blend should breakdown as DAN-PMMA co-polymer will displace the NAPyO-PS co-polymer to give two phase separated cross-linked co-polymers (AUPy-PMMA cross-linked to DAN-PMMA and NAPyO-PS cross-linked to itself). This has the potential to translate the self-sorting behaviour from the molecular level to polymer blends.

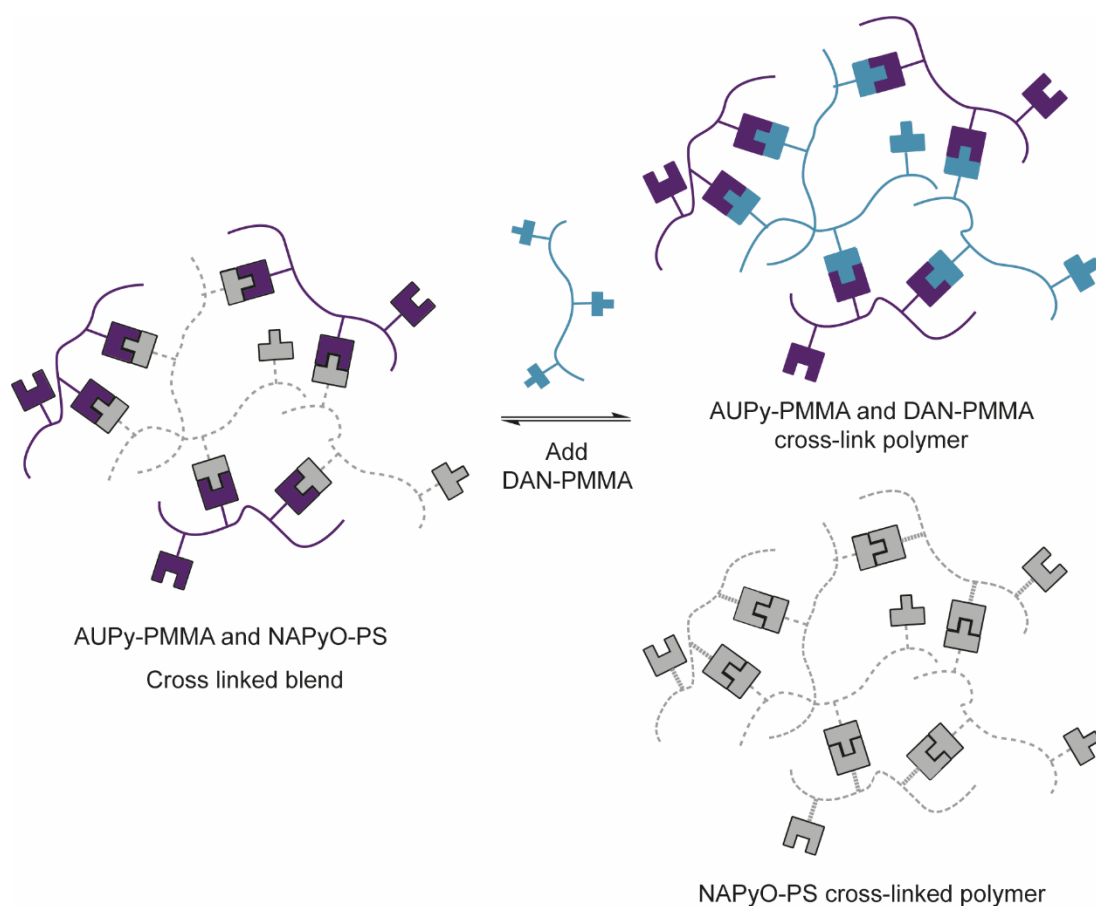


Figure 72. A schematic showing potential self-sorting in polymer blends due to side chain functionalisation with self-sorting hydrogen bonding motifs.

The first stage to achieving this goal was to design and synthesise copolymers with orthogonal set of complementary hydrogen bonding motifs that could form a supramolecular blend. For this we turned to hydrogen bonding motifs that are well established and known to self-sort as described in Chapter 2 as well as previously reported polymer blends. In the previous study carried out by the Wilson group, poly(styrene) and poly(methyl methacrylate) polymers functionalised with *DAD* and *ADA* hydrogen bonding motifs respectively.¹⁰⁶ These complementary triply hydrogen bonding motifs have relatively weak dimerisation energy $k_a \sim 56 \text{ M}^{-1}$ (in CHCl_3) (due to secondary electrostatic repulsion). Yet with 6% *DAD* and 14% *ADA* incorporation into the

respective PS and PMMA co-polymers, the additive affinity was sufficient to form a polymer blend between the immiscible polymers. With this previously described system in mind,¹⁰⁶ complementary hydrogen bonding motifs AIC and UIM with *DAA* and *ADD* arrays described previously were selected as ideal candidates. As well as being orthogonal to the reported *DAD:ADA* array, this *DAA:ADD* array had the benefit of a higher association constant at $K_a \sim 3 \times 10^4 \text{ M}^{-1}$. It was hypothesised that due to the higher affinity of the *DAA:ADD* array in comparison to the affinity of the *DAD:ADA* array previously reported, a lower degree of incorporation of the hydrogen bonding motif into the co-polymer would be required for the same degree of blend formation.

The aim of this project was to create an alternative polymer blend with orthogonal complementary hydrogen bonding partners to meet three objectives. The first objective was to create an alternative polymer blend to confirm hydrogen bonding induced blending of immiscible polymers was reproducible. The second objective was to study the properties of the blend to understand how blending the two polymers may alter their materials properties in comparison to the pure polymer and the previously reported system. The final objective would be to probe if these orthogonal system it would be suitable to develop self-sorting polymer blends.

The strategy to create polymer blend with *DDA:AAD* complementary hydrogen bonding partners is outlined in Figure 73. AIC-styrene and UIM-MMA co-monomers are designed and synthesised, then co-polymerised by RAFT to form functionalised co-polymers, which are subsequently mixed to create a supramolecular polymer blend.

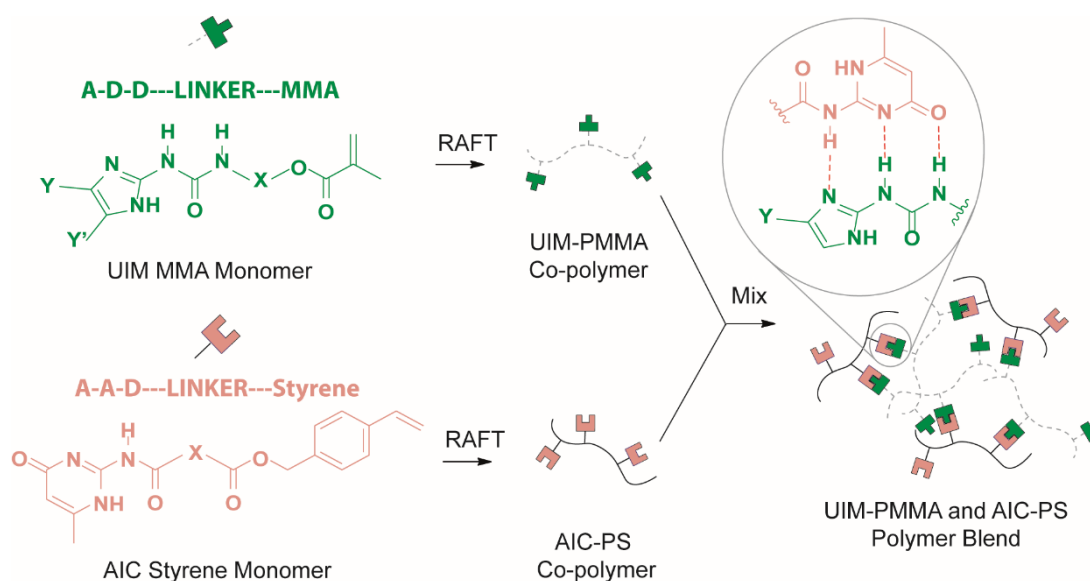


Figure 73. A schematic outlining the strategy for the formation of a supramolecular blend between UIM-PMMA and AIC-PS co-polymers.

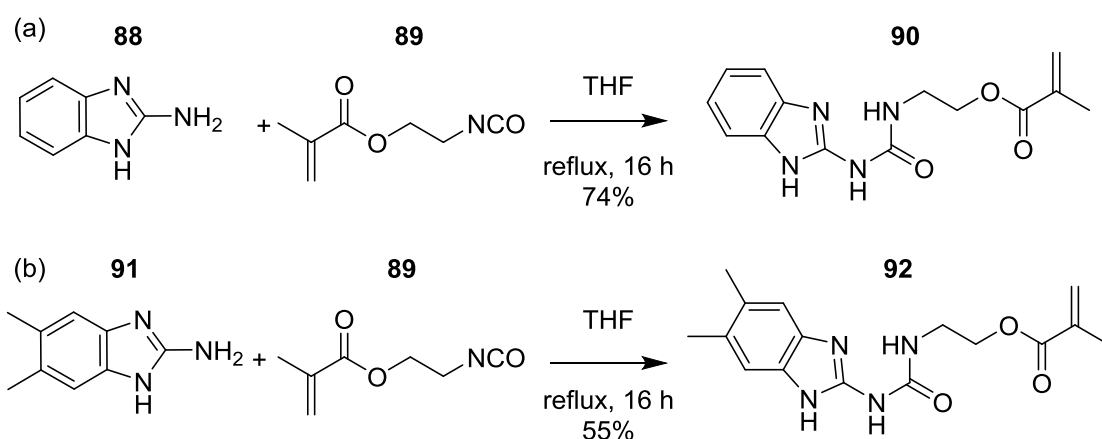
The design and synthesis of the co-monomers are described in section 4.1. Previous research from Rotello, Zimmerman and Wilson proved that polymers functionalised with side chain hydrogen bonding motifs could be created by direct co-polymerisation and post polymerisation modification strategies.^{17,106,164,165} Early work by Rotello required post polymerisation modification reaction, because of the incompatibility of the recognition motifs with the free radical polymerisation methods used to obtain the poly(styrene) backbones.^{165,166} Other groups tried to overcome this problem by using living and functional group tolerant polymerisation methods such as ring-opening metathesis polymerisation (ROMP).^{167,168} The Wilson group concluded that direct co-polymerisation by means of reversible addition fragmentation chain transfer (RAFT) offered greater control over the polymer composition, both degree of polymerisation and percentage incorporation of hydrogen bonding motifs, hence this methodology was selected for the current study.¹⁰⁶

After the synthesis of the co-polymers two complementary co-polymers would be combined to form a cross-linked polymer blend, and the (material) properties of the polymer blend would be investigated. Having a clear understanding of how two complementary side chain co-polymers interrelate is essential prior to the development of a self-sorting polymer network comprising many functionalised co-polymers. Ideally, physical markers, such as glass transition temperature (T_g), would be used to differentiate between a cross-linked or separated state initially in a two-component system. There is widely accepted evidence that blends which display a single T_g are miscible.¹⁵⁷ In turn, these markers would be used to monitor blend formation in a more complex mixture of co-polymers and hence investigate if self-sorting of co-polymers is viable. In this work visual observations and the T_g are used as indicators for polymer blending.

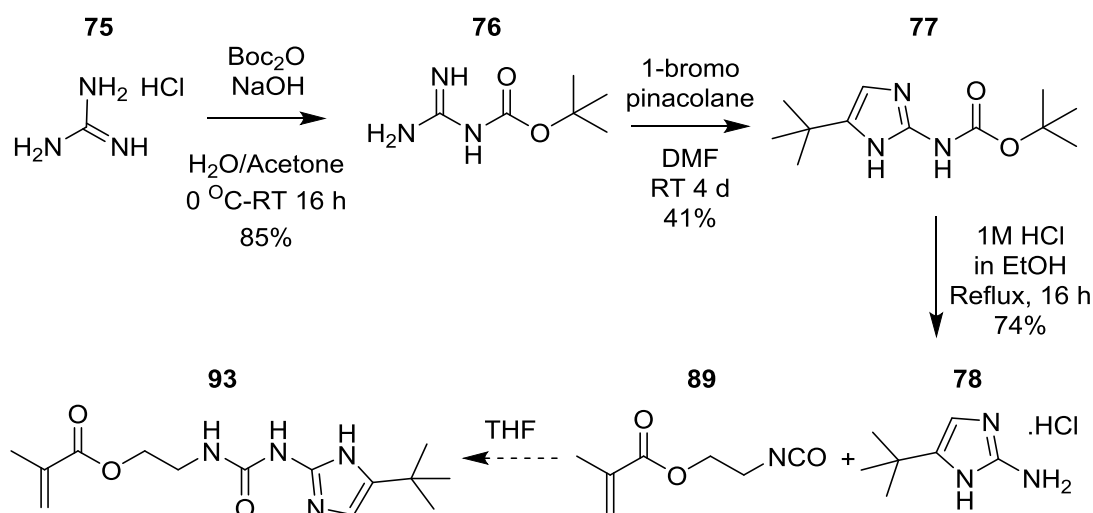
4.1 Monomer design and synthesis

4.1.1 DDA functionalised methacrylate monomers

Methacrylate functionalised polymerisable compounds **90** and **92**, presenting a *DDA* hydrogen bonding array, were synthesised from the reaction of isocyanate **89** with amines **88** and **91** respectively (Scheme 11). This synthetic method was adapted from literature procedures reported by the Wilson group.¹⁰⁶ The work up of the reaction was simplified because the product precipitated out of the reaction mixture in both cases, was filtered and dried rather than requiring further purification by column chromatography and recrystallisation. However, the solubility of these two monomers was poor in organic solvents which could create problems for polymerisation reactions. We rationalised that the replacement of the benzimidazole motif with a *tert*-butyl imidazole would increase the solubility of the resulting monomer. As such the synthesis of methyl methacrylate monomer **93** was attempted (Scheme 12).



Scheme 11. The synthetic route for preparation of methacrylate monomers (a) **90** and (b) **92** adapted from synthesis previously reported by the Wilson group.¹⁰⁶



Scheme 12. The synthetic route for preparation of methacrylate monomer 93 adapted from the syntheses previously reported by the Wilson group.^{40,106}

The synthesis of monomer **93** combines two synthetic methods previously reported by the Wilson group (Scheme 12).^{40,106} *N-tert* butoxy carbonyl guanidine **76** and protected imidazole **77** were synthesised following the literature procedure.⁴⁰ The literature notes that the *tert* butyl deprotection of imidazole **77** using hydrochloric acid in ethanol results in an unstable amine **78** which was shown to degrade. Consequently, as a precaution, following the deprotection of imidazole **77** the resulting amine **78** was not isolated was reacted immediately with isocyanate **89** to form methacrylate monomer **93**. NMR studies of this monomer were odd as several of the NH peaks were overlapped or not present. NOESY and NOE data of this molecule with a complementary monomer did not show the expected interactions. Eventually, a crystal structure was obtained which revealed a single nucleophilic addition occurred at the N1 position of imidazole ring rather than the expected exocyclic primary amine (Figure 74).

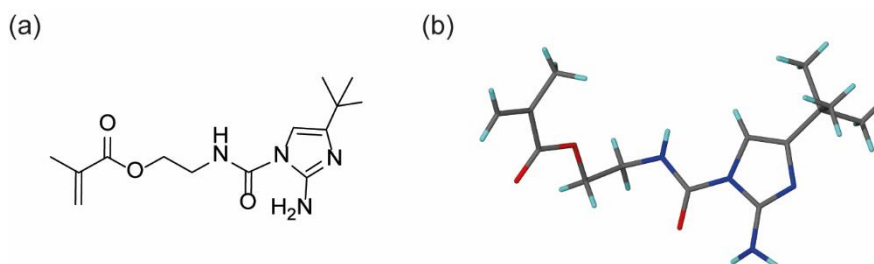
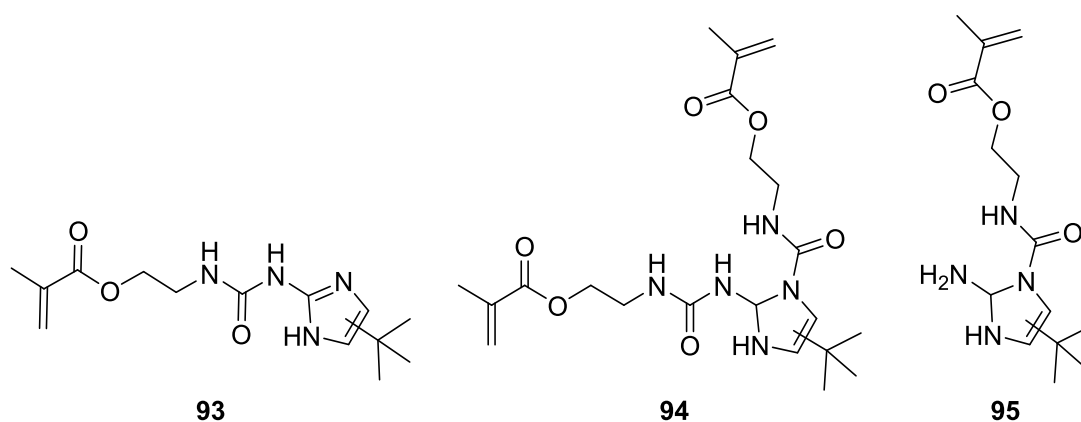
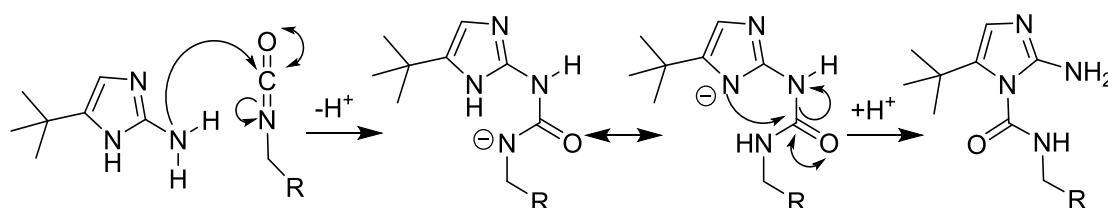


Figure 74. The product from the reaction of tert-butyl imidazole amine 78 with isocyanate 89 (a) structure and (b) crystal structure.

This led to the question: Does the nucleophilic addition take place at both the N1 position of imidazole ring and exocyclic primary amine? to give a mixture of three products (Scheme 13), or: Does the nucleophilic addition first occur at the exocyclic primary amine and then rearrangement occur to result in acylation of the imidazole ring? (Scheme 14).



Scheme 13. Potential products of the reaction between tert-butyl imidazole amine 78 and isocyanate 89.

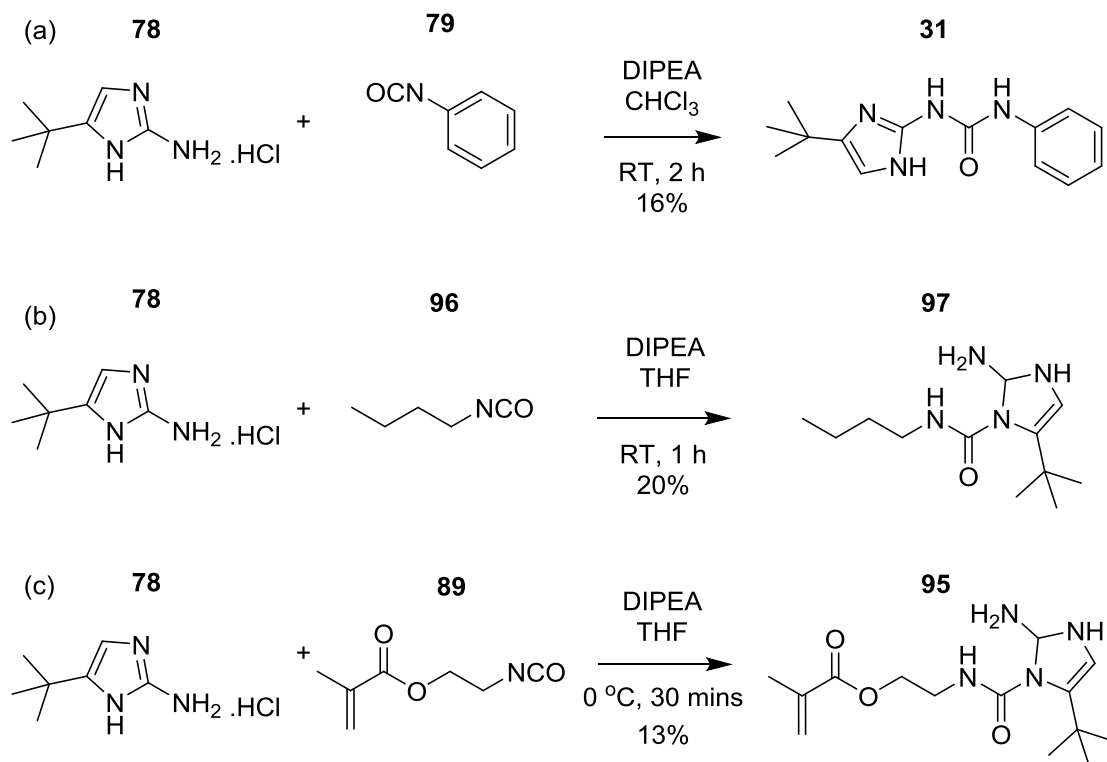


Scheme 14. Potential rearrangement reaction for the formation of 95.

As a result, attempts were made to control the reaction to give the desired product by changing the reagent stoichiometries and reducing the temperature to slow down the reaction while monitoring over time. This showed that the reaction occurs quickly with mono-substituted and di-substituted compounds forming after five minutes on ice. This suggested that nucleophilic addition was very fast occurred at both positions rather than a rearrangement occurring. However, the NMR of the isolated mono-substituted compound was still ambiguous as to the regioselectivity of the nucleophilic addition. Crystal structures have been previously reported confirming that the reaction of the *tert*-butyl imidazole with several phenyl isocyanate analogues results in nucleophilic attack from the exocyclic NH₂ as desired.¹²³ In fact, the synthesis of the hydrogen bonding motif UIM **31** described in Chapter 2 confirms the reaction of *tert*-butyl imidazole **78** with phenyl isocyanate **79** gives the desired product **31** (Scheme 15 (a)) with reaction on the exocyclic NH₂. This led to the question: Do aromatic substrates react at the exocyclic primary amine preferentially while alkyl substrates react at the N1 position of the imidazole ring?

Consequently, a test reaction was carried out with the *tert*-butyl imidazole **78** and *neo*-butyl isocyanate **96** (Scheme 15 (b)). Compound **97**, formed by the reaction of alkyl isocyanate **96** at the N1 position of the imidazole ring, was identified as the isolated product. This correlated well with the crystal structure of the isolated product **95** from the reaction between *tert*-butyl imidazole **78** and isocyanate **89** (Scheme 15 (c)). This suggests alkyl isocyanates preferentially form the product from a single nucleophilic addition at the position of the imidazole ring.¹⁶⁹ However when considering the isolated yields

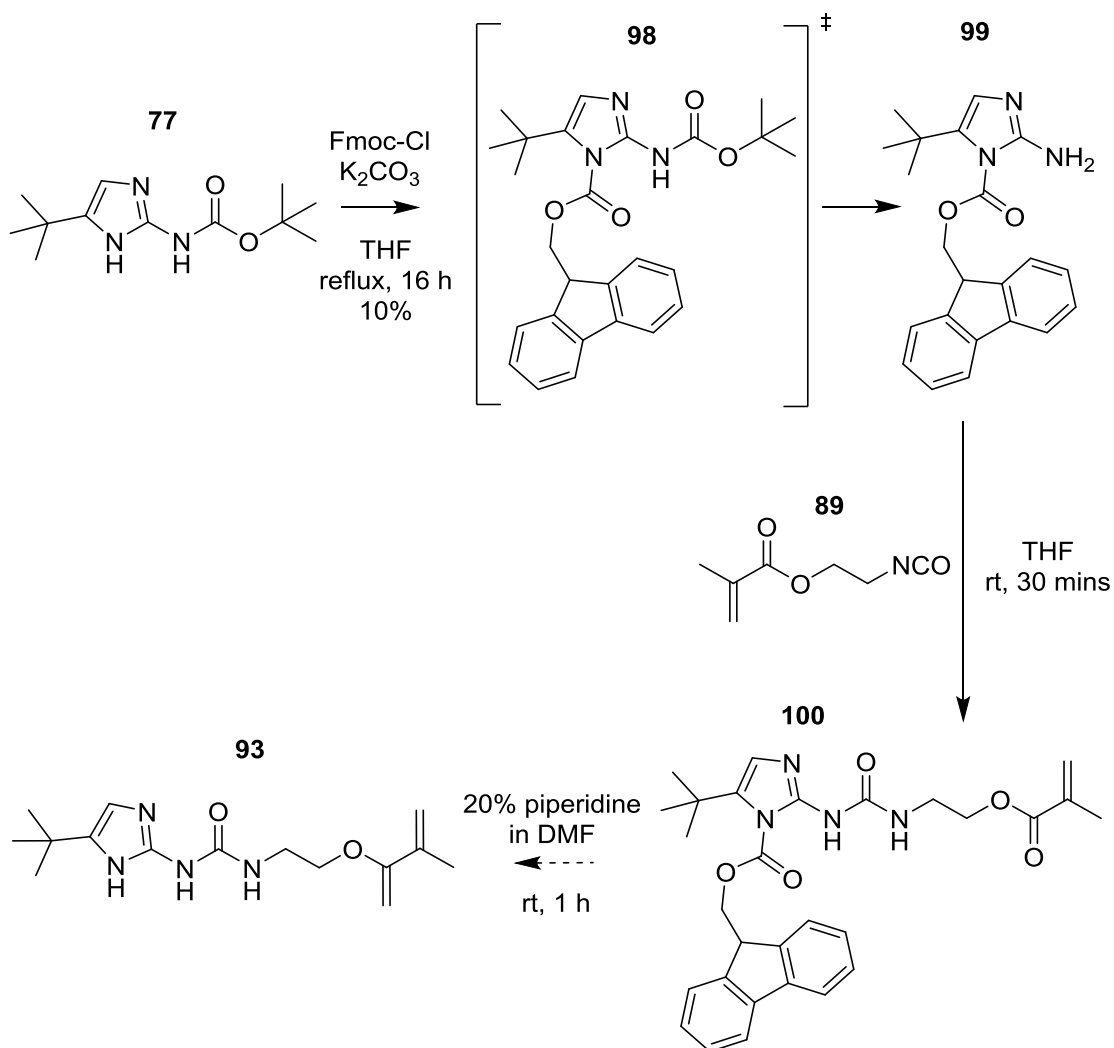
of compounds **31**, **97** and **95** (Scheme 15) range from 13-20% it's clear no real conclusions can be made about the most favourable site of reaction or potential rearrangement.



Scheme 15. The synthetic route for the formation of **31, **97** and **95**.**

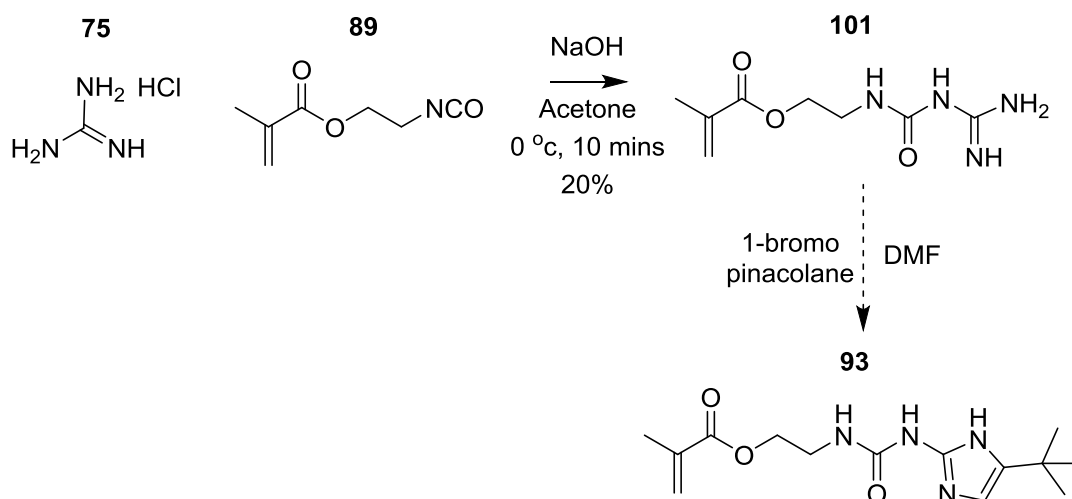
To avoid the nucleophilic addition at the imidazole ring, an alternative synthetic route was devised which protected the amine on the imidazole ring with a fluorenylmethyloxycarbonyl (Fmoc) moiety (Scheme 16). Fmoc was chosen as an orthogonal protecting group to Boc, so the Fmoc group would remain during Boc deprotection of compound **98** to form the primary amine **99**. It was thought that the Fmoc group would block the site for nucleophilic addition on the imidazole ring and force the reaction of the exocyclic primary amine in compound **99** to react with isocyanate **89** to form compound **100**.

The Fmoc group would then be cleaved to give the target molecule **93**. Although there was evidence the reaction was successful, isolation and purification of the target molecule could not be achieved in sufficient quantities at this stage.



Scheme 16. The proposed synthesis of methacrylate monomer **93** using Fmoc protection.

Additionally, the synthesis of compound **93** was also attempted following Scheme 17 in which isocyanate **89** is reacted with guanidine HCl salt **75** to form intermediate **101** followed by a cyclisation reaction to form the *tert*-butyl imidazole moiety. Unfortunately, there was no evidence of the formation of compound **93** in this synthesis. The synthesis of target molecule **93** was explored no further and instead efforts turned to the design of a monomer containing a *tert*-butyl imidazole moiety with a urea link to a phenyl moiety and a methyl methacrylate end group (Scheme 18).

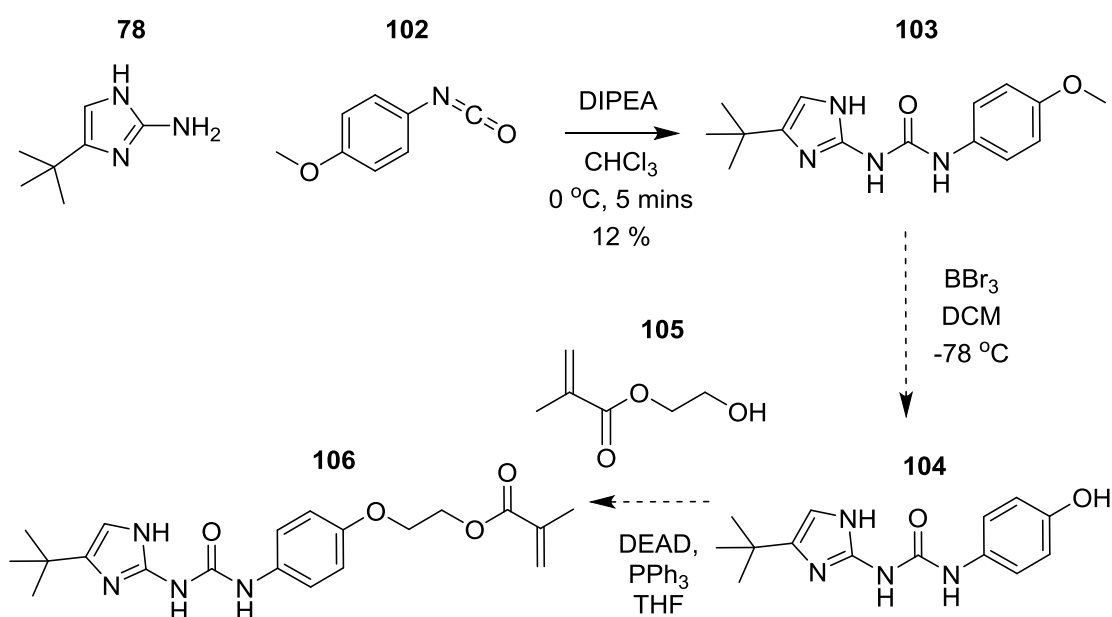


Scheme 17. The proposed synthesis of methacrylate monomer **93 forming the urea prior to the *tert*-butyl imidazole.**

Scheme 18 shows the reaction of *tert*-butyl imidazole **78** and 4-methoxyphenyl isocyanate **102** to form urea **103** followed by ether cleavage to give the alcohol **104**. A Mitsunobu reaction between alcohols **104** and **105** forms the methyl methacrylate monomer **106**. Test reactions with phenyl analogues showed that the ether cleavage and Mitsunobu reactions were feasible in the presence of the methacrylate moiety. However due to the low yield of the reaction

between imidazole **78** and isocyanate **102** this synthesis was no longer pursued.

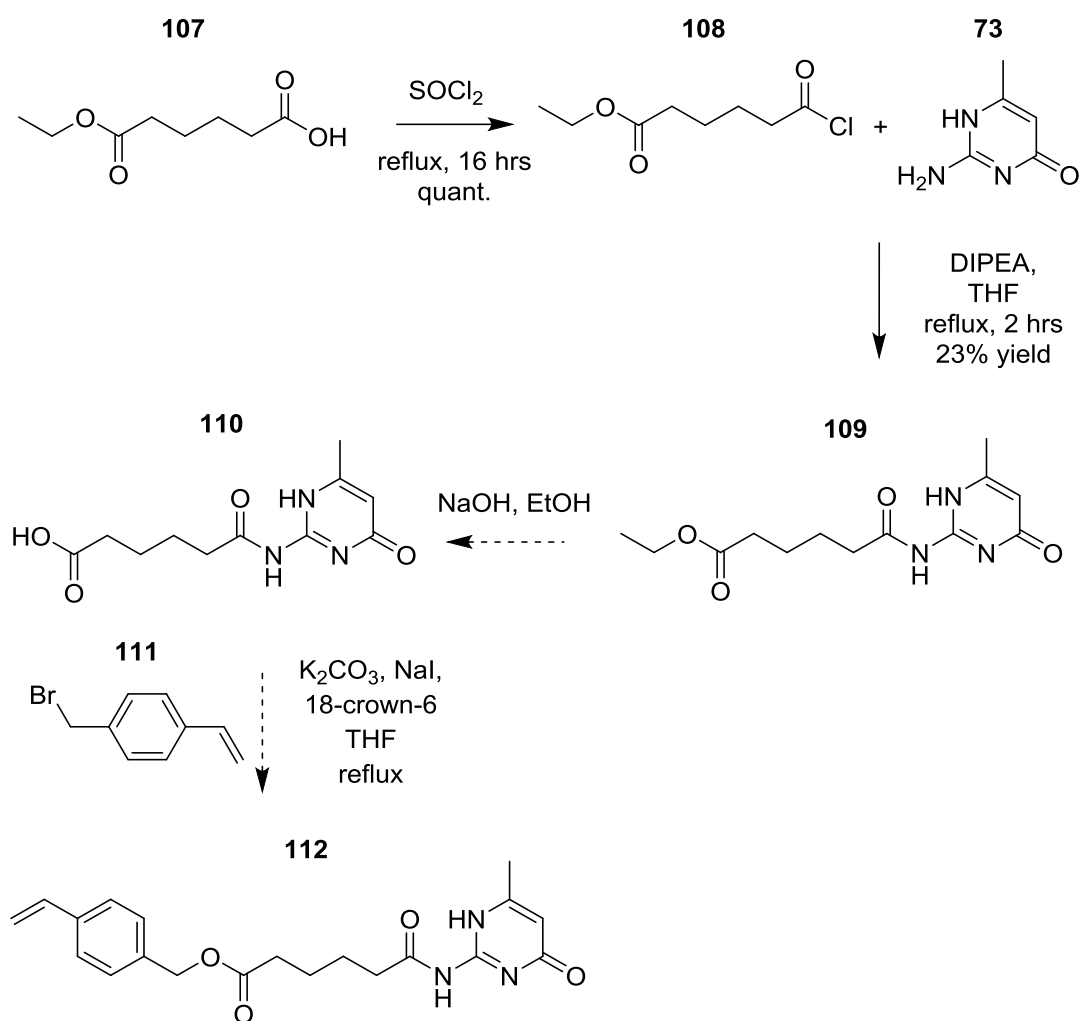
It was decided that further design and synthetic optimisation of a potentially more soluble methacrylate monomer would not be beneficial to the project at this stage and so the less soluble monomers **90** and **92** were taken forward in co-polymerisations.



Scheme 18. Potential synthetic route for preparation of an aromatic containing methyl methacrylate monomer 106.

4.1.2 AAD functionalised styrene monomers

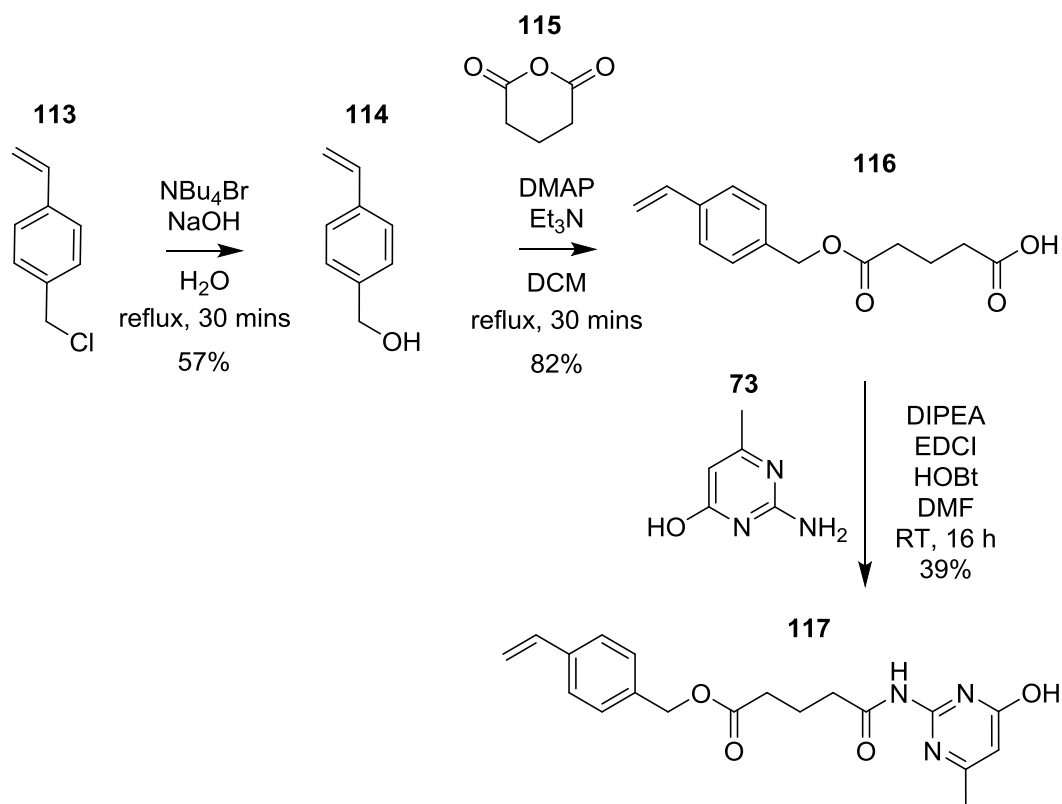
Compound **112** was initially designed as a complementary AAD functionalised styrene monomer. The synthetic route outline in Scheme 19 was adapted from a literature procedure previously reported by the Wilson group.¹⁰⁶ The acid chloride **108** was synthesised from the acid **107** and assuming a quantitative yield was reacted immediately with 2-amino-4-methyl-6-hydroxypyrimidine **73** to form ethyl ester **109**. The hydrolysis of the ethyl ester **109** to the acid **110** was first carried out using pH 13 sodium hydroxide at reflux temperature but resulted in cleavage of the amide bond. This hydrolysis was then repeated several times to find optimal conditions. However, the hydrolysis of the ethyl ester in the presence of the amide was not possible in the conditions tested.



Scheme 19. The synthetic route for preparation of styrene monomer **112** adapted from a synthesis previously reported by the Wilson group.¹⁰⁶

This led to the design of a different *AAD* array functionalised styrene monomer **117** in which the amine coupling occurs in the final step and no hydrolysis in the presence of the amine is required. Monomer **117** was initially synthesised by the reactions shown in Scheme 20. The synthetic route A was adapted from several literature procedures to form a styrene containing monomer with a suitable length linker between the *AAD* motif and styrene moiety. However, the reproducibility of the final reaction between **116** and **73** to give **117** was poor. The purification of **116** and **117** was problematic as the crude mixture

often became gelatinous and insoluble in organic solvents over time hindering further purification. It was thought that the styrene moiety had covalently cross-linked (polymerised) to form an insoluble polymer.



Scheme 20. The synthetic route A for the preparation of styrene monomer 117.

Consequently, an alternative synthetic route B was attempted in which the styrene moiety was introduced in the final synthetic step (Scheme 21). Synthetic route B proved to be advantageous as the synthesis was shorter and purification easier. For example, intermediate **118** and product **117** could be isolated by trituration without the requirement for further purification, column chromatography was only used to purify the filtrate and increase the yield of the final step.

4.1.3 ^1H NMR Studies of Heterocomplementary Monomer

Components

Prior to the co-polymerisation of the functionalised monomers **90**, **92** and **117** ^1H NMR studies were attempted to confirm the expected triple hydrogen bonding interaction. Ideally these studies would be carried out in an aprotic solvent such as CDCl_3 to ensure the solvent wouldn't interfere with the hydrogen bonding interactions; however, MMA-UIM monomer **90** was not soluble in CDCl_3 . MMA-UIM monomer **90** was soluble in DMSO, but as a polar aprotic solvent this competes with the hydrogen bonding by acting as a hydrogen bond acceptor. Thus when the two monomers were combined in a 1:1 ratio in deuterated DMSO solvent there was no change in the chemical shifts of diagnostic resonances (Figure 75).

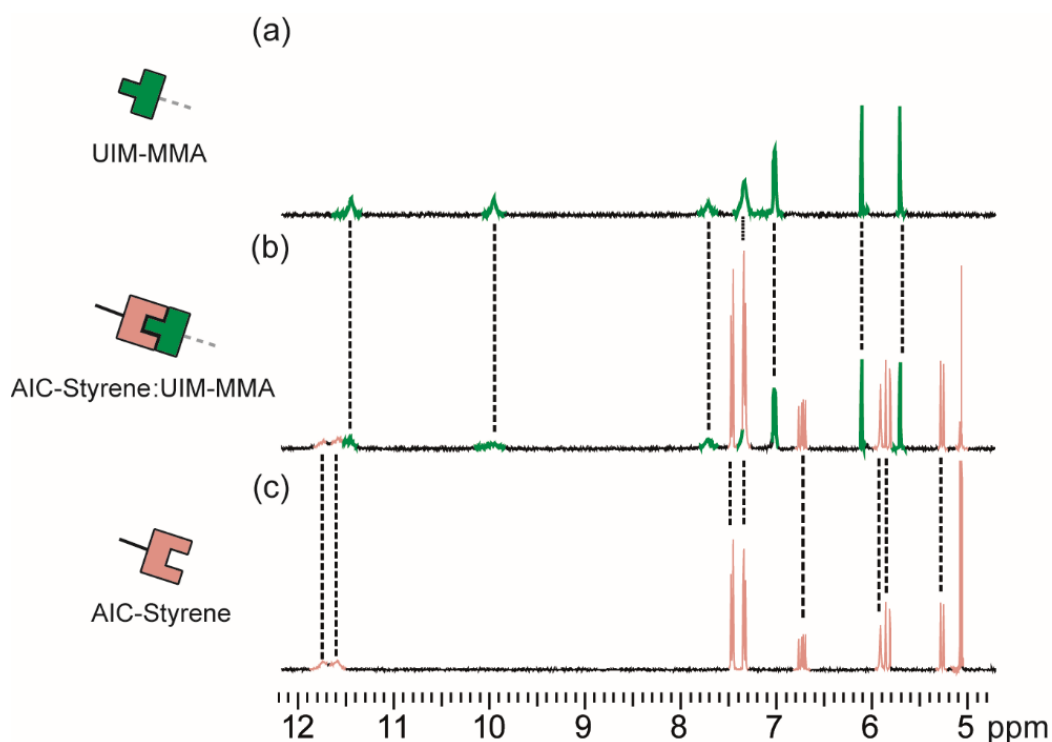
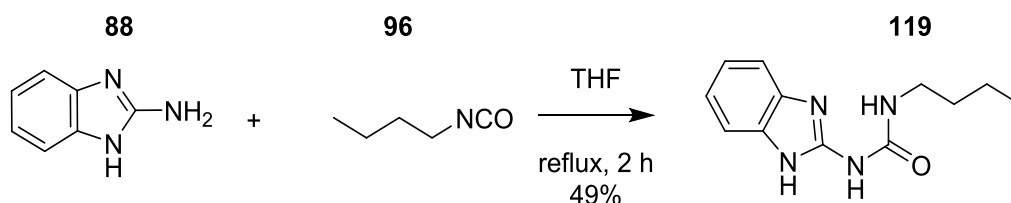


Figure 75. ^1H NMR (400 MHz, DMSO, 5 mM) (a) MMA-UIM monomer **90**, (b) MMA-UIM monomer **90** and AIC-Styrene co-monomer **117** and (c) AIC-Styrene monomer **117**.

This problem of solubility of amino imidazole UIM motifs was previously recognised by the Wilson group.¹⁷⁰ In the prior work, the problem was overcome when the amino imidazole UIM motif was combined with its complementary partner (AIC analogue). The 1:1 mixture of UIM and AIC analogues was soluble in CDCl₃ and diagnostic changes in resonances were observed for the AIC motif indicating a hydrogen bonding dimerisation interaction was occurring. However, in this system even a mixture of monomers **90** and **177** was not soluble enough to give a well resolved ¹H NMR spectrum. A more soluble n-butyl analogue of the 2-amino imidazole UIM co-monomer **199** was synthesised (Scheme 22) and in combination with co-monomer **117** diagnostic changes in resonances were observed in ¹H NMR (Figure 76).



Scheme 22. Synthesis of n-butyl imidazole UIM analogue 119.

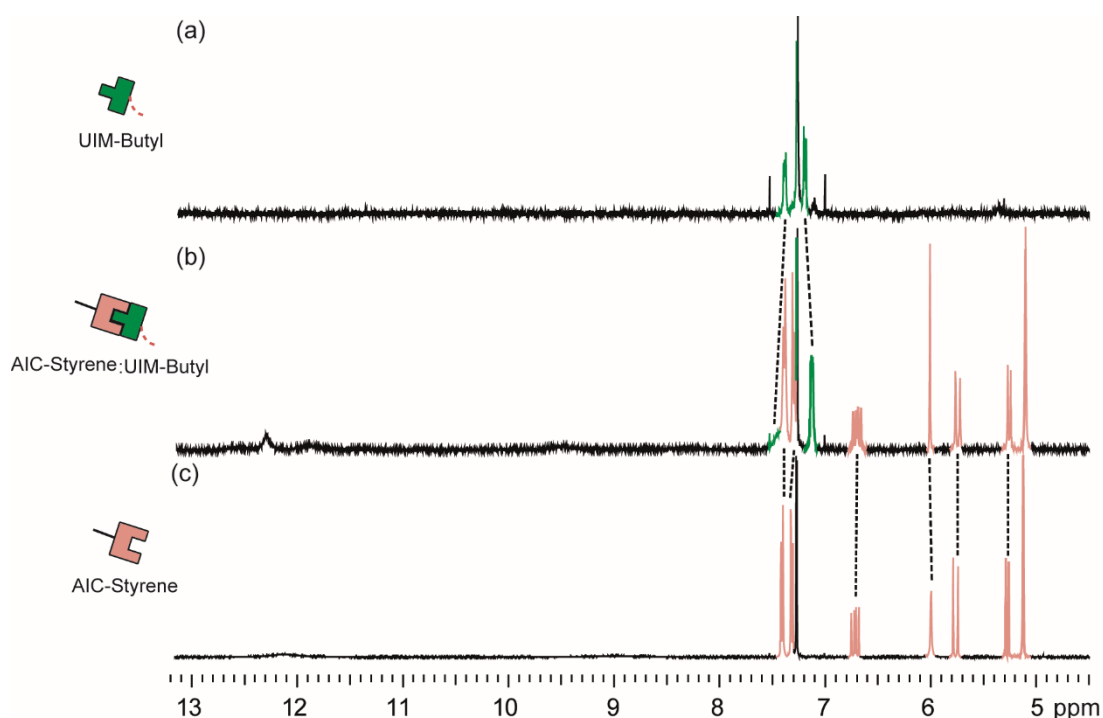


Figure 76. ^1H NMR (400 MHz, CDCl_3 , 5 mM) (a) UIM-butyl analogue 119, (b) 1:1 UIM-butyl analogue 119 and AIC-Styrene monomer 117 and (c) AIC-Styrene monomer 117.

In previous research, amino imidazole UIM motifs and AIC have been utilised in the creation of elastomers.⁹⁸ Here the hydrogen bonding interaction between the two hydrogen bonding motifs was implied by the formation and material properties the elastomer and IR data. By comparing the ^1H NMR data in Figure 75 & Figure 76 with similar previously reported systems it was rationalised that the complementary co-monomers and subsequent co-polymers should have a sufficient association energy to facilitate polymer blending. In addition molecular modelling was carried out to provide further evidence that the desired *DDA-AAD* hydrogen bonding interaction was possible between the co-monomers. A hybrid Monte Carlo Molecular Mechanics (MCM) conformational search was carried out on monomers **90** and **117** in a chloroform medium, using Macromodel 10.3 from Schrödinger

software and the Merck Molecular Force Field (MMFF) without restraints. 10000 conformers were generated by MCMM and low energy conformers (up to 10 kJ mol⁻¹ of relative energy) were retained. All of the conformers retained, 399 in total, displayed the desired *DDA-AAD* intermolecular hydrogen bonding interactions as well as the expected intramolecular hydrogen bonds. Figure 77 shows the lowest energy conformer, the methacrylate and styrene moieties point in opposite directions with potential π -stacking between the aromatic ring and the pyrimidone ring of the styrene-AIC monomer **117**.

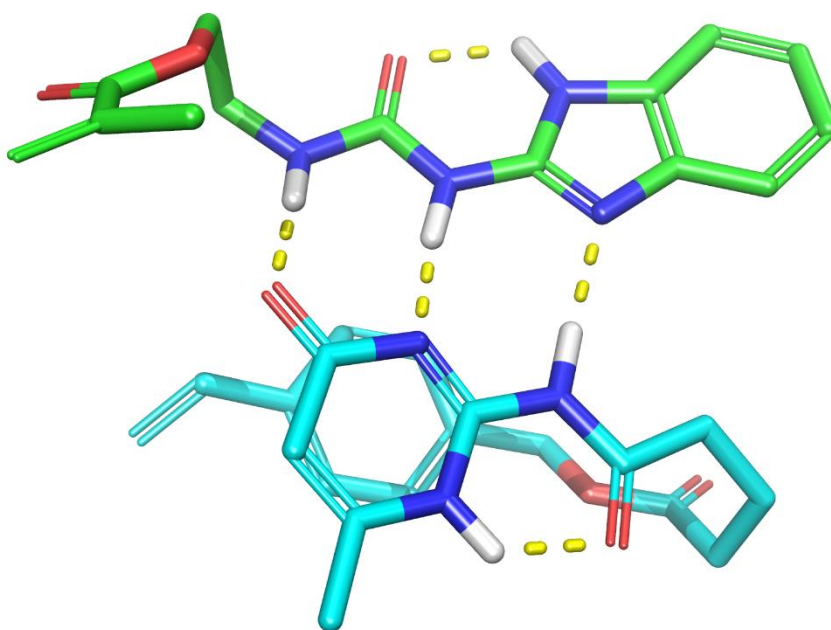


Figure 77. Molecular model diagram of the lowest energy conformation found when merge MMA-UIM monomer 90 and Styrene-AIC monomer 117 showing the desired intermolecular and intramolecular hydrogen bonding interaction. MMA-UIM monomer 90 in green, styrene-AIC monomer 117 in blue, hydrogen bonds in yellow.

4.2 First generation co-polymerisation

4.2.1 RAFT co-polymerisation and characterisation

Reversible-addition-fragmentation-chain transfer (RAFT) polymerisation was chosen as the technique for co-polymerisation as it is a controlled living polymerisation procedure. The mechanism and reaction conditions were discussed in Chapter 1.¹⁷¹⁻¹⁷³ The main advantages of RAFT include: low polydispersity; application to many different polymerisable monomers; tolerance to unprotected functionality in monomers and solvent and ease of implementation.¹⁰⁰

The aim was to co-polymerise MMA-UIM monomers **90** and **92** with methyl methacrylate and Styrene-AIC monomer **117** with styrene following literature precedent.¹⁰⁶ The polymerisation of methyl methacrylate monomers was carried out using an initiator, azo-*bis*-isobutyronitrile (AIBN) and a chain transfer agent (4-cyano-4-((dodecylsulfanylthiocarbonyl)sulfanyl) pentanoic acid). The polymerisation of styrene monomers were carried out with a chain transfer agent (cyanomethyl dodecyl trithiocarbonate) and heat as the initiator. The polymerisation reactions were initially carried out in bulk (solvent free conditions) using the relevant monomer as solvent.

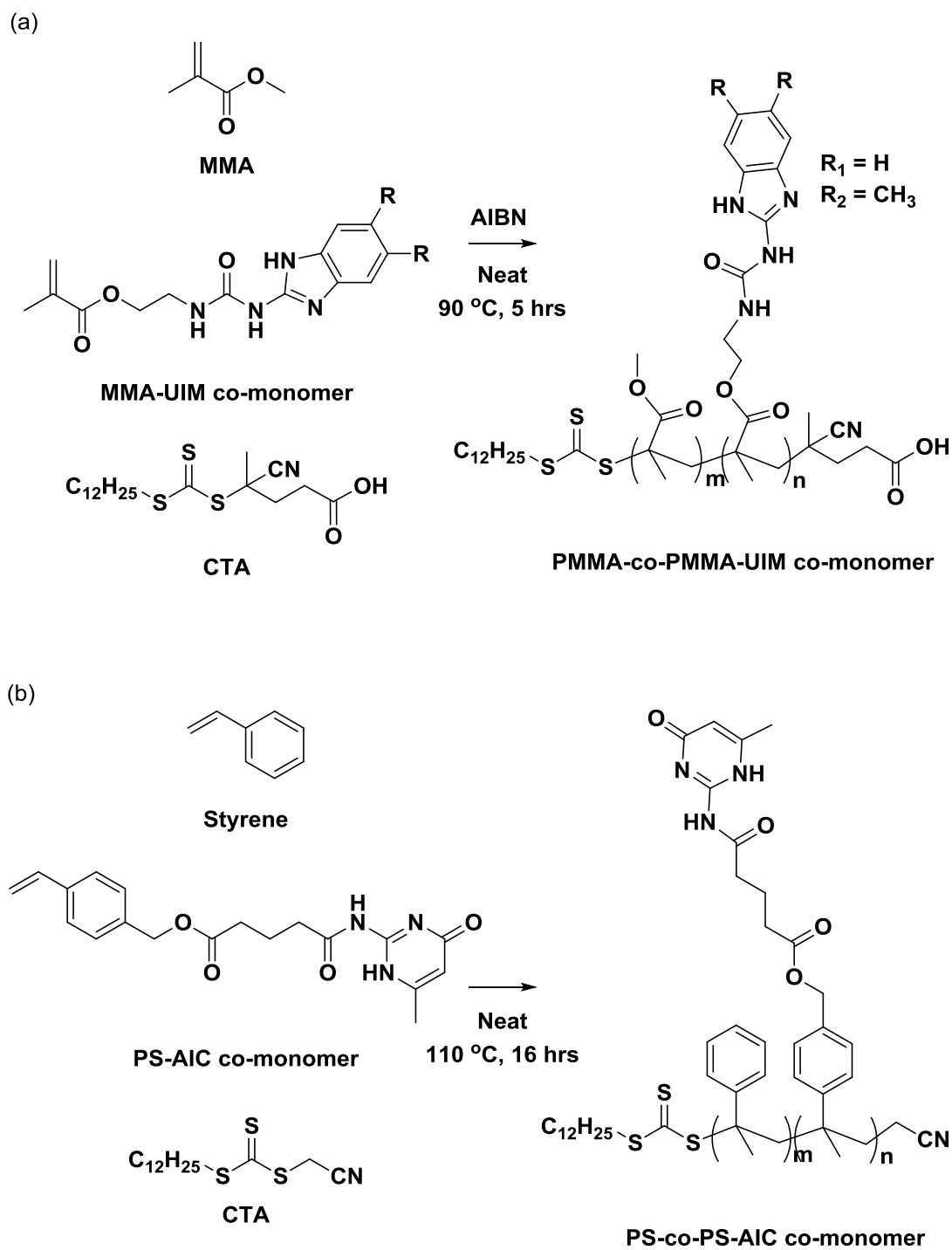
Prior to the synthesis of co-polymers with the functionalised monomers, a series of RAFT polymerisations were carried out to synthesise standard polymethylmethacrylate and polystyrene samples. The objective was to confirm the reported conditions were appropriate and the polymerisation reaction was living. For a living polymerisation, the PDI should be close to 1 and the molecular length should increase linearly with time until all monomer

is consumed or intentionally terminated.¹⁷⁴ To test this, polymerisations were set up with the same reactions conditions (i.e. reagents, concentration, and solvent) but the reaction time was varied. It was thought that with increasing time the molecular length would increase while maintaining a constant PDI. The polymer length and PDI of the resultant polymers were quantified using a Waters advanced polymer chromatography (APC) in DMF or THF as shown in Table 3. The Waters APC works in the same way as a conventional GPC in terms of the separation and analysis of polymers but the systems runs at higher back pressure using different columns for a reduced time. The molecular weight and PDI of the polymers are calculated relative to a calibration curve of the system (see experimental for details). For both the polymethylmethacrylate and polystyrene, the molecular weight increases with time. Small fluctuations can be seen for the PDI, particularly for the polymethylmethacrylate samples, but overall the PDI was low enough for the polymerisation to be considered as living. To support this assumption, additional uncontrolled polymerisations were carried out for polymethylmethacrylate (**127**) and polystyrene (**128**). Similar reaction conditions were used for the uncontrolled polymerisations but the absence of a CTA resulted in significantly larger PDI at 2.96 and 2.93 respectively (Table 3). Comparison of the PDI value for these uncontrolled polymerisations with polymers **120-126** suggest a variation of 1.03-1.24 in PDI is insignificant. Hence, it was inferred that these reaction conditions for RAFT polymerisation, with a CTA, were living and appropriate to use for co-polymerisations with functional monomers.

Polymer	Monomer	Time (hrs)	CTA	Initiator	Solvent for analysis	Mn (10^3 g mol ⁻¹)	PDI
120	MMA	3	Yes	AIBN	DMF	12.0	1.20
121	MMA	5	Yes	AIBN	DMF	22.9	1.03
122	MMA	6	Yes	AIBN	DMF	31.0	1.06
123	MMA	8	Yes	AIBN	DMF	47.3	1.24
124	Styrene	4.5	Yes	Heat	THF	8.4	1.06
125	Styrene	8	Yes	Heat	THF	10.7	1.11
126	Styrene	15	Yes	Heat	THF	12.3	1.09
127	MMA	1.5	No	AIBN	DMF	200.8	2.96
128	Styrene	15	No	Heat	THF	262.6	2.93

Table 3. APC data for first generation test polymerisations created by from neat polymerisation conditions. See Appendix F for APC RI traces against time.

Scheme 23 outlines the reaction conditions used for RAFT co-polymerisation, with methyl methacrylate or styrene monomer acting as the solvent, following literature precedent.¹⁰⁶ For the co-polymerisation of methyl methacrylate monomers, five hours was identified as a suitable reaction time because during the test polymerisations (Table 3) the lowest PDI was achieved with Mn close to the projected value at five hours. For the co-polymerisation of styrene monomers, 15 hours was selected from the tested systems. At this longer reaction time, the longest polystyrene polymer was obtained, even though it was slightly shorter than the target length. It was thought the longer reaction time was necessary for the styrene monomers because the polymerisation is self-initiated thermally; hence, its rate is slower than for the methyl methacrylate monomers which are initiated by the decomposition of AIBN.¹⁷⁵



Scheme 23. First generation RAFT co-polymerisation of (a) MMA and MMA-UIM co-monomer (b) styrene and PS-AIC co-monomer.

A series of co-polymers (first generation) were produced in this way, with between 1-12% of hydrogen bonding functionalised co-monomers (**90**, **92** and **117**) to methyl methacrylate and styrene monomers (Table 4). The copolymers were characterised by ^1H NMR to confirm incorporation of the respective functionalised co-monomer into the polymer backbone. The integration of the co-monomer resonances relative to polymer backbone resonances in the ^1H NMR spectra revealed that the percentage of incorporation of co-monomer was in agreement with the percentage added. The polymer length and PDI were initially characterised using an APC system was discussed above this works in the same way as conventional GPC (Table 4). The polymer length for these co-polymers were comparable to the test reactions. The PDI values for the methyl methacrylate co-polymers were reasonable at <1.4 however the polystyrene co-polymer were higher than ideal. Additionally the conversion rate for the polystyrene co-polymerisations were low with $M_n \sim 11000 \text{ g mol}^{-1}$ for a theoretical $M_n \sim 20000 \text{ g mol}^{-1}$. This suggested that a controlled polymerisation had been inhibited for the polystyrene co-polymer. One explanation is that the CTA is not working efficiently in the reaction conditions (i.e. in the presence of the co-monomer) or is decomposing. Alternatively small impurities in the reagents or oxygen radicals could be terminating the polymer propagation. Another reason could be that thermal initiation of the co-monomer is less efficient than styrene. However at this stage it was clear the creation of hydrogen bonding functionalised co-polymers was possible from the NMR spectrum, and so these co-polymers were taken forward for blend formation and characterisation.

Co-polymer	Monomer	HBM	HBM %	Mn (10 ³ g mol ⁻¹)	PDI
129	MMA	UIM (90)	3	15.1	1.34
130	MMA	UIM (90)	12	19.1	1.31
131	MMA	UIM (92)	3	27.2	1.24
132	MMA	UIM (92)	6	20.3	1.28
133	MMA	UIM (92)	12	20.9	1.36
134	Styrene	AIC (117)	1	16.0	1.77
135	Styrene	AIC (117)	3	11.1	1.85
136	Styrene	AIC (117)	6	11.4	1.82
137	Styrene	AIC (117)	9	10.7	1.77

Table 4. APC data for first generation co-polymers created by neat polymerisation conditions. See Appendix F for APC RI traces against time.

4.2.2 Blends formation

Blend formation was initially investigated visually by comparing films of the standard polymers and functionalised co-polymers obtained by RAFT polymerisation. For this purpose a series of polymer films were prepared by solution casting into glass petri dishes. Films were prepared from 1:1 mixtures of co-polymers in dichloromethane solution (20 mg mL⁻¹ of each component by mass). The samples were left to dry at room temperature, after 20 hours the dichloromethane solution had evaporated creating a polymer film. It is expected that on blend formation a transparent and homogeneous film would be created whereas a phase separated sample would result in an opaque film.¹⁷⁶

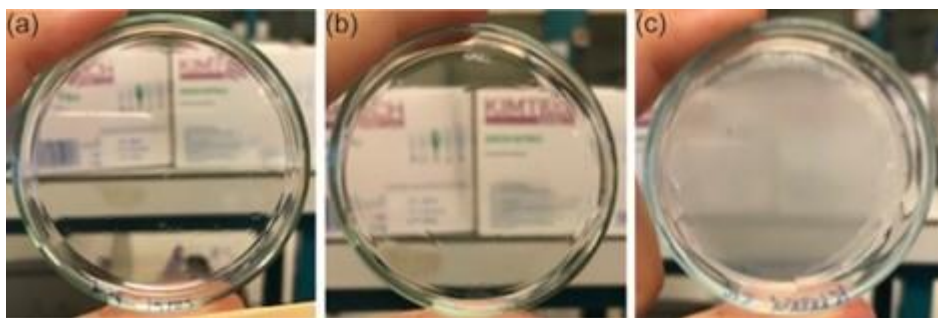


Figure 78. Films of (a) 122 (PS), (b) 126 (PMMA) and (c) 1:1 mixture of 122 and 126 (PS:PMMA).

A control film made of 1:1 mixture standard polymers **126** and **122** revealed an opaque film as expected from two immiscible polymers (Figure 78 (c)). The films of separate samples of polystyrene **126** and polymethylmethacrylate **122** were transparent (Figure 78 (a) & (b)), suggesting that the opacity of the 1:1 mixture was a result of phase separation rather than an inherit property of the respective polymers. Additional control films combining standard polymers of one polymer type with functionalised co-polymers of the opposite polymer type also displayed the expected opacity of a phase separated sample (Figure 79 (a-c)). This suggested that the incorporation of a single hydrogen bonding motif in the functionalised co-polymer does not increase the transparency of a film but rather the incompatibility of the polymer backbone results in an opaque film. However, films composed of equal amounts of heterocomplementary functionalised co-polymer were completely transparent in appearance (Figure 79 (d-f)), suggesting a stable single phase. For example when co-polymer **129** containing 3% UIM **92** monomer was mixed with co-polymer **135** containing 3% of the complementary AIC monomer **117** the resultant film was transparent. This result taken together with the control

films suggest that the interaction of complementary hydrogen bonding motifs are responsible for blend formation.

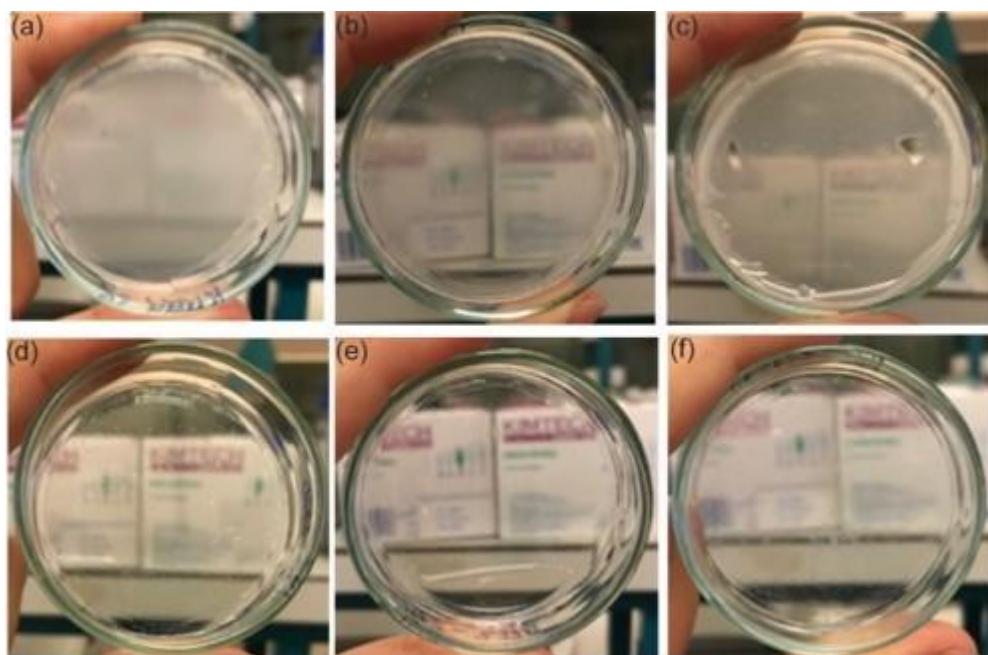


Figure 79. Films of 1:1 mixtures of co-polymers (a) 122 (PMMA) and 126 (PS), (b) 129 (3% UIM-PMMA) and 126 (PS), (c) 122 (PMMA) and 135 (3% AIC-PS), (d) 129 (3% UIM-PMMA) and 135 (3% AIC-PS), (e) 131 (3% UIM-PMMA) and 135 (3% AIC-PS) and (f) 132 (6% UIM-PMMA) and 136 (6% AIC-PS).

On visual inspection of the transparent films formed between complementary functionalised co-polymers, films with a lower percentage of hydrogen bonding motif (3%) were identified as more homogenous. This is somewhat surprising as one would expect a more stable crosslinked network with a greater number of hydrogen bonding interactions. However, the film for a 1:1 mixture of co-polymers **132** and **136** with 6% incorporation of hydrogen bonding motifs was less homogenous than a film of co-polymers with 3% incorporation (**129**, **131** and **135**) (Figure 79 (d-f)). This could be a result of intramolecular interactions of the co-polymers at higher hydrogen bond monomer incorporation and hence reducing heterocomplementary hydrogen bonding between the co-polymers. Alternatively, it could be a result of the

aggregation of the hydrogen bonding motifs becoming more significant at higher concentrations resulting in crystalline domains in the polymeric matrix. It is clear, therefore, that to form a homogeneous polymer blend a balance needs to be reached between the polymer length, the strength of hydrogen bonding incorporation and degree of hydrogen bonding motif present to form a cross-linked network without aggregation.

4.2.3 Differential scanning calorimetry analysis

Differential scanning calorimetry (DSC) was performed on films of co-polymer samples in order to evaluate the effect of side-chain interactions upon phase transition characteristics, in particular the glass transition. DSC measures the heat flow of a given sample in comparison to a reference sample to produce a curve for heat flow against temperature. Changes in the gradient of this curve in relation to temperature indicate a phase transition. The glass transition temperature (T_g) is the temperature at which a polymer changes from a hard, brittle state into a molten rubber like state and is characterised by a subtle change in the gradient of the DSC curve (Figure 80). As shown in Figure 80, the T_g is generally taken at the midpoint of the slope between two flat (less steep) sections ("baselines") of the curve. It was anticipated that phase separated polymers would have two distinct T_g indicative of the two distinct co-polymers present, whereas blended co-polymers would exhibit a single T_g indicating a combination of both co-polymers.¹⁷⁷

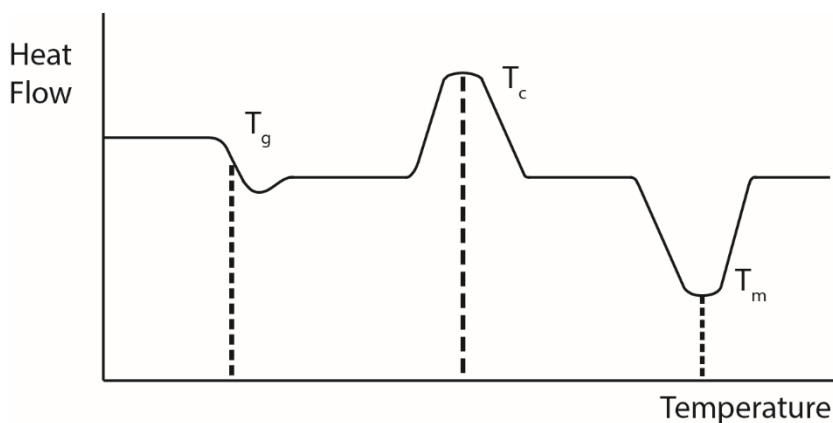


Figure 80. Schematic of a DSC thermogram showing typical phase transitions; glass transition (T_g), crystallisation (T_c) and melting (T_m).

The samples used for DSC were prepared as discussed in section 4.3.1 (blends formation) by solution casting into glass petri dishes. Films were prepared for isolated co-polymers and 1:1 mixes of co-polymers in dichloromethane solution (20 mg mL^{-1} of each component by mass) followed by drying at room temperature for a minimum of 20 hours. The resultant films (5-10 mg) were transferred to a standard aluminium DSC pan and sealed for use.

Typically glassy polymer films created by solvent casting are annealed prior to carrying out DSC experiments to ensure any solvent trapped in the polymer is removed. The presence of solvent in the polymer film sample is known to decrease the T_g .¹⁷⁸⁻¹⁸⁰ Consequently it is standard practise to dry the samples in a vacuum oven by heating above the expected T_g under vacuum to remove any solvent trapped in the glassy state. To test if this was required for the polymer films formed in this project DSC experiments were carried out on the same polymer film sample with different degrees of drying. Comparison of the DSC heat flow curves revealed that the T_g was unchanged for a samples

without drying, drying for 24 hours and drying for 72 hours in a vacuum oven heated to 120 °C. This suggested that solvent was not trapped in the polymer film and that the vacuum drying procedure was not necessary for these samples. Hence, it was decided that the films created from drying at room temperature were suitable to use directly in the DSC measurements.

The DSC experiments were initially carried out by cycling three times from 25 °C to 100 °C then back to 25 °C, at a heating and cooling rate of 10 °C per minute. These conditions were taken from previous literature, 100 °C was chosen as a suitable maximum temperature to prevent any reinitiation of the polystyrene based polymers on heating.¹⁰⁶ This data was analysed using TA Universal Analysis 2000 software. However, it was not possible to determine the T_g accurately when using this temperature range. This was a result of the T_g being close to the maximum temperature of the cycle (100 °C); hence, it was difficult to set the “baselines” of the T_g slope to calculate the midpoint of the T_g slope. The conditions were then changed: cycle 1 heated from 25 °C to 100 °C and cooled back to 25 °C; cycle 2 and 3 heated from 25 °C to 150 °C and back to 25 °C. This system was beneficial as cycle 2 and 3 provided enough data to calculate T_g values up to approximately 130 °C. Additionally, it was thought that comparison of the curve from cycle 1 to the curves from cycles 2 and 3 may indicate if polymerisation was reinitiated at the higher temperature, i.e. if all the curves are the same there is no reinitiation.

To begin a control DSC experiment was carried out using standard polymers **122** and **126**. The DSC curves of the separate transparent polymer films were compared to the opaque film of 1:1 mixture of the standard polymers **122** and **126**. On heating the separate samples showed single transitions, the T_g of

PMMA polymer **122** was calculated at 102 °C (blue curve) and the T_g of polystyrene polymer **126** was calculated at 99 °C (red curve) using TA universal analysis software (Figure 81). The 1:1 mixture displayed two distinct transitions at $T_g = 88$ °C and $T_g = 105$ °C (green curve). The presence of two transitions is in line with the polymers being immiscible as expected and suggested from the opacity.

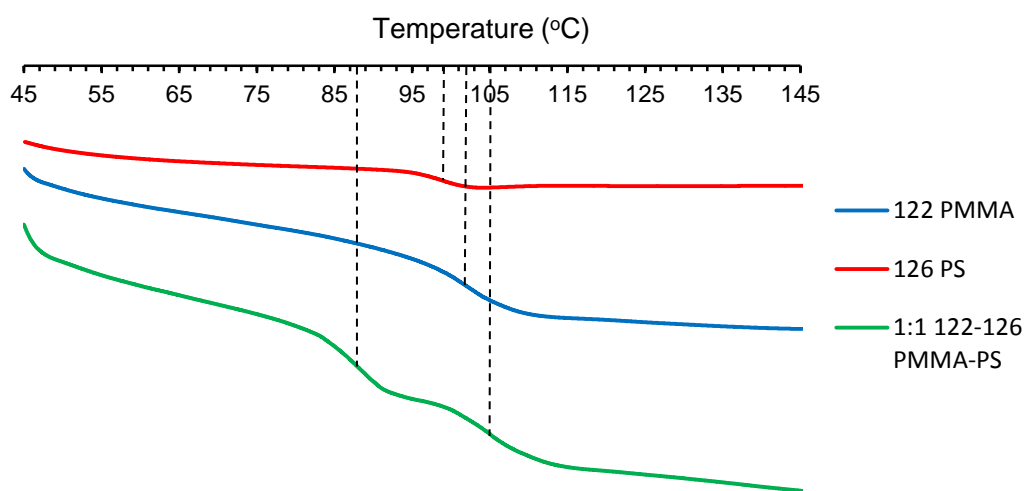


Figure 81. DSC thermogram on heating of polymer 122 (PMMA) blue, polymer 126 (PS) red and 1:1 mixture of 122 and 126 (PMMA:PS) green (dashed line highlighting the calculated T_g).

However, the T_g values in the mixture are not identical to the separate samples. This suggests that the samples are not completely immiscible but the system has some compatibility.¹⁷⁷ This shift in T_g for the mixture can be explained in terms of entropy on mixing; positive entropy lowers the T_g and negative entropy, as in the case of strongly interacting mixtures, the domain of the glassy state expands, increasing T_g .¹⁸¹ Another perspective is to consider the mixture as an impurity which causes a change (mainly decrease) in T_g compared to a pure polymer in a similar way that an impurity in a small

molecule would change the melting temperature (T_m). For small molecules, the impurity disrupts the crystal lattice energy and so depresses the melting point, applying this to polymers, the mixture of polymeric chains could disrupt the interactions between the pure polymers thus shift the T_g . Overall, it is evident that the two standard polymers do not form a miscible blend. As with the blend formation, more control experiments were conducted combining standard polymers and co-polymers with different polymeric backbones. The DSC curves of these mixtures also displayed two distinct transitions, indicating blending did not occur. For example, two distinct transitions were observed for the mixture of co-polymer **129** (composed of PMMA with 3% UIM monomer) and polymer **126** (PS) (Figure 82). The DSC curves for other control experiments can be found in the Appendix B.

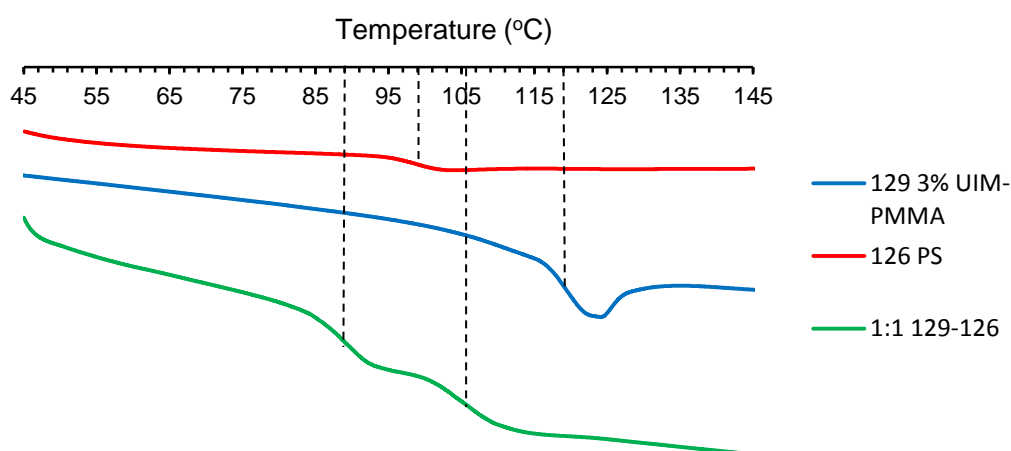


Figure 82. DSC thermogram on heating of co-polymer 129 (PMMA with 3% UIM co-monomer 90) blue, polymer 126 (PS) red and 1:1 mixture of 129 and 126 (3% UIM-PMMA:PS) green (dashed line highlighting the calculated T_g).

Following the control experiments DSC was carried out on the transparent films of complementary co-polymers believed to be miscible blends in

comparison to pure co-polymer films. The single transitions were observed in the DSC curves of films of pure co-polymers **129-137** (Table 5).

Polymer	Monomer	HBM	HBM %	Mn (10 ³ g mol ⁻¹)	PDI	T _g (°C)
122	MMA	N/A	0	31.0	1.06	102
129	MMA	UIM (90)	3	15.1	1.34	119
130	MMA	UIM (90)	12	19.1	1.31	120
131	MMA	UIM (92)	3	27.2	1.24	130
132	MMA	UIM (92)	6	20.3	1.28	121
133	MMA	UIM (92)	12	20.9	1.36	121
126	Styrene	N/A	0	12.3	1.09	99
135	Styrene	AIC (117)	3	11.1	1.85	107
136	Styrene	AIC (117)	6	11.4	1.82	106
137	Styrene	AIC (117)	9	10.7	1.77	105

Table 5. Glass transition temperatures of polymers calculated from DSC experiments on polymer films.

The trend observed on comparison of the T_g values for standard polymers and co-polymers contrasts the trend observed on comparison between the co-polymers. T_g is known to increase with molecular weight according the Flory Fox equation, due to the decrease in free volume. However, on inspection of the methyl methacrylate standard polymers against the co-polymers, the co-polymers have a lower Mn than the standard polymer **122** but a larger T_g. This suggests that the change in polymer composition (introduction of hydrogen bonding motifs) has a greater effect on the T_g than the change in Mn. The increase in T_g for co-polymers is likely due to the hydrogen bonding motifs interacting favourably with themselves or the polymer backbone through non-covalent interactions and hence reducing the free volume of the polymer. Conversely, on the comparison of the series co-polymers the T_g does not

increase with increasing incorporation of hydrogen bonding motif but here the T_g increases with M_n . For example, co-polymer 130 with 12% UIM monomer and M_n of $19.1 \times 10^3 \text{ gmol}^{-1}$ has a lower T_g at 120 °C compared to co-polymer **131** containing 3% UIM monomer and M_n of $27.2 \times 10^3 \text{ gmol}^{-1}$ which has a $T_g = 130 \text{ °C}$. These contrasting trends highlight the complexity associated with determining and understanding the T_g of different polymers. Consequently, with this series of polymers and co-polymers it was not possible to directly relate a shift in T_g with a specific variable of the polymer.

Nevertheless, DSC experiments were carried out on the transparent films from 1:1 mixtures of complementary co-polymers. As expected for a miscible polymer blend, a single transition was observed in the DSC curve, albeit broad for some mixtures (full series of curves in Appendix B). Focusing of the 1:1 mixture of co-polymers **129** and **135** with 3% incorporation of complementary UIM and AIC hydrogen bonding motifs respectively (Figure 83), a single $T_g = 102 \text{ °C}$ was observed (green curve). It can be inferred this blend formation is a direct consequence of hydrogen bonding between the complementary arrays, rather than the result of interactions between hydrogen bonding motifs and polymer backbone, because the control samples of these functionalised co-polymers exhibit two T_g s when mixed with polymer standards as discussed above.

As seen on the mixture of polymer standards, the T_g of the blend is lower than the separate samples, $T_g = 119 \text{ °C}$ for co-polymer **129** with 3% UIM.MMA monomer incorporation (blue curve) and $T_g = 107 \text{ °C}$ for co-polymer **135** containing 3% AIC.styrene monomer (red curve) (Figure 83). Rationalising this shift in T_g is difficult because the inferred hydrogen bonding should

increase the enthalpy between the co-polymers and so increase the T_g , yet when compared to the pure co-polymer samples it is obvious the blend is impure and hence the T_g would decrease. An additional observation for the blended system is that the transition is much broader compared to the pure co-polymer samples. This a broadening is common for miscible blends, in the same way the melting point range increases for impure crystalline compounds. Possible reasons for this broadening in miscible blends include concentration fluctuations, different polymer orientations and superposition of the co-polymers.¹⁸²⁻¹⁸⁴ On balance, the results of the DSC experiments indicated the functionalised co-polymers synthesised in the project were able to form a miscible when complementary co-polymers were combined.

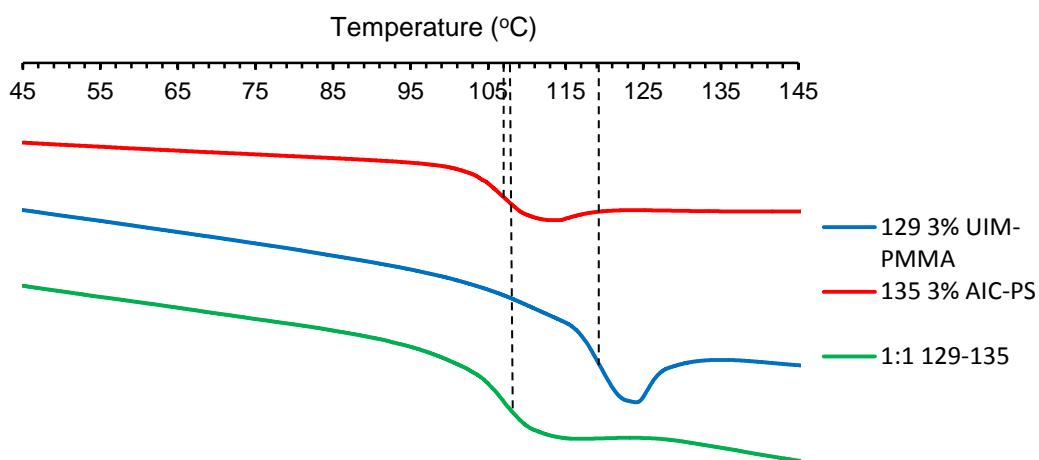


Figure 83. DSC thermogram on heating of co-polymer 129 (PMMA with 3% UIM hydrogen bonding motifs 90) blue, co-polymer 135 (PS with 3% AIC hydrogen bonding motifs 117) red and 1:1 mixture of 129 and 135 (3% UIM-PMMA:3% AIC-PS) green (dashed line highlighting the calculated T_g).

4.2.4 Dynamic light scattering analysis

Dynamic light scattering can be used to estimate the hydrodynamic radius distribution of an ensemble of macromolecules. A laser is directed at a dilute solution of particles and light is scattered from the particles in solution. The particles move due to "Brownian motion," which depends on particle size, solution viscosity, temperature, and particle density. Fluctuations in the intensity of the scattered light, caused by the interference with surrounding particles, are a measure of this Brownian motion and the translational diffusion coefficient can be inferred. The translational diffusion coefficient is related to the hydrodynamic diameter through the Stokes–Einstein relation, allowing for the calculation of the hydrodynamic radius.

It was thought that DLS could be used to confirm blend formation in this work. If a blend is formed the diffusion coefficient of the blend should increase in comparison to the separate co-polymers and hence the hydrodynamic radius would increase. This was described in previous work by Zimmerman whereby a functionalised poly(butyl) methacrylate (PBMA) co-polymer was titrated with a functionalised polystyrene co-polymer in chloroform.¹⁰⁴ The DLS data indicated growth of aggregates (solvodynamic radius) on titration to a 1:1 mixture. However, when this methodology was applied to the UIM-PMMA and AIC-PS co-polymers in chloroform at a concentration range of 10-100 mg mL⁻¹ a measurement was not possible on the Zetasizer Nano system from Malvern Panalytical. It was initially thought that the solvent may be affecting the DLS measurement for two reasons; chloroform had not been used of the system before, hence it was possibly a technical issue with the setup (even though the system is believed to be compatible), or chloroform was directly

changing the polymer shape as both organic and aqueous solvents are known to influence the particle size.¹⁸⁵ To test the theory that the solvent was influencing the shape of the polymers, the DLS measurements were repeated for polystyrene samples in toluene (toluene has been used for PS in previous studies),¹⁸⁶ however, it was still not possible to obtain a reading. Additionally, it was not possible to carry out the DLS measurements in water because the polymers were not soluble.¹⁸⁷ This led to a third hypothesis that the polymers may be non-spherical making it impossible to use DLS to determine a solvodynamic radius (particle size). Consequently it was decided that DLS was not a suitable tool for investigating the blending of these functionalised co-polymers and no further DLS experiments were attempted.

4.3 Second generation co-polymerisation

As the project progressed, it was ascertained that the APC system may not be suitable for the characterisation of the co-polymers tested. Several issues arose with the system including calibration, high pressure and low reproducibility of data. Consequently, it was decided that analysis of the co-polymers should be repeated using gel permeation chromatography (GPC). The series of generation one co-polymers were analysed again using this system (Table 6). A DMF solvent system was used for analysing methyl methacrylate based co-polymers and a THF solvent system for analysing styrene-based co-polymers.

Co-polymer	Monomer	HBM	HBM %	APC		GPC	
				Mn (10 ³ g mol ⁻¹)	PDI	Mn (10 ³ g mol ⁻¹)	PDI
129	MMA	UIM (90)	3	15.1	1.34	11.6	1.70
130	MMA	UIM (90)	12	19.1	1.31	10.8	1.98
131	MMA	UIM (92)	3	27.2	1.24	24.4	1.27
132	MMA	UIM (92)	6	20.3	1.28	14.8	1.61
133	MMA	UIM (92)	12	20.9	1.36	12.5	1.76
134	Styrene	AIC (117)	1	16.0	1.77	18.8	2.39
135	Styrene	AIC (117)	3	11.1	1.85	6.9	2.93
136	Styrene	AIC (117)	6	11.4	1.82	7.7	2.37
137	Styrene	AIC (117)	9	10.7	1.77	8.4	2.52

Table 6. APC and GPC data for first generation co-polymers created by solvent free polymerisation. See Appendix F for APC RI traces against time and Appendix G for GPC RI traces against time.

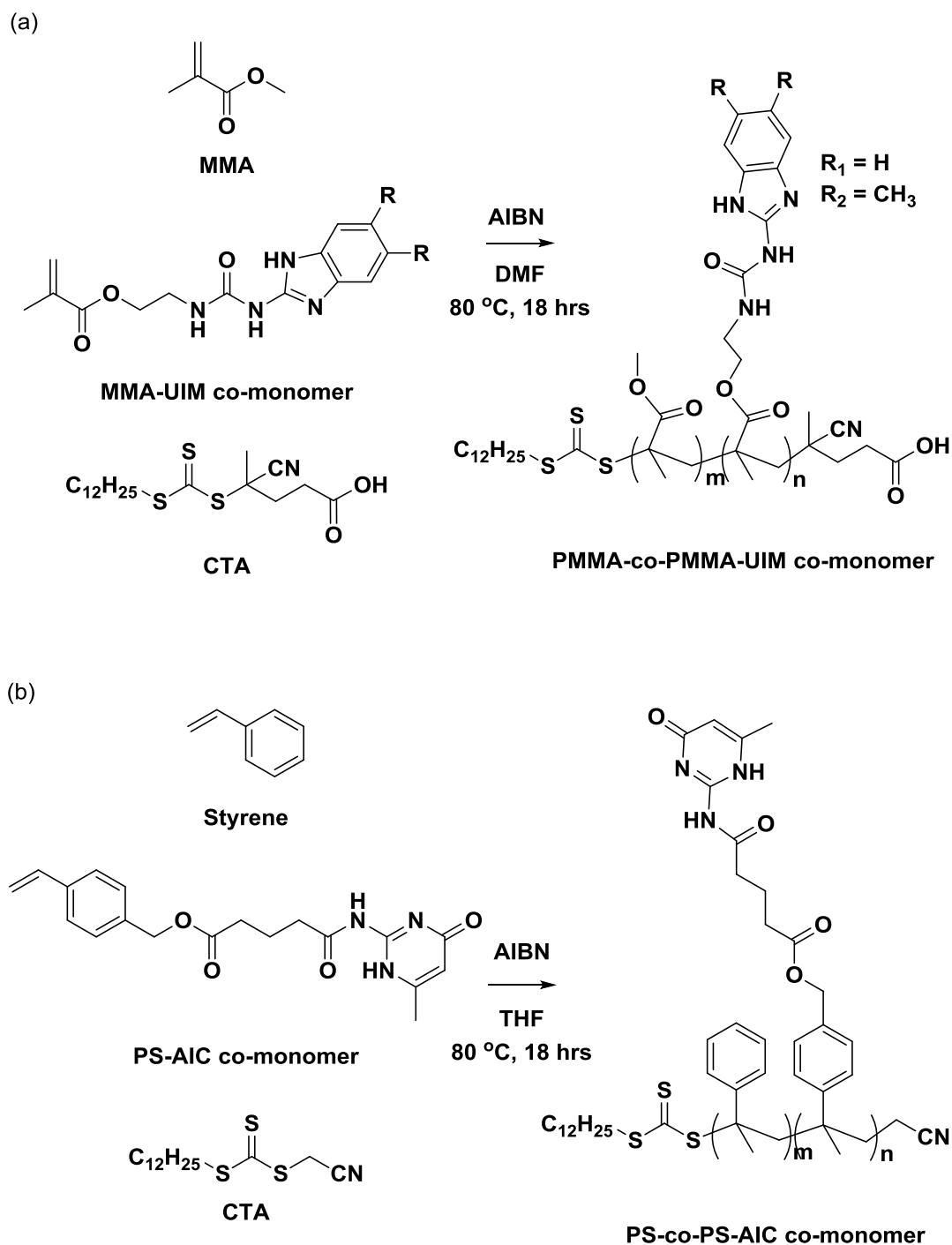
In comparison to the APC data, the GPC showed lower M_n values but the trend remained the same. However, the PDI values were higher than expected for a controlled polymerisation, especially for the styrene-based co-polymers. This raised the issue that the number of hydrogen bonding units in each polymer could not reliably be predicted. Ideally the PDI would be close to 1 to confidently estimate the number of hydrogen bonding units in each polymer chain. For example, if a co-polymer had 3% incorporation of hydrogen bonding co-monomers and M_n value of 50000 g mol^{-1} , each polymer chain would have an average of 500 monomers and an average of 15 hydrogen bonding motifs would be expected per chain. However, if the PDI is greater, (e.g. 2) even though the average number of monomers per chain is still 500 many more chains will be small or larger than 500. Because of this increased distribution it is more difficult to predict the number of hydrogen bonding motifs per chain with confidence. Depending on the length of the polymer, some chains may not be functionalised at all. This also raises a further issue in that blending of complementary co-polymers may be affected by the lack of dispersity of hydrogen bonding units. Overall this lack of control brings into question the degree of hydrogen bonding required for co-polymer blending.

4.3.1 RAFT co-polymerisation second generation

Consequently, a second series of test polymerisations was carried out with the aim to decrease the PDI, increase the length of the polymer chain and ensure all the polymer chains were functionalised with the appropriate hydrogen bonding units. It was thought that using a radical initiator in the styrene co-polymerisations rather than heat would be beneficial to decrease the required reaction time and offer improved control of the polymerisation. To increase the polymer length, the ratios of monomer to CTA and initiator were varied as well as reaction time. Table 7 shows the GPC analysis of the test polymerisations (**138-145**) in the relevant solvent systems. A ratio of 500:1:0.2 monomer:CTA:initiator and reaction time of 18 hours were found to be optimal, giving a good correlation between the theoretical and experimental polymer length with reasonable PDI values for both polymers (**138** and **141**).

Polymer	Monomer	Ratio M:CTA:I	Time (hrs)	Conv ersio n	Mn Theory (10 ³ g mol ⁻¹)	Mn (10 ³ g mol ⁻¹)	PDI
138	MMA	500:1:0.2	18	0.89	44.5	45.0	1.21
139	MMA	1000:1:0.2	18	0.69	69.0	81.9	1.30
140	Styrene	100:1:0.2	18	0.96	10.0	11.2	1.16
141	Styrene	500:1:0.2	18	0.49	25.5	20.5	1.26
142	Styrene	1000:1:0.2	18	0.44	45.8	25.6	1.33
143	Styrene	1000:1:0.2	2.5	0.24	25.0	12.0	1.65
144	Styrene	1000:1:0.2	19.5	0.39	40.6	18.9	1.60
145	Styrene	1000:1:0.2	116	1	100.8	38.7	1.64

Table 7. GPC data for the second generation polymer standards created by solvent free polymerisation. See Appendix G for GPC RI traces against time.



Scheme 24. Second generation RAFT co-polymerisation of (a) MMA and MMA-UIM co-monomer (b) styrene and PS-AIC co-monomer.

Another modification considered was to add solvent to the co-polymerisations, DMF for the UIM-MMA monomer **90** and THF for AIC-styrene monomer **117**. It was hypothesised that solvent would decrease the viscosity of the reaction and so reduce the number of termination events, which could be beneficial for

longer polymer chains and improve the PDI. The addition of solvent could also aid solubilisation of the co-monomers and increase the percentage of incorporation of hydrogen bonding monomers. The implementation of these modifications resulted in the synthesis of a second generation of co-polymers (Scheme 24).

The GPC data (Table 8) revealed for the PMMA-UIM co-polymer **146** the polymer length had increased almost two-fold compared to the PMMA-UIM co-polymers from generation 1 while the PDI was kept relatively low at 1.29. However The GPC data for the PS-AIC co-polymers **147-150** indicated that the changes to the polymerisation conditions did not result in the expected improved polymer length or PDI. It is noteworthy that the PDI of co-polymers **149** and **150** could not be reliably determined by GPC because the co-polymers eluted together with the solvent in the void volume. Hence it was not possible to differentiate between the signal for the polymer and the solvent. This is a restriction of the columns used on the available GPC instrument which have a lower limit of 5000 g mol^{-1} , so any polymers lower or close to this limit cannot be accurately quantified. Furthermore, inspection of the GPC traces revealed the signals to be unsymmetrical; there was often a broad tail indicating that the distribution is not normal. Rather, the distribution is made up of more shorter polymer chains than longer polymer chains. Another explanation for this tail is that the polymer chains interact with the column, causing the polymer chains to stick to the column for a longer time and slowing down the elution. Polymers containing NH groups, such as polyurethanes and polyamides, can exhibit this behaviour in GPC analysis.^{188,189} Consequently this could lead to an exaggerated PDI value as the tailing effect is not accounted

for in the calibration. Running the GPC with additives may solve the problem but was not possible with the equipment available.

Co-polymer	Monomer	HBM	HBM %	Reaction Solvent	Solvent for analysis	Mn (10 ³ g mol ⁻¹)	PDI
146	MMA	UIM (90)	2	DMF	DMF	39.0	1.29
147	Styrene	AIC (117)	2.5	THF	THF	6.8	2.24
148	Styrene	AIC (117)	2.5	THF	THF	7.9	2.24
149	Styrene	AIC (117)	4.5	THF	THF	5.3	2.85*
150	Styrene	AIC (117)	5	THF	THF	5.8	2.78*

Table 8. GPC data for second generation co-polymers (*samples elute with solvent). See Appendix G for GPC RI traces against time.

Overall, the co-polymers produced in generation two seem, to an extent, to be consistent with the first generation of co-polymers. It was clear from both series that incorporation of the AIC hydrogen bonding motif influences the polymerisation reaction. The resultant styrene-AIC co-polymers had a large PDI (greater than 2) and low molecular weight (less than 10000 g mol⁻¹). This implies that the polymerisation was not living and there is a fundamental limit on the degree of polymerisation which can be achieved in the presence of the AIC hydrogen bonding motif. It was evident in both generations of co-polymerisations that; as the percentage of incorporation of the styrene-AIC co-monomer was increased, the PDI increased and the average polymer length decreased. One explanation for this observation, is that the styrene-

AIC co-monomer could be acting as a radical trapping agent. This could hinder the desired RAFT polymerisation in at least two ways. First, it could lead to an excess of free radical species during the polymerisation. This could shift the RAFT equilibrium causing the active polymeric chain radicals to combine with excess free radical species present in solution (co-monomer) irreversibly thus forming dead polymeric chains. Some groups have used excess of a free radical in post polymerisation modification for the elimination of thiocarbonylthio polymeric chains, however in this case it would hinder the formation of the desired co-polymer.^{190,191} Alternatively, the styrene-AIC co-monomer could be capping the end of polymer chains as seen in Radical Trap-Assisted Atom Transfer Radical Coupling (RTA-ATRC) polymerisations.^{192,193} Depending on the nature of the radical trap used in these reactions, polymerisation can be halted by an end-capped polymer.¹⁹⁴ It also explains, to some extent, why high co-monomer incorporation (above 6%) was difficult, despite being initially considered a monomer solubility problem. With this in mind a comparative study incorporating the hydrogen bonding units after RAFT polymerisation could probe some of these questions, but due to time this was not explored further.

4.3.2 Blend formation and characterisation

Polymer films of these second generation co-polymers were made by the same procedure as the first generation of co-polymers. On visual inspection similar trends were observed for the second generation of standard polymers and functionalised co-polymers (Figure 84). Opaque films were formed from the mixture of standard polymers (**138** and **142**) with each other and mixtures with functionalised co-polymers (**146**, **148** and **149**) (Figure 84 (a-c)). Mixtures of co-polymers functionalised with heterocomplementary hydrogen bonding motifs produced transparent films indicative of blending (Figure 84 (d-e)).

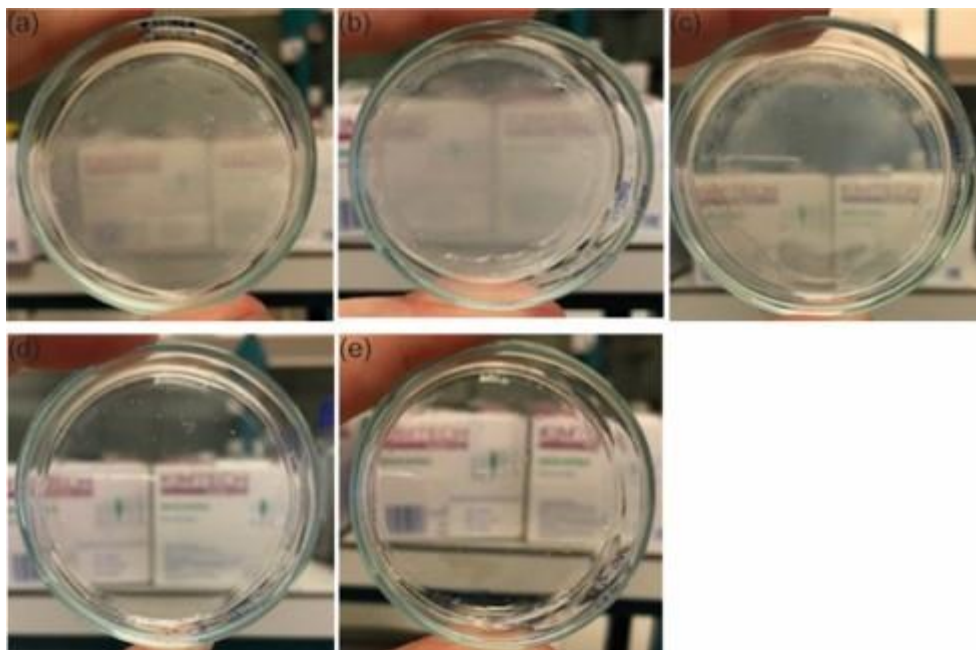


Figure 84. Films of 1:1 mixtures of co-polymers (a) 138 (PMMA) and 142 (PS), (b) 146 (2% UIM-PMMA) and 142 (PS), (c) 138 (PMMA) and 148 (2.5% AIC-PS), (d) 146 (2% UIM-PMMA) and 148 (2.5% AIC-PS), and (e) 146 (2% UIM-PMMA) and 149 (4.5% AIC-PS).

DSC studies carried out on the second generation of co-polymers also illustrated blend formation in the same way as the first generation of functionalised co-polymers. Control DSC experiments on the opaque films displayed two distinct transitions mirroring that of the first generation as expected (see Appendix B for thermograms). Meanwhile, the DSC curves for the transparent films made up of 1:1 mixtures of complementary co-polymers exhibited a single transition indicating blending. Figure 85 shows a single transition at 107 °C for the 1:1 mixture of co-polymer **146** (with 2% UIM-MMA monomer **90**) and co-polymer **149** (with 4.5% AIC-styrene monomer **117**) compared to the isolated co-polymers with T_g of 112 °C and 98 °C respectively. Unlike the blends described above in which the T_g is lowered on mixing, here the T_g is between that of the separate samples. This suggests that the positive and negative contributions to entropy on mixing are balanced.

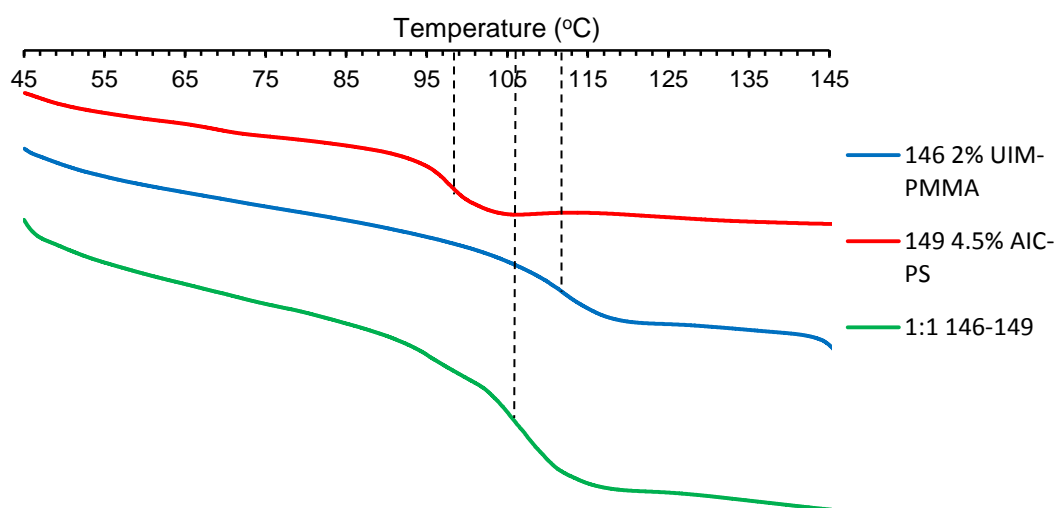


Figure 85. DSC thermogram on heating of co-polymer **146** (2% UIM hydrogen bonding motifs) blue, co-polymer **149** (4.5% AIC hydrogen bonding motifs) red and 1:1 mixture of **146** and **149** (2% UIM-PMMA:4.5% AIC-PS) green (dashed line highlighting the calculated T_g).

The shape of the curve for the mixture of co-polymer **146** (with 2% UIM-MMA monomer **90**) and co-polymer **148** (with 2.5% AIC-styrene monomer **117**) is different (Figure 86). The T_g is calculated at 96 °C rather than at the middle of the slope suggesting that the broad transition is made up of more than one T_g . Work is ongoing to try to understand this behaviour and if it is possible to differentiate two T_g in close proximity.

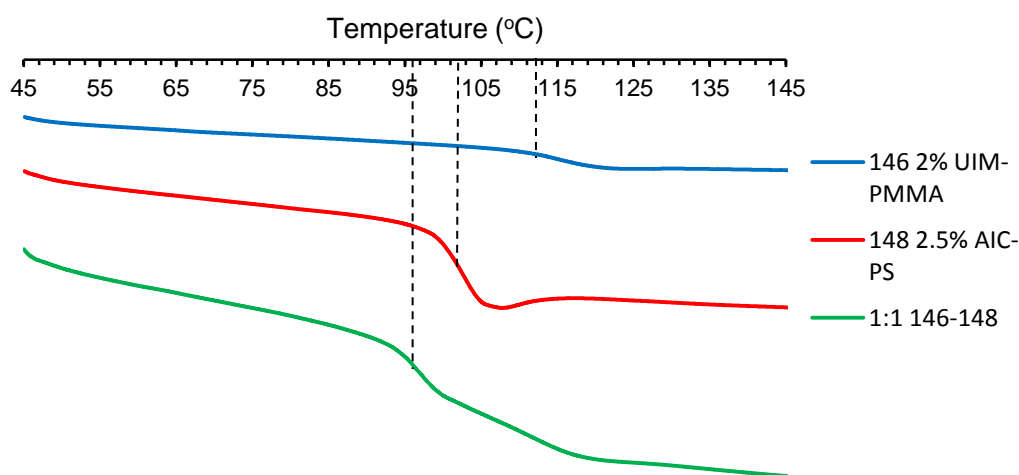


Figure 86. DSC thermogram on heating of co-polymer 146 (2% UIM hydrogen bonding motifs) blue, co-polymer 148 (2.5% AIC hydrogen bonding motifs) red and 1:1 mixture of 146 and 148 (2% UIM-PMMA:2.5% AIC-PS) green (dashed line highlighting the calculated T_g).

Additional blend characterisation was carried out on the second generation of co-polymers to probe the degree of phase separation, if any, of the polymer blend films. Optical polarised microscopy was used to compare samples of the transparent film of a 1:1 mixture of co-polymers **146** and **148** with the opaque film of a 1:1 mixture of pure polymers **138** and **142**. The samples were prepared by spin casting a solution of the 1:1 mixture (20 mg of each component in 2 mL of dichloromethane) on to a glass microscope slide. The samples were visualised using a polarised microscope with reflective

transition on 50x magnification. Figure 87(a) shows that the opaque film of a 1:1 mixture of pure polymers **138** and **142** undergo microphase separation. Two distinct regions can be seen as expected for immiscible polymers polystyrene and PMMA (The green and purple streaks are believed to be solvent drying effects). For the transparent film with hydrogen bonding motifs no features suggesting phase separation can be seen on the same scale of magnification (x50) (Figure 87(b)). This indicates that the hydrogen bonding between the co-polymers is resulting in a miscible blend. Further microscopy such as AFM and SEM may probe if phase separation is occurring on a smaller scale but so far the optical microscopy and visual observation are positive.

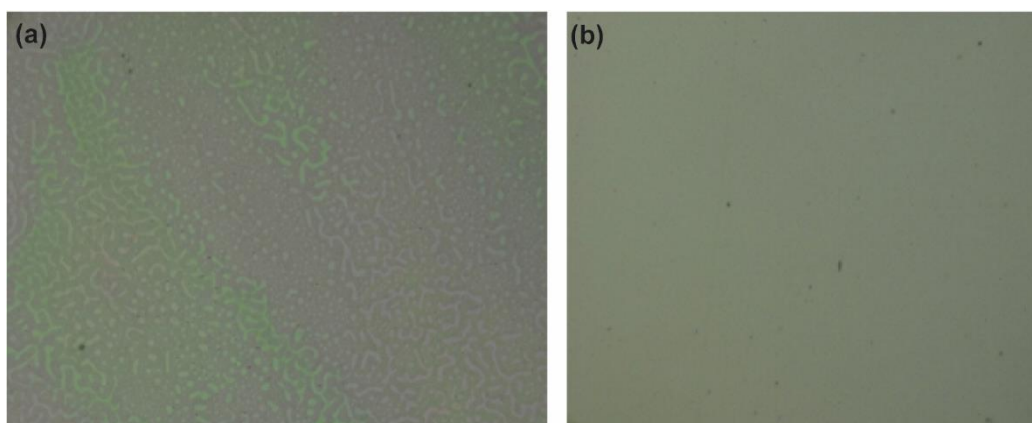


Figure 87. Optical polarised microscopy images at 50x magnification of (a) 1:1 mixture of pure polymers 138 (PMMA) and 142 (PS) and (b) 1:1 mixture of co-polymers 146 and 148 (2% UIM-PMMA:2.5% AIC-PS).

4.4 Conclusions

Two methyl methacrylate monomers containing a *DDA* interacting array were designed and synthesised. A complementary styrene-based monomer containing an *AAD* interacting array was also synthesised. 3-12% of these monomers were co-polymerised with the respective monomer using RAFT

polymerisation to create a series of co-polymers. Optimisation of the reaction conditions for the RAFT co-polymerisation, particularly for the polystyrene co-polymerisation, were attempted to form co-polymers suitable for hydrogen bond mediated blend formation. However it was concluded that the incorporation of styrene-AIC co-monomers limited the degree of polymerisation and resulted in large PDI values not expected for a controlled polymerisation. There are several possible explanations for this including; the co-monomer acted as a radical trapping agent terminating the propagation, the CTA does not work efficiently or decomposes during the reaction and impurities are terminating the propagation.

Visual inspection, optical microscopy and DSC studies suggested that miscible polymers of polymethylmethacrylate and polystyrene were created through hydrogen bonding of complementary *DDA* and *AAD* arrays. The characterisation of the co-polymers and blends produced in this project provide another example of hydrogen bonding driven blending of immiscible polymers, in line with previously reported polymer blends.^{98,104,161} This represents progress for developing self-sorting materials in terms of creating more blends with different hydrogen bonding motifs.

However, at this stage, limited conclusions can be made about the system due to discrepancies in the properties of the co-polymer. Hence it was not possible to infer the degree of hydrogen bonding required for blending in comparison to other systems. Additionally, it was revealed that subtleties in polymer composition can greatly influence the DSC data, interpretation of the DSC data is more complex than initially thought as many factors influence T_g hence physical markers for a blended or separated polymeric system could

not be inferred. Furthermore nothing can be concluded in terms of the type of blending that is infer from the DSC measurements and visual observations. Optical microscopy suggest these blends do not phase separate on the same are required to probe if these blends are fully miscible or phase separate on a smaller scale. It is clear that a more detailed study with greater control of the polymer composition is required for conclusions to be made on the effects hydrogen bonding on blending before self-sorting polymers can be established.

5. Summary and Future work

5.1 Thesis Summary

This thesis began with investigating the self-sorting behaviour of six hydrogen bonding motifs with an aim to imitate natural self-sorting processes. Pairwise hydrogen bonding interactions of the motifs were examined experimentally and computationally to understand their social and narcissistic self-sorting preferences. A self-sorting network was established comprising of several sequential self-sorting pathways. The use of hydrogen bonding motifs with varying degrees of fidelity and promiscuity was essential in creating these sequential self-sorting pathways. These contrasting characteristics allowed for the development of cross-talking between some pathways within the network. Additionally, other orthogonal pathways were shown to operate in parallel despite containing building block capable of cross-talk. The product distribution of the overall system was understood in terms of orthogonal recognition. Although the final product distribution was consistent for the six hydrogen bonding motifs examined, the product distribution at each stage of the pathway provided interesting results. The study revealed that thermodynamically less preferential complexes can be formed during self-sorting to maximise the stability of the whole system.

Next, efforts were made to introduce reversibility to the self-sorting network to closer mimic the cellular signalling cascades seen in biological systems. It was hypothesised that an external stimulus could reversibly switch the self-sorting preferences of specific hydrogen binding motifs and hence alter the product distribution of a given mixture. The hydrogen bonding motif UIM **31** was

identified as a potential responsive motif and a series of protonated analogues were created. Reversible switching between a protonated and neutral state was observed by ^1H NMR depending on the presence of acid or base, to produce different interacting arrays (*DDD* or *DDA*). The neutral and protonated species of UIM were shown to preferentially interact, self-sort, with their complementary partners AIC **46** and BB1 **85** in a three-component mixture. Finally, the self-sorting of the three hydrogen bonding motifs, the responsive hydrogen bonding motif (**31**) and the two complementary partners (**46** and **85**) were reversibly switched *in situ* between two self-sorted states. This *in situ* switching of molecular recognition between motifs highlights the potential to switch self-sorting in more complexed networks.

With the aim to development self-sorting materials, the final section of the thesis describes the translation of hydrogen bonding motifs capable of self-sorting into a supramolecular blends. Methylmethacrylate and styrene monomers containing UIM (**31**) and AIC (**46**) hydrogen bonding motifs were designed, synthesised and co-polymerised using RAFT polymerisation. The resultant co-polymers with complementary side chain functionalities were combined to create glassy polymer films. Characterisation of these polymer films suggested the formation of polymer blends was possible through the hydrogen bonding of the complementary monomers.

5.2 Future Directions

A future objective could be to combine the responsive switching between two self-sorted states described in Chapter 3 with the sequential self-sorting pathways explored in Chapter 2. This could result in the direction of a self-sorting pathway being reversed by an external stimulus. This would require careful consideration of potential changes to the molecular recognition of all the hydrogen bonding motifs in the network as well as the desired switching. Another method could be to design and synthesis an alternative responsive hydrogen bonding motif in which the switching is induced with an orthogonal mechanism such as light. The use of responsive hydrogen bonding motifs which can be activated in an orthogonal and selective manner would be beneficial in more complexed networks.

Chapter 4 concluded that blending between UIM and AIC functionalised co-polymers was possible. However the characterisation of blending was made more complex by variation in the co-polymers properties such as polymer length. Although some optimisation was carried out during this project it was not possible to achieve consistency of all parameters. The control of the properties of the co-polymers is required for conclusions to be made about the influence of the hydrogen bonding motifs and degree of blending achieved. A detailed study optimising the co-polymerisation conditions, by direct co-polymerisation and post-polymerisation modification, could be advantageous for future investigations of blends. Greater control of the co-polymerisation would limit the variability of co-polymers and so give more confidence to the data interpretation. Future work should also probe if the polymer films are truly a single phase using additional techniques. Microscopy experiments could be

used to distinguish if blends are phase separated.¹⁹⁵ Polarized light microscopy is suitable for determining immiscible blends. Scanning electron microscopy (SEM) and atomic force microscopy (AFM) can be used for studying the surface morphology. Transmission electron microscopy (TEM) has very good resolution and can thus be used for the study of very fine dispersion in miscible blends. Additional physical techniques such as rheology could be used to determine the viscoelastic or glassy properties of the blends and quantify the strength of the films created.

To realise the long term goal of creating materials capable of self-sorting, a variety of co-polymers functionalised with complementary and orthogonal hydrogen bonding motifs would need to be combined. This could involve combining the co-polymers previously reported by Zimmerman and Wilson or developing new co-polymers with side chain functionalisation of different hydrogen bonding motifs such as AUPy and NAPyO.

6. Experimental

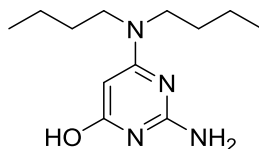
6.1 General materials and methods for synthesis

Solvents and reagents were purchased from Sigma Aldrich or Fisher Scientific and used without further purification unless otherwise stated. Where anhydrous solvents were required, dichloromethane, chloroform, tetrahydrofuran and acetonitrile were obtained from the in-house solvent purification system Innovative Inc. PureSolv®. Anhydrous dimethyl formamide and *N,N*-diisopropylethylamine were obtained from Sigma Aldrich equipped with Sure/Seal™. Anhydrous pyridine was placed over KOH for 24 hours before being refluxed for 2 hours and distilled over Linde 5Å molecular sieves and solid KOH before use. All non-aqueous reactions were carried out under a nitrogen atmosphere. Chloroform-*d* was dried over Linde 5Å molecular sieves or placed on CaCl₂ before being distilled and stored on KOH prior to use in ¹H NMR experiments. For reactions under non-anhydrous conditions, the solvents used were HPLC quality and provided by Sigma Aldrich or Fisher. Water in aqueous solutions and used for quenching was deionised. Mixtures of solvents are quoted as ratios and correspond to a volume: volume ratio. Analytical thin layer chromatography was performed on Merck Kieselgel 60 F254 0.25 mm pre-coated aluminium plates. Product spots were visualised under UV light ($\lambda_{\text{max}} = 254 \text{ nm}$) or using a suitable stain. Flash chromatography was carried out using Merck Kieselgel 60 silica gel using pressure by means of head bellows or using disposable RediSepRf silica flash columns on an automated Biotage Isolera One system. Nuclear magnetic resonance spectra were obtained at 298 K (unless stated) using a Bruker

AV500 spectrometer operating at 11.4 T (500 MHz for ^1H and 125 MHz ^{13}C) and JEOL ECA600ii operating at 14.1 T (150 MHz for ^{13}C) and NOESY spectra as stated. Infra-red spectra were obtained using a Bruker Alpha Platinum ATR where absorption maxima (ν_{max}) are quoted in wavenumbers (cm^{-1}) and only structurally relevant absorptions have been included. High Resolution Mass Spectra (HRMS) were recorded on a BrukerDaltonicsmicroTOF using electrospray ionisation (ESI). Liquid Chromatography and Mass Spectrometry (LC-MS) was performed using an Agilent Technologies 1200 series LC and a Bruker HCT ultra ion-trap MS. Gel permeation chromatography (GPC) measurements were conducted using an Agilent 1260 Infinity system fitted with two 5 μm Mixed-C columns plus a guard column, a refractive index detector and an UV/Vis detector operating at 309nm. DMF eluent was used at flow rate of 1.0 mL min^{-1} and temperature of 60 $^{\circ}\text{C}$. THF eluent contained 1.0 % v/v triethylamine (TEA) and 0.05 % w/v butylated hydroxyl toluene (BHT) at a flow rate of 1.0 mL min^{-1} and temperature of 30 $^{\circ}\text{C}$. A series of ten near-monodisperse poly(styrene) standards in THF and poly(methylmethacrylate) standards in DMF (M_p ranging from 400 to 2,300,000 g mol^{-1}) were employed as calibration standards in conjunction with RI detector for determining molecular weights. Advanced Polymer Chromatography (APC) measurements were conducted using Waters Acquity APC system fitted with three 2.4 μm columns plus a guard column and a refractive index detector. DMF and THF eluent was used at a flow rate of 0.5 mL min^{-1} and temperature of 40 $^{\circ}\text{C}$. A series of 6 near-monodisperse poly(methylmethacrylate) standards in DMF and THF (M_p ranging from 2,000 to 100,000 g mol^{-1}) were employed as calibration standards in conjunction with RI detector for determining molecular weights.

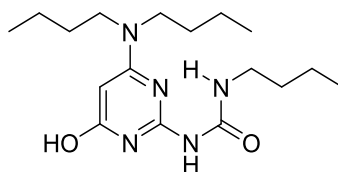
6.2 Experimental Chapter 2

2-Amino-6-(dibutylamino) 4-pyrimidinol (69)



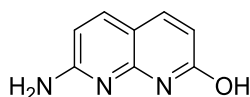
2-Amino-6-chloro-4-pyrimidinol (10.01 g, 68.70 mmol) was dissolved in ethyleneglycol (170 mL) and dibutylamine (29 mL, 171.80 mmol) was added. The solution was heated for 5 hours at 135 °C after which it was allowed to cool to room temperature. The solution was poured into saturated aqueous NH₄Cl solution (500 mL) and extracted three times with ethyl acetate. The combined organic layers were evaporated *in vacuo* to a volume of 100 mL and extracted with a saturated aqueous NaHCO₃ solution (300 mL) and a saturated aqueous NaCl solution (300 mL). The organic layer was dried, filtered and evaporated *in vacuo*. The yellow solid was recrystallised with acetonitrile twice affording 2-amino-6-(dibutylamino) 4-pyrimidinol (10.44 g, 64%) as a colourless solid. ¹H-NMR (500 MHz, CDCl₃) δ: 12.39 (s, 1H, OH), 5.02 (s, 2H, NH₂), 4.81 (s, 1H, Ar-H), 3.29 (bs, 4H, N-CH₂), 1.54-1.49 (m, 4H, NCH₂-CH₂), 1.28 (sext, *J* 7.2, 4H, NCH₂CH₂-CH₂), 0.91 (t, *J* 7.2, 6H, CH₃); ¹³C-NMR (125 MHz, CDCl₃) δ: 165.8, 163.6, 154.4, 76.3, 48.1, 29.6, 20.1, 13.9; *v*_{max} (solid state): 3317, 3166, 2956, 2930, 2871, 2730, 1586, 1558, 1490, 1453 cm⁻¹; MS (ESI+) *m/z* [M+H]⁺ calculated for C₁₂H₂₂N₄O: 239.18., found: [M+H]⁺ 239.17.

1-Butyl-3-(4-(dibutylamino)-6-hydroxypyrimidin-2-yl)urea (66)



A suspension of 2-amino-6-(dibutylamino) 4-pyrimidinol (5.00 g, 21.07 mmol), butyl isocyanate (3.56 mL, 31.60 mmol) and 4-*N,N*-dimethylaminopyridine (6.44 g, 52.70 mmol) in anhydrous chloroform (150 mL) was heated under nitrogen at 70 °C overnight. After cooling, the solution was concentrated. Dissolved in dichloromethane and filtered through silica to remove excess 4-*N,N*-dimethylaminopyridine. Ether (20 mL) was added and the white precipitate formed was further purified by recrystallisation (acetone) affording 1-(4-(dibutylamino)-6-hydroxypyrimidin-2-yl)-3-dodecylurea (0.68 g, 10%) as a colourless solid. ¹H-NMR (500 MHz, CDCl₃) δ: 12.57 (bs, 1H, OH), 11.18 (bs, 1H, NH), 9.54 (bs, 1H, NH), 5.31 (s, 1H, Ar-H), 3.40-3.20 (m, 6H, N-CH₂), 1.63-1.47 (m, 8H, NCH₂-CH₂), 1.43-1.27 (m, 4H, NCH₂CH₂-CH₂), 0.98-0.88 (m, 9H, CH₃) ppm; ¹³C-NMR (125 MHz, CDCl₃) δ: 170.9, 162.5, 157.4, 157.0, 78.7, 50.0, 40.0, 31.9, 30.3, 29.6, 29.4, 14.0 ppm; ν_{max} (solid state) = 3218, 3127, 3019, 2955, 2922, 2852, 2548, 1674, 1613, 1559, 1524, 1504, 1454 cm⁻¹; MS (ESI+) m/z [M+H]⁺ calculated for C₁₇H₃₁N₅O₂: 338.2556., found: [M+H]⁺ 338.2566.

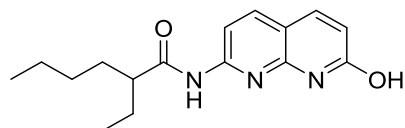
7-Amino-1,8-naphthridin-2-ol (71)



Concentrated sulfuric acid (40 mL), was added drop wise at 0 °C to a ground mixture of 2,6-diaminopyridine (6.67 g, 61.1 mmol) and D-malic acid (9.07 g, 67.6 mmol). The reaction mixture was then heated to 110 °C for 4 hours before

being cooled back to 0 °C. Saturated aqueous NH₄OH solution was then added drop wise to pH 9, before the reaction mixture was filtered and subsequently washed with water and diethyl ether, to give 7-amino-1,8-naphthridin-2-ol (5.31 g, 54 %) as an olive green solid. ¹H-NMR (500 MHz, DMSO-*d*₆) δ: 7.67 (m, 2H, Ar-*H*), 6.99 (s, 2H, NH₂), 6.37 (d, 1H, *J* 8.5 Hz, Ar-*H*), 6.14 (d, 1H, *J* 9.2 Hz, Ar-*H*) ppm; ¹³C-NMR (125 MHz, DMSO-*d*₆) δ: 164.1, 160.9, 150.7, 140.1, 137.7, 115.2, 105.6, 105.4 ppm; ν_{max} (solid state): 3500-2500 (broad), 1617, 1513 cm⁻¹; MS (ESI+) *m/z* [M+H]⁺ calculated for C₈H₈N₃O: 162.0667, found: [M+H]⁺ 161.9396.

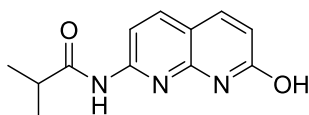
2-Ethyl-*N*-(5methyl-1,5-naphthyridine)hexanamide (67)



2-Ethylhexanoyl chloride (1.2 mL, 7.14 mmol) was slowly added to a solution of 7-amino-4-methyl-1,8-naphthyridin-2(1H)-one (1.00 g, 5.71 mmol) in dry pyridine (10.0 mL). The mixture was heated to 110 °C for 24 h and the solvent removed in vacuo. The residue was diluted with dichloromethane (100 mL). The organic phase was washed with 0.1 M aqueous HCl solution (10 mL), water (10 mL), saturated NaHCO₃ solution (10 mL) and dried. After evaporation of the solvent the crude product was purified by re-crystallisation from acetone yielding 2-ethyl-*N*-(5methyl-1,5-naphthyridine)hexanamide (1.07 g, 65%) as a colourless powder. ¹H-NMR (500 MHz, CDCl₃) δ: 12.83 (s, 1H, NH), 11.73 (s, 1H, NH), 8.45 (d, *J* 8.6 Hz, 1H, Ar-*H*), 7.91 (d, *J* 8.6 Hz, 1H; Ar-*H*), 7.73 (d, *J* 9.4 Hz, 1H, Ar-*H*), 6.62 (dd, *J*₁ 9.4 Hz, *J*₂ 1.9 Hz, 1H, Ar-*H*), 2.92-2.77 (m, 1H; CH), 1.81-1.69 (m, 2H; CH₂), 1.54-1.45 (m, 4H; CH₂), 1.40-1.25 (m, 4H; CH₂), 0.96 (t, *J* 7.2 Hz, 3H; CH₃), 0.85 (t, *J* 7.2 Hz, 3H; CH₃) ppm; ¹³C-

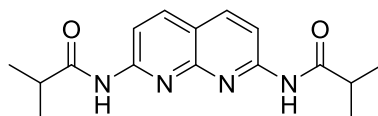
NMR (125 MHz, CDCl₃) δ : 177.8, 154.0, 148.5, 148.4, 136.0, 119.0, 112.0, 110.6, 48.4, 32.5, 29.7, 26.2, 22.9, 18.6, 14.0, 11.9 ppm; ν_{\max} (solid state) = 3175, 3135, 3069, 2960, 2933, 1705, 1657, 1616, 1579, 1525 cm⁻¹; MS (ESI+) m/z [M+H]⁺ calculated for C₁₆H₂₁N₃O₂: 288.38., found: [M+H]⁺ 288.40

7-[(Propan-2-yl)amino]-1,8-naphthyridin-2-ol (72)



Isobutyryl chloride (134 mg, 1.26 mmol) was slowly added to a solution of 7-amino-4-methyl-1,8-naphthyridin-2(1H)-one (100 mg, 0.63 mmol) in dry pyridine (5.0 mL). The mixture was heated to 110 °C for 1 h. Precipitate was filtered, washed with methanol and recrystallised from acetonitrile to give colourless crystals of 7-[(propan-2-yl)amino]-1,8-naphthyridin-2-ol (95 mg, 66%). ¹H-NMR (500 MHz, DMSO-*d*₆) δ : 11.82 (s, 1H, NH), 10.46 (s, 1H, NH), 8.04 (d, *J* 8.6 Hz, 1H, Ar-*H*), 7.95 (d, *J* 8.6 Hz, 1H; Ar-*H*), 7.84 (d, *J* 9.4 Hz, 1H, Ar-*H*), 6.42 (d, *J* 9.4 Hz, 1H, Ar-*H*), 2.86 (quintet, *J* 6.8 Hz, 1H, CH), 1.09 (s, 3H, CH₃), 1.08 (s, 3H, CH₃) ppm; ¹³C-NMR (125 MHz, DMSO-*d*₆) δ : 177.7, 155.8, 154.7, 153.2, 140.9, 140.1, 121.9, 119.4, 115.7, 35.2, 19.7 ppm; ν_{\max} (solid state) = 3044, 2972, 2925, 2868, 1700, 1624, 1525 cm⁻¹; MS (ESI+) m/z [M+H]⁺ calculated for C₁₂H₁₄N₃O₂: 232.1081, found: [M+H]⁺ 232.1080.

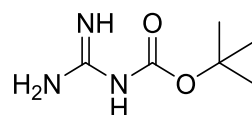
N2,N7-Bis(propan-2-yl)-1,8-naphthyridine-2,7-diamine (81)



7-[(propan-2-yl)amino]-1,8-naphthyridin-2-chloride (75 mg, 0.30 mmol), isobutyramide (31 mg, 0.36 mmol), potassium carbonate (58 mg, 0.42 mmol),

palladium(II) acetate (3 mg, 0.015 mmol) and xantphos (17 mg, 0.03 mmol) were suspended in 1,4-dioxane (5 mL) in a schlenck tube. The reaction mixture was heated to 100 °C for 23 h before being cooled to room temperature and filtered through celite. The solvent was evaporated in vacuo and the crude product was purified by crystallisation (MeOH) to give *N*2,*N*7-bis(propan-2-yl)-1,8-naphthyridine-2,7-diamine (32 mg, 34%) as colourless needles; ¹H-NMR (400 MHz, CDCl₃) δ: 8.42 (d, *J* 8.6 Hz, 1H, Ar-*H*), 8.21 (s, 1H, NH), 8.10 (d, *J* 8.6 Hz, 1H, Ar-*H*), 2.60 (m, *J* 6.8 Hz, 1H, CH), 1.28 (s, 3H, CH₃), 1.26 (s, 3H, CH₃) ppm; ¹³C-NMR (100 MHz, CDCl₃) δ: 176.0, 153.9, 153.7, 139.0, 121.9, 118.4, 113.4, 37.1, 19.3 ppm; ν_{max} (solid state) = 3284, 3138, 2967, 2933, 2872, 1690, 1499 cm⁻¹; MS (ESI+) *m/z* [M+H]⁺ calculated for C₁₆H₂₁N₄O₂: 301.1620, found: [M+H]⁺ 301.0924.

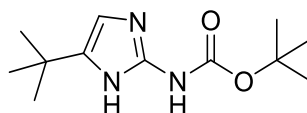
***N*-tert-Butoxycarbonylguanidine (76)**



Guanidine hydrochloride (13.1 g, 138 mmol) was dissolved in deionised water (80 mL). Sodium hydroxide (11.0 g, 275 mmol) was added in portions with stirring, then di-*tert*-butyl dicarbonate (10.0 g, 46 mmol) in acetone (100 mL) was added at 0 °C and the reaction mixture was left to stir for 20 hrs, once reaching room temperature. The volatiles were removed *in vacuo* to provide an aqueous suspension, which was extracted into ethyl acetate (2 x 150 mL). The organic layer was dried with sodium sulfate, filtered and concentrated under reduced pressure. The resultant solid was triturated (2:1 hexane:ethyl acetate) to provide *N*-*tert*-Butoxycarbonylguanidine (6.19 g, 85%) as a colourless solid; ¹H-NMR (500 MHz, DMSO-*d*₆): δ 6.81 (br s, 4H, CNH₂ and 2x

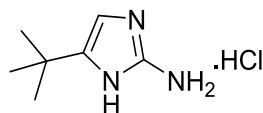
CNH), 1.36 (s, 9H, CH_3 (t Bu)) ppm; ^{13}C -NMR (125 MHz, DMSO- d_6) δ 163.4, 162.7, 75.5, 28.2 ppm; ν_{max} (solid state) = 3440, 3402, 3312, 1599, 1531 cm^{-1} ; ESI-HRMS m/z found 182.0899 $[M + Na]^+$ $C_6H_{13}N_3NaO_2$ requires 182.0900.

Tert-Butyl 5-tert-1H-imidazol-2-yl-carbamate (77)



1-Bromopinacolone (1.70 mL, 12.6 mmol) was added to a solution of *N*-tert-butoxycarbonylguanidine (6.00 g, 37.6 mmol) in anhydrous dimethylformamide (40 mL). The reaction was stirred at room temperature for 72 hr. The solution was filtered and the precipitate was dried providing tert-Butyl 5-tert-1H-imidazol-2-yl-carbamate (708 mg, 23%) as a colourless powder. The filtrate was refrigerated to give a second crop (554 mg, 18%); 1H -NMR (500 MHz, DMSO- d_6): δ 6.43 (s, 1H, imidazole-*H*), 6.41 (br s, 2H, 2xNH), 1.55 (s, 9H, CH_3 (O^t Bu)), 1.14 (s, 9H, CH_3 (C^t Bu)) ppm; ^{13}C -NMR (125 MHz, DMSO- d_6): δ 149.8, 149.0, 148.0, 102.9, 84.0, 31.2, 29.1, 27.5 ppm; ν_{max} (solid state) = 3433, 3279, 2971, 1724, 1640 cm^{-1} ; ESI-HRMS m/z found 262.1525 $[M + Na]^+$ $C_{12}H_{21}N_3NaO_2$ requires 262.1526.

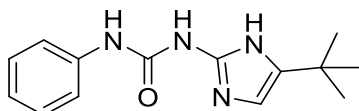
4-tert-Butyl-1H-imidazole-2-amine hydrochloride (78)



Tert-butyl 5-tert-1H-imidazol-2-yl-carbamate (750 mg, 3.10 mmol) was dissolved in 1M HCl in ethanol (30 mL) and refluxed for 16 hrs. The reaction was allowed to cool, concentrated and dried under pressure to give a colourless solid (400 mg, 2.28 mmol, 74%) 1H -NMR (500 MHz, $CDCl_3$): δ

11.83 (s, 1H, NH), 11.23 (s, 1H, NH). 6.24 (s, 1H, imidazole-H), 5.53 (br s, 2H, NH₂), 1.25 (s, 9H, CH₃ (C^tBu)) ppm; ¹³C-NMR (125 MHz, DMSO-*d*₆): δ 147.1, 135.8, 106.1, 29.8, 28.6 ppm; ν_{max} (solid state) = 3500-2800 (broad) cm⁻¹; ESI-HRMS *m/z* found 140.1190 [M + H]⁺ C₇H₁₄N₃ requires 140.1188.

1-(4-*tert*-Butyl-1*H*-imidazol-2-yl)-3-phenylurea (31)



Tert-Butyl imidazole (3.5 g, 20 mmol) was dissolved in anhydrous chloroform (100 mL) and anhydrous *N,N*-diisopropylethylamine (1.78 mL, 9.99 mmol) under a nitrogen atmosphere. Reaction was cooled to 0 °C and phenylisocyanate (1.09 mL, 9.99 mmol) was added dropwise and stirred for 1 hour. The resulting solution was concentrated under reduced pressure and purified via column chromatography (SiO₂, 9:1 dichloromethane:ethylacetate) and recrystallised from acetonitrile:methanol to give 1-(4-*tert*-Butyl-1*H*-imidazol-2-yl)-3-phenylurea (300 mg, 1.16 mmol, 12%). ¹H-NMR (500 MHz, CDCl₃): δ 7.28 (d, *J* 8.3, 2H, Ar-*H*), 7.19 (t, *J* 8.0, 2H, Ar-*H*), 6.97 (t, *J* 7.4, 1H, Ar-*H*), 6.22 (s, 1H, imidazole-*H*), 1.19 (s, 9H, CH₃ (C^tBu)) ppm; ¹³C-NMR (125 MHz, CDCl₃): δ 180.6, 154.7, 144.4, 138.3, 130.0, 123.3, 119.7, 101.6, 30.6, 29.7 ppm; ν_{max} (solid state) = 3184, 3069, 2961, 1549 cm⁻¹; ESI-HRMS *m/z* found 259.1561 [M + H]⁺ C₁₄H₁₉N₄O requires 259.1514.

Benzamido-5-methylisocytosine (46)

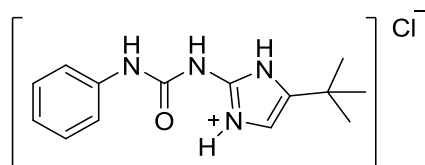


To a stirred mixture of methylisocytosine (3.00 g, 24.0 mmol) and 4-*N,N*-dimethylaminopyridine (150 mg, cat.) in anhydrous chloroform (120 mL) at room temperature under N₂ was added anhydrous *N,N*-diisopropylethylamine (6.30 ml, 36 mmol) and benzoyl chloride (3.00 mL, 26.4 mmol) and the reaction heated to reflux for 16 h. After cooling to room temperature the reaction mixture was washed with water (3 x 100 mL). The organic phase was dried over sodium sulfate, filtered and concentrated under reduced pressure. The product was purified by column chromatography (SiO₂, 1:9 ethylacetate:dichloromethane) to yield Benzamido-5-methylisocytosine as an off-white solid (4.10 g, 17.9 mmol, 75%); ¹H-NMR (500 MHz, CDCl₃) δ 8.11 (d, *J* 7.6, 2H, Ar-*H*), 7.58 (t, *J* 7.6, 1H, Ar-*H*), 7.44 (t, *J* 7.6, 2H, Ar-*H*), 6.42 (s, 1H, PyCH), 2.34 (s, 3H, PyCH₃) ppm; ¹³C NMR (125 MHz, DMSO-*d*₆) δ 171.6, 166.2, 163.7, 163.3, 134.1, 130.4, 128.7, 128.7, 102.0, 24.1 ppm; ν_{max} (solid state) = 3483, 3296, 3144, 1744 cm⁻¹; ESI-HRMS *m/z* found 230.0923 [M + H]⁺ C₁₂H₁₂N₃O₂ requires 230.0924.

6.3 Experimental Chapter 3

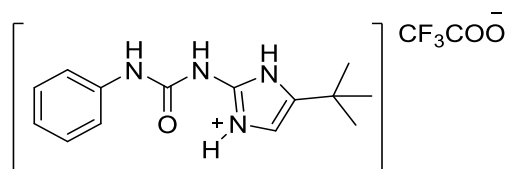
General Procedure for 1-(4-*tert*-Butyl-1*H*-imidazol-2-yl)-3-phenylurea acid salts

Hydrochloric acid salt



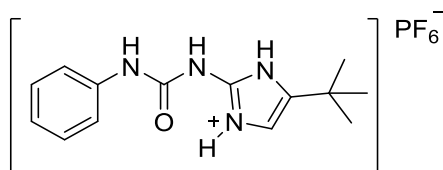
1-(4-*tert*-Butyl-1*H*-imidazol-2-yl)-3-phenylurea was dissolved in 4M hydrochloride in 1,4-dioxane (1-4 equivalents) and stirred for 1 hour. The solution was concentrated under pressure and dried to give 1-(4-*tert*-Butyl-1*H*-imidazol-2-yl)-3-phenylurea hydrochloride.

Trifluoroacetic acid salt



1-(4-*tert*-Butyl-1*H*-imidazol-2-yl)-3-phenylurea hydrochloride was dissolved in chloroform (2-10 mM). Trifluoroacetic acid (1 equivalent) was added to give 1-(4-*tert*-Butyl-1*H*-imidazol-2-yl)-3-phenylurea trifluoroacetic acid which was used immediately.

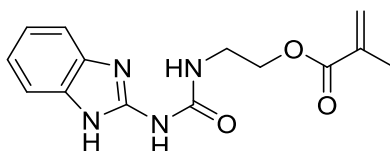
Hexafluorophosphoric acid salt



1-(4-tert-Butyl-1H-imidazol-2-yl)-3-phenylurea hydrochloride was dissolved in chloroform (2-10 mM). Silver hexafluorophosphate (1 equivalent) was added and stirred for one hour at room temperature. The resultant precipitate was filtered and the filtrate was concentrated under reduced pressure to give 1-(4-tert-Butyl-1H-imidazol-2-yl)-3-phenylurea hexafluorophosphoric acid.

6.4 Experimental Chapter 4

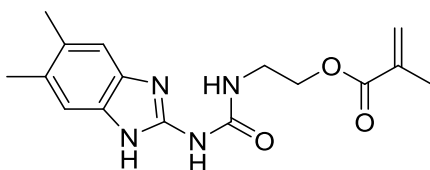
2-(3-1H-Benzo[d]imidazol-2-ylureido)ethyl methacrylate (90)



A solution of 2-aminobenzimidazole (786 mg, 5.90 mmol) in anhydrous tetrahydrofuran (12 mL) was stirred at reflux under nitrogen atmosphere for 3 hr. 2-Isocyanatoethyl methacrylate (1.00 mL, 7.08 mmol) was then added dropwise to the reaction mixture over 10 minutes. The reaction was stirred at reflux for a further 20 hr. The precipitate was isolated and dried under vacuum to give 2-(3-1H-Benzo[d]imidazol-2-ylureido)ethyl methacrylate as a colourless solid; (1.26 g, 4.37 mmol, 74%) ^1H NMR (500 MHz, $\text{DMSO-}d_6$) δ 11.45 (br. s., 1H, NH), 9.99 (br. s., 1H, NH), 7.73 (br. s., 1H, NH), 7.25 - 7.45 (m, 2H, Ar-H), 7.03 (dd, J_1 5.58, J_2 3.06, 2H, Ar-H), 6.15-6.06 (m, 1H, CCHH), 5.75-5.69 (m, 1H, CCHH'), 4.23-4.17 (m, 2H, OCH_2), 3.56-3.48 (m, 2H, NHCH_2), 1.98-1.86 (m, 3H, CH_3) ppm; ^{13}C NMR (125 MHz, $\text{DMSO-}d_6$) δ 166.5, 154.4, 148.4, 135.9, 125.6, 120.5, 120.5, 113.5, 63.5, 38.4, 17.8 ppm; ν_{max} (solid state) = 3341, 2941, 1707, 1531 cm^{-1} ; ESI-HRMS m/z found 311.1114 $[\text{M} + \text{Na}]^+$ $\text{C}_{14}\text{H}_{16}\text{N}_4\text{NaO}_3$ requires 311.1115.

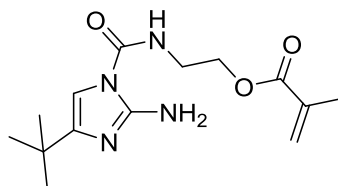
2-(3-(5,6-Dimethyl-1H-benzo[d]imidazol-2-yl)ureido)ethyl methacrylate

(92)



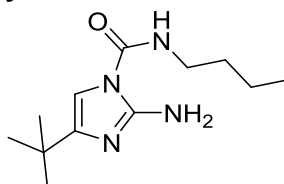
A solution of 2-amino-5,6-dimethylbenzimidazole (951 mg, 5.90 mmol) in anhydrous tetrahydrofuran (12 mL) was stirred at reflux under a nitrogen atmosphere for 3 hr. 2-Isocyanatoethyl methacrylate (1.00 mL, 7.08 mmol) was then added dropwise to the reaction mixture over 10 minutes. The reaction was stirred at reflux for a further 20 hr. The precipitate was isolated and dried under vacuum to give 2-(3-(5,6-Dimethyl-1H-benzo[d]imidazol-2-yl)ureido)ethyl methacrylate as a colourless solid (1.03 g, 3.25 mmol, 55%); ^1H NMR (500 MHz, $\text{DMSO-}d_6$) δ 11.20 (br. s., 1H, NH), 9.85 (br. s., 1H, NH), 7.73 (br. s., 1H, NH), 7.16-7.08 (m, 2H, Ar-H), 6.14-6.10 (m, 1H, CCHH'), 5.74-5.69 (m, 1H, CCHH'), 4.23-4.17 (m, 2H, OCH₂), 3.54-3.48 (m, 2H, NHCH₂), 2.28-2.23 (m, 6H, Ar-CH₃), 1.94-1.89 (m, 3H, CH₃) ppm; ^{13}C NMR (125 MHz, $\text{DMSO-}d_6$) δ 166.5, 154.4, 147.7, 135.9, 128.4, 128.4, 125.9, 113.9, 63.6, 38.2, 19.8, 18.0 ppm; ν_{max} (solid state) = 3349, 3017, 2970, 1707, 1523 cm^{-1} ; ESI-HRMS m/z found 339.1428 $[\text{M} + \text{Na}]^+$ $\text{C}_{16}\text{H}_{20}\text{N}_4\text{NaO}_3$ requires 339.1428.

2-(2-Amino-4-*tert*-butyl-1*H*-imidazole-1-carboxamido)ethyl methacrylate (95)



Tert-Butyl imidazole (1.16 g, 8.36 mmol) was dissolved in anhydrous tetrahydrofuran (150 mL) and anhydrous *N,N*-diisopropylethylamine (1.46 mL, 8.36 mmol) under a nitrogen atmosphere. Reaction was cooled to 0 °C and 2-isocynatoethylmethyleate (0.95 mL, 6.69 mmol) was added dropwise and stirred for 30 minutes. The resulting solution was concentrated under reduced pressure and purified via column chromatography (SiO₂, 9:1 dichloromethane:ethylacetate) to give 2-(2-Amino-4-*tert*-butyl-1*H*-imidazole-1-carboxamido)ethyl methacrylate (255 mg, 0.87 mmol, 13%). ¹H NMR (500 MHz, CDCl₃): δ 7.19 (s, 1H, *NH*), 6.24 (s, 1H, imidazole-*H*), 6.09 (m, 1 H, CCH*H*'), 6.04 (s, 1H, *NH*), 5.60 (br s, 2H, *NH*₂), 5.57 (m, 1H, CCH*H*'), 4.30 (m, 2H, CH₂O), 3.59 (m, 2H, CH₂NH), 1.89 (m, 3H, CH₃), 1.25 (s, 9H, *t*Bu-CH₃) ppm; ¹³C NMR (125 MHz, CDCl₃): δ 168.0, 151.8, 150.2, 150.0, 135.8, 126.6, 101.8, 63.1, 40.3, 31.5, 29.3, 18.3 ppm; ν_{\max} (solid state) = 3472, 3361, 3200, 2955, 1722, 1693 cm⁻¹; ESI-HRMS *m/z* found 295.1796 [M + H]⁺ C₁₄H₂₂N₄O₃ requires 295.1725.

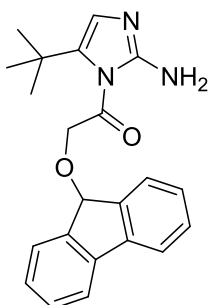
2-Amino-4-*tert*-butyl-*N*-butyl-1*H*-imidazole-1-carboxamide (97)



Tert-Butyl imidazole chloroform (20 mL) and anhydrous *N,N*-diisopropylethylamine (0.052 mL, 0.29 mmol) under a nitrogen atmosphere.

Reaction was cooled to 0 °C and butylisocyanate (0.064 mL, 0.57 mmol) was added dropwise and stirred for 25 minutes. The resulting solution was concentrated under reduced pressure and purified via column chromatography (SiO₂, 9:1 dichloromethane:ethylacetate) to give 2-Amino-4-tert-butyl-1H-imidazole-1-carboxamide (27 mg, 0.114 mmol, 20%).¹H NMR (500 MHz, CDCl₃): δ 6.22 (s, 1H, imidazole-*H*), 5.71 (br s, 2H, NH₂), 5.44 (s, 1H, NH), 3.29 (dd, *J*₁ 12.9 *J*₂ 6.9, 2H, CH₂NH), 1.52 (quin, *J* 7.4, 2H, CH₂CH₂NH), 1.33 (sext, *J* 7.4, 2H, CH₂CH₂CH₂NH), 1.15 (s, 9H, ^tBu-CH₃), 0.89 (t, *J* 7.4, 3H, CH₃CH₂) ppm; ¹³C NMR (125 MHz, CDCl₃): δ 151.8, 150.3, 150.0, 101.6, 40.4, 31.7, 31.5, 29.3, 20.0, 13.7 ppm; ν_{max} (solid state) = 33556, 2961, 2928, 2860, 1699 cm⁻¹; ESI-HRMS *m/z* found 239.1880 [M + H]⁺ C₁₂H₂₃N₄O requires 239.1827.

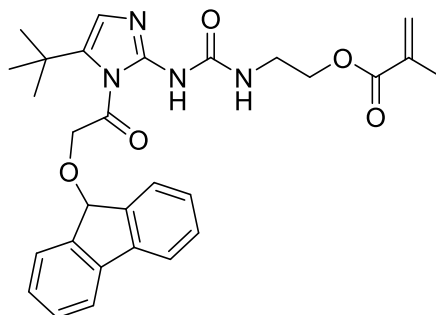
1-(2-Amino-4-tert-butyl-1H-imidazol-1-yl)-2-(9H-fluoren-9-yloxy)ethan-1-one (99)



Tert-Butyl 5-tert-1H-imidazol-2-yl-carbamate (2.00 g, 8.36 mmol), potassium carbonate (1.15 g, 8.36 mmol) and fluorenylmethoxycarbonyl chloride (2.37 g, 9.12 mmol) was refluxed in anhydrous tetrahydrofuran (150 mL) under a nitrogen atmosphere for 20 hours. The resulting solution was concentrated under reduced pressure and purified via column chromatography (SiO₂, 9:1 dichloromethane:ethylacetate) to give 1-(2-amino-4-tert-butyl-1H-imidazol-1-yl)-2-(9H-fluoren-9-yloxy)ethan-1-one (230 mg, 0.64 mmol, 8%). Crude ¹H NMR (500 MHz, CDCl₃): δ 7.76 (d, *J* 7.9, 2H, Ar-*H*), 7.63 (d, *J* 7.9, 2H, Ar-*H*),

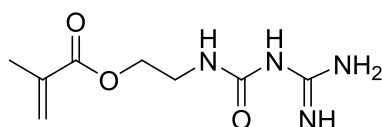
7.39 (t, J 7.7, 2H, Ar-H), 7.29 (t, J 7.7, 2H, Ar-H), 6.36 (s, 1 H, imidazole-H), 4.45 (d, J 7.3, 2H, OCH₂), 4.27 (t, J 7.3, 1H, OCH₂CH), 1.26 (s, 9H, ^tBu-CH₃) ppm. LC-MS m/z found 362.47 [M + H]⁺ C₂₂H₂₄N₃O₂ requires 362.4530.

2-(((4-Tert-butyl-1-[2-(9H-fluoren-9-yloxy)acetyl]-1H-imidazol-2-yl)carbamoyl)amino]ethyl-2-methylprop-2-enoate (100)



1-(2-amino-4-tert-butyl-1H-imidazol-1-yl)-2-(9H-fluoren-9-yloxy)ethan-1-one (200 mg, 0.55 mmol) was dissolved in anhydrous tetrahydrofuran (20 mL) and anhydrous *N,N*-diisopropylethylamine (0.03 mL, 0.23 mmol) under a nitrogen atmosphere. 2-isocyanatoethylmethylate (0.07 mL, 0.55 mmol) was added dropwise and the reaction was stirred for 30 minutes. The resulting solution was concentrated under reduced pressure and crude product used in the next step. LC-MS m/z found 517.59 [M + H]⁺ C₂₉H₃₃N₄O₅ requires 517.6060.

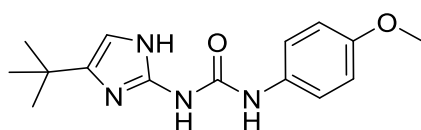
2-[(Carbamimidoyl)carbamoyl]amino]ethyl-2-methylprop-2-enoate (101)



Guanidine hydrochloride (200 mg, 2.09 mmol) was dissolved in deionised water (10 mL). Sodium hydroxide (84 g, 2.09 mmol) was added in portions with stirring, then 2-isocyanatoethylmethylacrylate (0.10 mL, 0.70 mmol) in acetone (10 mL) was added at room temperature and the reaction was stirred

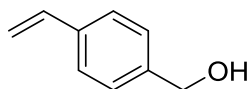
for 2 hours. The resulting solution was concentrated under reduced pressure and crude product used in the next step. Crude ^1H NMR (500 MHz, $\text{DMSO-}d_6$): δ 6.59 (br s, 1H, NH), 6.24 (s, 1H, CH_2NH), 6.06 (m, 1 H, CCHH'), 5.60 5.67 (t, J 1.5, 1 H, CCHH'), 4.07 (t, J 5.8, 2H, CH_2O), 3.24 (dd, J_1 5.8, J_2 11.5, 2H, CH_2NH), 1.89 (m, 3H, CH_3) ppm; LC-MS m/z found 215.37 $[\text{M} + \text{H}]^+$ $\text{C}_8\text{H}_{15}\text{N}_4\text{O}_3$ requires 215.2330.

3-(4-*Tert*-butyl-1H-imidazol-2-yl)-1-(4-methoxyphenyl)urea (103)



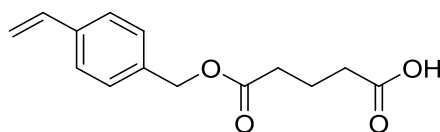
Tert-Butyl imidazole (500 mg, 2.86 mmol) was dissolved in anhydrous tetrahydrofuran (50 mL) and anhydrous *N,N*-diisopropylethylamine (0.50 mL, 2.86 mmol) under a nitrogen atmosphere at room temperature. 4-methoxy phenylisocyanate (0.19 mL, 1.43 mmol) was added dropwise and stirred for 2 hours. The resulting solution was concentrated under reduced pressure and purified via column chromatography (SiO_2 , 8:2 dichloromethane:ethylacetate) to give 3-(4-*tert*-butyl-1H-imidazol-2-yl)-1-(4-methoxyphenyl)urea (56 mg, 0.19 mmol, 14%). ^1H NMR (500 MHz, CDCl_3): δ 7.20 (d, J 8.9, 2H, Ar-*H*), 6.79 (d, J 8.9, 2H, Ar-*H*), 6.23 (s, 1 H, imidazole-*H*), 3.74 (s, 3H, OCH_3), 1.21 (s, 9H, CH_3 (C^tBu)) ppm; ^{13}C NMR (125 MHz, CDCl_3): δ 168.6, 167.9, 166.1, 156.4, 122.8, 114.4, 55.5, 30.6, 29.7 ppm. LC-MS m/z found 289.36 $[\text{M} + \text{H}]^+$ $\text{C}_{15}\text{H}_{21}\text{N}_4\text{O}_2$ requires 289.3590.

4-Ethenylphenyl)methanol (114)



4-Vinylbenzylchlorine (5 mL, 35.6 mmol) is added to a solution of sodium hydroxide (142 mg, 3.56 mmol) and tetrabutylammonium bromide (13.0 g, 35.6 mmol) in water (120 mL). The mixture was refluxed for 30 minutes, cooled and extracted with ethyl acetate (3x100 mL). The organic portions were combined and dried over sodium sulfate, filtered and concentrated under reduced pressure. The product was purified by column chromatography (SiO₂, 1:5 ethylacetate:hexane) to yield the (4-ethenylphenyl)methanol as a colourless oil (3.46 g, 25.8 mmol, 72%); ¹H NMR (500 MHz, CDCl₃): δ 7.44 (d, *J* 8.2, 2H, Ar-*H*), 7.34 (t, *J* 8.2, 2H, Ar-*H*), 6.75 (dd, *J*₁ 17.7, *J*₂ 10.9, 1H, CHCHH'), 5.79 (d, *J* 17.7, 1H, CHCHH'), 5.28 (d, *J* 10.9, 1H, CHCHH'), 4.69 (s, 2H, Bn-CH₂), 2.14 (br s, 1H, OH) ppm; ¹³C NMR (125 MHz, CDCl₃): δ 140.5, 137.0, 136.5, 127.2, 126.4, 113.9, 64.9 ppm.

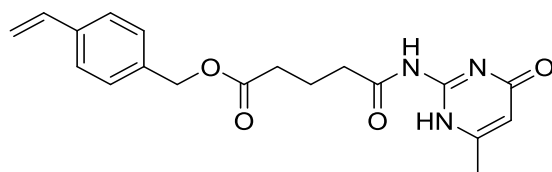
5-[(4-Ethenylphenyl)methoxy]-5-oxopentanoic acid (116)



4-Vinylbenzylalcohol (3.32 g, 24.7 mmol) is added to a solution of glutaric anhydride (5.62 g, 49.4 mmol), 4-dimethylaminopyridine (50 mg, cat) and anhydrous *N,N*-diisopropylethylamine (4.30 mL, 24.7 mmol) in anhydrous dichloromethane (100 mL). The mixture was stirred for 30 minutes and concentrated under reduced pressure. The product was purified by column chromatography (SiO₂, 1:9 ethylacetate:dichloromethane) to yield 5-[(4-ethenylphenyl)methoxy]-5-oxopentanoic acid as an off-white solid (2.50 g,

10.1 mmol, 41%); ^1H NMR (500 MHz, CDCl_3): δ 7.75 (br s, 1H, OH), 7.44 (d, J 8.2, 2H, Ar-H), 7.34 (t, J 8.2, 2H, Ar-H), 6.75 (dd, J_1 17.7, J_2 10.9, 1H, CHCHH'), 5.79 (d, J 17.7, 1H, CHCHH'), 5.28 (d, J 10.9, 1H, CHCHH'), 5.14 (s, 2H, Bn- CH_2), 2.54-2.42 (m, 4H, $\text{CH}_2\text{CH}_2\text{CH}_2$), 2.05-1.97 (m, 2H, $\text{CH}_2\text{CH}_2\text{CH}_2$) ppm; ^{13}C NMR (125 MHz, CDCl_3): δ 178.9, 172.8, 158.7, 135.9, 128.7, 128.6, 128.3, 128.3, 66.3, 33.2, 33.0, 19.8 ppm; ν_{max} (solid state) = 3325, 3058, 2929, 1651 cm^{-1} ; LC-MS m/z found 271.08 $[\text{M} + \text{Na}]^+$ $\text{C}_{14}\text{H}_{16}\text{NaO}_4$ requires 271.0946

(4-Ethenylphenyl)methyl 4-[(6-methyl-4-oxo-1,4-dihydropyrimidin-2-yl) carbamoyl]butanoate (117)



Method A

To a stirred solution of 2-amino-4-methyl-6-hydroxypyrimidine (1.26 g, 10.09 mmol), anhydrous *N,N*-diisopropylethylamine (4.4 mL, 25.0 mmol), 1-ethyl-3-(3-dimethylaminopropyl)carbodiimide (2.12 mL, 12.11 mmol) and hydroxybenzotriazole (1.64 g, 12.11 mmol) in anhydrous dimethylformamide (100 mL) was added 5-(4-vinylbenzyloxy-5-oxo-)pentanoic acid (2.50 g, 10.09 mmol). The reaction was stirred at room temperature for 20 hours. The reaction mixture was poured onto water and extracted with ethylacetate (5x50 mL). The organic layer was reduced in volume and washed with brine (3x50 mL), dried over sodium sulfate, filtered and concentrated under reduced pressure. The oil was dissolved in small amount of dichloromethane and

trituated with hexane and filtered to give (4-ethenylphenyl)methyl 4-[(6-methyl-4-oxo-1,4-dihydropyrimidin-2-yl) carbamoyl]butanoate as a colourless soild (1.23 mg, 3.45 mmol, 34%)

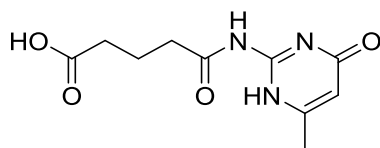
Method B

A suspension of 4-[(6-methyl-4-oxo-1,4-dihydropyrimidin-2-yl)carbamoyl]butanoic acid (2.00 g, 8.36 mmol) and anhydrous triethylamine (0.97 mL, 6.97 mmol) in anhydrous dimethylformamide (100 mL) was heated to 100 °C until a solution was reached. The reaction was cooled to 50 °C and 4-vinylbenzyl chloride (0.98 mL, 6.97 mmol) was added dropwise over 1 hour. The reaction was stirred at 50 °C for 48 hours. The reaction mixture was cooled and poured onto water. The resulting precipitate was filtered and filtrate was extracted with ethylacetate (5x50 mL). The organic layer was reduced in volume, combined with the precipitate and washed with brine (5x50 mL), dried over sodium sulfate, filtered and concentrated under reduced pressure. The product was purified by column chromatography (SiO₂, 5:95 methanol:dichloromethane) to yield (4-ethenylphenyl)methyl 4-[(6-methyl-4-oxo-1,4-dihydropyrimidin-2-yl) carbamoyl]butanoate as an off-white solid (1.14 g, 3.20 mmol, 46%);

¹H NMR (500 MHz, CDCl₃): δ 7.04 (d, *J* 8.2, 2H, Ar-*H*), 7.31 (d, *J* 8.2, 2H, Ar-*H*), 6.71 (dd, *J*₁ 17.3, *J*₂ 11.2, 1H, CHCHH'), 5.99 (s, 1H, Py-CH), 5.75 (d, *J* 17.3, 1H, CHCHH'), 5.27 (d, *J* 11.2, 1H, CHCHH'), 5.11 (s, 2H, Bn-CH₂), 2.60-2.51 (m, 2H, OCOCH₂), 2.49 (t, *J* 7.2, 2H, NHCOCH₂), 2.12-1.99 (m, *J* 7.2, 2H, CH₂CH₂CH₂) ppm; ¹³C NMR (125 MHz, CDCl₃): δ 172.7, 166.1, 162.7, 149.3, 137.6, 135.3, 128.4, 126.4, 114.4, 108.0, 66.2, 35.9, 33.1, 23.9, 19.8

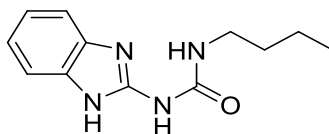
ppm; ν_{\max} (solid state) = 3118, 3061, 2945, 2888, 1731, 1664 cm^{-1} ; ESI-HRMS m/z found 356.1621 $[\text{M} + \text{H}]^+$ $\text{C}_{19}\text{H}_{21}\text{N}_3\text{O}_4$ requires 356.1566.

4-[(6-Methyl-4-oxo-1,4-dihydropyrimidin-2-yl)carbamoyl]butanoic acid (118)



Glutaric anhydride (10.9 g, 96.0 mmol) and 2-amino-4-methyl-6-hydroxypyrimidine (10.0 g, 80.0 mmol) were heated at 100 °C in anhydrous dimethylformamide (150 mL) for 2 hours. The mixture was cooled to room temperature and the product was triturated on addition of methanol. The precipitated was filtered and dried to give 4-[(6-methyl-4-oxo-1,4-dihydropyrimidin-2-yl)carbamoyl]butanoic acid as an off-white solid (13.7 g, 57.5 mmol, 72%); ^1H NMR (400 MHz, $\text{DMSO}-d_6$): δ 11.79 (br s, 2H, NH), 5.92 (s, 1H, imidazole-H), 2.46 (t, J 7.3, 2H, OCOCH_2), 2.27 (t, J 7.3, 2 H, NHCOCH_2), 1.82-1.74 (m, 2H, $\text{CH}_2\text{CH}_2\text{CH}_2$) ppm; ^{13}C NMR (100 MHz, DMSO) δ 176.5, 174.4, 165.2, 161.1, 150.8, 107.4, 35.6, 33.1, 23.7, 20.0 ppm; ν_{\max} (solid state) = 3207, 2917, 1663, 1577 cm^{-1} ; ESI-HRMS m/z found 240.0976 $[\text{M} + \text{H}]^+$ $\text{C}_{10}\text{H}_{14}\text{N}_3\text{O}_4$ requires 240.0979

1-(1H-1,3-Benzodiazol-2-yl)-3-butylurea (119)



A solution of 2-aminobenzimidazole (100 mg, 0.75 mmol) in anhydrous tetrahydrofuran (2 mL) was stirred at reflux under nitrogen atmosphere. *N*-butylisocyanate (0.10 mL, 0.90 mmol) was then added dropwise to the reaction mixture and the reaction was stirred at reflux for 2 hours. The precipitate was isolated and dried under vacuum to give 1-(1H-1,3-benzodiazol-2-yl)-3-butylurea as a colourless solid; (86 mg, 0.37 mmol, 49%) ¹H NMR (500 MHz, DMSO-*d*₆) δ 11.45 (br. s., 1H, *NH*), 9.76 (br. s., 1H, *NH*), 7.35 (br. s., 1H, *NH*), 7.38-7.31 (m, 2H, *Ar-H*), 7.04-6.97 (m, 2H, *Ar-H*), 3.19 (dd, *J*₁ 12.9, *J*₂ 6.7, 2H, *CH*₂*NH*), 1.52-1.42 (m, 2H, *CH*₂). 1.40-1.28 (m, 2H, *CH*₂), 0.91 (t, *J* 7.3, 3H, *CH*₃) ppm; ¹³C NMR (125 MHz, DMSO-*d*₆) δ 154.7, 148.8, 120.9, 39.2, 32.6, 20.2, 14.1 ppm; ν_{max} (solid state) = 3280, 3053, 2957, 2872, 1702 cm⁻¹; ESI-HRMS *m/z* found 255.1215 [M + Na]⁺ C₁₂H₁₆N₄NaO requires 255.1216.

General Procedure for 1st generation PMMA and PMMA-co-MMA-UIM Polymerisation

The required amount of MMA-UIM co-monomer (if required) and solvent (if required) was transferred to an ampoule with stirrer bar under nitrogen atmosphere. A solution of the required amount of 4-cyano-4-((dodecylsulfanylthiocarbonyl)sulfanyl) pentanoic acid (CTA) (if required) and azobutyronitrile (AIBN) dissolved in methyl methacrylate monomer was also

prepared, and the required aliquot of stock solution was added to the ampoule by syringe addition. The reaction mixture was thoroughly degassed by purging with nitrogen for 30 minutes, followed by three freeze-pump-thaw cycles. The reaction mixture was placed into a preheated oil bath at 90 °C and stirred for the specified time. After this time, the flask was immediately cooled to 0 °C to prevent any further polymerisation. Precipitation with methanol twice, followed by removal of residual solvent under reduced pressure provided the title material as a flocculent colourless powder.

PMMA (120)

General Procedure was followed adding methyl methacrylate (1.06 mL, 9.99 mmol), 4-cyano-4-((dodecylsulfanylthiocarbonyl)sulfanyl) pentanoic acid (20 mg, 0.050 mmol) and AIBN (0.8 mg, 0.0050 mmol) to a schlenk tube and heated for 3 hours. Yield: 757 mg, 76%; M_n (g mol^{-1}): 11992 (APC); \bar{D} : 1.20 (APC); $^1\text{H NMR}$ (500 MHz, CDCl_3) δ 3.56 (polymer CH_3O), 2.10-1.60 (polymer CH_2), 1.10-0.70 (polymer CH_3) ppm.

PMMA (121)

General Procedure was followed adding methyl methacrylate (1.06 mL, 9.99 mmol), 4-cyano-4-((dodecylsulfanylthiocarbonyl)sulfanyl) pentanoic acid (20 mg, 0.050 mmol) and AIBN (0.8 mg, 0.0050 mmol) to a schlenk tube and heated for 5 hours. Yield: 373 mg, 38%; M_n (g mol^{-1}): 22937 (APC); \bar{D} : 1.03 (APC); $^1\text{H NMR}$ (500 MHz, CDCl_3) δ 3.65-3.45 (polymer CH_3O), 2.10-1.60 (polymer CH_2), 1.10-0.70 (polymer CH_3) ppm.

PMMA (122)

General Procedure was followed adding methyl methacrylate (1.06 mL, 9.99 mmol), 4-cyano-4-((dodecylsulfanylthiocarbonyl)sulfanyl) pentanoic acid (20

mg, 0.050 mmol) and AIBN (0.8 mg, 0.0050 mmol) to a schlenk tube and heated for 6 hours. Yield: 487 mg, 49%; Mn (g mol⁻¹): 30978 (APC); Đ: 1.06 (APC); ¹H NMR (500 MHz, CDCl₃) δ 3.56 (polymer CH₃O), 2.10-1.60 (polymer CH₂), 1.10-0.70 (polymer CH₃) ppm.

PMMA (123)

General Procedure was followed adding methyl methacrylate (1.06 mL, 9.99 mmol), 4-cyano-4-((dodecylsulfanylthiocarbonyl)sulfanyl) pentanoic acid (20 mg, 0.050 mmol) and AIBN (0.8 mg, 0.0050 mmol) to a schlenk tube and heated for 8 hours. Yield: 310 mg, 31%; Mn (g mol⁻¹): 47300 (APC); Đ: 1.24 (APC); ¹H NMR (500 MHz, CDCl₃) δ 3.56 (polymer CH₃O), 2.10-1.60 (polymer CH₂), 1.10-0.70 (polymer CH₃) ppm.

PMMA (127)

General Procedure was followed adding methyl methacrylate (0.50 mL, 4.67 mmol) and AIBN (0.5 mg, 0.003 mmol) to a schlenk tube and heated for 1.5 hours. Yield: 305 mg, 65%; Mn (g mol⁻¹): 200847 (APC); Đ: 2.96 (APC); ¹H NMR (500 MHz, CDCl₃) δ 4.00-3.40 (polymer CH₃O), 2.10-1.60 (polymer CH₂), 1.20-0.50 (polymer CH₃) ppm.

PMMA-co-MMA-UIM 3% (129)

General Procedure for PMMA-co-MMA-UIM polymerisation was followed adding methyl methacrylate (1.0 mL, 9.99 mmol), 4-cyano-4-((dodecylsulfanylthiocarbonyl)sulfanyl) pentanoic acid (27 mg, 0.067 mmol) and AIBN (1 mg, 0.0067 mmol) to a schlenk tube containing co-monomer **90** (86 mg, 0.30 mmol). Yield: 566 mg, 52%; Mn (g mol⁻¹) 20306 (APC), 11641: (GPC); Đ:1.34 (APC), 1.70 (GPC); ¹H NMR (500 MHz, CDCl₃) δ 7.39 (br. s, 2H, co-monomer imidazole-H), 7.10 (br. s, 2H, co-monomer imidazole-H),

4.22-3.94 (m, 4H, co-monomer $\text{CH}_2\text{CH}_2\text{O}$), 3.86-3.31 (polymer CH_3O), 2.10-1.60 (polymer CH_2), 1.10-0.58 (polymer CH_3) ppm.

PMMA-co-MMA-UIM 12% (130)

General Procedure for PMMA-co-MMA-UIM polymerisation was followed adding methyl methacrylate (1.0 mL, 9.99 mmol), 4-cyano-4-((dodecylsulfanylthiocarbonyl)sulfanyl) pentanoic acid (27 mg, 0.067 mmol) and AIBN (1 mg, 0.0067 mmol) to a schlenk tube containing co-monomer **90** (345 mg, 1.20 mmol). Yield: 764 g, 56% Mn (g mol^{-1}) 19114 (APC), 10753: (GPC); Đ :1.31 (APC), 1.98 (GPC); $^1\text{H NMR}$ (500 MHz, $\text{DMSO-}d_6$) δ 7.36 (br s, 2H, co-monomer imidazole-*H*), 7.05 (br s, 2H, co-monomer imidazole-*H*), 4.11-3.89 (m, 4H, co-monomer $\text{CH}_2\text{CH}_2\text{O}$), 3.77-3.36 (polymer CH_3O), 2.05-1.60 (polymer CH_2), 1.10-0.58 (polymer CH_3) ppm.

PMMA-co-MMA-UIM 3% (131)

General Procedure was followed adding methyl methacrylate (1.0 mL, 9.99 mmol), 4-cyano-4-((dodecylsulfanylthiocarbonyl)sulfanyl) pentanoic acid (27 mg, 0.067 mmol) and AIBN (1 mg, 0.0067 mmol) to a schlenk tube containing co-monomer **92** (94 mg, 0.3 mmol). Yield: 733 mg, 65%; Mn (g mol^{-1}) 27159 (APC), 24410: (GPC); Đ :1.24 (APC), 1.27 (GPC); $^1\text{H NMR}$ (500 MHz, $\text{DMSO-}d_6$) δ 7.28-7.00 (2H, br s, co-monomer imidazole-*H*), 4.50-3.94 (4H, m, co-monomer $\text{CH}_2\text{CH}_2\text{O}$), 3.57 (polymer CH_3O), 2.36-2.26 (6H, m, co-monomer imidazole- CH_3), 2.12-1.57 (polymer CH_2), 1.06-0.42 (polymer CH_3) ppm.

PMMA-co-MMA-UIM 6% (132)

General Procedure was followed adding methyl methacrylate (1.0 mL, 9.99 mmol), 4-cyano-4-((dodecylsulfanylthiocarbonyl)sulfanyl) pentanoic acid (27 mg, 0.067 mmol) and AIBN (1 mg, 0.0067 mmol) to a schlenk tube containing

co-monomer **92** (189 mg, 0.6 mmol). Yield: 470 mg, 39%; M_n (g mol^{-1}) 20291 (APC), 14758: (GPC); \bar{M}_w : 1.28 (APC), 1.61 (GPC); $^1\text{H NMR}$ (500 MHz, $\text{DMSO-}d_6$) δ 7.17 (2H, br s, imidazole-*H*), 4.20-3.90 (4H, m, co-monomer $\text{CH}_2\text{CH}_2\text{O}$), 3.57 (polymer CH_3O), 2.38-2.18 (6H, m, co-monomer imidazole- CH_3), 2.40-1.40 (polymer CH_2), 1.30-0.40 (polymer CH_3) ppm.

PMMA-co-MMA-UIM 12% (133)

General Procedure was followed adding methyl methacrylate (1.0 mL, 9.99 mmol), 4-cyano-4-((dodecylsulfanylthiocarbonyl)sulfanyl) pentanoic acid (27 mg, 0.067 mmol) and AIBN (1 mg, 0.0067 mmol) to a schlenk tube containing co-monomer **92** (379 mg, 1.20 mmol). Yield: 566 mg, 40%; M_n (g mol^{-1}): 20881 (APC), 12455 (GPC); \bar{M}_w : 1.36 (APC), 1.76 (GPC); $^1\text{H NMR}$ (500 MHz, $\text{DMSO-}d_6$) δ 7.17 (2H, br s, imidazole-*H*), 4.20-3.90 (4H, m, co-monomer $\text{CH}_2\text{CH}_2\text{O}$), 3.56 (polymer CH_3O), 2.44-2.18 (6H, m, co-monomer imidazole- CH_3), 2.35-1.30 (polymer CH_2), 1.10-0.30 (polymer CH_3) ppm.

General Procedure for 1st generation Polystyrene and Polystyrene-co-styrene-AIC Polymerisation

The required amount of styrene co-monomer (if required) and solvent (if required) was transferred to an ampoule with stirrer bar under nitrogen atmosphere. A solution of the required amount of cyanomethyldodecyltrithiocarbonate (CTA) (if required) dissolved in styrene monomer was also prepared, and the required aliquot of stock solution was added to the ampoule by syringe addition. The reaction mixture was thoroughly degassed by purging with nitrogen for 30 minutes, followed by three freeze-pump-thaw cycles. The reaction mixture was placed into a preheated oil bath at 110 °C and stirred for the specified time. After this time,

the flask was immediately cooled to 0 °C to prevent any further polymerisation. Precipitation with methanol twice, followed by removal of residual solvent under reduced pressure provided the title material as a flocculent colourless powder.

Polystyrene (124)

General procedure was followed styrene (0.55 mL, 4.80 mmol) and cyanomethyldodecyltrithiocarbonate (7.6 mg, 0.025 mmol) was heated for 4.5 hours Yield: 335 mg, 67%; Mn (g mol⁻¹):8414 (APC); Đ:1.06 (APC); ¹H NMR (500 MHz, CDCl₃) δ 7.20-6.84 (polymer Ar-*H*), 6.80-6.25 (polymer Ar-*H*), 2.00-1.60 (polymer CH-Ar), 1.60-1.20 (polymer CH₂CH-Ar) ppm.

Polystyrene (125)

General procedure was followed styrene (0.55 mL, 4.80 mmol) and cyanomethyldodecyltrithiocarbonate (7.6 mg, 0.025 mmol) was heated for 8 hours Yield: 475 mg, 95%; Mn (g mol⁻¹): 10659 (APC); Đ: 1.11 (APC); ¹H NMR (500 MHz, CDCl₃) δ 7.20-6.84 (polymer Ar-*H*), 6.80-6.25 (polymer Ar-*H*), 2.00-1.60 (polymer CH-Ar), 1.60-1.20 (polymer CH₂CH-Ar) ppm.

Polystyrene (126)

General procedure was followed styrene (0.5 mL, 4.40 mmol) and cyanomethyldodecyltrithiocarbonate (1.6 mg, 0.005 mmol) was heated for 15 hours Yield: 404 mg, 81%; Mn (g mol⁻¹): 12354 (APC); Đ: 1.09 (APC); ¹H NMR (500 MHz, CDCl₃) δ 7.20-6.84 (polymer Ar-*H*), 6.80-6.25 (polymer Ar-*H*), 2.00-1.60 (polymer CH-Ar), 1.60-1.20 (polymer CH₂CH-Ar) ppm.

Polystyrene (128)

General procedure was followed, styrene (0.5 mL, 4.40 mmol) was heated for 15 hours. Yield: 284 mg, 62%; M_n (g mol^{-1}):262643 (APC); \bar{D} :2.93 (APC); ^1H NMR (500 MHz, CDCl_3) δ 7.20-6.84 (polymer Ar-*H*), 6.80-6.25 (polymer Ar-*H*), 2.00-1.60 (polymer CH-Ar), 1.60-1.20 (polymer $\text{CH}_2\text{CH-Ar}$) ppm.

Polystyrene-co-styrene-AIC 0.8% (134)

General procedure for polystyrene-co-styrene-AIC polymerisation was followed adding styrene (0.5 mL, 4.40 mmol), cyanomethyldodecyltrithiocarbonate (1.6 mg, 0.005 mmol) and styrene-AIC co-monomer **117** (12.5 mg, 0.035 mmol). Yield: 255 mg, 54%; M_n (g mol^{-1}): 10600 (APC), 18751 (GPC); \bar{D} :1.77 (APC), 2.39 (GPC); ^1H NMR (500 MHz, CDCl_3) δ 7.22-6.86 (polymer Ar-*H*), 6.71-6.26 (polymer Ar-*H*), 6.02-5.96 (br s, 1H, co-monomer pyridyl-*H*), 5.10-4.95 (br s, 2H, co-monomer Bn- CH_2), 2.71-2.55 (m, 2H, co-monomer OC(O)CH_2), 2.55-2.34 (m, 2H, co-monomer NHC(O)CH_2), 2.34-2.14 (m, 3H, co-monomer pyridyl- CH_3), 2.14-2.00 (m, 2H, co-monomer $\text{CH}_2\text{CH}_2\text{CH}_2$), 2.00-1.70 (polymer CH), 1.68-1.16 (polymer CH_2) ppm.

Polystyrene-co-styrene-AIC 3% (135)

General procedure for polystyrene-co-styrene-AIC polymerisation was followed adding styrene (0.5 mL, 4.40 mmol), cyanomethyldodecyltrithiocarbonate (1.6 mg, 0.005 mmol) and styrene-AIC co-monomer **117** (46.9 mg, 0.132 mmol). Yield: 247 mg, 49%; M_n (g mol^{-1}): 11100 (APC), 6877 (GPC); \bar{D} :1.85 (APC), 2.93 (GPC); ^1H NMR (500 MHz, CDCl_3) δ 7.27-6.86 (polymer Ar-*H*), 6.71-6.25 (polymer Ar-*H*), 6.05-5.86 (br s, 1H, co-monomer pyridyl-*H*), 5.14-4.90 (br s, 2H, co-monomer Bn- CH_2), 2.72-2.53 (m, 2H, co-monomer OC(O)CH_2), 2.52-2.32 (m, 2H, co-monomer

NHC(O)CH₂), 2.27-2.12 (m, 3H, co-monomer pyridyl-CH₃), 2.11-2.00 (m, 2H, co-monomer CH₂CH₂CH₂), 2.00-1.68 (polymer CH), 1.68-1.16 (polymer CH₂) ppm.

Polystyrene-co-styrene-AIC 6% (136)

General procedure for polystyrene-co-styrene-AIC polymerisation was followed adding styrene (0.5 mL, 4.40 mmol), cyanomethyldodecyltrithiocarbonate (1.6 mg, 0.005 mmol) and styrene-AIC co-monomer **117** (93.8 mg, 0.264 mmol). Yield: 360 mg, 65%; Mn (g mol⁻¹): 11400 (APC), 7777 (GPC); Đ:1.82 (APC), 2.37 (GPC); ¹H NMR (500 MHz, CDCl₃) δ 7.22-6.86 (polymer Ar-H), 6.80-6.25 (polymer Ar-H), 6.05-5.90 (br s, 1H, co-monomer pyridyl-H), 5.13-4.91 (br s, 2H, co-monomer Bn-CH₂), 2.73-2.53 (m, 2H, co-monomer OC(O)CH₂), 2.52-2.32 (m, 2H, co-monomer NHC(O)CH₂), 2.26-2.11 (m, 3H, co-monomer pyridyl-CH₃), 2.11-2.00 (m, 2H, CH₂CH₂CH₂), 2.00 – 1.68 (polymer CH), 1.68 – 1.16 (polymer CH₂) ppm.

Polystyrene-co-styrene-AIC 9% (137)

General procedure for polystyrene-co-styrene-AIC polymerisation was followed adding styrene (0.5 mL, 4.40 mmol), cyanomethyldodecyltrithiocarbonate (1.6 mg, 0.005 mmol) and styrene-AIC co-monomer **117** (140.6 mg, 0.396 mmol). Yield: 325 mg, 54%; Mn (g mol⁻¹): 10700 (APC), 8366 (GPC); Đ:1.81 (APC), 2.52 (GPC); ¹H NMR (500 MHz, CDCl₃) δ 7.22-6.86 (polymer Ar-H), 6.71-6.26 (polymer Ar-H), 6.08-5.88 (br s, 1H, co-monomer pyridyl-H), 5.16-4.84 (br s, 2H, co-monomer Bn-CH₂), 2.73-2.54 (m, 2H, co-monomer OC(O)CH₂), 2.54-2.33 (m, 2H, co-monomer NHC(O)CH₂), 2.27-2.11 (m, 3H, co-monomer pyridyl-CH₃), 2.11-1.97 (m, 2H, CH₂CH₂CH₂), 1.97-1.68 (polymer CH), 1.68-1.16 (polymer CH₂) ppm.

General Procedure for 2nd generation PMMA and PMMA-co-MMA-UIM Polymerisation

The required amount of MMA-UIM co-monomer (if required) was dissolved in dimethylformamide and transferred to an ampoule with stirrer bar under nitrogen atmosphere. A solution of the required amount of 4-cyano-4-((dodecylsulfanylthiocarbonyl)sulfanyl) pentanoic acid (CTA) and azobutyronitrile (AIBN) dissolved in methyl methacrylate monomer was also prepared, and the required aliquot of stock solution was added to the ampoule by syringe addition. The reaction mixture was thoroughly degassed by purging with nitrogen for 30 minutes, followed by three freeze-pump-thaw cycles. The reaction mixture was placed into a preheated oil bath at 80 °C and stirred for 18 hours. After this time, the flask was immediately cooled to 0 °C to prevent any further polymerisation. Precipitation with methanol twice, followed by removal of residual solvent under reduced pressure provided the title material as a flocculent colourless powder.

PMMA (138)

General Procedure was followed adding methyl methacrylate (1.60 mL, 15.0 mmol), 4-cyano-4-((dodecylsulfanylthiocarbonyl)sulfanyl) pentanoic acid (12 mg, 0.03 mmol) and AIBN (1 mg, 0.006 mmol) to a schlenk tube and heated for 18 hours. Yield: 1.35 g, 89%; M_n (g mol^{-1}): 42705 (GPC); \bar{D} : 1.21 (APC); $^1\text{H NMR}$ (500 MHz, CDCl_3) δ 3.58 (polymer CH_3O), 2.00-1.66 (polymer CH_2), 1.06-0.70 (polymer CH_3) ppm.

PMMA (139)

General Procedure was followed adding methyl methacrylate (3.20 mL, 30.0 mmol), 4-cyano-4-((dodecylsulfanylthiocarbonyl)sulfanyl) pentanoic acid (12 mg, 0.03 mmol) and AIBN (1 mg, 0.006 mmol) to a schlenk tube and heated for 18 hours. Yield: 2.07 g, 69%; M_n (g mol^{-1}): 69393 (GPC); \bar{M}_w : 1.30 (GPC); $^1\text{H NMR}$ (500 MHz, CDCl_3) δ 3.57 (polymer CH_3O), 2.00-1.70 (polymer CH_2), 1.10-0.70 (polymer CH_3) ppm.

PMMA-co-MMA-UIM 2% (146)

General Procedure was followed adding methyl methacrylate (1.6 mL, 15.0 mmol), 4-cyano-4-((dodecylsulfanylthiocarbonyl)sulfanyl) pentanoic acid (12 mg, 0.03 mmol), AIBN (1 mg, 0.006 mmol) and co-monomer **90** (130 mg, 0.45 mmol) to a schlenk tube and heated for 18 hours. Yield: 850 mg, 51%; M_n (g mol^{-1}) 38962 (GPC); \bar{M}_w : 1.29 (GPC); $^1\text{H NMR}$ (500 MHz, CDCl_3) δ 7.40 (2H, br s, co-monomer imidazole-*H*), 7.16 (2H, br s, co-monomer imidazole-*H*), 4.24-4.00 (4H, m, co-monomer $\text{CH}_2\text{CH}_2\text{O}$), 3.59 (polymer CH_3O), 2.20-1.55 (polymer CH_2), 1.10-0.50 (polymer CH_3) ppm.

General Procedure for 2nd generation Polystyrene and Polystyrene-co-styrene-AIC Polymerisation

The required amount of styrene co-monomer (if required) was dissolved in tetrahydrofuran and transferred to an ampoule with stirrer bar under nitrogen atmosphere. A solution of the required amount of cyanomethyldodecyltrithiocarbonate (CTA) and azobutyronitrile (AIBN) dissolved in styrene monomer was also prepared, and the required aliquot of stock solution was added to the ampoule by syringe addition. The reaction mixture was thoroughly degassed by purging with nitrogen for 30 minutes, followed by three freeze-pump-thaw cycles. The reaction mixture was placed

into a preheated oil bath at 80 °C and stirred for 18 hours. After this time, the flask was immediately cooled to 0 °C to prevent any further polymerisation. Precipitation with methanol twice, followed by removal of residual solvent under reduced pressure provided the title material as a flocculent colourless powder.

Polystyrene (140)

General procedure was followed, styrene (0.36 mL, 3.15 mmol), cyanomethyldodecyltrithiocarbonate (10 mg, 0.03 mmol) and AIBN (1 mg, 0.006 mmol) to a schlenk tube and heated for 18 hours. Yield: 315 mg, 93%; Mn (g mol⁻¹): 11229 (GPC); Đ: 1.16 (GPC); ¹H NMR (500 MHz, CDCl₃) δ 7.32-6.88 (polymer Ar-H), 6.88-6.29 (polymer Ar-H), 2.00-1.68 (polymer CH-Ar), 1.68-1.22 (polymer CH₂CH-Ar) ppm.

Polystyrene (141)

General procedure was followed, styrene (1.82 mL, 15.7 mmol), cyanomethyldodecyltrithiocarbonate (10 mg, 0.03 mmol) and AIBN (1 mg, 0.006 mmol) to a schlenk tube and heated for 18 hours. Yield: 810 mg, 46%; Mn (g mol⁻¹): 20483 (GPC); Đ: 1.26 (GPC); ¹H NMR (500 MHz, CDCl₃) δ 7.32-6.85 (polymer Ar-H), 6.85-6.24 (polymer Ar-H), 2.00-1.65 (polymer CH-Ar), 1.65-1.17 (polymer CH₂CH-Ar) ppm.

Polystyrene (142)

General procedure was followed, styrene (3.64 mL, 31.5 mmol), cyanomethyldodecyltrithiocarbonate (10 mg, 0.03 mmol) and AIBN (1 mg, 0.006 mmol) to a schlenk tube and heated for 18 hours. Yield: 1.45 g, 42%; Mn (g mol⁻¹): 25562 (GPC); Đ: 1.33 (GPC); ¹H NMR (500 MHz, CDCl₃) δ 7.32-

6.84 (polymer Ar-*H*), 6.84-6.24 (polymer Ar-*H*), 2.00-1.65 (polymer CH-Ar), 1.65-1.18 (polymer CH₂CH-Ar) ppm.

Polystyrene (143)

General procedure was followed, styrene (3.64 mL, 31.5 mmol), cyanomethyldodecyltrithiocarbonate (10 mg, 0.03 mmol) and AIBN (1 mg, 0.006 mmol) to a schlenk tube and heated for 2.5 hours. Yield: 760 mg, 23%; Mn (g mol⁻¹): 11982 (GPC); Đ: 1.65 (GPC); ¹H NMR (500 MHz, CDCl₃) δ 7.32-6.84 (polymer Ar-*H*), 6.84-6.24 (polymer Ar-*H*), 2.00-1.66 (polymer CH-Ar), 1.66-1.16 (polymer CH₂CH-Ar) ppm.

Polystyrene (144)

General procedure was followed, styrene (3.64 mL, 31.5 mmol), cyanomethyldodecyltrithiocarbonate (10 mg, 0.03 mmol) and AIBN (1 mg, 0.006 mmol) to a schlenk tube and heated for 20 hours. Yield: 1.22 g, 37%; Mn (g mol⁻¹): 18855 (GPC); Đ: 1.60 (GPC); ¹H NMR (500 MHz, CDCl₃) δ 7.32-6.84 (polymer Ar-*H*), 6.88-6.25 (polymer Ar-*H*), 2.00-1.66 (polymer CH-Ar), 1.66-1.19 (polymer CH₂CH-Ar) ppm.

Polystyrene (145)

General procedure was followed, styrene (3.64 mL, 31.5 mmol), cyanomethyldodecyltrithiocarbonate (10 mg, 0.03 mmol) and AIBN (1 mg, 0.006 mmol) to a schlenk tube and heated for 116 hours. Yield: 3.20 g, 97%; Mn (g mol⁻¹): 38721 (GPC); Đ: 1.64 (GPC); ¹H NMR (500 MHz, CDCl₃) δ 7.32-6.84 (polymer Ar-*H*), 6.84-6.29 (polymer Ar-*H*), 2.00-1.68 (polymer CH-Ar), 1.68-1.22 (polymer CH₂CH-Ar) ppm.

Polystyrene-co-styrene-AIC 2.5% (147)

General procedure was followed, styrene (1.82 mL, 15.7 mmol), cyanomethyldodecyltrithiocarbonate (10 mg, 0.03 mmol), AIBN (1 mg, 0.006 mmol) and styrene-AIC co-monomer **117** (167 mg, 0.47 mmol) to a schlenk tube and heated for 18 hours. Yield: 650 mg, 36%; M_n (g mol^{-1}): 6792 (GPC); \bar{M}_w : 2.24 (GPC); $^1\text{H NMR}$ (500 MHz, CDCl_3) δ 7.22-6.86 (polymer Ar-*H*), 6.71-6.26 (polymer Ar-*H*), 6.02-5.94 (br s, 1H, co-monomer pyridyl-*H*), 5.10-4.93 (br s, 2H, co-monomer Bn- CH_2), 2.66-2.51 (m, 2H, co-monomer $\text{OC}(\text{O})\text{CH}_2$), 2.50-2.34 (m, 2H, co-monomer $\text{NHC}(\text{O})\text{CH}_2$), 2.26-2.12 (m, 3H, co-monomer pyridyl- CH_3), 2.12-1.98 (m, 2H, co-monomer $\text{CH}_2\text{CH}_2\text{CH}_2$), 1.98-1.68 (polymer *CH*), 1.68-1.16 (polymer CH_2) ppm.

Polystyrene-co-styrene-AIC 2.5% (148)

General procedure was followed, styrene (3.64 mL, 31.5 mmol), cyanomethyldodecyltrithiocarbonate (10 mg, 0.03 mmol), AIBN (1 mg, 0.006 mmol) and styrene-AIC co-monomer **117** (335 mg, 0.94 mmol) to a schlenk tube and heated for 18 hours. Yield: 945 mg, 26%; M_n (g mol^{-1}): 7935 (GPC); \bar{M}_w : 2.24 (GPC); $^1\text{H NMR}$ (500 MHz, CDCl_3) δ 7.22-6.86 (polymer Ar-*H*), 6.71-6.26 (polymer Ar-*H*), 6.03-5.94 (br s, 1H, co-monomer pyridyl-*H*), 5.10-4.93 (br s, 2H, co-monomer Bn- CH_2), 2.66-2.53 (m, 2H, co-monomer $\text{OC}(\text{O})\text{CH}_2$), 2.51-2.34 (m, 2H, co-monomer $\text{NHC}(\text{O})\text{CH}_2$), 2.25-2.12 (m, 3H, co-monomer pyridyl- CH_3), 2.12-1.99 (m, 2H, co-monomer $\text{CH}_2\text{CH}_2\text{CH}_2$), 1.99-1.68 (polymer *CH*), 1.68-1.16 (polymer CH_2) ppm.

Polystyrene-co-styrene-AIC 4.5% (149)

General procedure was followed, styrene (1.82 mL, 15.7 mmol), cyanomethyldodecyltrithiocarbonate (10 mg, 0.03 mmol), AIBN (1 mg, 0.006 mmol) and styrene-AIC co-monomer **117** (335 mg, 0.94 mmol) to a schlenk

tube and heated for 18 hours. Yield: 1.01 g, 51%; M_n (g mol^{-1}):5272 (GPC); \bar{M}_w :2.85 (GPC); $^1\text{H NMR}$ (500 MHz, CDCl_3) δ 7.22-6.86 (polymer Ar-*H*), 6.71-6.26 (polymer Ar-*H*), 6.03-5.96 (br s, 1H, co-monomer pyridyl-*H*), 5.10-4.93 (br s, 2H, co-monomer Bn- CH_2), 2.67-2.53 (m, 2H, co-monomer $\text{OC}(\text{O})\text{CH}_2$), 2.53-2.39 (m, 2H, co-monomer $\text{NHC}(\text{O})\text{CH}_2$), 2.20-2.11 (m, 3H, co-monomer pyridyl- CH_3), 2.11-1.97 (m, 2H, co-monomer $\text{CH}_2\text{CH}_2\text{CH}_2$), 1.97-1.68 (polymer *CH*), 1.68-1.16 (polymer CH_2) ppm.

Polystyrene-co-styrene-AIC 5% (150)

General procedure was followed, styrene (3.64 mL, 31.5 mmol), cyanomethyldodecyltrithiocarbonate (10 mg, 0.03 mmol), AIBN (1 mg, 0.006 mmol) and styrene-AIC co-monomer **117** (670 mg, 1.89 mmol) to a schlenk tube and heated for 18 hours. Yield: 1.62 g, 41%; M_n (g mol^{-1}):5757 (GPC); \bar{M}_w :2.78 (GPC); $^1\text{H NMR}$ (500 MHz, CDCl_3) δ 7.22-6.86 (polymer Ar-*H*), 6.71-6.26 (polymer Ar-*H*), 6.05-5.91 (br s, 1H, co-monomer pyridyl-*H*), 5.10-4.92 (br s, 2H, co-monomer Bn- CH_2), 2.70-2.52 (m, 2H, co-monomer $\text{OC}(\text{O})\text{CH}_2$), 2.52-2.37 (m, 2H, co-monomer $\text{NHC}(\text{O})\text{CH}_2$), 2.27-2.11 (m, 3H, co-monomer pyridyl- CH_3), 2.11-1.98 (m, 2H, co-monomer $\text{CH}_2\text{CH}_2\text{CH}_2$), 1.98-1.68 (polymer *CH*), 1.68-1.16 (polymer CH_2) ppm.

6.5 Crystal Structures

Crystal structure determination for 66: Single crystals were grown by the slow evaporation of **66** in acetonitrile. X-Ray diffraction data were collected at the University of Leeds. Crystal data. $\text{C}_{17}\text{H}_{31}\text{N}_5\text{O}_2$, $M = 337.47$, crystal size $0.21 \times 0.07 \times 0.04 \text{ mm}^3$, triclinic, $a = 5.1924(6)$, $b = 11.8545(15)$, $c = 15.3976(10) \text{ \AA}$, $\alpha = 97.911(8)$, $\beta = 93.859(7)$, $\gamma = 102.021(10)^\circ$, $U =$

913.65(17) Å³, T = 120.3(7) K, P-1, Z = 2, I = 0.661 mm⁻¹, λ = 1.54184 [Cu–Kα], 6466 reflections measured, 3410 unique (R_{int} = 0.0462), observed (I > 2σ(I)). The final R₁ was 0.0532 (observed reflections 0.0774) and wR(F²) was 0.1306 (all data 0.1468) for 232 parameters. CCDC 1868220 contains the supplementary crystallographic data for this paper. These data can be obtained free of charge from the Cambridge Crystallographic Data Centre via www.ccdc.cam.ac.uk/data_request/cif.

Crystal structure determination for 72: Single crystals were grown by the slow evaporation of **72** in acetonitrile. X-Ray diffraction data were collected at the University of Leeds. Crystal data. C₁₂H₁₃N₃O₂, M = 231.25, crystal size 0.15 × 0.06 × 0.03 mm³, monoclinic, a = 4.8837(11), b = 22.962(4), c = 9.9321(18) Å, α = 90, β = 101.26(2), γ = 90°, U = 1092.4(4) Å³, T = 120.00(10) K, P2₁/n, Z = 4, I = 0.811 mm⁻¹, λ = 1.54184 [Cu–Kα], 4018 reflections measured, 2121 unique (R_{int} = 0.0500), observed (I > 2σ(I)). The final R₁ was 0.0832 (observed reflections 0.1048) and wR(F²) was 0.2057 (all data 0.2223) for 164 parameters. CCDC 1868221 contains the supplementary crystallographic data for this paper. These data can be obtained free of charge from the Cambridge Crystallographic Data Centre via www.ccdc.cam.ac.uk/data_request/cif.

Crystal structure determination for 66·44: Single crystals were grown by the slow evaporation of a 1:1 mixture of **66** and **44** in acetonitrile. X-Ray diffraction data were collected at the University of Leeds. Crystal data. C₃₃H₅₁N₉O₄, M = 637.82, crystal size 0.29 × 0.11 × 0.08 mm³, monoclinic, a = 9.52157(15), b = 15.8558(3), c = 22.3751(3) Å, α = 90, β = 92.0659(13), γ = 90°, U = 3375.81(9) Å³, T = 119.99(13) K, P2₁/n, Z = 4, I = 0.684 mm⁻¹, λ =

1.54184 [Cu-K α], 13422 reflections measured, 6628 unique ($R_{\text{int}} = 0.0348$), observed ($I > 2\sigma(I)$). The final R_1 was 0.0412 (observed reflections 0.0541) and $wR(F^2)$ was 0.0996 (all data 0.1084) for 442 parameters. CCDC 1868219 contains the supplementary crystallographic data for this paper. These data can be obtained free of charge from the Cambridge Crystallographic Data Centre via www.ccdc.cam.ac.uk/data_request/cif.

Crystal structure determination for 78: Single crystals were grown by the slow evaporation of a solution of **78** in DCM. X-ray diffraction data were collected at the University of Leeds. Crystal data: $C_{14}H_{22}N_4O_3$, $M=294.35$, crystal size $0.18 \times 0.04 \times 0.02 \text{ mm}^3$, monoclinic, $a=10.8541(4)$, $b=23.4566(9)$, $c=12.2668(3)$, $\alpha=\gamma=90$, $\beta=93.920$, $U=3115.83(19) \text{ \AA}^3$, $T=120 \text{ K}$, $Z=8$, $\lambda=1.54184[\text{CuK}\alpha]$, 12467 reflections measured, 6131 unique [$R_{\text{int}}=0.0383$] observed [$I>2\sigma(I)$]. The final R_1 was 0.0476 (observed reflections 0.0742) and $wR(F_2)$ was 0.1066 (all data 0.1185) for 411 parameters.

Crystal structure determination for 95: Single crystals were grown by the slow evaporation of a solution of **95** in MeCN-hexane. X-ray diffraction data were collected at the University of Leeds. Crystal data: $C_7H_{14}N_3Cl$, $M=175.66$, crystal size $0.37 \times 0.22 \times 0.09 \text{ mm}^3$, triclinic, $a=8.7847(3)$, $b=10.5084(3)$, $c=10.8699(2)$, $\alpha=86.562$, $\beta=79.455$, $\gamma=80.992$, $U=973.81(18) \text{ \AA}^3$, $T=120 \text{ K}$, $Z=4$, $\lambda=1.54184[\text{CuK}\alpha]$, 10652 reflections measured, 3677 unique [$R(\text{int})=0.0245$], 3677 observed [$I>2\sigma(I)$]. The final R_1 was 0.0290 (observed reflections 0.0313) and $wR(F_2)$ was 0.0752 (all data 0.0774) for 237 parameters.

6.6 General procedures for ^1H NMR Experiments

6.6.1 Pairwise analysis (chapter 2)

The one-component and two-component ^1H NMR Experiments were ran on separate samples. The mass of each component was calculated to make a final concentration of 10 mM in 0.6 mL of CDCl_3 . The required mass of each component was dissolved in 0.6 mL of CDCl_3 . The sample was allowed to equilibrate for a minimum of ten minutes before acquisition. The acquired spectra of the one-component and two-component were compared for changes the chemical shifts of specific resonances indicative of hydrogen bonding.

6.6.2 Self-sorting pathways sequential addition (chapter 2)

The mass of each component was calculated to make a final concentration of 10 mM in 0.6 mL of CDCl_3 . The required mass of each component for the first step of the pathway was dissolved in 0.6 mL of CDCl_3 . The sample was allowed to equilibrate for a minimum of ten minutes before acquisition. The required mass of the next component in the pathway was added to the same sample tube. The sample was allowed to equilibrate for a minimum of ten minutes before acquisition. The remaining components were added in the same sequential manner after each acquisition until all the components were added and ^1H NMR spectra was acquired for each stage of the pathway.

6.6.3 Self-sorting pathways non-sequential addition (chapter 2)

The mass of each component at each stage of the pathway was calculated to make a final concentration of 10 mM in 0.6 mL of CDCl_3 . For each stage of the pathway a separate ^1H NMR experiment was carried out on a separate

sample tube for each stage. The required mass of each component was dissolved in 0.6 mL of CDCl_3 . The sample was allowed to equilibrate for a minimum of ten minutes before acquisition.

6.6.4 Switching interactions using system A (chapter 3)

The mass of each component was calculated to make a final concentration of 5 mM in 0.6 mL of CDCl_3 (apart from the experiment described in Figure 58 which was at 10 mM concentration). The required mass of the starting component(s) was dissolved in 0.6 mL of CDCl_3 . The sample was allowed to equilibrate for a minimum of ten minutes before acquisition. After acquisition the sample was protonated by the addition of 1 equivalent of 4M HCl in 1,4-dioxane solution directly to the sample tube. The sample was allowed to equilibrate for a minimum of ten minutes before acquisition. After acquisition the sample was transferred to a vial and deprotonated by the addition of excess basic NaHCO_3 solution. The aqueous layer was separated and the organic layer was dried and added to an NMR sample tube. The sample was allowed to equilibrate for a minimum of ten minutes before acquisition. Any additional components were added to the same sample when required and the protonation and deprotonation method was repeated as required.

6.6.5 Switching interactions using system B (chapter 3)

The mass of each component was calculated to make a final concentration of 5 mM in 0.6 mL of CDCl_3 . The required mass of the starting component(s) was dissolved in 0.6 mL of CDCl_3 . The sample was allowed to equilibrate for a minimum of ten minutes before acquisition. After acquisition the sample was protonated by the addition of 1 equivalent of TFA directly to the sample tube. The sample was allowed to equilibrate for a minimum of ten minutes before

acquisition. After acquisition the sample was deprotonated by the addition of 1 or 3 equivalents of DABCO directly to the sample tube. The sample was allowed to equilibrate for a minimum of ten minutes before acquisition. Any additional components were added to the same sample when required and the protonation and deprotonation method was repeated as required.

6.7 NOESY NMR experiments

Phase sensitive ^1H - ^1H NOESY experiments were performed on a 1:1 mixture of components at 50 mM concentration with respect to each component in CDCl_3 solvent. Spectra were recorded using a 750 ms mixing time with 256 increments, 2048 data points on a JEOL ECA600ii spectrometer at 298 K operating at 14.1 T (600 MHz for ^1H).

6.8 Isothermal titration calorimetry (ITC)

ITC experiments were carried out using Microcal ITC200i instrument (Malvern) at 25°C in chloroform. 100 μM DAN 4 was present in the cell and titrated with 1 mM AUPy 1 loaded into the syringe using 26, 1.4 μL injections with 120 s spacing between the injections for 26 injection. Heats of chloroform dilution was subtracted from each measurement raw data. Data was analysed using Microcal Origin 8 and fitted to a one-binding site model.

6.9 Molecular structure calculations (Chapter 2):

The computations were carried out by using the density functional theory-based program Amsterdam Density Functional (ADF) 2017.108^{128,196} at the BLYP-D3(BJ)/TZ2P¹²⁴⁻¹²⁷ level of theory, which is known to accurately

reproduce hydrogen bond strengths and lengths.^{129,197} Solvent effects were accounted for by using the implicit conductor-like screening model (COSMO), in which the solute molecule is surrounded by a dielectric medium.¹³⁰ All optimised structures have been verified to be true minima (zero imaginary frequencies). The molecular figures were illustrated using CYLview.¹³¹

6.10 Molecular modelling (Chapter 4):

A hybrid Monte Carlo Molecular Mechanics (MCMM) conformational search was carried out in a chloroform medium, using Macromodel 10.3 from Schrödinger software and the Merck Molecular Force Field (MMFF) without restraints. 10000 conformers were generated by MCMM and low energy conformers (up to 10 kJ mol⁻¹ of relative energy) were retained.

6.11 Differential scanning calorimetry (DSC)

Measurements were performed on a DSC Q100 from TA Instruments equipped with an auto sampler and a liquid nitrogen cooling system. 5-15 mg of sample were placed in a standard aluminium pan that was not hermetically sealed. Experiments were performed under a nitrogen atmosphere, using a scanning rate of 10 °C min⁻¹ in a cyclic manner between 25 °C and 150 °C. Data was analyzed using Universal Analysis 2000 software.

6.12 Optical microscopy

The samples were visualised with a Leica DLMP microscope and the pictures were taken with a Nikon D7200. The samples were prepared by spin casting, at 10 revolutions per second, a solution of the 1:1 mixture (20 mg of each

component in 2 mL of dichloromethane) on to a glass microscope slide. The samples were focussed at 50x magnification at the sample edge and then the slide was moved to image the centre of the sample.

List of References

- 1 A. J. Wilson, *Soft Matter*, 2007, **3**, 409–425.
- 2 R. P. Sijbesma and E. W. Meijer, *Curr. Opin. Colloid Interface Sci.*, 1999, **4**, 24–32.
- 3 D. Philp and J. F. Stoddart, *Angew. Chemie Int. Ed.*, 1996, **35**, 1154–1196.
- 4 G. A. Jeffrey and W. Saenger, in *Hydrogen Bonding in Biological Structures*, eds. G. A. Jeffrey and W. Saenger, Springer Berlin Heidelberg, Berlin, Heidelberg, 1991, pp. 351–393.
- 5 M. C. Etter, *J. Phys. Chem.*, 1991, **95**, 4601–4610.
- 6 M. Simard, D. Su and J. D. Wuest, *J. Am. Chem. Soc.*, 2011, **113**, 4696–4698.
- 7 P. Brunet, M. Simard and J. D. Wuest, *J. Am. Chem. Soc.*, 1997, **119**, 2737–2738.
- 8 F. Garcia-Tellado, S. Goswami, S. K. Chang, S. J. Geib and A. D. Hamilton, *J. Am. Chem. Soc.*, 1990, **112**, 7393–7394.
- 9 S. K. Chang, D. van Engen, E. Fan and A. D. Hamilton, *J. Am. Chem. Soc.*, 1991, **113**, 7640–7645.
- 10 S. K. Chang and A. D. Hamilton, *J. Am. Chem. Soc.*, 1988, **110**, 1318–1319.
- 11 F. Garcia-Tellado, S. J. Geib, S. Goswami and A. D. Hamilton, *J. Am. Chem. Soc.*, 1991, **113**, 9265–9269.
- 12 E. Fan, J. Yang, S. J. Geib, T. C. Stoner, M. D. Hopkins and A. D. Hamilton, *J. Chem. Soc. Chem. Commun.*, 1995, **0**, 1251–1252.
- 13 C. a. Hunter, *Angew. Chemie Int. Ed.*, 2004, **43**, 5310–5324.
- 14 F. H. Beijer, R. P. Sijbesma, J. J. M. Vekemans, E. W. Meijer, H. Kooijman and A. L. Spek, *J. Org. Chem.*, 1996, **61**, 6371–6380.
- 15 Y. Kyogoku, R. C. Lord and A. Rich, *Proc. Natl. Acad. Sci.*, 1967, **57**, 250–257.
- 16 S. C. Zimmerman and P. S. Corbin, in *Molecular Self-Assembly Organic Versus Inorganic Approaches*, ed. M. Fuiita, Springer Berlin Heidelberg, Berlin, Heidelberg, 2000, pp. 63–94.
- 17 S. K. Yang and S. C. Zimmerman, *Isr. J. Chem.*, 2013, **53**, 511–520.
- 18 J. R. Quinn and S. C. Zimmerman, *Org. Lett.*, 2004, **6**, 1649–1652.
- 19 S. Brammer, U. Lüning and C. Köhl, *European J. Org. Chem.*, 2002, **23**, 4054–4062.
- 20 T. R. Kelly, C. Zhao and G. J. Bridger, *J. Am. Chem. Soc.*, 1989, **111**, 3744–3745.
- 21 T. R. Kelly and M. P. Maguire, *J. Am. Chem. Soc.*, 1987, **109**, 6549–6551.
- 22 H. Zeng, R. S. Miller, R. A. Flowers and B. Gong, *J. Am. Chem. Soc.*, 2000, **122**, 2635–2644.
- 23 J. D. Watson and F. H. C. Crick, *Nature*, 1953, **171**, 737–738.
- 24 B. A. Blight, A. Camara-campos, S. Djurdjevic, M. Kaller, D. A. Leigh, F. M. Mcmillan, H. McNab and A. M. Z. Slawin, *J. Am. Chem. Soc.*, 2009, **131**, 14116–14122.
- 25 S. Djurdjevic, D. Leigh, H. McNab, S. Parsons, G. Teobaldi and F. Zerbetto, *J. Am. Chem. Soc.*, 2007, **129**, 476–477.
- 26 W. L. Jorgensen and J. Pranata, *J. Am. Chem. Soc.*, 1990, **112**, 2008–

- 2010.
- 27 J. Pranata, S. G. Wierschke and W. L. Jorgensen, *J. Am. Chem. Soc.*, 1991, **113**, 2810–2819.
- 28 Y. Kyogoku, R. C. Lord and A. Rich, *Biochim. Biophys. Acta - Nucleic Acids Protein Synth.*, 1969, **179**, 10–17.
- 29 T. J. Murray and S. C. Zimmerman, *J. Am. Chem. Soc.*, 1992, **114**, 4010–4011.
- 30 A. D. Hamilton and D. Van Engen, *J. Am. Chem. Soc.*, 1987, **109**, 5035–5036.
- 31 J. M. Lehn, *Angew. Chemie Int. Ed.*, 1990, **29**, 1304–1319.
- 32 J. Sartorius and H.-J. Schneider, *Chem. Eur. J.*, 1996, **2**, 1446–1452.
- 33 Y. Ducharme and J. D. Wuest, *J. Org. Chem.*, 1988, **13**, 5787–5789.
- 34 B. Gong, Y. Yan, H. Zeng, E. Skrzypczak-Jankunn, Y. W. Kim, J. Zhu and H. Ickes, *J. Am. Chem. Soc.*, 1999, **121**, 5607–5608.
- 35 D. H. Williams, C. T. Calderone, D. P. O'Brien and R. Zerella, *Chem. Commun.*, 2002, **0**, 1266–1267.
- 36 T. J. Murray and S. C. Zimmerman, *Tetrahedron Lett.*, 1995, **36**, 7627–7630.
- 37 M. C. Etter, *Acc. Chem. Res.*, 1990, **23**, 120–126.
- 38 F. H. Beijer, H. Kooijman, A. L. Spek, R. P. Sijbesma and E. W. Meijer, *Angew. Chemie Int. Ed.*, 1998, **37**, 75–78.
- 39 P. S. Corbin, S. C. Zimmerman, P. A. Thiessen, N. A. Hawryluk and T. J. Murray, *J. Am. Chem. Soc.*, 2001, **123**, 10475–10488.
- 40 A. M. McGhee, C. Kilner and A. J. Wilson, *Chem. Commun.*, 2008, **0**, 344–346.
- 41 C.-H. Chien, M. Leung, J.-K. Su, G.-H. Li, Y.-H. Liu and Y. Wang, *J. Org. Chem.*, 2004, **69**, 1866–1871.
- 42 A. Gooch, A. M. McGhee, L. C. Renton, J. P. Plante, C. I. Lindsay and A. J. Wilson, *Supramol. Chem.*, 2009, **21**, 12–17.
- 43 F. H. Beijer, R. P. Sijbesma, H. Kooijman, A. L. Spek and E. W. Meijer, *J. Am. Chem. Soc.*, 1998, **120**, 6761–6769.
- 44 P. S. Corbin and S. C. Zimmerman, *J. Am. Chem. Soc.*, 1998, **120**, 9710–9711.
- 45 P. S. Corbin, L. J. Lawless, Z. Li, Y. Ma, M. J. Witmer and S. C. Zimmerman, *Proc. Natl. Acad. Sci.*, 2002, **99**, 5099–5104.
- 46 J. Nelson, *Structure and Function in Cell Signalling*, Wiley, 2009.
- 47 B. Grzybowski, S. Otto and D. Philp, *Chem. Commun.*, 2014, **50**, 14924–14925.
- 48 E. Mattia and S. Otto, *Nat. Nanotechnol.*, 2015, **10**, 111–119.
- 49 G. Ashkenasy, T. M. Hermans, S. Otto and A. F. Taylor, *Chem. Soc. Rev.*, 2017, **46**, 2543–2554.
- 50 M. M. Safont-sempere, G. Fernández and F. Würthner, *Chem. Rev.*, 2011, **111**, 5784–5814.
- 51 A. Wu and L. Isaacs, *J. Am. Chem. Soc.*, 2003, **125**, 4831–4835.
- 52 M. J. Mayoral, C. Rest, J. Schellheimer, V. Stepanenko and G. Fernández, *Chem. Eur. J.*, 2012, **18**, 15607–15611.
- 53 A. S. Singh and S.-S. Sun, *Chem. Commun.*, 2012, **48**, 7392–7394.
- 54 W. Jiang and C. A. Schalley, *Proc. Natl. Acad. Sci.*, 2009, **106**, 10425–10429.
- 55 Z. He, W. Jiang and C. A. Schalley, *Chem. Soc. Rev.*, 2015, **44**, 779–789.

- 56 P. Mukhopadhyay, P. Y. Zavalij and L. Isaacs, *J. Am. Chem. Soc.*, 2006, **128**, 14093–14102.
- 57 N. Basilio, J. Mendoza, S. Gago and A. J. Parola, *Chem. Commun.*, 2017, **53**, 6472–6475.
- 58 C. Addicott, N. Das and P. J. Stang, *Inorg. Chem.*, 2004, **43**, 5335–5338.
- 59 M. L. Saha and M. Schmittel, *J. Am. Chem. Soc.*, 2013, **135**, 17743–17746.
- 60 A. Jiménez, R. A. Bilbeisi, T. K. Ronson, S. Zarra, C. Woodhead and J. R. Nitschke, *Angew. Chemie Int. Ed.*, 2014, **53**, 4556–4560.
- 61 L. Isaacs, *Acc. Chem. Res.*, 2014, **47**, 2052–2062.
- 62 M. Zhang, L. Cao and L. Isaacs, *Chem. Commun.*, 2014, **50**, 14756–14759.
- 63 K. Kim, N. Selvapalam, Y. H. Ko, K. M. Park, D. Kim and J. Kim, *Chem. Soc. Rev.*, 2007, **36**, 267–279.
- 64 S. Ghosh, A. Wu, J. C. Fettinger, P. Y. Zavalij and L. Isaacs, *J. Org. Chem.*, 2008, **73**, 5915–5925.
- 65 Y. Chen and Y. Liu, *Chem. Soc. Rev.*, 2010, **39**, 495–505.
- 66 L. Li, H.-Y. Zhang, J. Zhao, N. Li and Y. Liu, *Chem. Eur. J.*, 2013, **19**, 6498–6506.
- 67 M. Zhang, X. Yan, F. Huang, Z. Niu and H. W. Gibson, *Acc. Chem. Res.*, 2014, **47**, 1995–2005.
- 68 W. Jiang, D. Sattler, K. Rissanen and C. A. Schalley, *Org. Lett.*, 2011, **13**, 4502–4505.
- 69 L.-P. Cao, J.-G. Wang, J.-Y. Ding, A.-X. Wu and L. Isaacs, *Chem. Commun.*, 2011, **47**, 8548–8550.
- 70 E. R. Draper, J. R. Lee, M. Wallace, F. Jäckel, A. J. Cowan and D. J. Adams, *Chem. Sci.*, 2016, **7**, 6499–6505.
- 71 E. R. Draper, B. Dietrich and D. J. Adams, *Chem. Commun.*, 2017, **53**, 1864–1867.
- 72 A. M. Castilla, E. R. Draper, M. C. Nolan, C. Brasnett, A. Seddon, L. L. E. Mears, N. Cowieson and D. J. Adams, *Sci. Rep.*, 2017, **7**, 8380.
- 73 E. R. Cross, S. Sproules, R. Schweins, E. R. Draper and D. J. Adams, *J. Am. Chem. Soc.*, 2018, **140**, 8667–8670.
- 74 Y. Ma, S. V Kolotuchin and S. C. Zimmerman, *J. Am. Chem. Soc.*, 2002, **124**, 13757–13769.
- 75 T. Park, E. M. Todd, S. Nakashima and S. C. Zimmerman, *J. Am. Chem. Soc.*, 2005, **127**, 18133–18142.
- 76 T. Park, S. C. Zimmerman and S. Nakashima, *J. Am. Chem. Soc.*, 2005, **127**, 6520–6521.
- 77 T. F. A. de Greef, G. Ercolani, G. B. W. L. Ligthart, E. . W. Meijer and R. P. Sijbesma, *J. Am. Chem. Soc.*, 2008, **130**, 13755–13764.
- 78 X. Zhao, X. Z. Wang, X. K. Jiang, Y. Q. Chen, Z. T. Li and G. J. Chen, *J. Am. Chem. Soc.*, 2003, **125**, 15128–15139.
- 79 M. L. Pellizzaro, A. M. McGhee, L. C. Renton, M. G. Nix, J. Fisher, W. B. Turnbull and A. J. Wilson, *Chem. Eur. J.*, 2011, **17**, 14508–14517.
- 80 A. Gooch, A. M. McGhee, M. L. Pellizzaro, C. I. Lindsay and A. J. Wilson, *Org. Lett.*, 2011, **13**, 240–243.
- 81 M. L. Pellizzaro, K. A. Houton and A. J. Wilson, *Chem. Sci.*, 2013, **4**, 1825–1829.
- 82 K. A. Houton and A. J. Wilson, *Polym. Int.*, 2015, **64**, 165–173.

- 83 C. Fouquey, J.-M. Lehn and A.-M. Levelut, *Adv. Mater.*, 1990, **5**, 254–257.
- 84 T. Gulik-Krzywicki, C. Fouquey and J.-M. Lehn, *Proc. Natl. Acad. Sci.*, 1993, **90**, 163–167.
- 85 M. Kotera, J. M. Lehn, J. P. Vigneron, *J. Chem. Soc. Chem. Commun.*, 1994, **5**, 197–199.
- 86 R. P. Sijbesma, F. H. Beijer, L. Brunsveld, B. J. Folmer, J. H. Hirschberg, R. F. Lange, J. K. Lowe and E. W. Meijer, *Science*, 1997, **278**, 1601–1604.
- 87 W. H. Carothers, *J. Am. Chem. Soc.*, 1929, **51**, 2548–2559.
- 88 W. H. Carothers, *Trans. Faraday Soc.*, 1936, **32**, 39–49.
- 89 T. F. A. De Greef and E. W. Meijer, *Nature*, 2008, **453**, 171–173.
- 90 A. W. Bosman, R. P. Sijbesma and E. W. Meijer, *Mater. Today*, 2004, **7**, 34–39.
- 91 V. G. H. Lafitte, A. E. Aliev, P. N. Horton, M. B. Hursthouse, K. Bala, P. Golding and H. C. Hailes, *J. Am. Chem. Soc.*, 2006, **128**, 6544–6545.
- 92 V. G. H. Lafitte, A. E. Aliev, E. Greco, K. Bala, P. Golding and H. C. Hailes, *New J. Chem.*, 2011, **35**, 1522–1527.
- 93 E. Greco, A. E. Aliev, V. G. H. Lafitte, K. Bala, D. Duncan, L. Pilon, P. Golding and H. C. Hailes, *New J. Chem.*, 2010, **34**, 2634–2642.
- 94 X. Yang, F. Hua, K. Yamato, E. Ruckenstein, B. Gong, W. Kim and C. Y. Ryu, *Angew. Chemie Int. Ed.*, 2004, **43**, 6471–6474.
- 95 G. B. W. Ligthart, H. Ohkawa, R. P. Sijbesma and E. W. Meijer, *J. Am. Chem. Soc.*, 2005, **127**, 810–811.
- 96 T. Park and S. C. Zimmerman, *J. Am. Chem. Soc.*, 2006, **128**, 13986–13987.
- 97 A. Gooch, S. Barrett, J. Fisher, C. I. Lindsay and A. J. Wilson, *Org. Biomol. Chem.*, 2011, **9**, 5938–5940.
- 98 A. Gooch, C. Nedolisa, K. A. Houton, C. I. Lindsay, A. Saiani and A. J. Wilson, *Macromolecules*, 2012, **45**, 4723–4729.
- 99 M. Weck, *Polym. Int.*, 2006, **56**, 453–460.
- 100 G. Moad, E. Rizzardo and S. H. Thang, *Polymers*, 2008, **49**, 1079–1131.
- 101 J. Krstina, G. Moad, E. Rizzardo, C. L. Winzor, C. T. Berge and M. Fryd, *Macromolecules*, 1995, **28**, 5381–5385.
- 102 J. Krstina, C. L. Moad, G. Moad, E. Rizzardo, C. T. Berge and M. Fryd, *Macromol. Symp.*, 2018, **111**, 13–23.
- 103 K. E. Feldman, M. J. Kade, T. F. A. de Greef, E. W. Meijer, E. J. Kramer and C. J. Hawker, *Macromolecules*, 2008, **41**, 4694–4700.
- 104 T. Park and S. C. Zimmerman, *J. Am. Chem. Soc.*, 2006, **128**, 11582–11590.
- 105 T. Park and S. C. Zimmerman, *J. Am. Chem. Soc.*, 2006, **128**, 14236–14237.
- 106 A. Gooch, N. S. Murphy, N. H. Thomson and A. J. Wilson, *Macromolecules*, 2013, **46**, 9634–9641.
- 107 R. Nussinov and C. J. Tsai, *Cell*, 2013, **153**, 293–305.
- 108 P. Csermely, R. Palotai and R. Nussinov, *Trends Biochem. Sci.*, 2010, **35**, 539–546.
- 109 M. M. Safont-Sempere, G. Fernández and F. Würthner, *Chem. Rev.*, 2011, **111**, 5784–5814.
- 110 M. L. Saha, S. De, S. Pramanik and M. Schmittel, *Chem. Soc. Rev.*,

- 2013, **42**, 6860–6909.
- 111 B. S. Pilgrim, D. A. Roberts, T. G. Lohr, T. K. Ronson and J. R. Nitschke, *Nat. Chem.*, 2017, **9**, 1276.
- 112 C. S. Wood, C. Browne, D. M. Wood and J. R. Nitschke, *ACS Cent. Sci.*, 2015, **1**, 504–509.
- 113 C. D. Pentecost, K. S. Chichak, A. J. Peters, G. W. V. Cave, S. J. Cantrill and J. F. Stoddart, *Angew. Chemie Int. Ed.*, 2006, **119**, 222–226.
- 114 I. A. Riddell, M. M. J. Smulders, J. K. Clegg, Y. R. Hristova, B. Breiner, J. D. Thoburn and J. R. Nitschke, *Nat. Chem.*, 2012, **4**, 751–756.
- 115 D. M. Wood, W. Meng, T. K. Ronson, A. R. Stefankiewicz, J. K. M. Sanders and J. R. Nitschke, *Angew. Chemie Int. Ed.*, 2015, **54**, 3988–3992.
- 116 A. Sørensen, A. M. Castilla, T. K. Ronson, M. Pittelkow and J. R. Nitschke, *Angew. Chemie Int. Ed.*, 2013, **52**, 11273–11277.
- 117 D. Wu, N. Potluri, J. Lu, Y. Kim and F. Rastinejad, *Nature*, 2015, **524**, 303–308.
- 118 T. Felder, T. F. A. de Greef, M. M. L. Nieuwenhuizen and R. P. Sijbesma, *Chem. Commun.*, 2014, **50**, 2455–2457.
- 119 T. F. A. de Greef, G. B. W. L. Ligthart, M. Lutz, A. L. Spek, E. W. Meijer and R. P. Sijbesma, *J. Am. Chem. Soc.*, 2008, **130**, 5479–5486.
- 120 E. V Brown, *J. Org. Chem.*, 1965, **30**, 1607–1610.
- 121 M. L. Pellizzaro, S. A. Barrett, J. Fisher and A. J. Wilson, *Org. Biomol. Chem.*, 2012, **10**, 4899–4906.
- 122 M. L. Pellizzaro, A. M. McGhee, L. C. Renton, M. G. Nix, J. Fisher, W. B. Turnbull and A. J. Wilson, *Chem. Eur. J.*, 2011, **17**, 14508–14517.
- 123 A. M. McGhee, J. P. Plante, C. A. Kilner and A. J. Wilson, *Supramol. Chem.*, 2011, **23**, 470–479.
- 124 A. D. Becke, *Phys. Rev. A*, 1988, **38**, 3098–3100.
- 125 C. Lee, W. Yang and R. G. Parr, *Phys. Rev. B*, 1988, **37**, 785–789.
- 126 S. Grimme, J. Antony, S. Ehrlich and H. Krieg, *J. Chem. Phys.*, 2010, **132**, 154104.
- 127 E. R. Johnson and A. D. Becke, *J. Chem. Phys.*, 2005, **123**, 24101.
- 128 G. te Velde, F. M. Bickelhaupt, E. J. Baerends, C. Fonseca Guerra, S. J. A. van Gisbergen, J. G. Snijders and T. Ziegler, *J. Comput. Chem.*, 2001, **22**, 931–967.
- 129 C. Fonseca Guerra, T. van der Wijst, J. Poater, M. Swart and F. M. Bickelhaupt, *Theor. Chem. Acc.*, 2010, **125**, 245–252.
- 130 C. C. Pye and T. Ziegler, *Theor. Chem. Acc.*, 1999, **101**, 396–408.
- 131 C. Y. Legault, CYLview, <http://www.cylview.org>.
- 132 T. J. Murray and S. C. Zimmerman, *J. Am. Chem. Soc.*, 1992, **114**, 4010–4011.
- 133 C. Fonseca Guerra, J.-W. Handgraaf, E. J. Baerends and F. M. Bickelhaupt, *J. Comput. Chem.*, 2003, **25**, 189–210.
- 134 A. K. Dutta, J. Rösger and K. Rajarathnam, *Methods Mol. Biol.*, 2015, **1229**, 315–324.
- 135 J. Hu and S. Liu, *Acc. Chem. Res.*, 2014, **47**, 2084–2095.
- 136 E. Cabane, X. Zhang, K. Langowska, C. G. Palivan and W. Meier, *Biointerphases*, 2012, **7**, 9.
- 137 B. Taghizadeh, S. Taranejoo, S. A. Monemian, Z. Salehi Moghaddam, K. Daliri, H. Derakhshankhah and Z. Derakhshani, *Drug Deliv.*, 2015, **22**, 145–155.

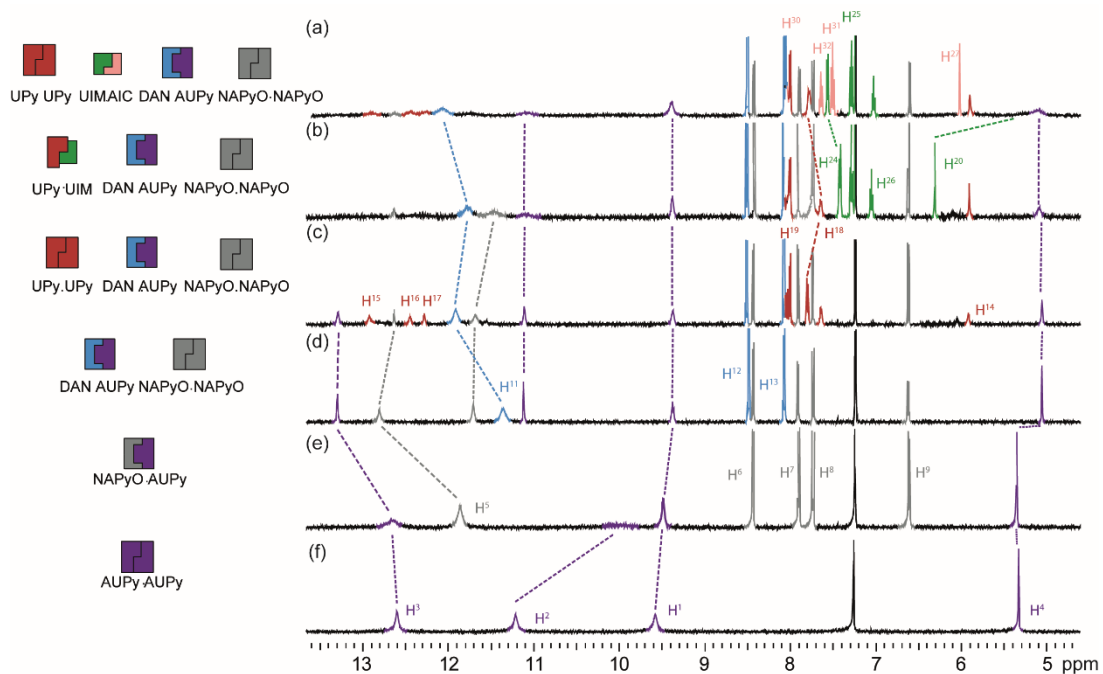
- 138 H. Wang, Q. Huang, H. Chang, J. Xiao and Y. Cheng, *Biomater. Sci.*, 2016, **4**, 375–390.
- 139 T.-G. Zhan, M.-D. Lin, J. Wei, L.-J. Liu, M.-Y. Yun, L. Wu, S.-T. Zheng, H.-H. Yin, L.-C. Kong and K.-D. Zhang, *Polym. Chem.*, 2017, **8**, 7384–7389.
- 140 L. Stricker, E.-C. Fritz, M. Peterlechner, N. L. Doltsinis and B. J. Ravoo, *J. Am. Chem. Soc.*, 2016, **138**, 4547–4554.
- 141 Y.-W. Yang, Y.-L. Sun and N. Song, *Acc. Chem. Res.*, 2014, **47**, 1950–1960.
- 142 I. Kocsis, D. Dumitrescu, Y.-M. Legrand, A. van der Lee, I. Grosu and M. Barboiu, *Chem. Commun.*, 2014, **50**, 2621–2623.
- 143 L. Maugeri, E. M. G. Jamieson, D. B. Cordes, A. M. Z. Slawin and D. Philp, *Chem. Sci.*, 2017, **8**, 938–945.
- 144 F. Muzika, T. Bánsági, I. Schreiber, L. Schreiberová and A. F. Taylor, *Chem. Commun.*, 2014, **50**, 11107–11109.
- 145 C. A. Nijhuis, B. J. Ravoo, J. Huskens and D. N. Reinhoudt, *Coord. Chem. Rev.*, 2007, **251**, 1761–1780.
- 146 S. Schoder and C. A. Schalley, *Chem. Commun.*, 2017, **53**, 9546–9549.
- 147 M. Herder, M. Pätzelt, L. Grubert and S. Hecht, *Chem. Commun.*, 2011, **47**, 460–462.
- 148 D. A. Bell and E. V. Anslyn, *Tetrahedron*, 1995, **51**, 7161–7172.
- 149 B. A. Blight, C. A. Hunter, D. A. Leigh, H. McNab and P. I. T. Thomson, *Nat. Chem.*, 2011, **3**, 244.
- 150 D. A. Leigh, C. C. Robertson, A. M. Z. Slawin and P. I. T. Thomson, *J. Am. Chem. Soc.*, 2013, **135**, 9939–9943.
- 151 J. Runt and J. Huang, in *Handbook of Thermal Analysis and Calorimetry*, ed. S. Cheng, Elsevier Science B.V., 2002, vol. 3, pp. 273–294.
- 152 M. T. Demeuse, in *Introduction to high temperature polymer blends*, ed. M. DeMeuse, Woodhead Publishing, 2014, pp. 1–13.
- 153 J. L. Koenig, in *Spectroscopy of Polymers*, ed. J. Koenig, Elsevier Science, New York, 1999, pp. 77–145.
- 154 W. J. MacKnight and F. E. Karasz, in *Comprehensive Polymer Science and Supplements*, eds. G. Allen and J. Bevington, Pergamon, Amsterdam, 1989, pp. 111–130.
- 155 L. A. Utracki, in *Polypropylene*, ed. J. Karger-Kocsis, Springer Netherlands, Dordrecht, 1999, pp. 601–605.
- 156 J. Mishra, S. K. Tiwari, M. M. Abolhasani, S. Azimi and G. C. Nayak, in *Micro and Nano Fibrillar Composites (MFCs and NFCs) from Polymer Blend*, eds. R. K. Mishra, S. Thomas and N. Kalarikkal, Woodhead Publishing, 2017, pp. 27–55.
- 157 E. Manias and L. A. Utracki, in *Polymer Blends Handbook*, eds. L. A. Utracki and C. A. Wilkie, Springer Netherlands, Dordrecht, 2014, pp. 171–289.
- 158 P. J. Flory, *Principles of Polymer Chemistry*, Cornell University Press, 1953.
- 159 A. I. Pesci and K. F. Freed, *J. Chem. Phys.*, 1989, **90**, 2017–2026.
- 160 J. S. Higgins, J. E. G. Lipson and R. P. White, *Philos. Trans. R. Soc. A*, 2010, **368**, 1009–1025.
- 161 S.-W. Kuo, *J. Polym. Res.*, 2008, **15**, 459–486.
- 162 L. M. Robeson, in *Polymer Blends*, Carl Hanser Verlag GmbH & Co.

- KG, 2007, pp. 11–64.
- 163 Y. Ochi, R. Kawakubo, D.-T. Van-Pham, Y. Kitamura, H. Nakanishi, T. Norisuye and Q. Tran-Cong-Miyata, *Adv. Nat. Sci. Nanosci. Nanotechnol.*, 2015, **6**, 45002.
- 164 U. Drechsler, R. J. Thibault and V. M. Rotello, *Macromolecules*, 2002, **35**, 9621–9623.
- 165 T. H. Galow, F. Ilhan, G. Cooke and V. M. Rotello, *J. Am. Chem. Soc.*, 2000, **122**, 3595–3598.
- 166 F. Ilhan, T. H. Galow, M. Gray, G. Clavier and V. M. Rotello, *J. Am. Chem. Soc.*, 2000, **122**, 5895–5896.
- 167 H. S. Bazzi and H. F. Sleiman, *Macromolecules*, 2002, **35**, 9617–9620.
- 168 W. Gerhardt, M. Črne and M. Weck, *Chem. Eur. J.*, 2004, **10**, 6212–6221.
- 169 N. Rabjohn and H. D. Barnstorff, *J. Am. Chem. Soc.*, 1953, **75**, 2259–2261.
- 170 A. Gooch, S. Barrett, J. Fisher, C. I. Lindsay and A. J. Wilson, *Org. Biomol. Chem.*, 2011, **9**, 5938–5940.
- 171 G. Moad, *Macromol. Chem. Phys.*, 2013, **215**, 9–26.
- 172 D. A. Shipp, *J. Macromol. Sci. Part C*, 2005, **45**, 171–194.
- 173 S. Perrier, *Macromolecules*, 2017, **50**, 7433–7447.
- 174 J. Chen and N. Seko, *Polymers*, 2017, **9**, 307.
- 175 M. Chanda, *Introduction to Polymer Science and Chemistry: A Problem-Solving Approach, Second Edition*, Taylor & Francis, 2013.
- 176 Y. Maruhashi and S. Iida, *Polym. Eng. Sci.*, 2004, **41**, 1987–1995.
- 177 W. Brostow, R. Chiu, I. M. Kalogerias and A. Vassilikou-Dova, *Mater. Lett.*, 2008, **62**, 3152–3155.
- 178 M. Eriksson, H. Goossens and T. Peijs, *Nanocomposites*, 2015, **1**, 36–45.
- 179 I. Hadj Romdhane, P. E. Price, C. A. Miller, P. T. Benson and S. Wang, *Ind. Eng. Chem. Res.*, 2001, **40**, 3065–3075.
- 180 A. Yoshioka and K. Tashiro, *Macromolecules*, 2004, **37**, 467–472.
- 181 R. Pinal, *Entropy*, 2008, **10**, 207–223.
- 182 T. P. Lodge and T. C. B. McLeish, *Macromolecules*, 2000, **33**, 5278–5284.
- 183 C. Pellerin, I. Pelletier, M. Pézolet and R. E. Prud'homme, *Macromolecules*, 2003, **36**, 153–161.
- 184 Y. Miwa, K. Usami, K. Yamamoto, M. Sakaguchi, M. Sakai and S. Shimada, *Macromolecules*, 2005, **38**, 2355–2361.
- 185 S. K. Motwani, R. K. Khar, F. J. Ahmad and S. Chopra, *J. Exp. Nanosci.*, 2006, **1**, 307–316.
- 186 L. Meistermann, M. Duval and B. Tinland, *Polym. Bull.*, 1997, **39**, 101–108.
- 187 M. T. García, I. Gracia, G. Duque, A. de Lucas and J. F. Rodríguez, *Waste Manag.*, 2009, **29**, 1814–1818.
- 188 T. Q. Nguyen, *J. Liq. Chromatogr. Relat. Technol.*, 2001, **24**, 2727–2747.
- 189 N. D. Hann, *J. Polym. Sci. Polym. Chem. Ed.*, 1977, **15**, 1331–1339.
- 190 Y. K. Chong, G. Moad, E. Rizzardo and S. H. Thang, *Macromolecules*, 2007, **40**, 4446–4455.
- 191 G. Moad, E. Rizzardo and S. H. Thang, *Polym. Int.*, 2010, **60**, 9–25.
- 192 M. E. Carnicom, A. J. Abruzzese, Y. Sidibe, D. K. Myers and S. E.

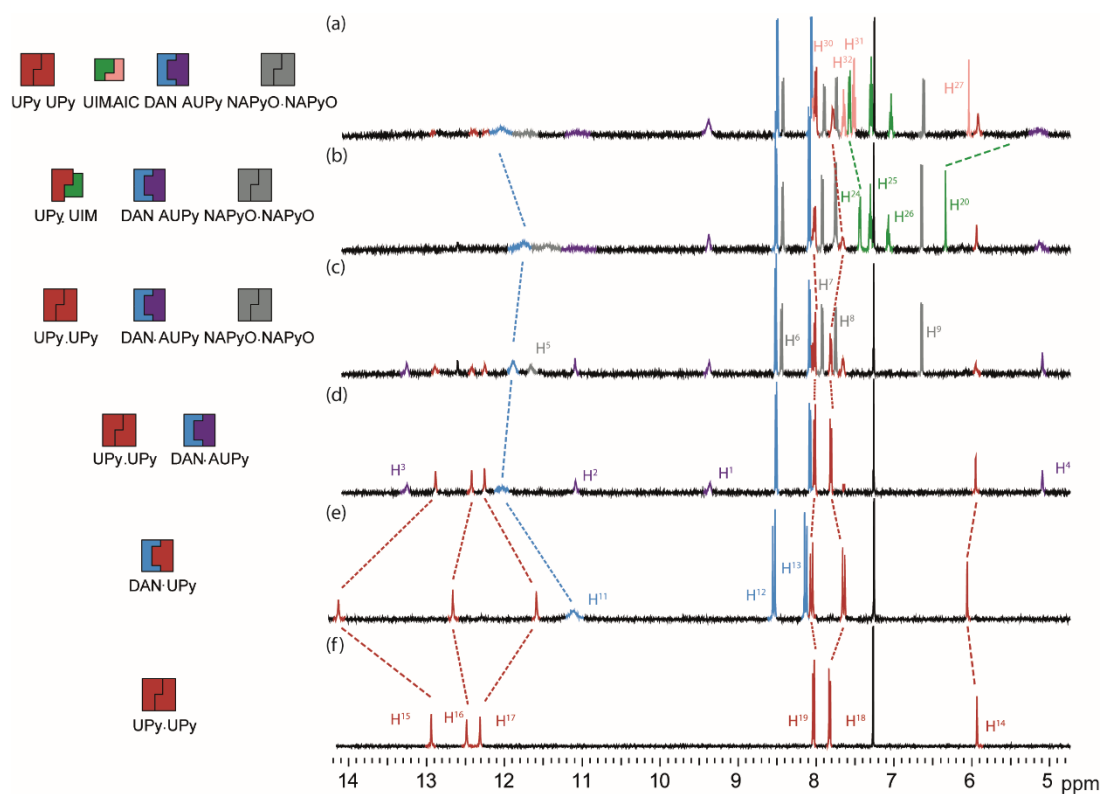
- Tillman, *Polymers*, 2014, 6, 2737–2751.
- 193 C. Pan and E. Tillman, *Polymers*, 2018, 10, 80.
- 194 K. E. Heiler, C. W. Pan, A. J. Heiler, J. P. Wu and E. S. Tillman, *Macromol. Chem. Phys.*, 2018, **219**, 1800171.
- 195 D. Vesely, *Polym. Eng. Sci.*, 1996, **36**, 1586–1593.
- 196 C. Fonseca Guerra, J. G. Snijders, G. te Velde and E. J. Baerends, *Theor. Chem. Acc.*, 1998, **99**, 391–403.
- 197 B. Brauer, M. K. Kesharwani, S. Kozuch and J. M. L. Martin, *Phys. Chem. Chem. Phys.*, 2016, **18**, 20905–20925.

Appendix A

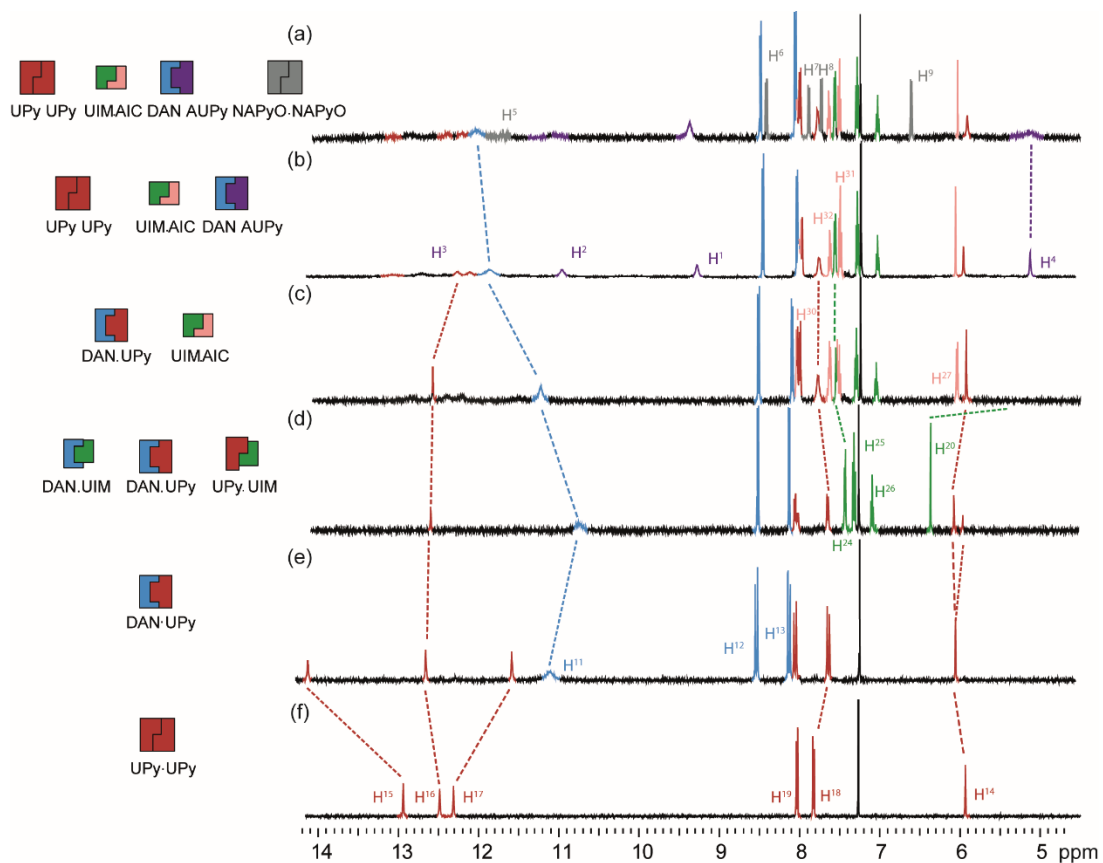
Supporting figures for Chapter 2



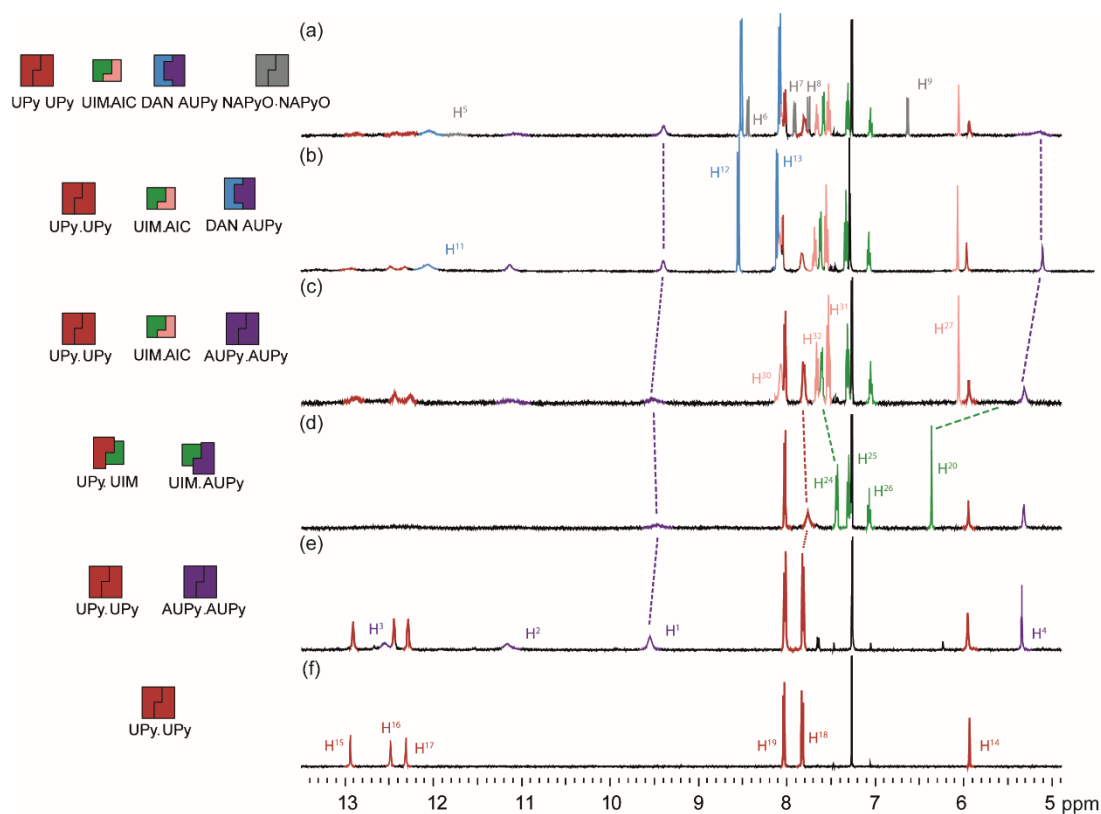
Appendix A Figure 1. Pathway A ¹H NMR (10 mM, CDCl₃) (a) UPY, UIM, AIC, DAN, AUPy and NAPyO, (b) UPY, UIM, DAN, NAPyO and AUPy, (c)UPY, DAN, AUPy AND NAPyO, (d)AUPy, DAN and NAPyO, (e)AUPy and NAPyO, (f) AUPy.



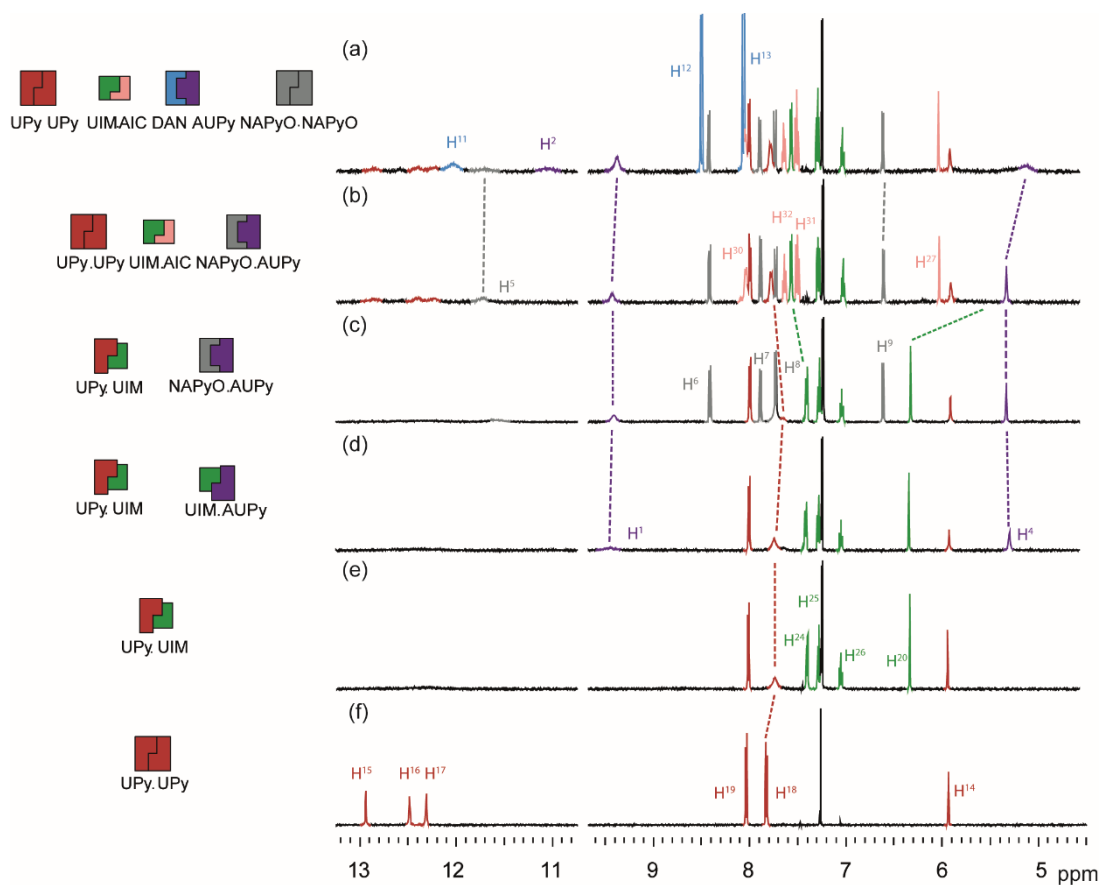
Appendix A Figure 2 Pathway B ^1H NMR (500 MHz, 10 mM, CDCl_3) (a) AUPy, NAPyO, DAN, UPy, UIM and AIC, (b) AUPy, NAPyO, DAN, UPy and UIM, (c) AUPy, NAPyO, DAN, UPy, (d) AUPy, DAN and UPy, (e) DAN and UPy and (f) UPy.



Appendix A Figure 3. Pathway C ^1H NMR (500 MHz, 10 mM, CDCl_3) (a) AUPy, NAPyO, DAN, UPy, UIM and AIC, (b) AUPy, DAN, UPy, UIM and AIC, (c) DAN, UPy, UIM and AIC, (d) DAN, UPy and UIM, (e) DAN and UPy and (f) UPy.



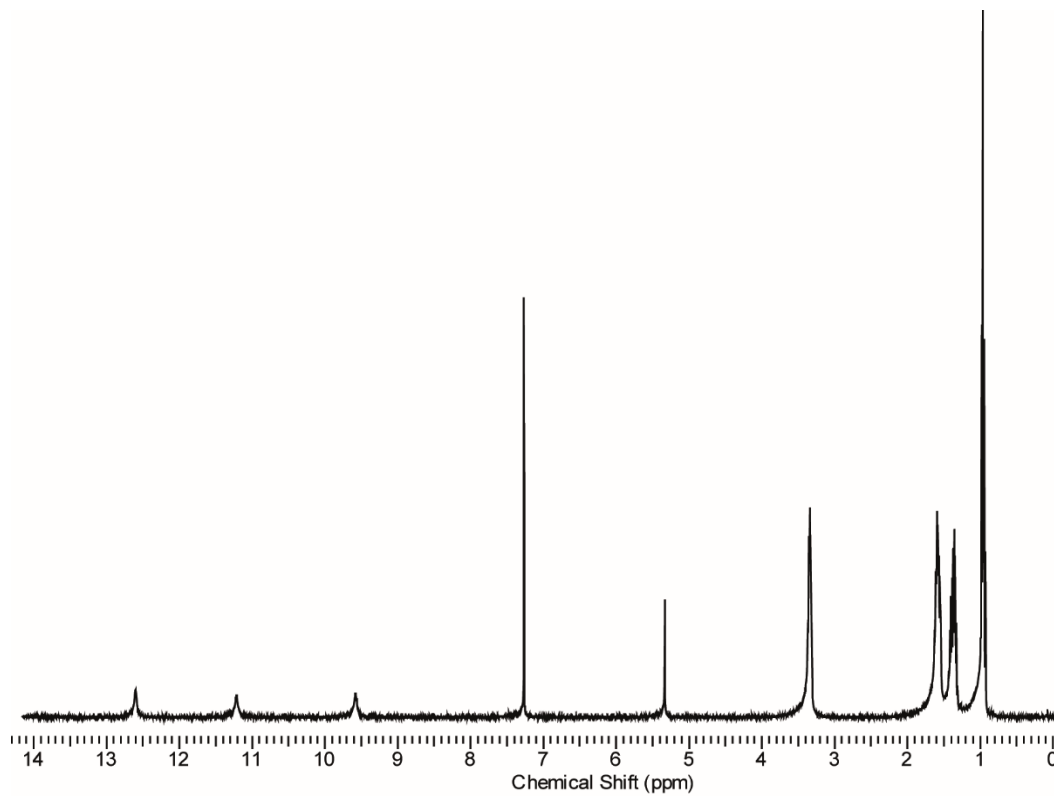
Appendix A Figure 4. Pathway D ^1H NMR (500 MHz, 10 mM, CDCl_3) (a) AUPy, NPyO, DAN, UPy, UIM and AIC, (b) AUPy, DAN, UPy, UIM, and AIC (c) AUPy, UPy, UIM and AIC, (d) AUPy, UPy and UIM (e) AUPy and UPy and (f) UPy.



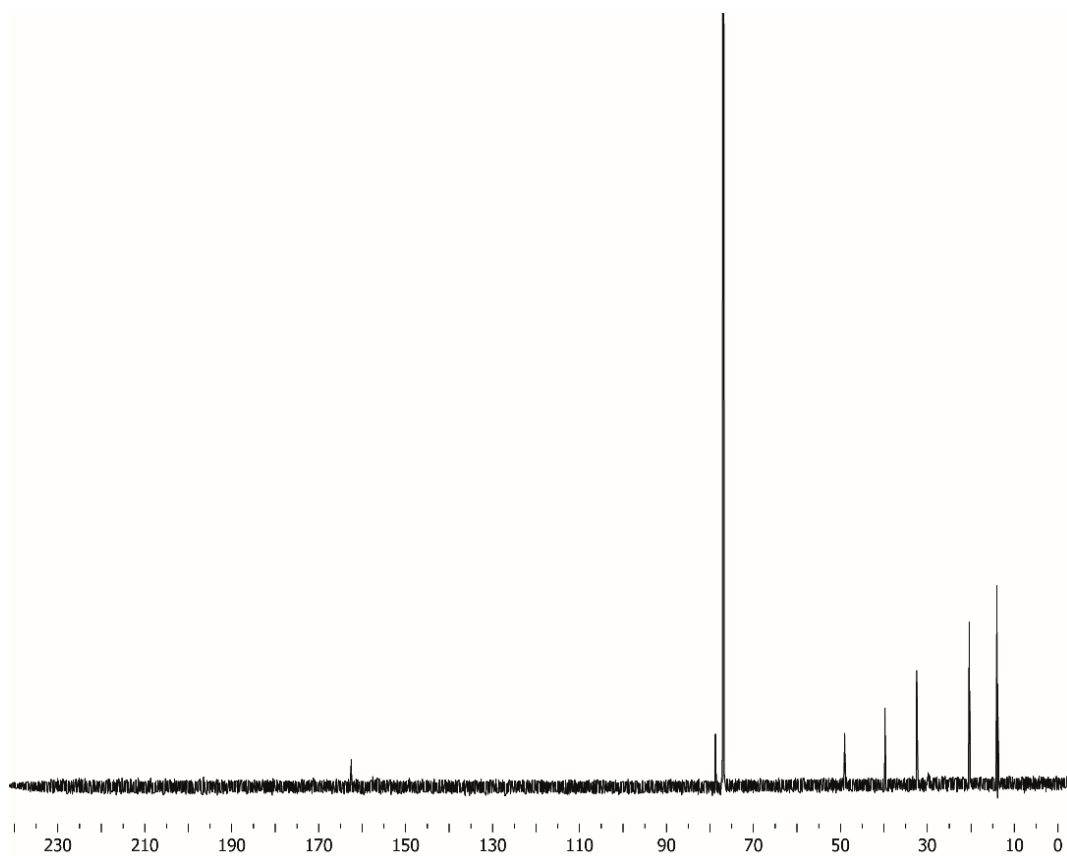
Appendix A Figure 5. Pathway F ^1H NMR (500 MHz, 10 mM, CDCl_3) (a) AUPy, NAPyO, DAN, UPy, UIM and AIC, (b) AUPy, NAPyO, UPy, UIM and AIC, (c) AUPy, NAPyO, UPy and UIM, (d) AUPy, UPy and UIM, (e) UPy and UIM and (f) UPy.

Appendix B

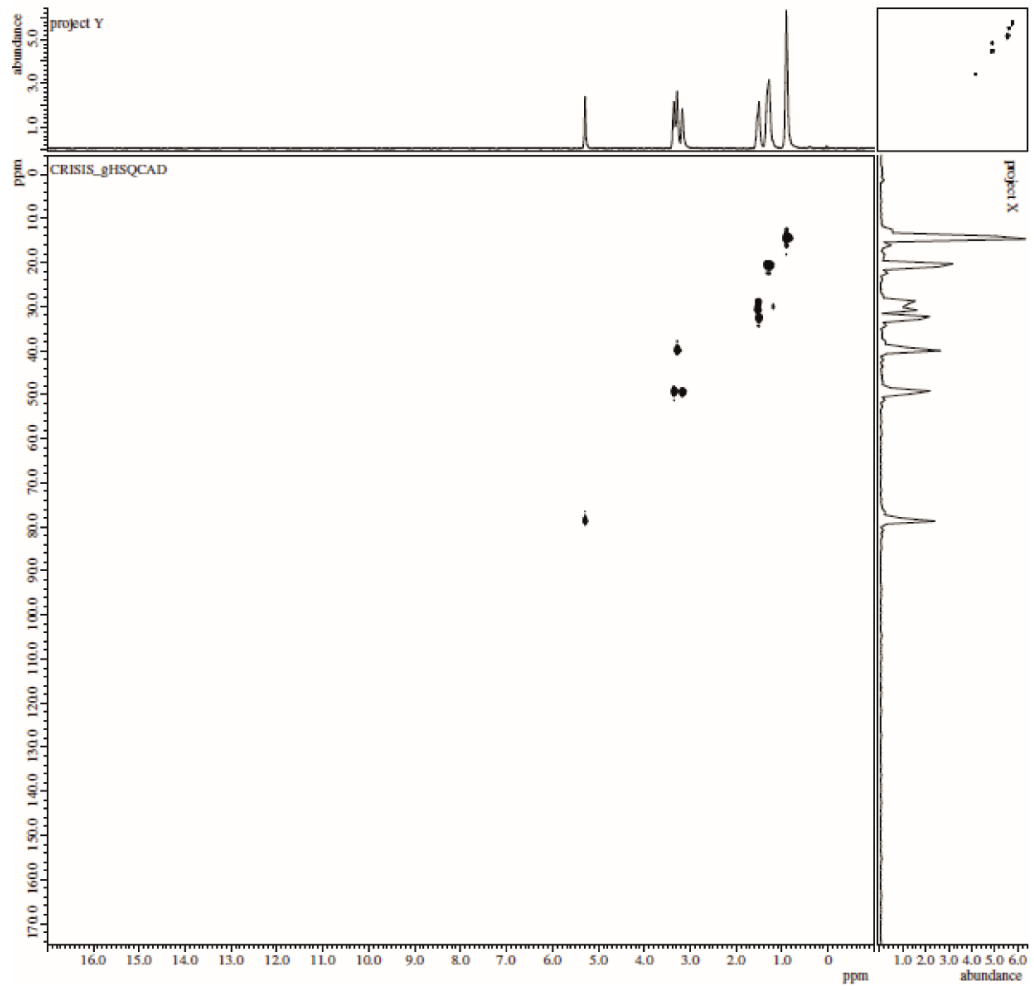
A representative selection of additional NMR spectra used for proton assignment of AUPy 66 from Chapter 2.



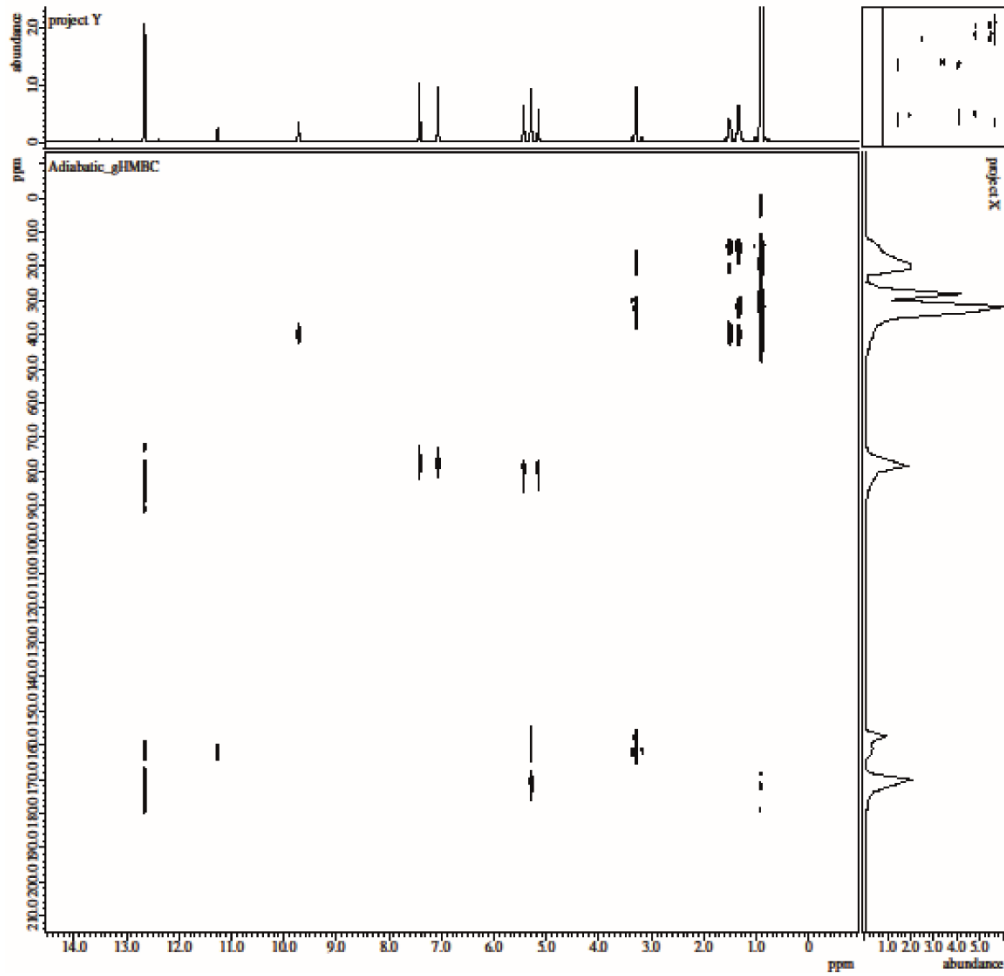
Appendix B Figure 1. ¹H NMR AUPy 66 (500 MHz, 10 mM, CDCl₃).



Appendix B Figure 2. ^{13}C NMR AUPy 66 (150 MHz, 30 mM, CDCl_3).



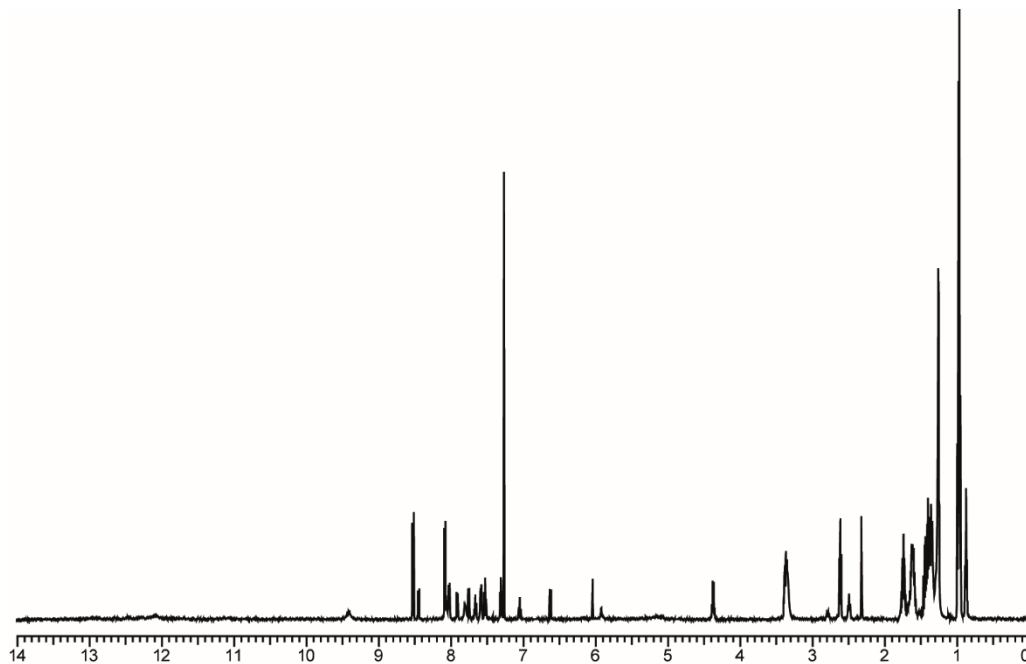
Appendix B Figure 3. HSQC NMR AUPy 66 (600 MHz, 30 mM, CDCl₃).



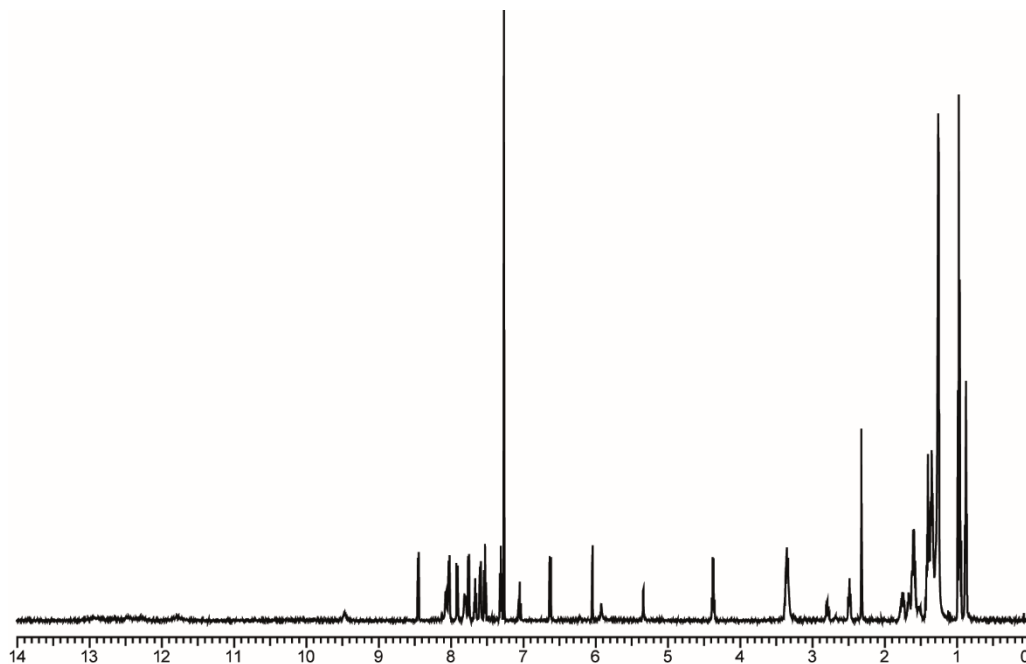
Appendix B Figure 4. HMBC NMR AUPy 66 (600 MHz, 30 mM, CDCl₃).

Appendix C

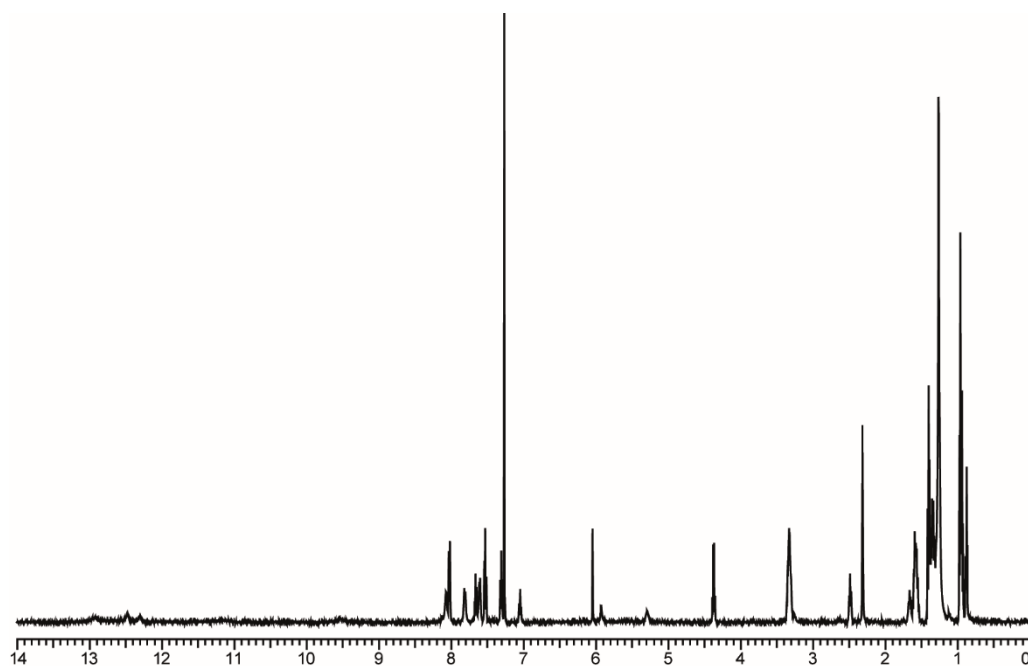
A representative selection of full ^1H NMR spectra taken from Pathway E
Figure 52 in Chapter 2.



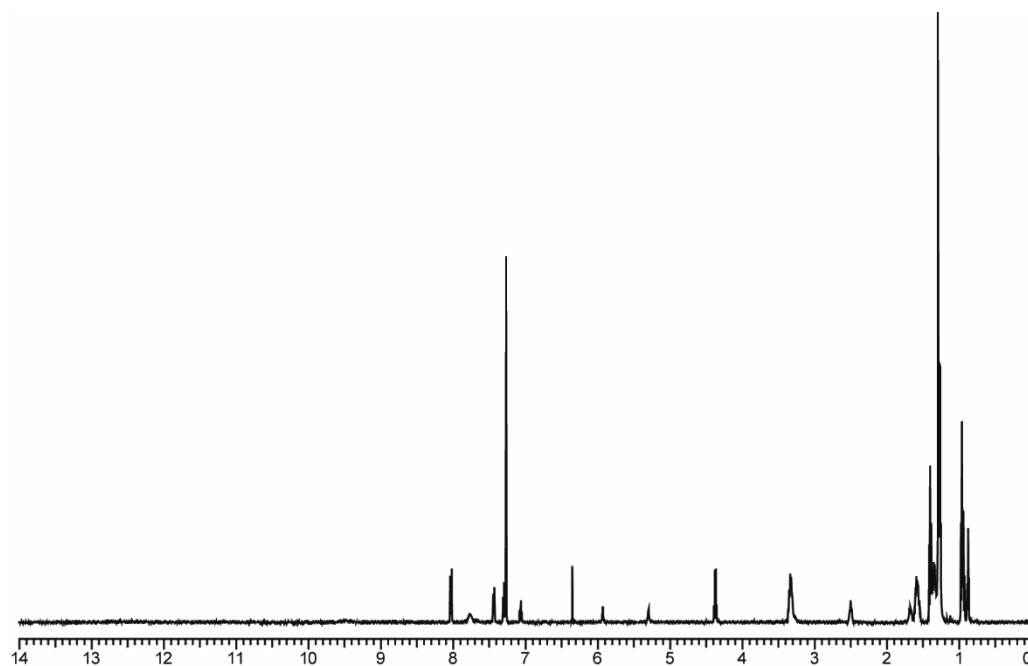
Appendix C Figure 1. Pathway E ^1H NMR (500 MHz, 10 mM, CDCl_3) (a)
AUPy 66, NAPyO 67, DAN 44, UPy 45, UIM 31, and AIC 46.



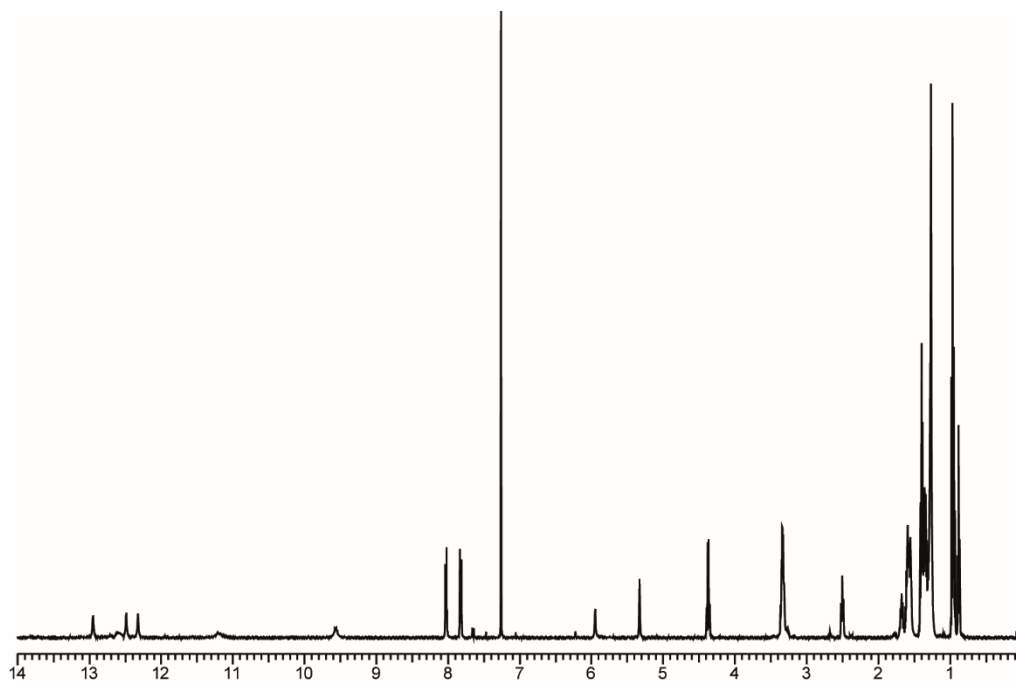
Appendix C Figure 2. Pathway E ^1H NMR (500 MHz, 10 mM, CDCl_3) (b)
AUPy 66, NAPyO 67, UPy 45, UIM 31, and AIC 46.



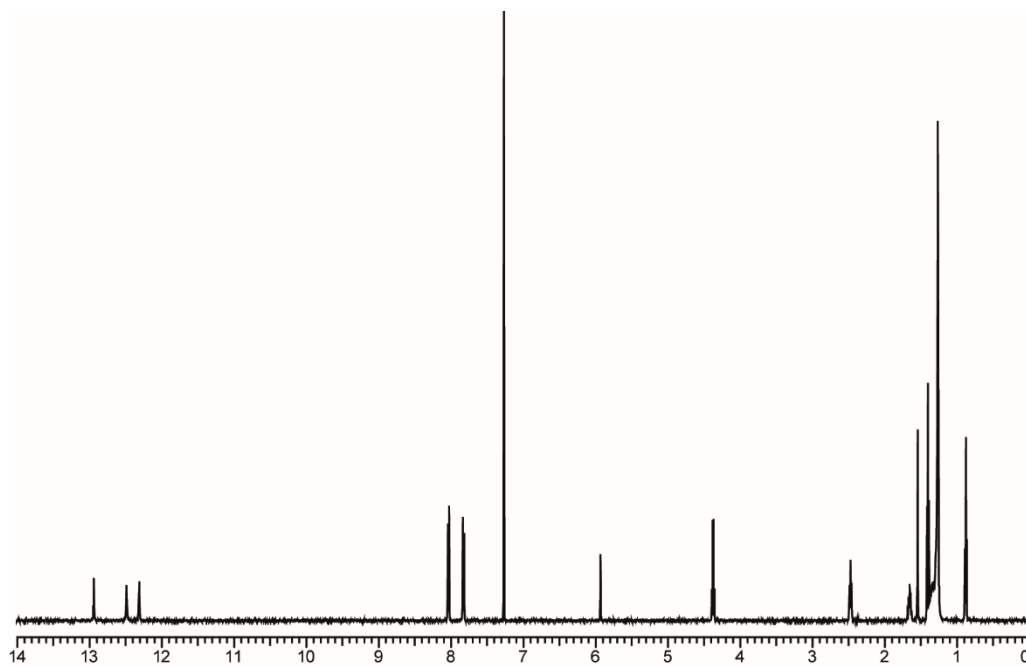
**Appendix C Figure 3. Pathway E ^1H NMR (500 MHz, 10 mM, CDCl_3) (c)
AUPy 66, UPY 45, UIM 31, and AIC 46.**



**Appendix C Figure 4. Pathway E ^1H NMR (500 MHz, 10 mM, CDCl_3) (d)
AUPy 66, UPY 45, and UIM 31.**



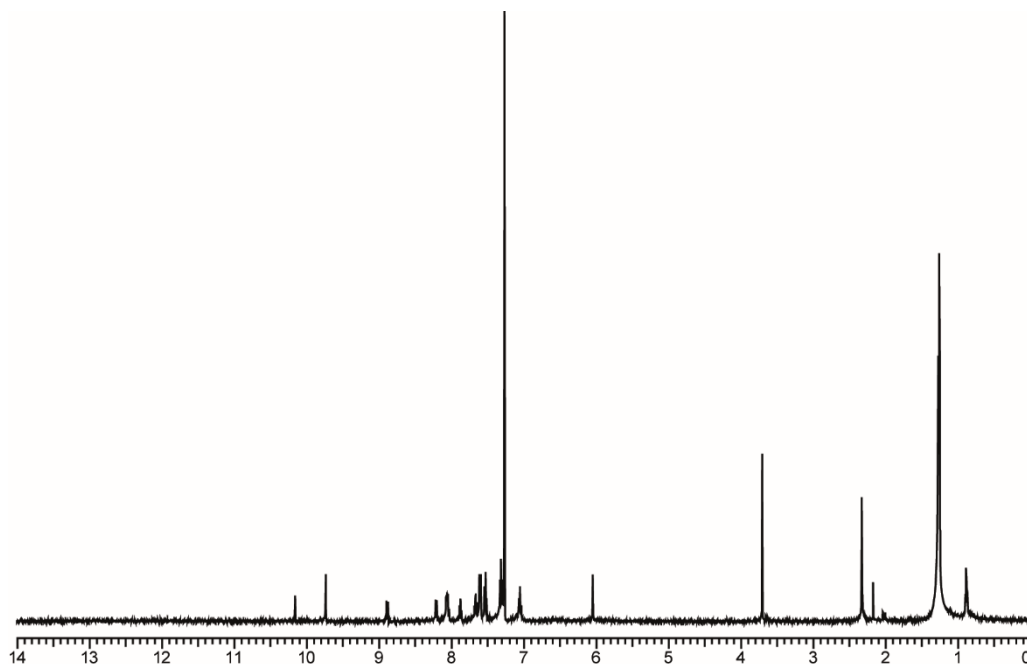
**Appendix C Figure 5. Pathway E ¹H NMR (500 MHz, 10 mM, CDCl₃) (e)
AUPy 66 and UPy 45.**



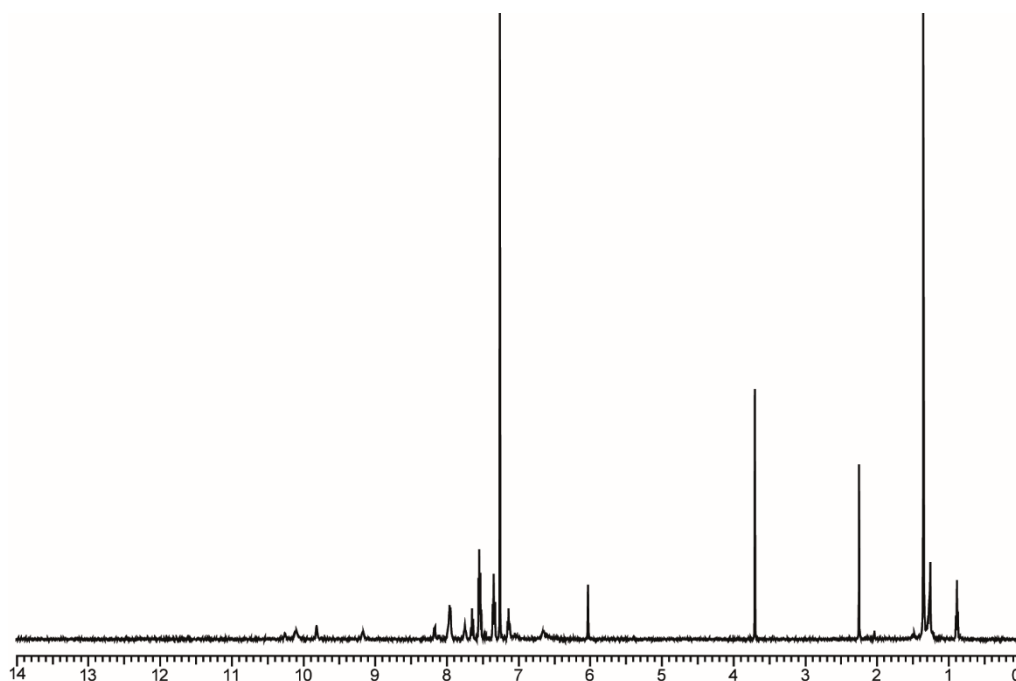
**Appendix C Figure 6. Pathway E ¹H NMR (500 MHz, 10 mM, CDCl₃) (f)
UPy.**

Appendix D

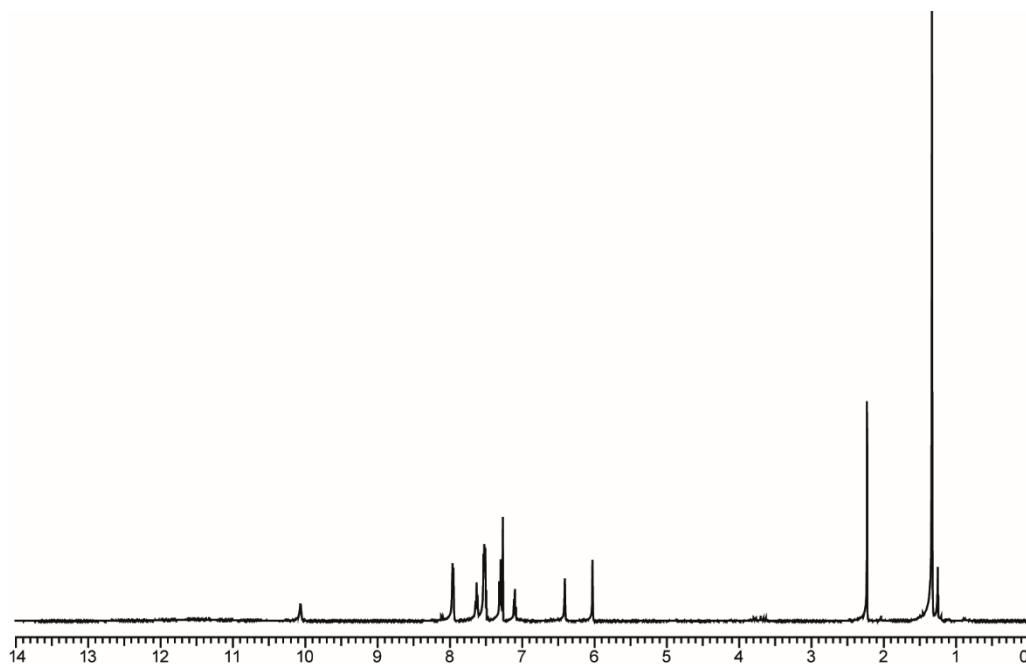
A representative selection of full ^1H NMR spectra taken from Figure 63 in Chapter 3.



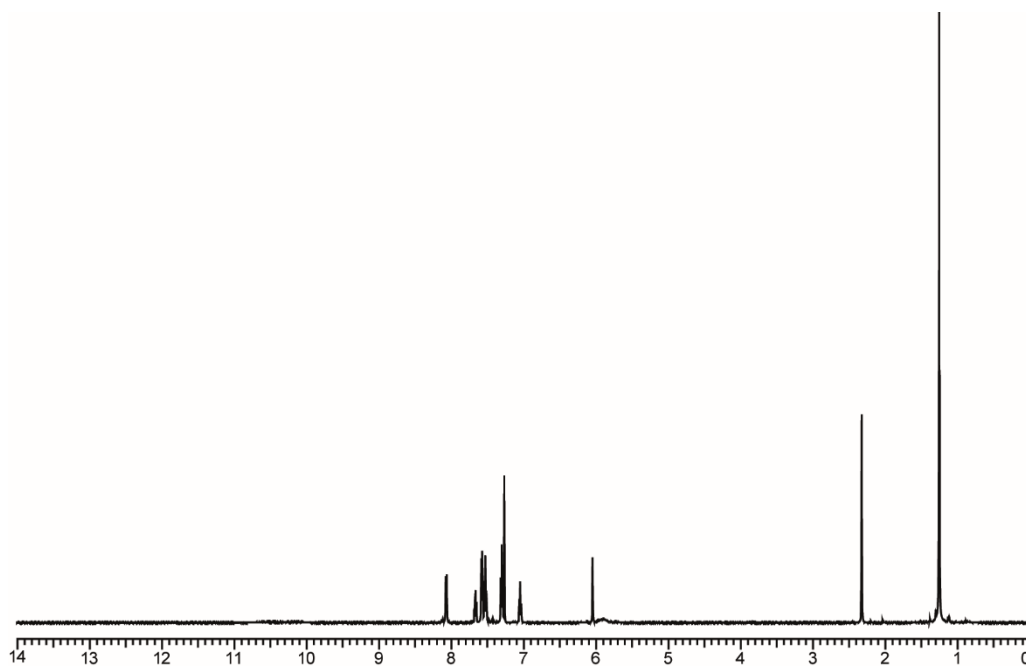
Appendix D Figure 1. ^1H NMR (500 MHz, 5 mM, CDCl_3) (a) UIM·AIC 31·46 dimer and BB1 85 formed after washing UIM-HCl·BB1 31*·85 dimer and AIC 46 mixture with NaHCO_3 .



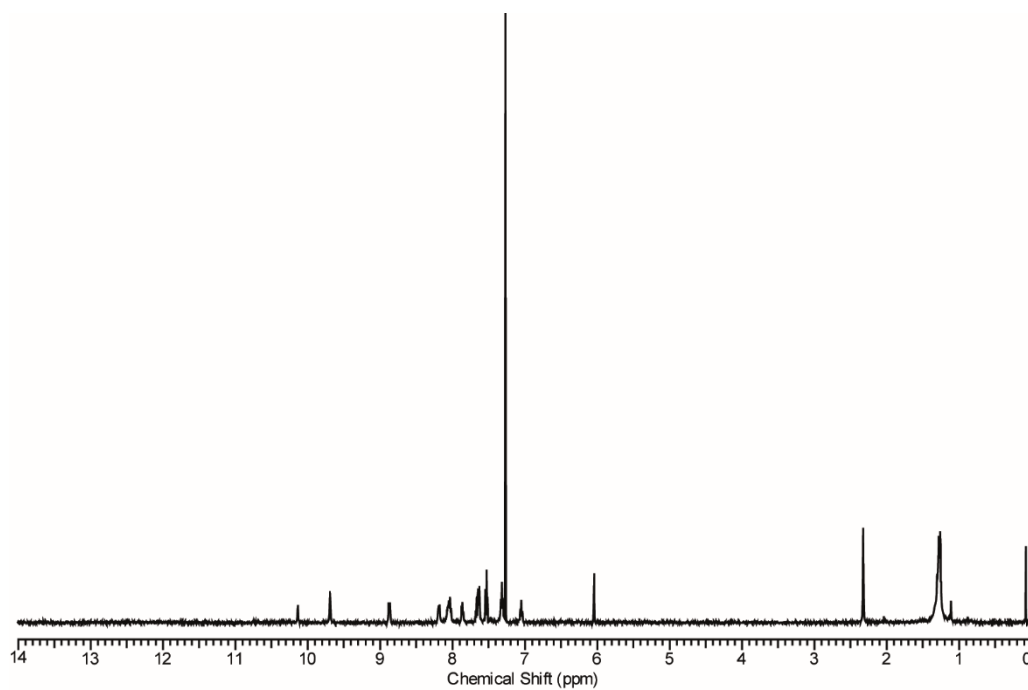
Appendix D Figure 2. ^1H NMR (500 MHz, 5 mM, CDCl_3) (b) UIM-HCl·BB1 31*·85 dimer (protonated with 4M HCl in 1,4-dioxane) and AIC 46.



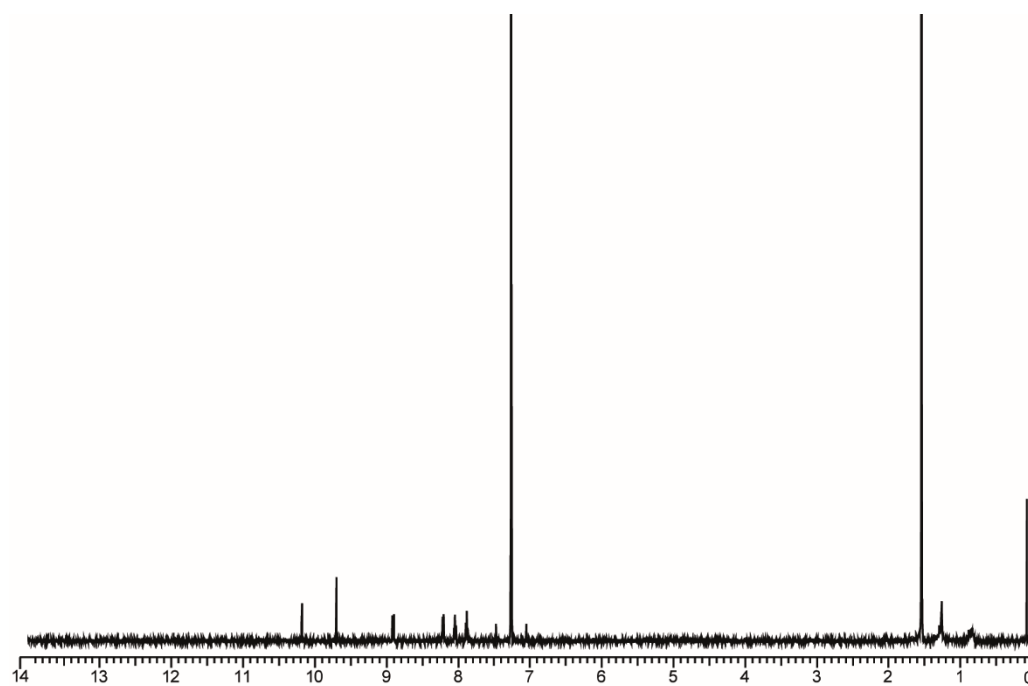
Appendix D Figure 3. ¹H NMR (500 MHz, 5 mM, CDCl₃) (c) UIM-HCl 31* (protonated with 4M HCl in 1,4-dioxane) and AIC 46.



Appendix D Figure 4. ¹H NMR (500 MHz, 5 mM, CDCl₃) (d) UIM·AIC 31·46 dimer.



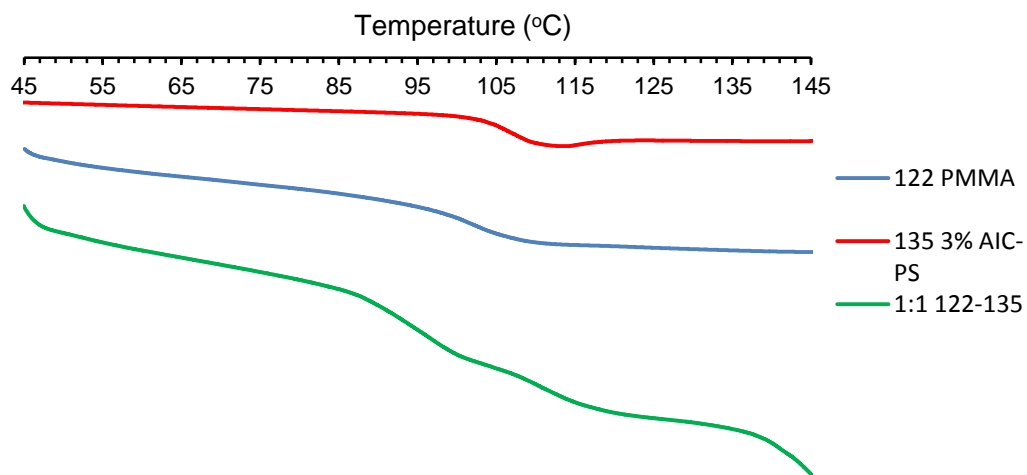
Appendix D Figure 5. ¹H NMR (500 MHz, 5 mM, CDCl₃) (e) UIM·AIC 31·46 dimer and BB1 85.



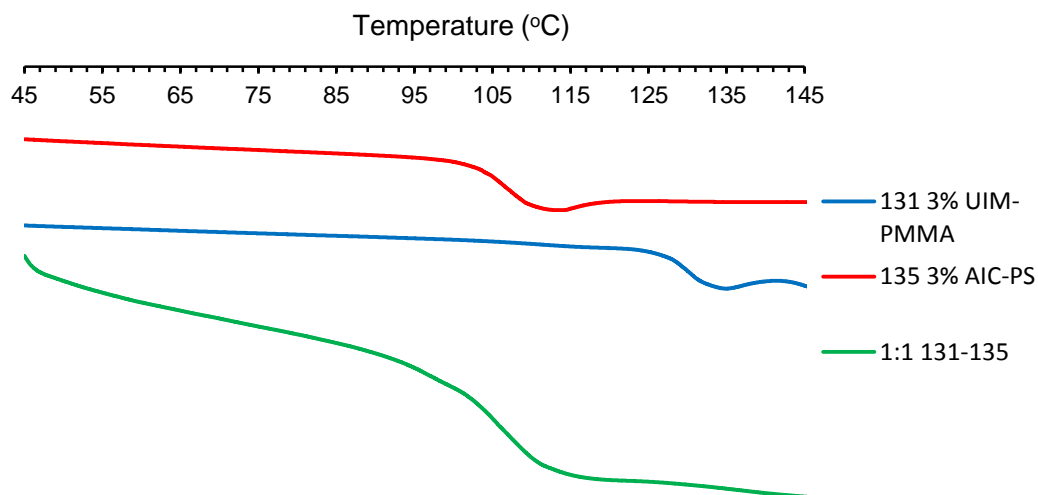
Appendix D Figure 6. ¹H NMR (500 MHz, 5 mM, CDCl₃) (f) BB1 85.

Appendix E

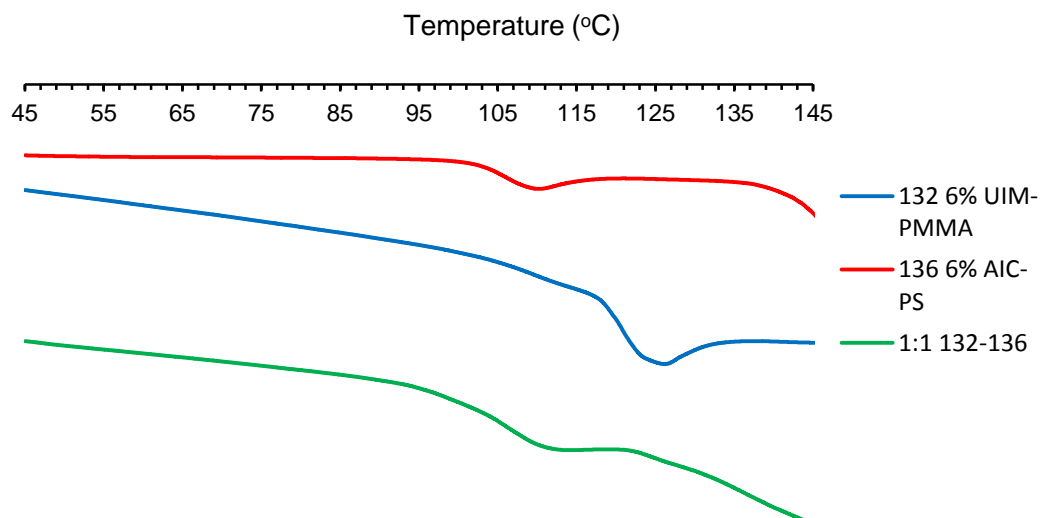
Supporting DSC thermograms for Chapter 4



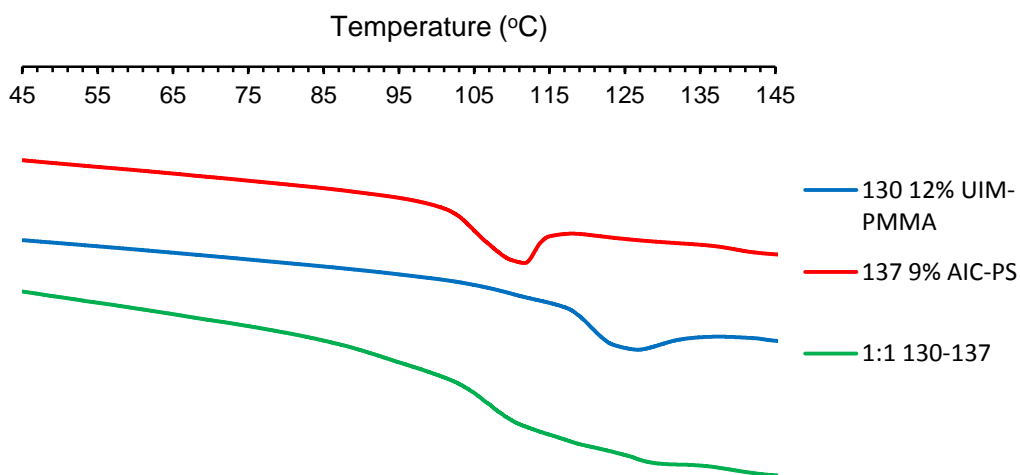
Appendix E Figure 1. DSC thermogram on heating of co-polymer 122 (PMMA) blue, co-polymer 135 (3% AIC hydrogen bonding motifs) red and 1:1 mixture of 122 and 135 (PMMA:3% AIC-PS) green.



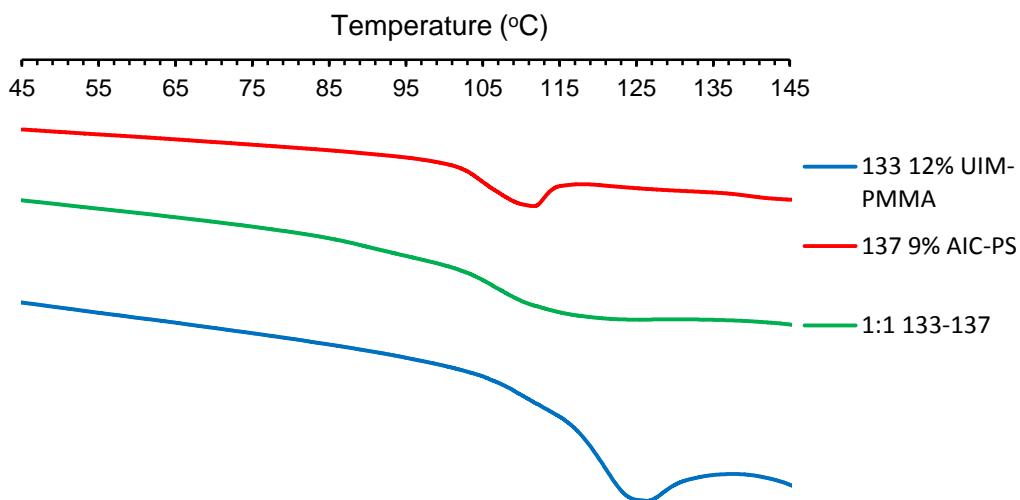
Appendix E Figure 2. DSC thermogram on heating of co-polymer 131 (3% UIM hydrogen bonding motifs) blue, co-polymer 135 (3% AIC hydrogen bonding motifs) red and 1:1 mixture of 131 and 135 (3% UIM-PMMA:3% AIC-PS) green.



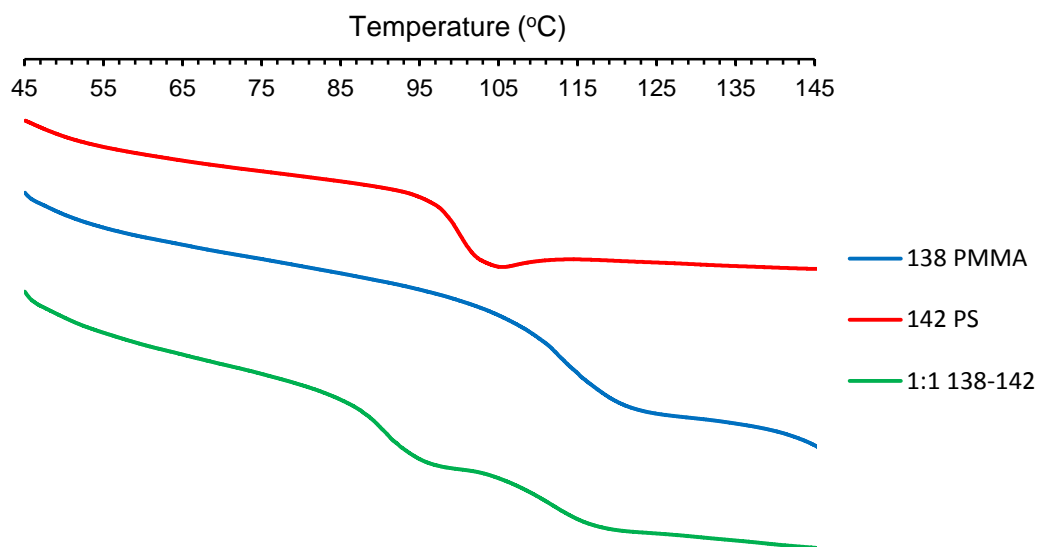
Appendix E Figure 3. DSC thermogram on heating of co-polymer 132 (6% UIM hydrogen bonding motifs) blue, co-polymer 136 (6% AIC hydrogen bonding motifs) red and 1:1 mixture of 132 and 136 (6% UIM-PMMA:6% AIC-PS) green.



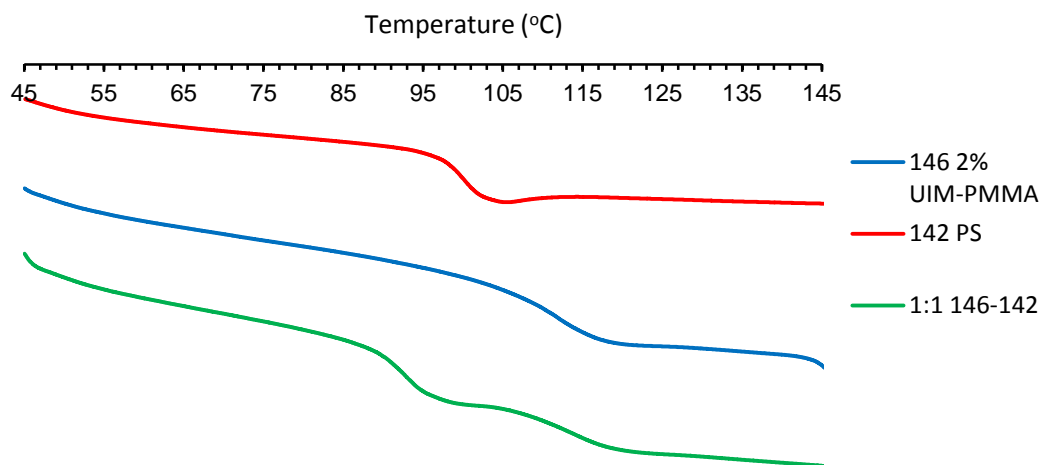
Appendix E Figure 4. DSC thermogram on heating of co-polymer 130 (12% UIM hydrogen bonding motifs) blue, co-polymer 137 (9% AIC hydrogen bonding motifs) red and 1:1 mixture of 130 and 137 (12% UIM-PMMA:9% AIC-PS) green.



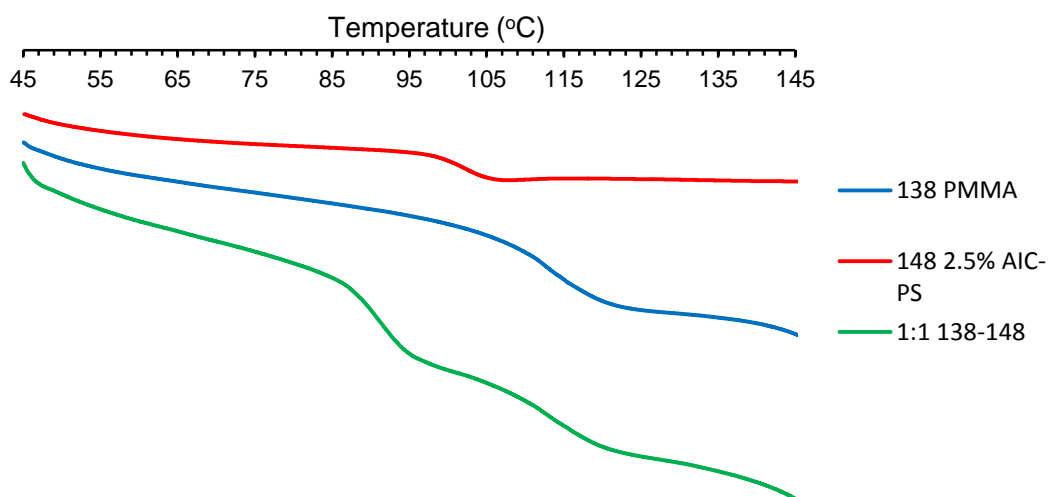
Appendix E Figure 5. DSC thermogram on heating of co-polymer 133 (12% UIM hydrogen bonding motifs) blue, co-polymer 137 (9% AIC hydrogen bonding motifs) red and 1:1 mixture of 133 and 137 (12% UIM-PMMA:9% AIC-PS) green.



Appendix E Figure 6. DSC thermogram on heating of co-polymer 138 (PMMA) blue, co-polymer 142 (PS) red and 1:1 mixture of 138 and 142 (PMMA:PS) green.



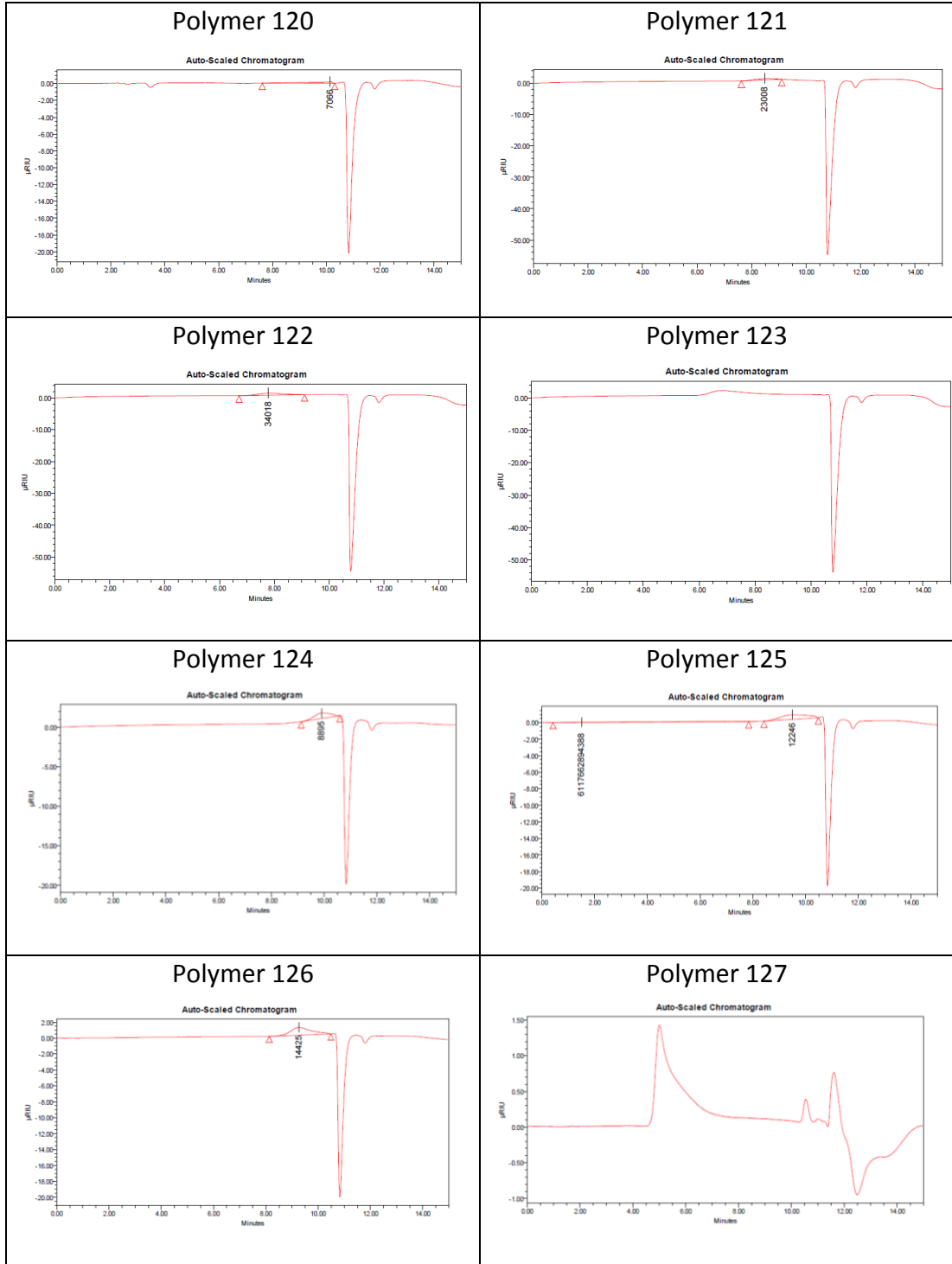
Appendix E Figure 7. DSC thermogram on heating of co-polymer 146 (2% UIM hydrogen bonding motifs) blue, co-polymer 142 (PS) red and 1:1 mixture of 146 and 148 (2% UIM-PMMA:PS) green.

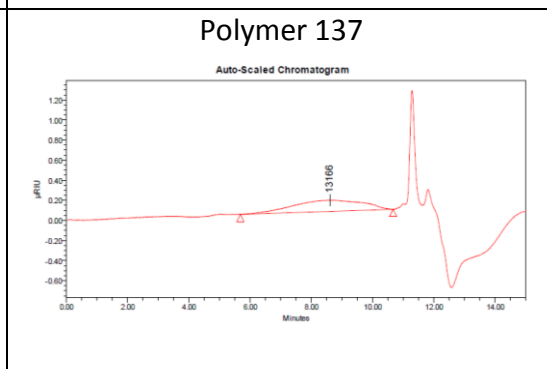
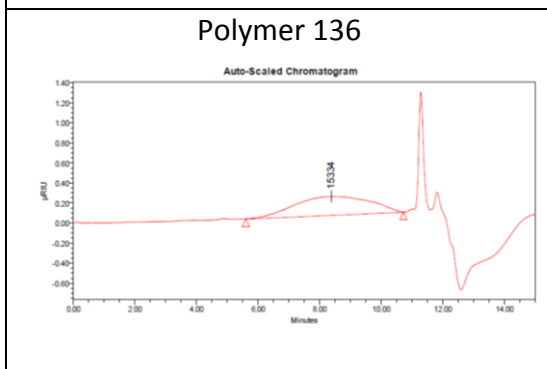
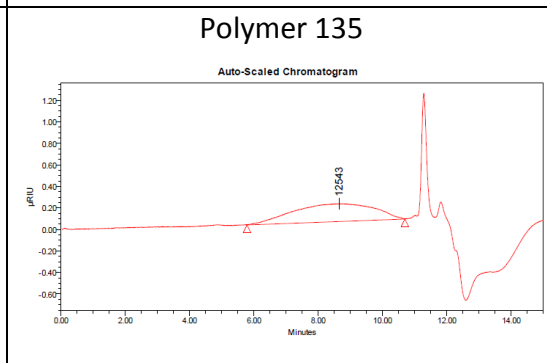
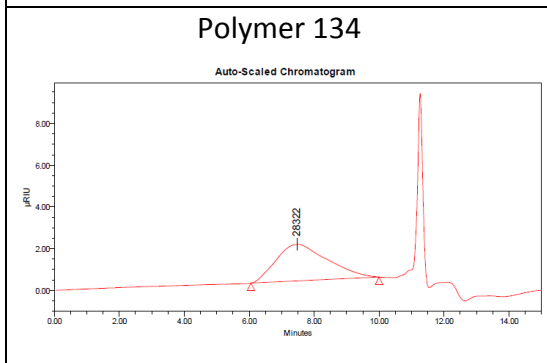
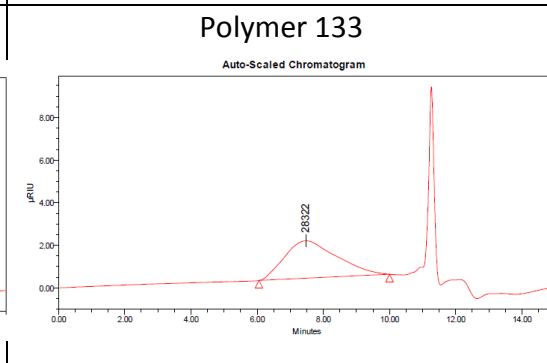
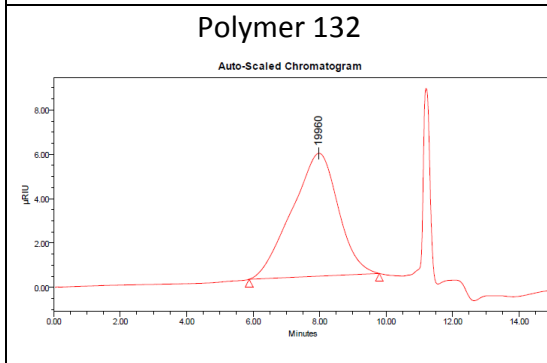
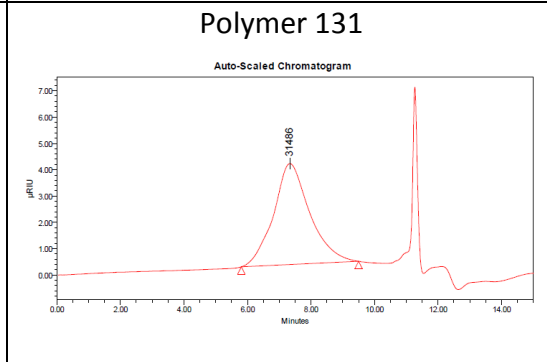
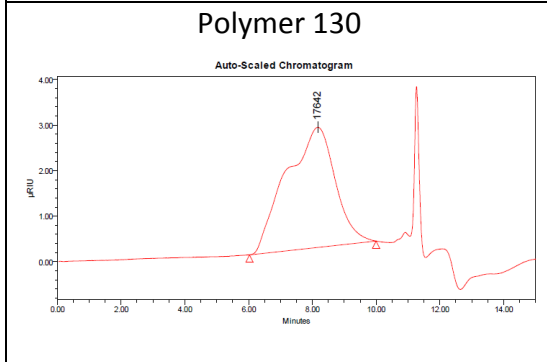
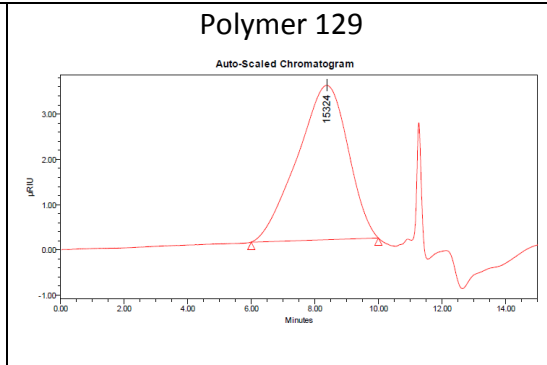
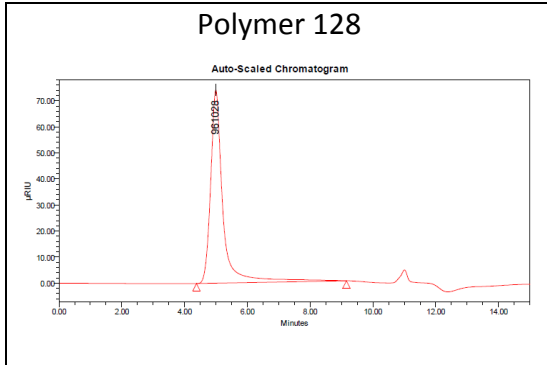


Appendix E Figure 8. DSC thermogram on heating of co-polymer 138 (PMMA) blue, co-polymer 148 (2.5% AIC hydrogen bonding motifs) red and 1:1 mixture of 138 and 148 (PMMA:2.5% AIC-PS) green.

Appendix F

Supporting table of APC traces of polymers from Chapter 4





Appendix G

Supporting table of GPC traces of polymers from Chapter 4

